DEVELOPMENT OF REVISED SAPRC AROMATICS MECHANISMS

Report to the California Air Resources Board
Contract No. 07-730 and 08-326

By

William P. L. Carter and Gookyoung Heo

April 12, 2012

Center for Environmental Research and Technology
College of Engineering
University of California
Riverside, California 92521

ABSTRACT

The representation of the gas-phase atmospheric reactions of aromatic hydrocarbons in the SAPRC-07 mechanism has been updated and revised to give better simulations of recent environmental chamber experiments. The SAPRC-07 mechanism consistently underpredicted NO oxidation and O_3 formation rates observed in recent aromatic - NO_x environmental chamber experiments carried out using generally lower reactant concentrations than the set of experiments used to develop SAPRC-07 and earlier mechanisms. The new aromatics mechanism, designated SAPRC-11, was evaluated against the expanded chamber database and gave better simulations of ozone formation in almost all experiments, except for higher (>100 ppb) NO_x benzene and (to a lesser extent) toluene experiments where O_3 formation rates were consistently overpredicted. This overprediction can be corrected if the aromatics mechanism is parameterized to include a new NO_x dependence on photoreactive product yields, but that parameterization was not incorporated in SAPRC-11 because it is inconsistent with available laboratory data. The new version incorporates a few minor updates to the base mechanism concerning acetylene, glyoxal and acyl peroxy + HO_2, has new parameterized mechanisms for phenolic compounds, and incorporates modifications and readjustments to the parameterized mechanisms representing reactive ring-opening products, but otherwise is the same as SAPRC-07. The new mechanism gives up to ~15% higher ozone concentrations under maximum incremental reactivity (MIR) conditions and gives ~0-50% higher MIR values for most aromatic compounds, and much higher reactivities for benzene and phenolic compounds. However, the mechanism revision has relatively small effects on O_3 predictions under NO_x-limited conditions, and the MIR values for non-aromatic compounds are not significantly affected.

ACKNOWLEDGEMENTS AND DISCLAIMERS

This work was carried out at the College of Engineering Center for Environmental Research and Technology (CE-CERT) at the University of California at Riverside (UCR). The mechanism development and analysis work and the preparation of this report were funded primarily by the California Air Resources Board (CARB) through contracts 07-730 and 08-326. In addition, the University of California Retirement System provided significant support to cover the efforts by William P. L. Carter for this project.

The environmental chamber experiments discussed in this report include new experiments carried out at CE-CERT and Commonwealth Scientific and Industrial Research Organisation (CSIRO) environmental chamber. The new CE-CERT experiments were carried out primarily under funding from CARB contract 08-326, William P. L. Carter and David R. Cocker III, co-investigators, and to a lesser extent from NSF grant ATM-0901282, Dr. David R. Cocker, III, principal investigator. Most of the new CE-CERT experiments are documented in a separate report being submitted to the CARB (Carter et al, 2012, in preparation).

The authors wishes to thank Dr. Ajith Kaduewela of the CARB for his support of this project and Dr. Stephen J. White for providing the CSIRO environmental chamber data, Mr. Dennis R. Fitz for assistance in administrating this project, and Wendy Goliff for helpful discussions.

The contents of this report reflect only the opinions and conclusions of the authors, and not CE-CERT, UCR, the CARB, or any of the individuals or institutions mentioned in this Acknowledgement or the body of the report. Mention of trade names and commercial products does not constitute endorsement or recommendation for use.

TABLE OF CONTENTS

TABLE OF CONTENTS (continued)

LIST OF TABLES

LIST OF TABLES (continued)

LIST OF FIGURES

LIST OF FIGURES (continued)

LIST OF FIGURES (continued)

EXECUTIVE SUMMARY

Background and Problem Statement

The chemical mechanism is the portion of the model that represents the processes by which emitted primary pollutants, such as volatile organic compounds (VOCs) and oxides of nitrogen (NO_x), interact in the gas phase to form secondary pollutants such as ozone (O_3) and other oxidants. The SAPRC-07 mechanism is the latest in the SAPRC series of gas-phase chemical mechanisms that are used for various airshed model applications. Simulations of environmental chamber data are important to mechanism development because mechanisms for many emitted VOCs are complex and have uncertainties, and available data, theories, and estimates are not sufficient to fully constrain the mechanism. For this reason, the predictive capabilities of the mechanisms need to be evaluated by determining if the mechanism can simulate the results of appropriate environmental chamber experiments, and in some cases uncertain portions of the mechanism may need to be adjusted for the mechanisms to give satisfactory simulations of these data. If a mechanism cannot adequately simulate results of well-characterized chamber experiments, it cannot be relied upon to give accurate predictions in airshed model applications.

Appropriate representation of the reactions of aromatic hydrocarbons is a priority for airshed models because of their high reactivity combined with their relatively large emissions. The need to evaluate and adjust mechanisms based on simulations of chamber data is particularly important for aromatics because of the complexities and significant uncertainties in their mechanisms, and the fact that much of their relatively high atmospheric reactivity is due to secondary reactions of poorly characterized products. Although results of a large number of environmental chamber experiments with aromatics were used in developing the aromatics mechanisms for SAPRC-07, most of these experiments were carried out at NO_x levels much higher than typically observed ambient NO_x levels, and comprehensive mechanism evaluation data were available for only a few representative compounds.

Since SAPRC-07 was developed, a large number of additional aromatic environmental chamber experiments were conducted, including experiments for additional compounds and many experiments at lower NO_x levels than previously available. Most of these were carried out to provide data to develop mechanisms for prediction of secondary organic aerosol (SOA) formation from aromatics, but they can also be used for gas-phase mechanism evaluation. It was found that SAPRC-07 did not perform well in simulating O_3 formation in many of the new experiments, particularly experiments at lower NO_x levels and also experiments with phenolic compounds that are important aromatic oxidation products. These new data indicate that the SAPRC-07 aromatics mechanisms do not give the best fits to the currently available chamber dataset, and need to be revised to take the new data into account.

Accomplishments

Although this work did not represent a complete update of SAPRC-07, a number of updates and revisions were made to SAPRC-07 to derive the updated version that is designated SAPRC-11. Almost all of the revisions concerned reactions of aromatics or aromatic oxidation products, with mechanisms updated for benzene, toluene, ethylbenzene, and all xylene, trimethylbenzene, ethyltoluene and propyl benzene isomers, as well as phenol, o-cresol, and 2,4-dimethylphenol. Mechanisms for other aromatics are derived based on those for these 17 representative compounds.

Several revisions were made to make the mechanism more consistent with recent literature data: Most of the revisions concerned aromatics, but an error was corrected in the temperature dependence for the reaction of OH radicals with acetylene, a few updates were made to the base mechanism concerning reactions of HO_2 with acetyl peroxy radicals ($RC(O)O_2\cdot$). Correcting the acetylene error does not affect predictions at ambient temperatures and the update to the HO_2 + acetyl peroxy reactions only affects product and radical predictions under low NO_x conditions and predictions of O_3 formation. The mechanism for glyoxal, an important aromatic oxidation product was also updated. The rate constants and yields of known oxidation products from the reactions of the aromatic hydrocarbons that are separately represented in the mechanism were updated to be consistent with current literature data. But the major changes concerned revisions made to improve model simulations of O_3 formation in aromatic - NO_x environmental chamber experiments. The quantum yields for radical formation from the model species representing unknown aromatic ring-opening products were adjusted to remove biases in model simulations of NO oxidation and O_3 formation rates in aromatic - NO_x experiments with NO_x levels lower than ~100 ppb. New mechanisms were derived for the reactions of the oxidation products phenol, cresols, and xylenols to improve model simulations of experiments with those compounds.

A second version of SAPRC-11, designated SAPRC-11A was developed in an attempt to account for an apparent dependence of mechanism evaluation results on total NO_x levels for certain compounds. This is the same as SAPRC-11 except that the possibility that adducts formed after OH radical addition to the aromatic ring may react with NO_2 to form less reactive compounds is considered.

The updated aromatics mechanisms were developed and evaluated by conducting model simulations of results of 410 aromatic - NO_x environmental chamber experiments carried out in 9 different environmental chambers at three different laboratories using five different types of light sources. Approximately half were new experiments not used when developing SAPRC-07, including data at lower NO_x levels more representative of ambient conditions and with new compounds, including phenolic products, that have not been experimentally studied previously. Many of these new experiments were carried out for the purpose of studying SOA formation from aromatics, but the data are suitable for gas-phase mechanism evaluation as well.

This mechanism was used as the starting point for the development of a mechanism for predicting aromatic SOA formation as discussed in a separate report (Carter et al, 2012). This involved adding model species and reactions for predicting SOA, but that did not affect gas-phase predictions. A discussion of this is beyond the scope of the present report, which focuses only on gas-phase predictions.

Results

The most significant finding is that it is not possible for the model to simulate the rates of NO oxidation and O_3 formation over the full range of available NO_x conditions for some important aromatic compounds without adding additional NO_x-dependent processes that were not previously considered in aromatics mechanisms used in airshed models. In order to simulate the data over the full range of NO_x conditions for these compounds it is necessary to assume that the OH-aromatic adduct formed from compounds reacts with O_2 sufficiently slowly that reaction of the adduct with NO_2 can become competitive at the NO_x levels in the higher NO_x experiments, forming less reactive products. However, this is not consistent with laboratory data and with known dependences of aromatic product yields on NO_x levels. Therefore, either there is an inconsistency between the chamber data and the published laboratory results, or there is a different, unknown, process that causes this additional NO_x dependence in the chamber experiments. This is applicable to benzene, toluene, ethylbenzene and p-xylene, but not to o- or m-xylene, the trimethylbenzenes and (probably) o-cresol. The data are not sufficient to determine whether it is applicable to the compounds studied.

However, this issue is probably not a practical concern for atmospheric modeling, where NO_x levels are generally lower than the 100 ppb level where use of SAPRC-11A is necessary. The SAPRC-11 mechanism gives good simulations not only for NO oxidation and O_3 formation rates at the lower NO_x levels (for which it was optimized), but also for maximum O_3 yields, for which it was not necessarily optimized. It represents a significant improvement over SAPRC-07, which tends to underpredict O_3 formation rates in many of the newer experiments, in this regard.

Although SAPRC-11 performs better than SAPRC-07 in simulating the available chamber experiments, it still has model performance issues and does not satisfactorily simulate all of the results of the available experiments. The mechanisms still systematically underpredicts OH radical levels in the aromatic - NO_x experiments by about ~30% on the average, the model performance for O_3 predictions depends on the aromatic / NO_x ratios for many compounds, and the mechanism still tends to underpredict O_3 at lower reactive organic / NO_x levels in chamber experiments with ambient surrogate experiments, though to a somewhat lesser extent than SAPRC-07. Therefore, although model performance in simulating the available data has improved with this update, it is still not entirely satisfactory.

Test simulations were carried out to assess the effects of mechanism updates on ambient O_3 simulations, using the 1-day box model scenarios used to develop the Carter (1994) reactivity scales. SAPRC-11 was found to give predictions of somewhat higher O_3 concentrations in ambient simulations, with 3-15% higher O_3 in higher NO_x, maximum incremental reactivity (MIR) conditions and ~2% higher O_3 at lower NO_x levels. The ozone impacts under MIR conditions were not significantly affected for non-aromatic compounds, but MIR values for aromatic compounds increased by factors of ~2.5-4 for phenolic compounds, by over a factor of 2 for benzene, by 30-50% for toluene and other monoalkylbenzenes, and by lesser and more variable amounts for other aromatic hydrocarbons. However, use of 3-D models is necessary to completely evaluate the effect of the mechanism updates on ambient simulations.

Recommendations

The new SAPRC-11 aromatics mechanism incorporates a number of updates to make it more consistent with recent literature data and performs significantly better in simulating O_3 formation observed in the available environmental chamber experiments, and therefore represents an improvement over SAPRC-07. However, this mechanism has not yet been completely adapted for ambient modeling, and additional work is needed before it is ready for use in airshed models and deriving updated MIR and other reactivity scales. Although progress has also been made in adapting this mechanism for modeling SOA formation from aromatics (see Carter et al, 2012), additional work is also needed before it can be used for modeling SOA formation in ambient atmospheres.

However, despite recent progress significant uncertainties and model performance issues still exist with current aromatics mechanism, and additional research is needed before this situation can be improved. Efforts to understand more of the details of the aromatics oxidation mechanisms, particularly the identity, yields, and reactions of the uncharacterized, highly reactive ring-opening products, need to continue. This will probably require new techniques and analytical methods before significant further progress can be made, and this may take many years. In the meantime, a thorough review of relevant information from the conflicting literature data and carrying out chamber experiments to test alternative mechanisms could provide nearer-term data needed to improve models for regulatory applications. There is also a need for additional environmental chamber experiments to evaluate the mechanisms for a wider range of conditions, and more well characterized experiments with arc light sources that are more representative of sunlight and allow temperature effects to be systematically studied. Without such data, attempts to develop more explicit mechanisms will probably not be useful or successful, and reactions of aromatics will continue to be a source of significant uncertainty in ambient air quality modeling.

INTRODUCTION

Airshed models are essential for the development of effective control strategies for reducing photochemical air pollution because they provide the only available scientific basis for making quantitative estimates of changes in air quality resulting from changes in emissions. The chemical mechanism is the portion of the model that represents the processes by which emitted primary pollutants, such as volatile organic compounds (VOCs) and oxides of nitrogen (NO_x), interact in the gas phase to form secondary pollutants such as ozone (O_3) and other oxidants. This is an important component of airshed models because if the mechanism is incorrect or incomplete in significant respects, then the model's predictions of secondary pollutant formation may also be incorrect, and its use might result in implementation of inappropriate or even counter-productive air pollution control strategies.

One airshed model application where the accuracy of the chemical mechanism is important is the calculation of reactivity scales that measure relative impacts of different types of VOCs on ozone formation. VOCs differ significantly in their impacts on O_3 formation, and regulations that take this into account are potentially much more cost-effective than those that regulate all VOCs equally. In view of this, several VOC regulations implemented (or being considered) in California take reactivity into account. The California regulations use the Maximum Incremental Reactivity (MIR) scale that was calculated using the SAPRC-99 chemical mechanism (Carter, 2000a), but these have been updated to values calculated using the more recently developed SAPRC-07 mechanism (Carter, 2010a,b).

The SAPRC-07 mechanism is the latest in the SAPRC series of gas-phase chemical mechanisms (Carter, 1990, 2000a, 2010a,b) that are designed for various airshed model applications. The detailed version of the mechanism, which has separate reactions for over 700 different types of VOCs and represents approximately 300 others using the "lumped molecule" approach (Dodge, 2000), is used for calculating the MIR and other ozone reactivity scales, and serves as the basis for deriving more condensed mechanisms for airshed model applications where such chemical detail is not required. For such applications, a lumped mechanism was developed where the many types of emitted VOCs are represented using a more limited number of lumped model species whose mechanisms are derived based on those of the mixture of compounds they represent in a standard ambient mixture taken as representative of anthropogenic VOC emissions (Carter, 2000b, 2010a). Even more condensed versions of lumped SAPRC-07 have been developed using various lumping approximations (Carter, 2009, 2010c,d), but a discussion of this is beyond the scope of this report. But the chemical basis of all these versions of SAPRC-07 is that of the detailed version.

The chemical basis of detailed SAPRC-07 is based on results of various laboratory studies, kinetic and mechanistic data evaluations (e.g., Atkinson, 1989; Atkinson and Arey, 2003; Calvert et al. 2000, 2002; IUPAC, 2006; NASA, 2006), theoretical or "best judgment" estimates, extrapolations, and interpolations, and results of model simulations of environmental chamber data. Simulations of chamber data are important because mechanisms for many emitted VOCs are complex and have uncertainties, and available data, theories, and estimates are not sufficient to fully constrain the mechanism. For this reason, the predictive capabilities of the mechanisms need to be evaluated by determining if the mechanism can simulate the results of appropriate environmental chamber experiments, and in some cases uncertain portions of the mechanism may need to be adjusted for the mechanisms to give satisfactory simulations of these data. If a mechanism cannot adequately simulate results of well-characterized chamber experiments, it certainly cannot be relied upon to give accurate predictions in airshed model applications.

The need to evaluate and adjust mechanisms based on simulations of chamber data is particularly important when deriving mechanisms for aromatic compounds, because of the complexities and

significant uncertainties in their mechanisms, and the fact that much of their relatively high atmospheric reactivity is due to secondary reactions of highly photoreactive but poorly characterized ring-opening products (Calvert et al, 2002 and references therein). Aromatics are important compounds in airshed models because of their relatively high reactivity combined with their relatively large emissions, so appropriate representation of their reactions in the mechanisms is a priority. The earlier versions SAPRC, such as SAPRC-90 (Carter, 1990) and SAPRC-99 (Carter, 2000a) use highly parameterized model species whose yields and photolysis rates are adjusted to fit chamber data to represent the photoreactive ring-opening products, and also used highly parameterized and adjusted mechanisms for the phenols and other major ring-retaining products. The availability of at least some data concerning the reactions of unsaturated dicarbonyl aromatic products resulted in SAPRC-07 having a slightly less parameterized representation of these products than the earlier versions, but significant uncertainties remain and photodecomposition quantum yields of the model species representing these products still have to be adjusted based on model simulations of chamber data.

The importance of chamber data in the development of aromatic mechanisms means that the predictive capabilities of this important aspect of the overall mechanism are highly dependent on the quality and comprehensiveness of the available data. The development of SAPRC-07 utilized results of over 2500 environmental chamber experiments, of which 226 were single aromatic - NO_x experiments that served as the basis for the adjustments in the aromatics mechanisms (Carter, 2010a). Because of uncertainties in characterizing light intensity and spectra of outdoor chamber runs, the adjustments were based on only indoor chamber runs with well-characterized blacklight or solar simulator arc light sources, with runs with significant measurement or characterization uncertainties or whose results appeared to be outliers compared to comparable runs not being utilized. Data were available for benzene, toluene, ethylbenzene, and all the xylene and trimethylbenzene isomers, with mechanisms for other alkylbenzenes being estimated based on the mechanisms derived for the most structurally similar compound where data were available.

Most of the experiments used in the SAPRC-07 aromatics mechanism development were carried out at our environmental chamber laboratories at the University of California at Riverside (UCR), with a majority of these being carried out in the older UCR chambers (Carter et al, 1995a) at NO_x levels of greater than ~200 ppb. The dataset did include 5 experiments carried out in the TVA chamber (Simonaitis and Bailey, 1995; Bailey et al, 1996; Simonaitis et al, 1997; Carter, 2004), most at lower NO_x levels, and ~60 were carried out at using the new UCR-EPA chamber (Carter, 2004; Carter et al, 2005) at NO_x levels of less than 100 ppb. However, the parameters derived for the SAPRC-07 aromatics mechanisms, like those in earlier version of SAPRC, reflect primarily results of older UCR chamber experiments carried out at generally higher than ambient NO_x levels.

Although the initial aromatics experiments carried out at lower NO_x levels in the UCR EPA chamber suggested that the mechanism could simulate results of very low NO_x experiments reasonably well (Carter, 2004), more recent low NO_x experiments, carried out under a wider variety of conditions, indicate that this may not be the case. Azzi et al (2010) reported results of model simulations of new toluene and m-xylene - NO_x experiments carried out in a new indoor chamber at the Commonwealth Scientific and Industrial Research Organisation (CSIRO) in Australia (Hynes et al, 2005; White et al, 2010) using the SAPRC-07 mechanism, and found that it consistently underpredicted O_3 formation in the toluene experiments, and had an underprediction bias in the m-xylene experiments at lower xylene / NO_x ratios. In addition, a large number of new aromatic - NO_x experiments were carried out in the UCR EPA chamber for the purpose of studying secondary organic aerosol (SOA) formation from aromatics (Carter et al, 2012), and the results also indicated significant biases in SAPRC-07 ozone predictions at lower NO_x or lower VOC/NO_x levels.

An indication of the biases in the SAPRC-07 aromatics mechanism in simulating the new CSIRO and UCR EPA chamber data is given in Figure 1, which gives plots of the model error in simulating amounts of NO oxidation and ozone formation[1] in benzene, toluene, m-xylene and o-cresol - NO_x experiments against initial NO_x and initial aromatic / NO_x ratios. Different symbols are used for the new CSIRO and UCR EPA experiments. Figure 1 shows that the mechanism tends to underpredict ozone formed and NO oxidized in essentially all the new experiments with benzene, toluene and (especially) o-cresol and indicates a general underprediction bias for m-xylene. There also appears to be a dependence of the underprediction bias on initial NO_x levels in the case of benzene and toluene, and on aromatic/NO_x ratios in the case of toluene and m-xylene.

Not shown on Figure 1 are the results of model simulations of new UCR-EPA chamber experiments for a number of other aromatic compounds, including other xylene isomers, the trimethylbenzenes, and compounds for which no chamber data were available when SAPRC-07 was developed, including the ethyltoluene and propylbenzene isomers and other phenolic compounds. It was found that SAPRC-07 had a tendency to underpredict ozone formation rates for many of these other compounds as well.

Therefore, the new data from the CSIRO and UCR EPA chambers indicate that the SAPRC-07 aromatics mechanisms do not give the best fits to the currently available chamber dataset, and need to be revised to take the new data into account. In addition, the data for benzene and toluene suggest a dependence of model bias on total NO_x levels that cannot be accounted for by any adjustments to the mechanism using its current formulation. Recent laboratory data (e.g., Nishino et al, 2010; Bethel et al 2000) indicates that there is a dependence of aromatic fragmentation product yields on total NO_x levels, which is not represented in the current mechanism. This is attributed to a competition between the OH-aromatic adduct reacting with O_2 and NO_2 (Koch et al, 2007), with the reaction with O_2 forming the expected fragmentation products and the reaction with NO_2 at high NO_x levels presumably forming other products. However, according to the laboratory data (Koch et al, 2007), the competing reaction with NO_2 only becomes significant at NO_2 levels greater than ~1 parts per million (ppm), which is much higher than the NO_x levels used in almost all of the experiments in the current evaluation dataset. Therefore, even if the mechanism were modified to take this aromatic-OH adduct + NO_2 reaction into account it would not give significantly different simulations of the chamber data unless other changes were made.

To address these problems, in this work we developed a revised version of the SAPRC-07 mechanism with the aromatics mechanisms that is updated and readjusted to give better fits to the chamber data. This modified aromatics version of SAPRC-07 is referred to as "SAPRC-11" in the subsequent discussion, though most of the non-aromatic portions of SAPRC-11 are the same as SAPRC-07 because a full update of the mechanism is beyond the scope of this project. This SAPRC-11 aromatics mechanism is used as the starting point for a PM-SAPRC11 mechanism developed to predict secondary organic aerosol (SOA) formation from aromatics, as discussed by Carter et al (2012).

[1] See the discussion of $\Delta([O_3]-[NO])$ model error in the mechanism evaluation section for the definitions of this and other measures used to evaluate mechanism performance.

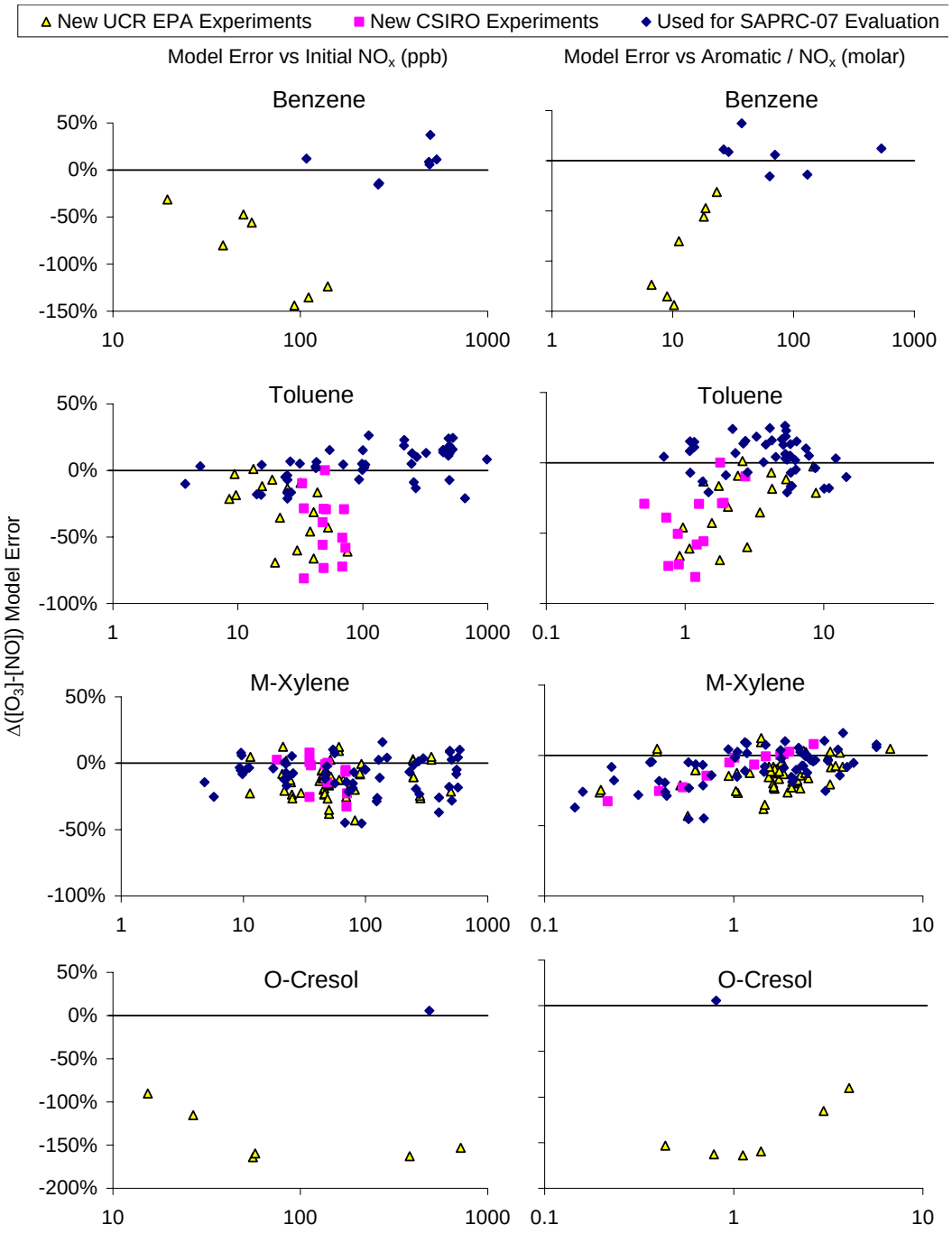

Figure 1. Plots of model error in SAPRC-07 model simulations of selected types of aromatic - NO_x experiments against initial NO_x and initial aromatic / NO_x ratios.

MECHANISM DESCRIPTION

General Mechanism

The starting point for the mechanisms developed in this work is the SAPRC-07 mechanism as documented by Carter (2010a,b). For this work, all portions of the mechanism were unchanged except as described in the following sections. Except for revisions to the general acyl peroxy + HO_2 reactions made as a result of an updated IUPAC recommendation (IUPAC, 2009), all of the revisions concerned the reactions of aromatics and model species used to represent aromatic photooxidation products. For simulations of chamber data, including the simulations used for adjusting the aromatics mechanisms, the reactions of each of the aromatic compounds present in the experiments were represented explicitly, rather than by a lumped model species (i.e., using TOLUENE rather than ARO1). This is the same approach as used when evaluating the SAPRC-07 mechanism against chamber data (Carter, 2010a,b).

A complete listing of the SAPRC-11 mechanisms used for the chamber and ambient simulations are given in Appendix A, where Table A-1 lists the model species and Table A-2 lists the reactions and rate constants. Table A-1 also indicates which species had changes to their mechanisms as part of this work, and footnotes to Table A-2 indicate which reactions were changed. If there is no footnote for a species or reaction in these tables then the mechanism is the same as given by Carter (2010a,b). The absorption cross sections and wavelength-dependent quantum yields are also the same as given by Carter (2010a,b), and are therefore not duplicated here.

Revisions to Base Mechanism

Table 1 lists the model species whose mechanisms were revised, added, or removed for this version of the base mechanism, and Table 2 lists the reactions involved. Footnotes to the table document the reasons for the changes or additions to the mechanisms, and additional discussion of these changes is given below. Note that except for the removed species listed in Table 1, the information on these two tables is a subset of the information in the complete mechanism listing given in Table A-1 and Table A-2 in Appendix A. Note that these tables do not include species and reactions that were added for the purpose of modeling aromatic SOA formation that are discussed by Carter et al (2012), since they do not affect the gas-phase that are the subject of this report. See Carter et al (2012) for a complete discussion of the revisions of the aromatics mechanism for SOA predictions.

Although a complete update of the mechanism based on a thorough review of current evaluations and data was beyond the scope of the present project, during the course of this project we became aware of revised evaluations that made changes to the base mechanism appropriate. These are summarized below.

Reaction of OH radicals with acetylene. The temperature dependence parameters used for acetylene in SAPRC-07 was based on the NASA (2006) evaluation, which is unchanged in the most recent NASA (2011) evaluation, should have had $k_0=5.5x10^{-30}$ cm^3 $molec^{-1}$ s^{-1}, independent of temperature, and $k_\infty=8.3x10^{-13}$ $(T/300)^2$ cm^3 $molec^{-1}$ s^{-1}. However, the $(T/300)^2$ temperature dependence was erroneously associated with k_0 in the mechanism. This has been corrected. This will not affect model performance for chamber simulations for this compound and have very little effect on atmospheric simulations at ambient temperatures.

Table 1. List of model species in the base mechanism that were added or deleted or whose mechanisms were changed in the current mechanism update. Species added by Carter et al (2012) that affect only SOA predictions are not included.

Species	Description	Discussion
Errors Corrected		
ACETYLEN	Acetylene (represented explicitly)	Error in temperature dependence parameters corrected. Does not affect evaluation against chamber data or atmospheric MIR predictions.
Mechanisms or Lumping Revised		
MECO3 RCO3 BZCO3 MACO3	All model species in the mechanism used to represent acyl peroxy radicals that react to form PAN or PAN analogues	Mechanism for reaction with HO_2 radicals revised based on new IUPAC (2009) evaluation.
GLY	Glyoxal	Mechanism for reaction with OH and NO_3 revised based on new IUPAC (2008a) evaluation.
CRES	Cresols	Now used to represent only cresols and not phenol or C_{8+} phenolic compounds, which are represented by separate model species. Mechanism revised to improve simulations of O_3 reactivity and SOA formation in o-cresol - NO_x chamber experiments.
AFG1 AFG2	Photoreactive monounsaturated dicarbonyl aromatic ring opening products and other unknown photoreactive aromatic ring opening products.	Yields reoptimized based on model simulations of aromatic - NO_x chamber experiments, including new experiments not available when SAPRC-07 was developed. Mechanisms are not changed other than removing reactions with O_3, which were found to be negligible under all conditions of interest.
AFG3	Used to represent di-unsaturated dicarbonyl ring opening products.	The change concerned only the set of compounds this model species is used to represent, not its mechanism. Previously AFG3 was also used for monounsaturated diketones, but now a separate model species, AFG4, is used for these compounds. The mechanism for AFG3 was not changed because it was based on estimated mechanisms for the di-unsaturated dicarbonyls only.
Model Species Added		
HCOCO3 [a]	Peroxy radical formed from H-abstraction reactions from glyoxal	This was previously represented by the lumped acyl peroxy radical species RCO3 but the current evaluations indicate that its reaction with NO_2 does not form stable PAN analogues so RCO3 is not an appropriate representation.
PHEN XYNL	Phenol and Xylenols and other C_{8+} phenolic compounds, respectively	These are now represented separately from cresols in order to represented differences in ozone reactivity and SOA formation from various types of

Table 1 (continued)

Species	Description	Discussion
		phenolic compounds. Parameterized mechanisms optimized to simulate of phenol - NO_x and 2,4-dimethyl phenol - NO_x chamber experiments.
AFG4 xAFG4 [a]	Monounsaturated diketones assumed not to be photoreactive, and the chemical operator representing the formation of AFG4 from peroxy radical reactions.	Separated from AFG3 for this version of the mechanism to appropriately represent differences in products formed and SOA formation potentials between monounsaturated diketones and di-unsaturated dicarbonyl ring opening products.
CATL	Catechols formed from reactions of phenolic compounds	These are added to the mechanism for the reactions of phenolic compounds primarily for the purpose of SOA prediction (Carter et al, 2012), but its reactions also affect radical and ozone predictions.
Model Species Deleted		
xAFG3 [a]	Chemical operator representing formation of AFG3, the model species used to represent di-unsaturated dicarbonyls, in peroxy radical reactions.	The revised mechanism no longer has AFG3 representing monounsaturated diketones that are formed following peroxy radical reactions. The model assumes that the di-unsaturated dicarbonyls that AFG3 represents are not formed following peroxy radical reactions.

[a] It is recommended that the steady state approximation be used for these xPROD species when the mechanism is implemented in models.

Reactions of Acyl Peroxy Radicals with HO_2.The SAPRC-07 mechanism representations for reactions of HO_2 with acyl peroxy radicals were based on the IUPAC (2006) recommendation for acyl peroxy radicals, which has ~70% of the reaction forming (1) O_2 + peroxyacetic acid, and ~30% of the reaction forming (2) O_3 + acetic acid. However, the most recent IUPAC (2009) recommendation recommends assuming these two pathways occur respectively 41% and 15% of the time, with a third pathway, forming (3) OH + O_2 + $CH_3C(O)O$ occurring 44% of the time. The mechanisms for all the acyl peroxy radical reactions in the mechanism were modified accordingly, with the model species used for the acid (CCOOH in the case of the acetic acid formed from MECO3) still being used to represent the peroxy acid formed in the first pathway. Thus the reaction for MECO3 (acetyl peroxy radicals) was changed from

MECO3 + HO2 = CCOOH + #.7 O2 + #.3 O3

to

MECO3 + HO2 = 0.44 {OH + MEO2 + CO2} + 0.41 CCOOH + #.15 {O3 + CCOOH}

Similar changes were made for the other acyl peroxy radicals in the mechanism. Note that the rate constant for the reaction was unchanged.

Reactions of Glyoxal. The reaction of glyoxal with OH and NO_3 radicals is assumed to involve a hydrogen abstraction reaction forming the intermediate HC(O)C(O)·. The SAPRC-07 mechanism assumed that this intermediate decomposes to CO + HCO and reacts with O_2 to form HC(O)C(O)OO· respectively 63% and 37% of the time. The HC(O)C(O)OO· is assumed to react analogously to other acyl peroxy radicals to form primarily PAN analogues in the presence of NO_2, and it is represented in the

Table 2. Reactions that were modified or added to the base mechanism for the updated aromatics mechanism developed for this project.

Label [a]	Reaction and Products [b]	Rate Parameters [c] k(300)	A	Ea	B	Notes [d]
Revised Reactions of Acyl Peroxy Radicals with HO_2						
BE10	ACETYLEN + OH = #.7 OH + #.3 HO2 + #.3 CO + #.7 GLY + #.3 HCOOH	7.56E-13	5.20e-13	-1.95		1
			0: 5.50e-30	0.00	0.00	
			inf: 8.30e-13	0.00	2.00	
Revised Reactions of Acyl Peroxy Radicals with HO_2						
BR22	MECO3 + HO2 = #.44 {OH + MEO2 + CO2} + #.41 CCOOH + #.15 {O3 + CCOOH}	1.36e-11	5.20e-13	-1.95		2
BR32	RCO3 + HO2 = #.44 {OH + RO2C + xHO2 + xCCHO + yROOH + CO2} + #.41 RCOOH + #.15 {O3 + RCOOH}		Same k as rxn BR22			2
BR43	BZCO3 + HO2 = #.44 {OH + BZO + RO2C + CO2} + #.41 RCOOH + #.15 {O3 + RCOOH}		Same k as rxn BR22			2
BR55	MACO3 + HO2 = #.44 {OH + HCHO + MECO3 + CO2} + #.41 RCOOH + #.15 {O3 + RCOOH}		Same k as rxn BR22			2
Revised Glyoxal + OH and NO_3 Reactions						
BP32	GLY + OH = #.7 HO2 + #1.4 CO + #.3 HCOCO3	9.63e-12	3.10e-12	-0.68		3,4
BP33	GLY + NO3 = HNO3 + #.7 HO2 + #1.4 CO + #.3 HCOCO3	1.02e-15	2.80e-12	4.72		4
BP80	HCOCO3 + NO = HO2 + CO + CO2 + NO2		Same k as rxn BR31			4
BP81	HCOCO3 + NO2 = HO2 + CO + CO2 + NO3		Same k as rxn BR28			4
BP82	HCOCO3 + HO2 = #.44 {OH + HO2 + CO + CO2} + #.56 GLY + #.15 O3		Same k as rxn BR22			2,4
Revised Mechanisms for Uncharacterized Photoreactive Aromatic Ring-Opening Products						
BP47	AFG1 + O3 = (products)	(Removed from mechanism)				5
BP50	AFG2 + O3 = (products)	(Removed from mechanism)				5
Added Mechanisms for Monounsaturated Diketone Aromatic Ring-Opening Products						
PO50	xAFG4 =	k is variable parameter: RO2XRO				6
PO51	xAFG4 = AFG4	k is variable parameter: RO2RO				6
BP89	AFG4 + OH = #.902 RO2C + #.098 RO2XC + #.098 zRNO3 + #.902 xMECO3 + #.902 xRCHO + yROOH	6.30e-11				6
Revised and Added Mechanisms for Phenolic Compounds						
BP38	CRES + OH = #.7 HO2 + #.1 BZO + #.17 xHO2 + #.03 OH + #.17 RO2C + #.7 CATL + #.03 AFG3 + #.085 xAFG1 + #.085 xAFG2 + #.085 xGLY + #.085 xMGLY + #.17 yRAOOH	4.06e-11	1.60e-12	-1.93		7,8

Table 2 (continued)

Label [a]	Reaction and Products [b]	Rate Parameters [c] k(300)	A	Ea	B	Notes [d]
BP39	CRES + NO3 = #.1 HNO3 + #.9 XN + #.7 HO2 + #.1 BZO + #.17 xHO2 + #.03 OH + #.17 RO2C + #.7 CATL + #.03 AFG3 + #.085 xAFG1 + #.085 xAFG2 + #.085 xGLY + #.085 xMGLY + #.170 yRAOOH	1.40e-11				7,9
BP83	PHEN + OH = #.7 HO2 + #.1 BZO + #.095 xHO2 + #.105 OH + #.095 RO2C + #.7 CATL + #.105 AFG3 + #.048 xAFG1 + #.048 xAFG2 + #.095 xGLY + #.095 yRAOOH	2.74e-11	4.70e-13	-2.42		10,11
BP84	PHEN + NO3 = #.1 HNO3 + #.9 XN + #.7 HO2 + #.1 BZO + #.095 xHO2 + #.105 OH + #.095 RO2C + #.7 CATL + #.105 AFG3 + #.048 xAFG1 + #.048 xAFG2 + #.095 xGLY + #.095 yRAOOH	3.80e-12				10,12
BP85	XYNL + OH = #.7 HO2 + #.07 BZO + #.23 xHO2 + #.23 RO2C + #.7 CATL + #.115 xAFG1 + #.115 xAFG2 + #.115 xGLY + #.115 xMGLY + #.23 yRAOOH	7.38e-11				13,14
BP86	XYNL + NO3 = #.07 HNO3 + #.93 XN + #.7 HO2 + #.07 BZO + #.23 xHO2 + #.23 RO2C + #.7 CATL + #.115 xAFG1 + #.115 xAFG2 + #.115 xGLY + #.115 xMGLY + #.23 yRAOOH	3.06e-11				13,15
BP87	CATL + OH = #.4 HO2 + #.2 BZO + #.2 xHO2 + #.2 OH + #.2 RO2C + #.2 AFG3 + #.1 xAFG1 + #.1 xAFG2 + #.1 xGLY + #.1 xMGLY + #.33 CNDPP + #.2 yRAOOH	2.00e-10				16
BP88	CATL + NO3 = #.2 HNO3 + #.8 XN + #.4 HO2 + #.2 BZO + #.2 xHO2 + #.2 OH + #.2 RO2C + #.2 AFG3 + #.1 xAFG1 + #.1 xAFG2 + #.1 xGLY + #.1 xMGLY + #.2 yRAOOH	1.70e-10				17

[a] Underlined reaction label indicates that the reaction was added to the mechanism. If not underlined, it is the same label as used in the SAPRC-07 listing given by Carter (2010a).

[b] Format of reaction listing: "=" separates reactants from products; "*#number*" indicates stoichiometric coefficient, "*#coefficient* {*product list*}" means that the stoichiometric coefficient is applied to all the products listed.

[c] Except as indicated, the rate constants are given by $k(T) = A \cdot (T/300)^{B} \cdot e^{-Ea/RT}$, where the units of k and A are cm^3 $molec^{-1}$ s^{-1}, Ea are kcal mol^{-1}, T is ^oK, and R=0.0019872 kcal mol^{-1} deg^{-1}. The following special rate constant expressions are used:

Falloff: The rate constant as a function of temperature and pressure is calculated using $k(T,M) = \{k0(T)\cdot[M]/[1 + k0(T)\cdot[M]/kinf(T)]\}\cdot F^{Z}$, where $Z = \{1 + [\log10\{k0(T)\cdot[M])/kinf(T)\}/N]^2\}^{-1}$, [M] is the total pressure in molecules cm^{-3}, F and N are as indicated on the table, and the temperature dependences of k0 and kinf are as indicated on the table.

Table 2 (continued)

Phot Set = *name*: The absorption cross sections and (if applicable) quantum yields for the photolysis reaction are given by Carter (2010a), where "*name*" indicates the photolysis set used. If a "qy=*number*" notation is given, the number given is the overall quantum yield, which is assumed to be wavelength independent.

Same K as Rxn xx: Uses the same rate constant as the reaction in the base mechanism with the same label.

k is variable parameter: xxx: The rate constant for this reaction of this chemical operator species is given by the indicated variable parameter, which is computed from peroxy radicals and NO_x levels as given by Carter (2010a) and also in footnotes to Table A-2.

[d] Footnotes discussing the rate constants and mechanisms used are given below. Unless indicated otherwise, the rate constants used are the same as those used in SAPRC-07 for the indicated reaction (Carter, 2010a).

1 Temperature dependence corrected. From NASA (2006), but unchanged in NASA (2011). Change would have no effect on simulations at 300 K, and have very minor or negligible effects on chamber or ambient simulations at normal temperatures.

2 Product distribution revised to be consistent with the most recent IUPAC (2009) recommendations. Three pathways are assumed for the HO2 + acyl peroxy radical reaction: (1) 41% O2 + peroxy acetic acid; (2) 15% O3 + acetic acid; and (3) 44% OH + O2 + CH3C(O)O·. The peroxy acetic acid is represented by acetic acid and the CH3C(O)O· is assumed to rapidly decompose to CO2 and methyl radicals. The mechanisms for reactions of HO2 with the other peroxyacyl radical model species are assumed to be analogous.

3 Rate constant revised and temperature dependence added based on the most recent IUPAC (2008a) recommendation. This results in a ~10% decrease in the rate constant at 300K.

4 Mechanism revised to be consistent with the most recent IUPAC (2008a) recommendation. Both OH and NO_3 reactions are assumed to involve initial formation of HC(O)C(O)·. IUPAC (2008a) does not give explicit recommendation for branching ratios for the subsequent reactions of this radicals, but the rate constants given there imply ~40% decomposition to HCO and CO and ~60% reaction with O_2 forming 50% HCO + 2 CO and 50% HC(O)C(O)OO· under atmospheric conditions at ~300K. This corresponds to the reactions indicated if it is assumed the major fate of HCO is HO_2 + CO. HC(O)C(O)OO· is represented by the HCOCO3 model species. Unlike other acyl peroxy radicals, data discussed by IUPAC (2008a) indicates that it reacts with NO_2 to form NO_3 + HCO + CO_2, so it is not appropriate to lump it with acyl peroxy radicals that react to form PAN analogues. However, the rate constants for the HCOCO3 reactions are the same as those used for the lumped acyl peroxy radical RCO3, which are given by Carter (2010a) and also in Table A-2. The HC(O)C(O)OH and HC(O)C(O)OOH predicted to be formed in the HCOCO3 + HO2 reaction is represented by the GLY model species.

5 The reactions of AFG1 and AFG2 with O_3 were calculated to be of minor importance under chamber or atmospheric conditions of interest so these reactions were deleted from the mechanisms. The mechanisms and rate parameters for the reactions of these model species with OH radicals and by photolysis are unchanged.

6 The model species AFG4 is added to represent the reactions of monounsaturated 1,4-diketones, which are assumed to not to undergo photodecomposition to a significant extent, other than perhaps cis-trans isomerization (Calvert et al, 2002). These compounds were previously represented using AFG3, whose mechanism is based on those estimated for diunsaturated dicarbonyls. In this version of the mechanism they are treated separately because they are expected to form products of different reactivity. The only significant net loss process is assumed to be reaction with OH radicals, and its mechanism is estimated using the SAPRC-07 mechanism generation system, based on the structure for cis-3-hexene-2,5-dione. The rate constant is from

Table 2 (continued)

Tuazon et al (1985), as recommended by Calvert et al (2002). The model species xAFG4 is added to represent the formation of AFG4 following reactions of peroxy radicals with NO (Carter, 2010a,b).

7 The CRES model species is now used to represent only reactions of cresols formed from toluene and lumped phenolic products formed from the lumped phenoxy radical model species BZO, not all phenolic compounds. As with SAPRC-07, its mechanism is derived based on laboratory and chamber data for o-cresol.

8 Rate constant is IUPAC (2008b) recommendation for OH + o-cresol. Parameterized mechanism derived and adjusted to fit results of environmental chamber experiments with o-cresol as discussed in the text and in Table 7.

9 Rate constant is IUPAC (2008c) recommendation for NO_3 + o-cresol. Mechanism is based on the parameterized mechanism derived for the OH reaction, but with HNO_3 as an additional product.

10 The PHEN model species is used to represent phenol formed from benzene; CRES is no longer used for this purpose.

11 Rate constant is IUPAC (2008d) recommendation for OH + phenol. Parameterized mechanism derived and adjusted to fit results of environmental chamber experiments with phenol as discussed in the text and in Table 7.

12 Rate constant is IUPAC (2008g) recommendation for NO_3 + phenol. Mechanism is based on the parameterized mechanism derived for the OH reaction, but with HNO_3 as an additional product.

13 The XYNL model species is used to represent phenolic products formed from xylenes and all other C_{8+} aromatics, including ethylbenzene. Its mechanism is derived based on chamber and laboratory data for 2,4-dimethyl phenol, a phenolic product formed in the reactions of xylenes.

14 Rate constant is from Thüner et al (2004) for 2,4-dimethyl phenol. Parameterized mechanism derived and adjusted to fit results of environmental chamber experiments with 2,4-dimethyl phenol as discussed in the text and in Table 7.

15 Rate constant is from Thüner et al (2004) for 2,4-dimethyl phenol. Mechanism is based on the parameterized mechanism derived for the OH reaction, but with HNO_3 as an additional product.

16 The CATL model species is used to represent dihydroxy phenol products formed from the reactions of phenols. The rate constant used for the OH radical reaction is based on the IUPAC (2008e) for 1,2-dihydroxy-3-methyl benzene. Its mechanism is based roughly on the parameterized mechanisms derived for phenolic products as described in Table 7. The contribution of Pathway 1 is adjusted to approximately ~40%, to best simulate PM formation in the phenol, o-cresol, and 2,4-dimethyl phenol chamber experiments, since this is assumed to be the main SOA formation pathway from phenolic compounds in the SOA version of this mechanism (Carter et al, 2012). There is no information or useable chamber data to serve as a basis for deriving contributions of the other three pathways given in Table 7, so we arbitrarily assume that all are equally important.

17 The rate constant is based on the IUPAC (2008f) recommendation for 1,2-dihydroxy-3-methyl benzene. As with the other phenolic compounds, the mechanism is based on the parameterized mechanism used for the OH reaction, but with HNO_3 as an additional product.

mechanism using the generic lumped acyl peroxy radical species RCO3. However, the discussion in the updated IUPAC (2008a) evaluation implies that the decomposition of HC(O)C(O)· occurs approximately 40% of the time, and that its reaction with O_2 forms approximately equal amounts of HC(O)C(O)OO· and 2 CO + HO_2. Furthermore, they point out that the data of Orlando and Tyndall (2001) indicate that reaction of HC(O)C(O)OO· with NO_2 does not form a PAN analogue, but instead probably forms HCO + CO + $NO_{3,}$, presumably following the initial formation of HC(O)C(O)O· + NO_3. Based on this, we added a separate model species HCOCO3 to form this radical, and represented its reactions separately. The overall mechanism used for the OH reaction was as follows, with the mechanism for the NO_3 changed analogously:

GLY + OH = 0.7 {HO2 + 2 CO} + 0.3 HCOCO3
HCOCO3 + NO = HO2 + CO + CO2 + NO2
HCOCO3 + NO2 = HO2 + CO + CO2 + NO3
HCOCO3 + HO2 = #.44 {OH + HO2 + CO + CO2} + #.56 GLY + #.15 O3

The rate constant for the glyoxal + OH reaction was updated based on the IUPAC (2008a) recommendation, but the change in the room temperature rate constant was small. The rate constants for the HCOCO3 reactions were the same as used for the lumped acyl peroxy radical RCO3. The mechanism for the HO_2 reaction was derived by analogy with the acyl peroxy + HO_2 reactions as discussed above, with GLY being used to represent the dicarbonyl acids and peroxy acids formed.

This revised glyoxal mechanism results in significantly improved fits of model simulations to chamber experiments with acetylene, which forms glyoxal in high yields. The effect of this change on the general aromatics mechanisms could not be assessed because of the changes to the mechanisms to the reactions of the more reactive aromatic photooxidation products.

Mechanisms for Uncharacterized Aromatic Products. Significant revisions were also made to the portion of the base mechanism representing reactions of phenolic compounds, and the possibility of making revisions to the mechanisms of the uncharacterized photoreactive products was investigated. The affected model species are listed on Table 1 and their revised mechanisms are shown on Table 2. These are considered part of the aromatics mechanisms and therefore are discussed in the following section.

Revisions to the Aromatics Mechanisms

The discussion in this report will focus only on benzene and those alkylbenzene compounds for which environmental chamber are available to us for evaluating their atmospheric reaction mechanisms. These 14 compounds, which include all the C_7 - C_9 alkylbenzene isomers, are listed in Table 3, along with rate constants used for their primary reactions as discussed below. Although these are only a subset of the aromatic hydrocarbons represented separately in the detailed version of SAPRC-07, the mechanisms derived for most of these compounds serves as the basis for the estimated or extrapolated mechanisms for all the other alkylbenzene compounds represented in SAPRC-07. (There were no available mechanism evaluation data for the ethyl toluenes and propyl benzenes at the time SAPRC-07 was developed, so their mechanisms were estimated based on those derived for the xylenes or ethylbenzene. Because there are now data available for these compounds, their mechanisms can be derived separately for the updated mechanism.) SAPRC-07 also has representations for naphthalenes, tetralins, and other bicyclic or oxygenated aromatics, but the mechanisms for these compounds are beyond the scope of this report because there are no new mechanism evaluation chamber data available for these compounds.

The major atmospheric consumption process for aromatic hydrocarbons is reaction with the hydroxyl (OH) radical. The rate constants for the OH radical reactions with the aromatic compounds whose mechanisms were updated for this work are listed in Table 3. Table 3 also lists the rate constants

Table 3. Rate constants assigned for the reactions of OH radicals aromatic hydrocarbons whose mechanisms were updated for this work. The estimated rate constants for the addition of OH radicals to the aromatic ring are also shown.

Compound	Total kOH [a]				Ring Addition [b]		
	k(300)	A	Ea	Note [c]	k(300)	Fract.	Note [d]
Benzene	1.22e-12	2.33e-12	193	1	1.22e-12	100%	1
Toluene	5.58e-12	1.81e-12	-338	1	5.18e-12	93%	2
Ethyl benzene	6.50e-12	-	-	2	5.11e-12	79%	3
n-Propyl benzene	6.13e-12	-	-	3	3.31e-12	54%	3
Isopropyl benzene (cumene)	6.20e-12	-	-	4	5.11e-12	82%	3
o-Xylene	1.36e-11	-	-	1	1.29e-11	95%	4
m-Xylene	2.31e-11	2.31e-11	0	1	2.20e-11	95%	4
p-Xylene	1.43e-11	1.43e-11	0	1	1.29e-11	90%	4
1,2,3-Trimethyl benzene	3.27e-11	-	-	1	3.13e-11	96%	3
1,3,5-Trimethyl benzene	5.67e-11	-	-	1	5.48e-11	97%	4
1,2,4-Trimethyl benzene	3.25e-11	-	-	1	3.12e-11	96%	4
o-Ethyl toluene	1.19e-11	-	-	1	1.00e-11	84%	3
m-Ethyl toluene	1.86e-11	-	-	1	1.67e-11	90%	3
p-Ethyl toluene	1.18e-11	-	-	1	9.94e-12	84%	3

[a] Total rate constant for the reactions of the aromatic with OH radicals. Temperature dependence is given by A exp(-Ea/T), where T is the temperature in degrees K, and the units of k(300) (the rate constant at 300K) and A are cm^3 $molec^{-1}$ s^{-1}, and Ea is the activation energy in degrees K. The notes indicate the source of the rate constant used. A "-" in the activation energy (Ea) column means that there is no information in the reference cited about the temperature dependence of the rate constant, and a "0" in that column means that there are experimental data indicating that the temperature dependence is negligible.

[b] The estimated rate constant for the addition of OH radicals to the aromatic ring in cm^3 $molec^{-1}$ s^{-1} and the fraction reacted by addition in percent. The notes column indicates how this was estimated. The rate constants or fractions reacted by abstraction from the methyl or ethyl substituent are the differences between the total rate constant or fraction and the rate constant or fraction for addition to the aromatic ring.

[c] Sources for the total OH rate constants used are as follows:

1 As recommended or tabulated by Atkinson and Arey (2003). Same as used in SAPRC-07 (Carter, 2010a,b).

2 Average of 6.03×10^{-12} cm^3 $molec^{-1}$ s^{-1} (Ohta and Ohyama, 1985), 6.49×10^{-12} cm^3 $molec^{-1}$ s^{-1} (Lloyd et al., 1976; measured at ~305 K), 7.95×10^{-12} cm^3 $molec^{-1}$ s^{-1} (Ravishankara et al., 1978; measured at 200 torr He), 5.85×10^{-12} cm^3 $molec^{-1}$ s^{-1} (Anderson et al., 2003) and 6.2×10^{-12} cm^3 $molec^{-1}$ s^{-1} (Anderson et al., 2004).

3 Average of the rate constants reported by Ravishankara et al. (1978), $(6.4 \pm 0.36) \times 10^{-12}$ cm^3 $molec^{-1}$ s^{-1} at 20 torr He, $(5.86 \pm 0.16) \times 10^{-12}$ cm^3 $molec^{-1}$ s^{-1} at 200 torr He, This is very close to 6.14×10^{-12} cm^3 $molec^{-1}$ s^{-1} rate constant from Ohta and Ohyama (1985).

Table 3 (continued)

4 Average of 5.82 x 10^{-12} cm^3 $molec^{-1}$ s^{-1} (Ohta and Ohyama, 1985), 4.97 x 10^{-12} cm^3 $molec^{-1}$ s^{-1} (Lloyd et al., 1976) and 7.79 x 10^{-12} cm^3 $molec^{-1}$ s^{-1} (Ravishankara et al., 1978).

[d] Sources for estimates of rate constants for OH radical addition to the aromatic rings are as follows:

1 Reactions other than addition to the aromatic ring are assumed to be negligible.

2 Derived from the observed yields of benzaldehyde and benzyl nitrate, which are assumed to be the major products for the competing abstractions from the aromatic rings. The benzaldehyde yield used is given in Table 5 and the benzyl nitrate yields used is ~0.8%, based on data tabulated by Calvert et al (2002).

3 Estimated from the ratios of rate constants estimated for OH abstraction from the group off the ring relative to the total OH rate constant. The estimated rate constant for abstraction was derived using structure-activity relationship (SAR) techniques, using the parameters given on Table 4.

4 Derived from the ratio of addition to abstraction rate constants derived from the measured yield of the aromatic aldehyde expected to be formed following the abstraction reaction from the methyl groups, corrected for the estimated organic nitrate yields in the peroxy radical reactions as given in Table 9 of Carter (2010a).

Table 4. Group additivity parameters used to estimate rate constants for H-atom abstraction by OH radicals from alkyl groups on aromatic rings.

Group	Partial Rate Constant (cm^3 $molec^{-1}$ s^{-1})	Substituent Correction Factor	Note
CH_3	1.39e-13	1.00	[a]
CH_2	9.41e-13	1.23	[a]
CH	1.94e-12	1.23	[a]
CH_3(Bz)	4.75e-13	1.00	[b]
CH_2(Bz)	1.21e-12	1.23	[b]
CH(Bz)	7.47e-13	1.23	[b]

[a] These are for alkyl groups not adjacent to aromatic rings. Based on Kwok and Atkinson (1995). Parameters are the same as used for SAPRC-07 (Carter, 2010a).

[b] These are for alkyl groups attached to the aromatic ring. Average of values derived based on measured product yield data for toluene, the xylenes, and 1,2,4- and 1,3,5-trimethylbenzene as given on Table 5, and estimated organic nitrate yields from peroxy + NO reactions. The partial rate constants are somewhat different than used for SAPRC-07. The substituent correction factors were not changed, and are assumed to be the same as used for alkyl groups not bonded to aromatic ring.

for OH addition to the aromatic ring, which are based on measured product yields in the case of toluene, measured or estimated product yields in the case of the xylenes and 1,2,4- and 1,3,5-trimethylbenzene, and on structure-reactivity estimates using parameters given in Table 4 for the other compounds. Footnotes to the table give the sources for the rate constants that were used. Most of these rate constants are the same as used for these compounds in SAPRC-07, though the rate constants for ethyl benzene and the propyl benzenes have been updated based on a review of the more recent literature.

Except as discussed below, the basic structure and level of chemical detail for the updated aromatic mechanisms are the same as that used for SAPRC-07. Figure 2 shows a schematic of the major features of the SAPRC-07 aromatics mechanisms, with additional processes considered when developing this version of the mechanism shown in the dashed-line box. As discussed by Carter (2010a,b), the major reaction of aromatic hydrocarbons is reaction of OH radicals, either by OH abstracting from the alkyl group off the ring (if present) (pathway 1 on Figure 2), or by adding to the ring forming an OH-aromatic adduct (pathway 2). The reactions following abstractions involve formation of an organic nitrate following the reactions of the peroxy radical with NO (pathway 3) or formation of an alkoxy radical that ultimately reacts to form HO_2 and various abstraction products (pathway 4). If the abstraction is from a methyl group, the product formed would be an aromatic aldehyde represented by the BALD model species; otherwise the product is either a ketone (represented by the PROD2 species) or an aldehyde with the carbonyl away from the aromatic group (represented by RCHO), depending on the location of the abstraction. This portion of the mechanism is not considered to be particularly uncertain and is not discussed further here (see Carter, 2010a,b).

The most uncertain portion of the aromatics mechanism concerns the reactions following OH addition to the aromatic ring (pathway 2 on Figure 2). The OH-aromatic adduct is assumed to react with O_2 either by abstraction to form HO_2 and a phenolic compound (pathway 5), or by addition forming an OH-aromatic-O_2 adduct (pathway 6) that reacts further. The OH-aromatic-O_2 adduct is then assumed to undergo two competing unimolecular reactions, one (pathway 7) involving cyclization by O_2 addition to an internal double bond to form a bicyclic radical that then reacts with O_2 to form a bicyclic peroxy radical, which then reacts with NO either to form an organic nitrate (pathways 9) or the corresponding alkoxy radical (pathway 10) that decomposes to ultimately form HO_2, an α-dicarbonyl such as glyoxal (GLY), methylglyoxal (MGLY) or biacetyl (BACL), and a monounsaturated dicarbonyl co-product represented by AFG1, AFG2, and (for the updated mechanism) AFG4 model species as discussed below. These pathways and measured or estimated product yields are not sufficient to account for all the reaction routes, so it is necessary to assume that the OH-aromatic-O_2 adduct undergoes an additional unimolecular reaction, designated pathway 8 on Figure 2, competing with pathway 7. In SAPRC-07 pathway 8 is assumed to involve formation of OH and a di-unsaturated dicarbonyl product that is represented by the AFG3 model species. This assumption is retained in this version of the mechanism. Additional reactions, shown on Figure 2 as pathways A and B within the dashed-line box, are considered in various test calculations discussed below, but are not part of the final SAPRC-11 mechanism. This is almost certainly an oversimplification of the actual aromatic ring-opening mechanism and products formed (e.g., see Calvert et al, 2002), but given the current state of information and uncertainties in the mechanism this is considered appropriate for the level of detail and predictive capability of the current mechanism.

Figure 2 also shows the two pathways for formation of hydroperoxides from the reactions of peroxy radicals with HO_2 (pathways 1H and 2H). These pathways are not significant to predictions of O_3 formation and found not to be important in predictions of radical levels (unpublished results from this laboratory) and are not discussed further in this section. However, as discussed by Carter et al (2012), hydroperoxides formed from peroxy radicals formed following OH addition to the aromatic ring (pathway 2H) are believed to be important in predictions of aromatic SOA formation, and therefore need to be represented in the mechanism.

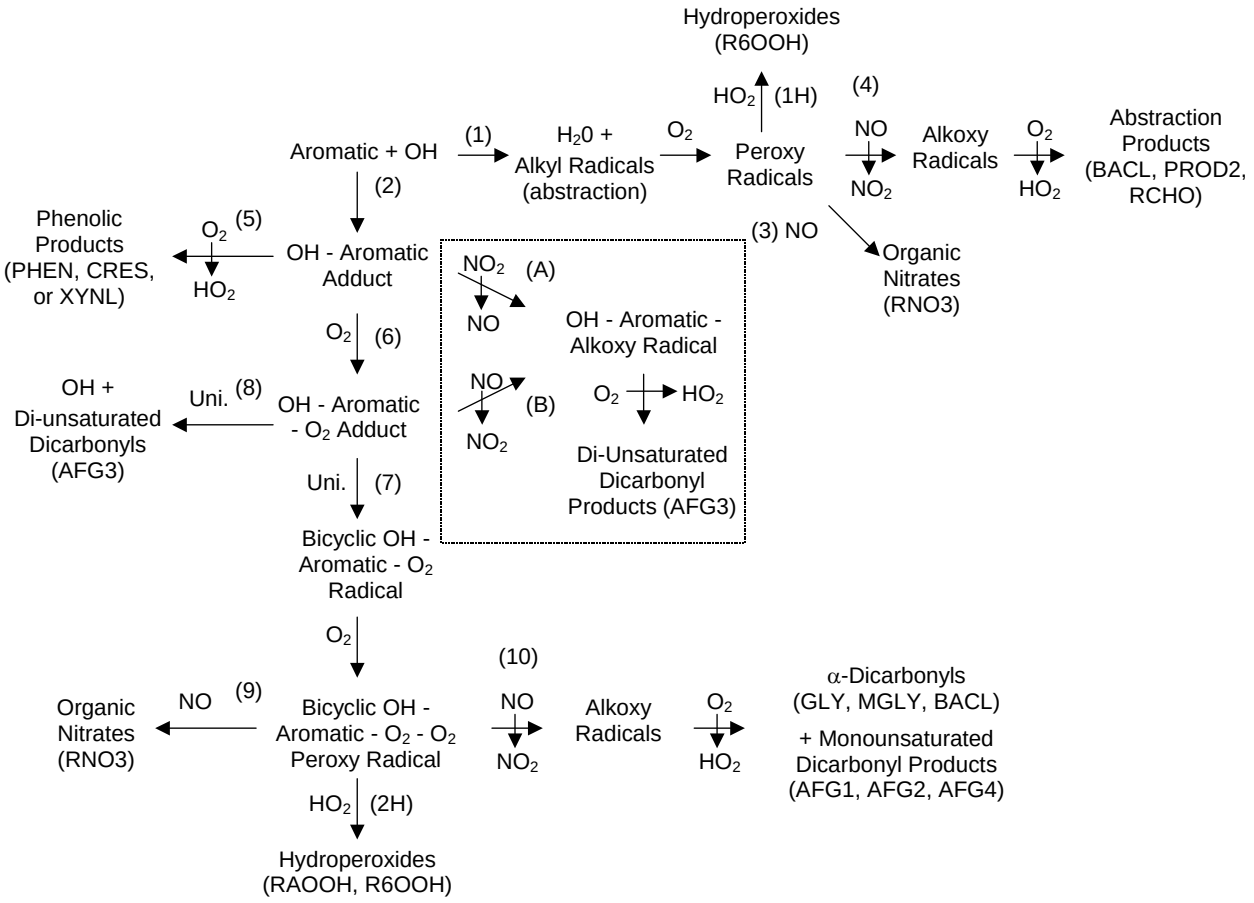

Figure 2. Schematic of major overall features of the initial reactions of alkylbenzenes in the presence of NO_x in the current SAPRC aromatics mechanisms. Processes not used in SAPRC-07 but considered for SAPRC-11 are shown in the dashed-line box. Model species used for reactive products are given in parentheses.

The yields of oxidation products that can be derived or estimated based on available measurement data and that are used in the current updated mechanism are summarized on Table 5, and the yields for the other pathways that had to be estimated are summarized on Table 6. The yields on Table 5 and Table 6 account for all the final pathways that occur in the presence of NO_x that are shown on Figure 2 outside the dotted line box. These include nitrate formation (pathways 3+9), formation of abstraction products (pathway 4), formation of phenolic products (pathway 5), formation of dicarbonyls and monounsaturated dicarbonyls (pathway 10), and formation of unknown products assumed to be diunsaturated dicarbonyls (pathway 8). The other pathways shown on Figure 2 outside the dotted line box refer to intermediate processes that give rise to these pathways that give the final products.

Footnotes to Table 5 and Table 6 indicate the sources of these yields and also indicates which are changed relative to SAPRC-07. The organic nitrate yields are derived based on the estimated or measured yields of the products formed from the competing alkoxy radical reaction and the estimated nitrate yields from the reaction of NO with the corresponding peroxy reaction as indicated in the footnotes to Table 6. The yields for the abstraction products (pathway 4) given in Table 5 are derived either from measurements of the predicted products or from estimates of the fraction of OH reaction that occurs via abstraction, reduced by the estimated relative organic nitrate yield (pathway 3). The yields for pathway 5

Table 5. Summary of yields of aromatic products that can be derived or estimated based on available product yield measurement data.

Compound	Yields and Notes [a]											
	Pathway 4: Products of Abstractions from Alkyl Groups [b]				Pathway 5: Phenolic products [c]		Pathway 10: Glyoxal (GLY)		Alkyl glyoxals (MGLY)		Biacetyl (BACL)	
	BALD	PROD2	RCHO	Note	Yield	Note	Yield	Note	Yield	Note	Yield	Note
Benzene					57%	1,9	31%	18				
Toluene	7%			1,2	18%	1,10	29%	19	25%	26		
Ethyl benzene		16%	2%	3	15%	11	25%	20	21%	20		
n-Propyl benzene		36%	2%	3	10%	11	17%	20	15%	20		
Isopropyl benzene		10%	5%	3	16%	11	26%	20	22%	20		
o-Xylene	5%			1,4	11%	12	13%	21	33%	21	19%	31
m-Xylene	4%			1,4	11%	13	11%	22	45%	27		
p-Xylene	8%			1,5	13%	14	37%	23	20%	28		
1,2,3-Trimethylbenzene	4%			6	3%	15	6%	24	17%	24	47%	32
1,3,5-Trimethylbenzene	3%			7	4%	16			61%	29		
1,2,4-Trimethylbenzene	3%			8	2%	17	8%	25	36%	30	11%	33
o-Ethyl toluene	3%	8%	1%	3	10%	1,11	12%	20	29%	20	17%	20
m-Ethyl toluene	2%	5%	1%	3	10%	1,11	10%	20	42%	20		
p-Ethyl toluene	3%	9%	1%	3	12%	1,11	35%	20	19%	20		

[a] Yields derived based on measurement data for the subject compounds are underlined, and notes indicating the sources of the yields used are given below. Yields that are not underlined are estimated as indicated in the notes. "Pathways" refer to pathways shown on Figure 2.

[b] Aromatic aldehydes such as benzaldehyde and tolualdehydes that are represented by the model species BALD; aromatic ketones such as methyl phenyl ketone that are represented by the model species PROD2, and aldehydes separated from the aromatic group such as phenyl acetaldehyde formed when OH abstracts from the methyl group in the ethyl or propyl benzenes. If more than one type of product can be formed the relative yields are estimated using structure-reactivity methods using the parameters given on Table 4.

[c] Phenol formed from benzene represented by PHEN, cresols formed from toluene represented by CRES, and all other phenolic products represented by XYNL.

Notes giving the sources of the data or estimates are as follows:

1 Unchanged from SAPRC-07

2 Benzaldehyde yields tabulated by Calvert et al (2002) range from 5-12%. Value used is average of data from studies published since 1989, which tend to be reasonably consistent as a group. Same as used by SAPRC-07.

Table 5 (continued)

3 Yields of products formed from abstraction from the methyl, ethyl or propyl groups derived from the estimated amount of non-ring abstraction calculated using the structure-reactivity parameters given on Table 4, corrected for the estimated nitrate yield. Abstraction from a -CH2- group is assumed to form an aromatic ketone represented by PROD2 and abstraction from a methyl group is assumed to form an aldehyde represented by RCHO. Abstraction from the -CH< group in isopropyl benzene is assumed to form methyl peroxy radicals + methyl phenyl ketone.

4 Most of the recent o-tolualdehyde or m-tolualdehyde yield data tabulated by Calvert et al (2002) are around 5%, and the value used is the average of those studies. A few studies indicate higher yields, but these are not used in computing the average.

5 Average of the various measurements tabulated by Calvert et al (2002). There is not particularly good agreement, but there are no obvious outliers to exclude from the average.

6 Derived from the estimated amount of non-ring abstraction, corrected for the estimated nitrate yield.

7 Based on the 3,5-dimethylbenzaldehyde yield from Smith et al (1999).

8 Sum of yields of 2,4-, 2,5-, and 3,4-dimethylbenzaldehyde from Smith et al (1999)

9 Average of values of Berndt and Böge (2006) (61%) and Volkamer et al (2002) (53%). The 51% yield reported by Noda et al. (2009) was not used in the average due to uncertainty implied by their reported high dealkylation branching ratio for m-xylene.

10 Total of yields for individual cresol isomers from Calvert et al (2002)

11 Estimated from the aromatic ring addition product yields from toluene (for monoalkylbenzenes) or the comparable xylene isomer (for methyl toluenes), after correction for estimated differences in fractions reacting at the aromatic ring and (for dicarbonyl products) for estimated differences in nitrate formation from peroxy + NO reactions.

12 The total dimethylphenol (DMP) yield of Atkinson et al (1991), 16.1%, calibrated by the ratio of the average of 13.8% (Bethel et al., 2000) and 13% (Smith et al., 1999) to 18.8%, the DMP yield reported by Aktinson et al. (1991), for p-xylene. This calibration resulted in reduction by 30% (i.e., reduction from 16% to 11%). Atkinson and Aschmann (1994) reported a yield of 2,3-dimethylphenol from o-xylene lower by ~40% than 9.7% reported by Atkinson et al. (1991).

13 The total dimethylphenol yield reported by Smith et al (1999) was used because Smith et al. (1999) used relatively low initial NOx compared to Atkinson et al. (1991). 21% reported by Atkinson et al. (1991) was not used.

14 Average of 2,5-dimethylphenol yields, 13% (Smith et al., 1999) and 13.8% (Bethel et al., 2000). 18.8% reported by Atkinson et al (1991) was not used.

15 No data available. The average of the assigned phenolic product yield for the other trimethylbenzenes is used.

16 Based on the 2,4,6-trimethylphenol yield from Smith et al (1999).

17 Sum of 2,4,5-, 2,3,5-, and 2,3,6-trimethylphenol from Smith et al (1999)

18 Average of values of Berndt and Boge (2006) and Volkamer et al (2002) (29% and 32%, respectively).

19 Average of 23.8% (Smith et al., 1998), 30.6% (Volkamer et al., 2001, 2005), 37% (Gómez-Alvarez et al., 2007) and 26% (Nishno et al., 2010) which were measured in experiments with relatively low NOx compared to 10.5% (Tuazon et al., 1986) and 15% (Bandow et al., 1985). 17%, a yield reported by Arey et al. (2009) was not used because Arey et al. (2009) did not independently measure the yields but did rely on product yields (e.g., for glyoxal, methylglyoxal and biacetyl) reported by other researchers for quantitative detection.

20 Estimated from the aromatic ring addition product yields from toluene (for monoalkylbenzenes) or the comparable xylene isomer (for ethyl toluenes), after correction for estimated differences in

Table 5 (continued)

fractions reacting at the aromatic ring and (for dicarbonyl products) for estimated differences in nitrate formation from peroxy + NO reactions.

21 The low-NOx limit data reported by Nishino et al. (2010) were used to avoid complexity caused by using high NOx during experiments.

22 Average of 13% (Bandow and Washida, 1985a), 7.9% (Smith et al., 1999) and 11.4% (Nishino et al., 2010). 8.6%, a yield reported by Tuazon et al (1986) was not used.

23 Average of 31.9% (Volkamer et al., 2001, 2005), 39.4% (Smith et al., 1999) and 38.9% (Nishino et al., 2010).

24 Yields reported by Bandow and Washida (1985b) and Nishino et al. (2010) are used because Nishino et al. (2010) reported that glyoxal and methylglyoxal formation yields were relatively independent of the NO_x level for 123-TMB. However, yields reported by Tuazon et al. (1986) were not used.

25 Yields reported by Bandow and Washida (1985b; 7.8%), Smith et al. (1999; 6.6%) and Nishino et al. (2010; 8.7%) are used because Nishino et al. (2010) reported that glyoxal and methylglyoxal formation yields relatively independent of the NOx level for 124-TMB. However, 4.8%, a yield reported by Tuazon et al. (1986) was not used.

26 Average of 16.7% (Smith et al., 1998), 37% (Gómez-Albrez et al., 2007) and 21.5% (Nishino et al., 2010) which were measured in experiments with relatively low NOx compared to 14.6% (Tuazon et al., 1986) and 14% (Bandow et al., 1985). 16%, a yield reported by Arey et al. (2009) was not used because Arey et al. (2009) did not independently measured but did rely on product yields (e.g., for glyoxal, methylglyoxal and biacetyl) reported by other researchers for quantitative detection.

27 Average of 42% (Bandow and Washida, 1985a), 40% (Smith et al., 1999) and 51.5% (Nishino et al., 2010). 31.9%, a yield reported by Tuazon et al (1986) was not used.

28 Average of 18.7% (Nishino et al., 2010) and 21.7% (Smith et al., 1999). 10.5% (Tuazon et al., 1986) and 12% (Bandow and Whashida, 1985a) were not used to exclude yields measured from experiments where relatively high NOx was used.

29 Average of 64% (Bandow and Washida, 1985b) and 58% (Nishino et al., 2010). Yields reported by Smith et al (1999) and Tuazon et al (1986) were not used.

30 Average of 37% (Bandow and Washida, 1985b), 44% (Smith et al., 1999) and 27.2% (Nishino et al., 2010). 35.7%, a yield reported by Tuazon et al (1986) was not used.

31 The low NO_x limit value of Atkinson and Aschmann (1994) is used. It is reasonably consistent with data from other studies at lower NOx levels tabulated by Calvert et al (2002).

32 Average of 45% (Bandow and Washida, 1985b), 44.4% (Atkinson and Aschmann, 1994) and 52% (Bethel et al., 2000). 31.6%, a yield reported by Tuazon et al (1986) was not used.

33 Average of 11% (Bandow and Washida, 1985b), 11.4% (Smith et al., 1999), and 10.2% (Bethel et al., 2000). 4.8%, a yield reported by Tuazon et al. (1986) was not used.

Table 6. Summary of yields of lumped model species used to represent other aromatics products used in the current updated aromatics mechanism.

Compound	Yields and Notes [a]								
	Paths 3+9: Total Organic Nitrates (RNO3)		Pathway 10: Photoreactive Ring-Opening Products (AFG1 + AFG2) [b]			Pathway 10: Unsaturated Diketones (AFG4) [c]		Pathway 8: Diunsaturated Dicarbonyyls (AFG3) [d]	
	Yield	Note	Yield	Rad. QY	Note	Yield	Note	Yield	Note
Benzene	3%	1	31%	59% [e]	3,4			9%	8
Toluene	7%	2	54%	60% [e]	3,4			14%	8
Ethyl benzene	10%	1	46%	40% [e]	3,4			10%	8
n-Propyl benzene	14%	1	31%	57%	3,4			6%	8
Isopropyl benzene	13%	1	48%	38%	3,4			9%	8
o-Xylene	11%	1	65%	45%	3,4			8%	8
m-Xylene	10%	1	56%	57%	3,4			19%	8
p-Xylene	11%	1	20%	89% [e]	4,5	37%	6	11%	8
1,2,3-Trimethylbenzene	15%	1	70%	40%	3,4			8%	8
1,3,5-Trimethylbenzene	13%	1	61%	39%	3,4			19%	8
1,2,4-Trimethylbenzene	12%	1	38%	48%	4,5	17%	7	28%	8
o-Ethyl toluene	14%	1	58%	55%	3,4			5%	8
m-Ethyl toluene	12%	1	53%	67%	3,4			16%	8
p-Ethyl toluene	13%	1	19%	100%	4,5	35%	6	8%	8

[a] "Pathways" refer to pathways shown on Figure 2. Notes, indicating the sources of the yields used, are given below.

[b] The model species AFG1 and AFG2 are used to represent monounsaturated dialdehydes or aldehyde ketones such as 2-butene-1,4-dial, which are assumed to be highly photoreactive. The mechanisms for AFG1 and AFG2 are the same except that AFG1 photolyzes to form radicals, while AFG2 photolyzes to form stable products. The "yield" column gives the total AFG1 + AFG2 yield and "Rad. QY" column gives the quantum yield for radical formation in the photolysis reaction, which is also the fraction of AFG1+AFG2 products that is AFG1 [i.e., the AFG1/(AFG1+AFG2) yield ratio.]

[c] The model species AFG4 is used to represent monounsaturated diketones, which are assumed not to be photoreactive. Such products can only be formed from aromatics with para substituents.

[d] This gives the yields used for Pathway 8 on Figure 2. The AFG3 model species is used to represent the uncharacterized aromatic products formed in this pathway, which are assumed to be primarily diunsaturated dicarbonyls.

[e] See Table 8 for the yields derived for the SAPRC-11A version of the mechanism..

Notes giving the sources of the yields used are as follows.

1 Estimated based on estimated total amounts of peroxy radical formation estimated to occur as discussed in the text and estimated nitrate yields in the reactions of the peroxy radicals with NO.

Table 6 (continued)

The latter are assumed to depend only on the carbon number of the aromatic compounds, and are estimated based on yields derived using the SAPRC mechanism generation system (Carter, 2010a) for secondary peroxy radicals formed from n-alkanes, multiplied by a factor of 0.81. The 0.81 factor is derived so the estimated nitrate yield for toluene is consistent with the yield ratios for benzyl nitrate and benzaldehyde from toluene as described in Note 2.

2 The nitrate yield per peroxy radical reaction with NO is based on the ratio of the average benzyl nitrate yield reported by Calvert et al (2002) to the benzaldehyde yield given on Table 5. The nitrate yields from the other C_7 peroxy radicals are assumed to be the same. The total nitrate yield is also determined by the total amount of peroxy radical formation estimated to occur as discussed in the text.

3 The total AFG1 + AFG2 yield is assumed to be the same as the sum of the yields given for the all α-dicarbonyl products given in Table 5.

4 The yield ratis for AFG1/(AFG1+AFG2) are adjusted based on model simulations of results of aromatic - NO_x chamber experiments as discussed in the Mechanism Evaluation section, below.

5 The total AFG1 + AFG2 + AFG4 yield is assumed to be the same as the sum of the yields given for the all α-dicarbonyl products given in Table 5. The AFG1 + AFG2 yield is derived from this and the yield assigned for AFG4.

6 The unsaturated diketone (AFG4) is assumed to be the co-product from glyoxal, so its yield is the same as given on Table 5 for glyoxal.

7 An unsaturated diketone is the only possible co-product with glyoxal, but an unsaturated diketone could also be a co-product from methyl glyoxal, which can have four other possible co-products. We assume that the total unsaturated diketone (AFG4) yield is equal to the yield for glyoxal + ¼ the yield of methyl glyoxal as given on Table 5.

8 The yield for this pathway is set at 100% - the sum of the estimated or measured yields for all the other pathways given on Table 5 and Table 6.

are based on measured or estimated yields of the corresponding phenolic products as given in Table 5. The yields for pathway 10 are based on measured α-dicarbonyl yields given on Table 5, which serve as the basis for the total yields of their assumed co-products as given on Table 6. The measured or estimated yields for these pathways are not sufficient to account for 100% of the reaction of the aromatic with OH radicals, so pathway 9, assumed to be formation of OH and a diunsaturated dicarbonyl, to account for the remaining, unknown, reaction pathway(s).

Representation of Reactions of Uncharacterized Aromatics Products

Photoreactive Products. In order for aromatic mechanisms to adequately simulate rates of NO oxidation and O_3 formation in chamber experiments, it must be assumed that additional highly photoreactive products are formed besides the observed photoreactive α-dicarbonyls. Based on available data discussed by Calvert et al (2002), it is assumed that the additional photoreactive products are the monounsatured dialdehydes or aldehyde-ketones formed as co-products to the α-dicarbonyls in pathway (10) on Figure 2. These photoreactive products are represented in SAPRC-07 and the updated mechanism by the model species AFG1 and AFG2 as discussed below. However, the monounsaturated diketones that can be formed from para- or 1,4-disubstuted aromatics are not believed to photolyze to form radicals at a significant rate (Calvert et al, 2002), so in SAPRC-07 these are also represented in AFG3, though in the updated mechanism a separate, also non-photoreactive, model species AFG4 is used for this purpose. In addition, the diunsaturated dicarbonyls formed in pathway (8) are believed not to be as photoreactive and

thus the model species AFG3 used to represent them in both SAPRC-07 and the updated mechanism does not photolyze.

In order for the model to fit the chamber data, it is necessary to treat either the yields or the radical-forming photolysis rates of the uncharacterized photoreactive products (i.e., the model species used to represent the monounsatured dialdehydes or aldehyde-ketones) as adjustable parameters for each aromatic compound for which there are chamber data (Carter, 1990, 2000a 2010a,b). Since the yields of these products are determined by the known (or independently estimated) α-dicarbonyl yields, only the radical-forming photolysis rates can be treated as adjustable parameters in the mechanism as currently formulated. In SAPRC-07 this is done by representing these compounds using two model species, AFG1 and AFG2, that react in the same way except that AFG1 photolyzes to form radical products and AFG2 photolyzes to form stable products, both with unit quantum yields. The AFG1/(AFG1+AFG2) yield ratio can then be adjusted for each aromatic compound to represent varying quantum yields for photolysis to form radical products, without having to have separate model species for each compound. Their mechanisms are based on those for the representative monounsaturated dicarbonyls 2-butene 1,4-dial (10%), 2-methyl-2-butene-1,4-dial (21%), 4-oxo-2-pentenal (37%), and 2-methyl-4-oxo-2-pentenal (32%), with the weighting factors based on estimated yields of these or similar compounds from toluene and the di- and tri-methylbenzene isomers, each weighed equally (Carter, 2010a). The AFG1/(AFG1+AFG2) yield ratio is used to represent the quantum yield for radical formation for the products formed from each individual compound, and adjusted or estimated separately for each compound based on chamber data or adjusted values for similar compounds. This approach is retained for SAPRC-11.

As discussed in the mechanism evaluation section, below, the SAPRC aromatic mechanisms have a consistent bias towards underpredicting OH radical levels in the aromatic - NO_x experiments, but increasing radical initiation processes in the ring fragmentation to fit the OH levels results in overpredictions of NO oxidation and O_3 formation rates. An analysis of initiation and termination processes during the periods where OH becomes underpredicted, indicate that formation of PAN analogues in the reactions of the model species representing these fragmentation products is the major radical termination process during the period when OH radicals are underpredicted, and somewhat better simulations of OH radical levels in models adjusted to fit NO oxidation and O_3 formation rates can be obtained if the yields of PAN analogues in the reactions of these products are reduced. Therefore, as part of this mechanism update project we investigated whether revising the AFG1 and AFG2 mechanisms to reduce the formation of PAN analogues would improve this bias towards underpredicting OH radical levels.

The main source of PAN analogues in the SAPRC-07 representation of the reactions of the photoreactive ring fragmentation products comes from assuming the following reactions occur following H abstraction from the aldehyde groups, as shown for example in the 2-butene 1,4-dial system:

$$OH + HC(O)CH=CHCHO \rightarrow H_2O + HC(O)CH=CHC(O)\cdot$$
$$HC(O)CH=CHC(O)\cdot + O_2 \rightarrow HC(O)CH=CH\text{-}C(O)OO\cdot$$
$$HC(O)CH=CH\text{-}C(O)OO\cdot + NO_2 \rightarrow HC(O)CH=CH\text{-}C(O)OONO_2$$

The model species MACO3 and MAPAN are used in the mechanism to represent the reactions of the acyl peroxy radicals and PAN analogues formed in these reactions. These species are also assumed to be formed in the photolysis reactions, following C(O)..H bond scission. Although there is no direct evidence for the formation of these PAN analogues in these systems, the available product laboratory and chamber data are insufficient to rule out its formation. However, this mechanism is inconsistent with the data of Bierbach et al (1994), who found that maleic anhydride is formed in ~50% yields in the reaction of OH radicals with 2-butene-1,4-dial. This inconsistency can be eliminated, and formation of PAN analogues in the AFG reactions will be reduced, if it is assumed that instead of reacting with O_2 forming the acyl

peroxy radical as shown above, it undergoes a cyclization reaction that should ultimately give rise to maleic anhydride:

$$HC(O)CH=CHC(O)\cdot \rightarrow \underline{\text{┌OCH(·)CH=CHC(O)┐}}$$
$$\underline{\text{┌OCH(·)CH=CHC(O)┐}} + O_2 \rightarrow \underline{\text{┌OCH(OO·)CH=CHC(O)┐}}$$
$$\underline{\text{┌OCH(OO·)CH=CHC(O)┐}} + NO \rightarrow NO_2 + \underline{\text{┌OCH(O·)CH=CHC(O)┐}}$$
$$\underline{\text{┌OCH(O·)CH=CHC(O)┐}} + O_2 \rightarrow HO_2 + \underline{\text{┌OC(O)CH=CHC(O)┐}} \text{ (maleic anhydride)}$$

The fact that the maleic anhydride yield is less than 100% is not inconsistent with this cyclization mechanism dominating because some of the reaction of OH with the 2-butene-1,4-dial proceeds via addition to the double bond, giving rise to other products. The SAPRC-07 mechanism estimation/generation system predicts that ~56% of the OH reaction proceeds via H-abstraction from HCO forming the species shown above, which is reasonably consistent with the observed maleic anhydride yields if the cyclization reaction dominates over acyl peroxy radical formation.

The products formed in the photolysis of the model species representing the photoreactive ring fragmentation products are actually more important than those formed in the OH reaction because rapid photolysis is the major fate of these model species. The radical-forming photolysis mechanisms in SAPRC-07 are derived from the mechanism estimation system assuming that photolysis involves breaking the =CH--CHO and the =CHC(O)--H with approximately equal probability. This is almost certainly an oversimplification of the actual mechanism but available information on the product yields are not sufficient to derive an adequate alternative mechanism that explains the significant tendency of these reactions to form radicals when they photolyze (Calvert et al, 2002). The latter process was previously assumed to form acyl peroxy radicals and PAN analogues, but as discussed above it is probably more reasonable to assume it forms maleic anhydride. In addition, it is probably not reasonable to assume that scission of =CH--CHO bonds are important photodecomposition products of unsaturated 1,4-dicarbonyls because if it were then one would expect the $=CH--C(O)CH_3$ scission to be equally important in the photolysis of unsaturated 1,4-diketones, but these compounds in fact do not appear to undergo photodecomposition to a significant extent (Calvert et al, 2002).

Based on these considerations, we re-derived the representation of the monounsaturated dialdehyde or aldehyde-ketone ring-opening reactions assuming that the cyclization reaction forming maleic anhydride and analogous compounds is the main process for radicals such as HC(O)CH=CHC(O)·, and also that the photolysis forming radicals only involves scission of CO..H bonds. The latter assumption is also almost certainly an oversimplification, but at least it is consistent with the observation that an aldehyde group must be present in these 1,4-dicarbonyls for the compounds to be highly photoreactive. In terms of SAPRC-07 (and SAPRC-11) model species, the resulting mechanisms for the reactions of AFG1 and AFG2 with OH radicals, and for the photolysis of AFG1 forming radicals, are as follows:

AFG1 or AFG2 + OH → 0.927 RO2C + 0.073 RO2XC + 0.073 zRNO3 + 0.756 xHO2 + 0.026 xMEO2 + 0.146 xMECO3 + 0.336 xCO + 0.353 xRCHO + 0.129 xMEK + 0.153 xGLY + 0.313 xMGLY + 0.212 xMEK + yR6OOH

AFG1 + HV → HO2 + 0.927 RO2C + 0.073 RO2XC + 0.073 zRNO3 + 0.454 xHO2 + 0.473 xMEO2 + 0.927 xMEK + yR6OOH

The mechanism for the photolysis of AFG2, forming non-radical compounds represented by the model species PROD2, was not changed. Note that the SAPRC-07 model species MEK is used to represent maleic anhydride based on considerations of its reactivity.

These revised AFG1 and AFG2 mechanisms were incorporated in a preliminary version of SAPRC-11, and the AFG1/(AFG1+AFG2) yield ratio were optimized for each compounds based on the

simulations of the chamber data using the procedures discussed in the "Mechanism Evaluation" section, below. However, this modified mechanism did not significantly improve the simulations of the integrated OH radical levels and resulted in a non-negligible degradation in the model performance in simulating final O_3 yields compared to the alternative version of SAPRC-11 where the mechanisms for the reactions of AFG1 and AFG2 with OH radicals and by photolysis were kept the same as in SAPRC-07. This is shown in Figure 3, which gives plots of model errors for maximum O_3 yields against initial NO_x concentrations for the two versions of SAPRC-11 in simulating the toluene - NO_x and the m-xylene - NO_x chamber experiments. Note that the maximum O_3 yield is the final O_3 yield in experiments where a "true" O_3 maximum was obtained, i.e., experiments where the final O_3 concentration is not affected by the NO oxidation and O_3 formation rate. Note also that the adjustments of the AFG1/(AFG2+AFG2) were based on fits to the NO oxidation and O_3 formation rates, so the predictions of the maximum O_3 yields provide an independent test of the mechanisms. (See the "Methods" subsection of the "Mechanism Evaluation" section for the definitions of "maximum O_3 yield" and "model error" used and the optimization methods employed.)

Figure 3 shows that the version of the mechanism that was revised as discussed above had a non-negligibly greater tendency to overpredict maximum O_3 yields than the version where the AFG mechanisms are unchanged. A similarly increased tendency to overpredict maximum O_3 is seen for most of the other compounds, but because of the smaller number of experiments and the run-to-run variability in model performance it is less clear whether the difference is statistically significant than is the case for toluene and m-xylene. Because of this, the revisions to the AFG1 and AFG2 mechanisms discussed above were not adopted.

The SAPRC-07 mechanism also has the AFG1 and AFG2 species reacting with O_3. However, an analysis of reaction rates in simulations of representative chamber experiments and atmospheric conditions indicated that the rate of reaction of these model species with O_3 was negligible compared to

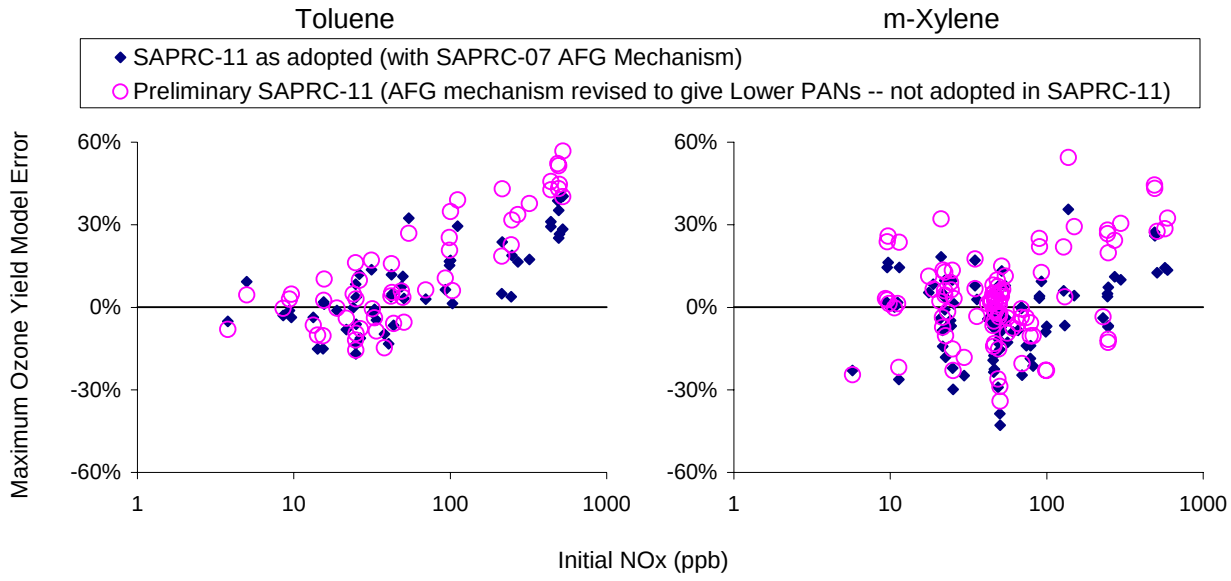

Figure 3. Plots of model errors in simulations of maximum O_3 yields in the toluene and m-xylene - NO_x experiments using versions of the SAPRC-11 mechanism with different treatments of the AFG1 and AFG2 mechanisms.

photolysis and OH radical reaction. Therefore, the O_3 reactions were deleted in the updated mechanism. As shown on Table 2, this is the only revision made to the AFG1 and AFG2 mechanisms.

Non-Photoreactive Products. The model species AFG3 is used to represent the reactions of uncharacterized non-photoreactive ring fragmentation products, which are assumed to be primarily diunsaturated dicarbonyls. In SAPRC-07 AFG3 is also used for monounsaturated 1,4-diketones predicted to be formed from the reactions of alkylbenzenes with substituents in the para position, but in the updated mechanism a separate model species, AFG4, is used for this purpose. Both of these types of compounds are assumed to be relatively unreactive with respect to photolysis, and thus are represented separate model species from AFG1 and AFG2 discussed above. The mechanism for AFG3 is based on those estimated for the representative diunsaturated dicarbonyl products 3-methyl 2,4-hexadien-1,6-dial (40.5%), 6-oxo-2,4-heptadienal (53.7%), and 3,5-octadien-2,7-dione (5.8%).[2] The weighting factors used are based on estimated diunsaturated dicarbonyls for toluene and the di- and tri-methylbenzene isomers, each weighed equally, with 2,4-hexadien-1,6-dial representing all dialdehydes, 6-oxo-2,4-heptadienal representing aldehyde-ketones, and 3,5-octadien-2,7-dione representing the diketones. The estimated mechanisms for monounsaturated diketones were not taken into account because they are not predicted to be formed from the majority of aromatics. The AFG3 mechanism was not revised for this update, though it is included in Table 2 for completeness.

Since the monounsaturated diketones are expected to have different mechanisms and form different products than the diunsaturated species used to derive the mechanism for AFG3, for this version of the mechanism a separate model species, AFG4, was added to represent only the monounsaturated 1,4-diketones. The mechanism for AFG3 was not revised because it was based on neglecting the contributions of these monounsaturated diketone compounds. The only significant net loss process for these AFG4 compounds is assumed to be reaction with OH radicals, and its mechanism was estimated using the SAPRC-07 mechanism generation system, based on the structure for cis-3-hexene-2,5-dione. The rate constant is from Tuazon et al (1985), as recommended by Calvert et al (2002). The model species xAFG4 is added to represent the formation of AFG4 following reactions of peroxy radicals with NO (Carter, 2010a,b), and the model species xAFG3 is removed because the diunsaturated dicarbonyls are not assumed to be formed following peroxy radical reactions.

Revised Mechanisms for Phenolic Compounds

Because of their importance for aromatic SOA formation as discussed by Carter et al (2012), an effort was made in this project to improve the representation of phenolic products such as phenols, cresols (methyl phenols), xylenols (dimethyl phenols), and catechols (dihydroxy benzenes). In SAPRC-07 the model species CRES is used to represent all these compounds, and a parameterized mechanism was developed based on environmental chamber model simulations of a single, relatively high concentration (~0.5 ppm NO_x) o-cresol - NO_x chamber experiment carried out in 1978 in the SAPRC evacuable chamber (EC281). Because of their expected importance for SOA formation, for this project a number of new chamber experiments have been carried out with cresols and other representative phenolic compounds, and the results are poorly simulated by the SAPRC-07 mechanism that was adjusted to fit the data for EC281. Therefore, revised mechanisms for phenolic compounds were developed for this work.

The first revision was that separate model species are used to represent reactions of phenol (PHEN), cresols (CRES), xylenols and other higher molecular weight alkyl phenols (XYNL), and catechols (CATL) predicted to be formed in the reactions of the phenolic products. These are represented

[2] Note that the documentation given in Carter (2010a,b) had incorrect contribution factors that exceeded 100%. The factors given here are those that were actually used, which correctly add to 100%.

separately primarily because they are expected to have different SOA formation potentials (see Carter et al, 2012), but they are also expected to have somewhat different ozone formation potentials as well. Parameterized and simplified mechanisms are still used to represent the reactions of these species, but the parameterization approach was updated for improved SOA and gas-phase predictions, and the mechanisms were adjusted to simulate a much more comprehensive set of environmental chamber experiments than was available at the time SAPRC-07 was developed.

The pathways that were used in the parameterized mechanisms to represent the reactions of phenolic compounds are listed and discussed in Table 7. As discussed in the table, the relative contributions of the four pathways used for the PHEN, CRES, and XYNL model species were derived based on consideration of the available product data for representative phenolic compounds, and adjustments to optimize model simulations to results of phenol (for PHEN), o-cresol (for CRES) and 2,4-dimethyl phenol (for XYNL) environmental chamber experiments.

The phenolic compounds are consumed both by reactions with OH and NO_3 radicals. Although the mechanisms and products formed from these reactions are probably different, the data are insufficient to derive separate mechanisms for both processes. Therefore, for simplicity and to avoid the use of more uncertain and adjustable parameters than the data can support, we assume that the mechanisms for the OH and NO_3 reactions are similar, except that the NO_3 reaction also results in the formation of either HNO_3 for reactions assumed to involve abstraction, or loss of reactive nitrogen (represented by formation of the XN model species) for the other processes. This is also shown on Table 7. This is almost certainly an oversimplification.

The catechol model species, CATL, is added to the mechanism because catechols are observed to be formed in relatively high yields in the reactions of OH radicals with phenolic compounds, and their subsequent reactions are believed to be important in contributing to SOA formation from aromatics (Carter et al, 2012). The pathways used in the parameterized mechanism for this model species are also summarized in Table 7. As indicated there, they are based on those used for the phenolic model species except that the process representing catechol formation is replaced by condensable product formation (e.g., formation of CNDCA instead of CATL as shown in Table 7 for Pathway 1), and the contribution of this process is adjusted to optimize model simulation of SOA levels in experiments with phenolic compounds as discussed by Carter et al (2012). The relative contributions of the other processes are unknown, and they are arbitrarily assumed to be equal.

Mechanism with Additional NO_x Dependence of Aromatic Reactivity (SAPRC-11A)

The simplest way to update SAPRC-07 to improve the fits to the newer chamber data is to re-adjust the AFG1/(AFG1+AFG2) yield ratios to give better fits to the available data. As discussed in the "Mechanism Evaluation" section, below, this was found to be sufficient for the xylenes and the other di- and tri-substituted aromatics, but does not account for the apparent dependence of model error on total NO_x levels for benzene, toluene, ethylbenzene, and p-xylene. Since SAPRC-07 tends to underpredict NO oxidation and O_3 formation for the newer experiments with NO_x levels less than about 100 ppb but gives reasonably good fits to or overpredicts these data in the earlier, higher NO_x, experiments, this suggests that there must be some other process, that SAPRC-07 and SAPRC-11 are missing, that accounts for increasing NO_x causing decreased reactivities for these compounds. Therefore, we investigated possible modifications to the mechanism to include additional NO_x - dependent processes that might allow the chamber data to be simulated at both high and low NO_x levels.

Possible processes that could account for this apparent NO_x dependence of aromatic reactivity are shown as pathways (A) and (B) on Figure 2. In both cases, if the NO_x reaction is assumed result in formation of a non-photoreactive diunsaturated dicarbonyl product, in competition with the formation of

Table 7. Pathways used to in the parameterized mechanisms used to represent the reactions of OH and NO_3 radicals with phenolic compounds and catechols

No.	Reaction Product Model Species	Discussion	Yields Used
1	OH: CATL + HO2 (for phenols) or HO2 + unreactive species (for CATL) NO_3: Same as above, except + XN (loss of reactive nitrogen)	This pathway is assumed to occur ~70% of the time for phenolic compounds, based on dihydroxybenzene yields reported by Olariu et al (2002) for phenol and cresol isomers. For catechols, the formation of the catechol model species as the product is replaced by an unreactive condensable catechol product model species whose yield in the OH reaction is adjusted to give best fits to SOA formation in chamber experiments with phenol, o-cresol, and 2,4-dimethyl phenol, as discussed by Carter et al (2012).	PHEN 70% CRES 70% XYNL 70% CATL 40%
2	OH: BZO NO_3: BZO + HNO3	Represents various pathways that result in the formation of nitrophenols. This pathway is assumed to occur about 10% of the time for phenolic compounds, based roughly on measured nitrophenol yield data given by Berndt and Böge (2003) for phenol and Olariu et al (2002) for cresols. It is reduced to 7% for XYNL because the yield of Pathway 3 required to fit the data for 2,4-dimethylphenol would otherwise make the total for all pathways exceed 100%. No useful information is available for the appropriate yield of this pathway for the catechols, so we arbitrarily assume that pathways 2-4 are equally important, so 20% is assumed to give a total of 100% for all pathways.	PHEN 10% CRES 10% XYNL 7% CATL 20%
3	OH: xHO2 + RO2C + xGLYs + xAFGs + yRAOOH NO_3: Same as above, except + XN (loss of reactive nitrogen)	Represents ring-opening reactions forming highly photoreactive products. xGLYs is xGLY for phenol and 0.5 {xGLY + xMGLY} for the other phenolics and catechols, and xAFGs is arbitrarily represented by xAFG1 + xAFG2, i.e., assuming a 50% quantum yield for radical forming products. For the phenolic compounds the contributions were adjusted to simulate rates of NO oxidation and O_3 formation in phenol - NO_x, o-cresol - NO_x , and 2,4-dimethyl phenol - NO_x experiments for PHEN, CRES, and XYNL, respectively. For CATL the same yield is used as discussed above for Pathway 2.	PHEN 9.5% CRES 17% XYNL 23% CATL 20%
4	OH: OH + AFG3 NO_3: Same as above, except + XN (loss of reactive nitrogen)	Represents all other ring-opening routes and is analogous to the di-unsaturated dicarbonyl-forming route used in the general aromatic hydrocarbon mechanism. Contributions were adjusted to yield 100% for all the routes, so they depend on the contributions assigned for the other routes as discussed above.	PHEN 9% CRES 3% XYNL 0% CATL 20%

the photoreactive α-dicarbonyls and monounsaturated dicarbonyls formed in pathway (10), then this may account for lower reactivity at higher NO_x levels. There are laboratory and product data indicating that these NO_x-dependent pathways indeed occur, but at rates too low to be significant at atmospheric NO_x levels or even the NO_x levels used in the environmental chamber experiments used for mechanism evaluation. Available kinetic and mechanistic data indicate that the reactions of the aromatic-OH adduct with NO_2 (pathway A on Figure 2) becomes competitive with the reaction of the adduct with O_2 (pathways 5 and 6) only with NO_2 concentrations greater than about 1 ppm for benzene (Koch et al, 2007) or ~3 ppm for toluene or ~5 ppm higher for xylenes (Nishino et al, 2010 and references therein). Available data also indicate that the reaction of the aromatic-OH-O_2 adduct with NO (pathway B) becomes competitive with unimolecular reactions of this adduct (processes 7 and 8) only at NO concentrations greater than about 2 ppm for benzene and 5 ppm for toluene (Nishino et al, 2010; Bohn and Zetzch, 1999; Klotz et al, 2002). These NO and NO_2 levels are not only considerably higher than currently occur even in polluted urban atmospheres, but also higher than occur in most of the chamber experiments used for evaluating the SAPRC aromatics mechanisms.

Nevertheless, in order to investigate whether the model can simulate the dependence of reactivities observed in environmental chamber experiments with benzene and toluene, we developed a version of the mechanism, designated SAPRC-11A, where Pathway A was assumed to occur at non-negligible rates for compounds that appeared to have lower reactivity at higher NO_x levels. The rate constant for the reaction of NO_2 with the OH-aromatic adduct was assumed to be 3.6×10^{-11} cm^3 $molec^{-1}$ s^{-1}, based on the rate constant used by Koch et al (2007) for this reaction in the toluene system. The total rate constants for the competing reactions with O_2 (pathways 5+6) was treated as an adjustable parameter to minimize the NO_x-dependence on the model error in simulating the aromatic - NO_x chamber experiments as discussed in the "Mechanism Evaluation" section, below. Table 8 gives the best fit parameter values that best fit the chamber data for the four compounds where this additional pathway was necessary in order to simulate the data over the full range of NO_x levels. As indicated on the table, the adduct + O_2 rate constants that fit the data were much smaller than indicated by the laboratory data of Koch et al. (2007) or Nishino et al. (2010) and references therein for all four of these compounds. For that reason, this version of the mechanism is only used for the sensitivity calculations and is not incorporated in the final mechanism developed for this project.

We also investigated the reaction of NO with the OH-aromatic-O_2 adduct (pathway B on Figure 2) competing with the unimolecular reactions of this adduct (pathways 7 and 8) as the source of this apparent additional NO_x dependence. This is considered to be less likely than pathway A being the source

Table 8. Adjusted mechanism parameters used in the SAPRC-11A mechanism with an additional NO_x dependence on aromatic product reactivity.

Compound	O_2 + OH-Aromatic Rate Constant		AFG1 + AFG2 Quantum Yield	
	(cm^3 $molec^{-1}$ s^{-1})	[NO_2] such that k[NO_2]=k[O_2]	SAPRC-11A	SAPRC-11 (from Table 6)
Benzene	3.44×10^{-18}	20 ppb	67%	59%
Toluene	3.44×10^{-17}	0.2 ppm	58%	60%
Ethyl benzene	8.60×10^{-18}	50 ppb	48%	40%
p-Xylene	5.16×10^{-18}	30 ppb	100%	89%

of the dependence because the product yield data referenced above indicate that higher NO_x levels are required for this to be important than is the case for pathway A. The results of test calculations using Pathway B with adjustable competing unimolecular reaction rates gave were similar to those using pathway A as discussed above, and are therefore not presented here.

MECHANISM EVALUATION

Methods

Chamber Experiments Used

The updated aromatics mechanisms were developed and evaluated by conducting model simulations of results of 410 aromatic - NO_x environmental chamber experiments carried out in 9 different environmental chambers at three different laboratories using five different types of light sources. The experiments used are summarized in Table B-1 in Appendix B, and the environmental chambers whose data were used are summarized in Table 9. The chambers listed in Table 9 are a subset of those used by Carter (2010a,b) to develop and evaluate the SAPRC-07 mechanism, except that for this work we also used new data from the CSIRO indoor chamber (Hynes et al, 2005; White et al, 2010; Azzi et al, 2010) that were not available to us when SAPRC-07 was developed. Approximately half, or 217, of the experiments used in this work were also used for SAPRC-07 development and evaluation, with the remaining 221 experiments being new experiments that were used for this work. Of these, 25 were CSIRO experiments, and the remaining 196 were new aromatics - NO_x experiments carried out in the UCR EPA chamber, mostly using the blacklight light source. Most of these experiments were carried out for the purpose of studying SOA formation from aromatics, but the data are sufficiently well characterized that they are suitable for gas-phase mechanism evaluation as well.

More significantly from the perspective of this report, the new experiments consisted of data for a number of aromatic compounds for which suitable mechanism evaluation data were not available, or were only available at relatively high reactant concentrations. New compounds for which mechanism evaluation data are now available include all the ethyltoluene and propylbenzene isomers, phenol, 2,4-dimethylphenol, and, and a more complete dataset is available for o-cresol. Thus mechanism evaluation data are now available for all C_6-C_9 alkylbenzene isomers and at representative C_6-C_8 phenolic products. This allowed adjusted mechanisms to be developed for all these 17 aromatic compounds.

Because of difficulties and uncertainties in characterizing conditions in outdoor chamber experiments with natural sunlight, all experiments used for mechanism evaluation in this report are indoor chamber experiments utilizing artificial light sources. As indicated on Table 9 and Table B-1, mechanism evaluation data are available from chambers with a variety of light sources. Representative relative spectral distributions of these light sources are shown on the two top plots on Figure 4, with a representative solar spectrum shown for comparison. The bottom plot shows action spectra or absorption cross sections for representative photolysis reactions or photoreactive species, indicating the wavelength regions that are important for those reactions. Most of the reactions that are not shown are sensitive to the low wavelength such as shown for "RCHO". Note that the photolyses of α-dicarbonyls such as glyoxal and methyl glyoxals and the photoreactive unsaturated dicarbonyls represented by AFG1 are particularly important in affecting reactivities of aromatics.

Figure 4 shows that the arc light sources such as used in the all of the UCR EC, CTC, and XTC and some of the UCR EPA chamber experiments give the best representation of solar spectrum, but the blacklights used in the other UCR experiments and the mixed lights used in the TVA chamber give a fair representation of the spectral region in the lower wavelength region and also the mid-wavelength region important for the photolysis of NO_2, glyoxal and AFG1. The "blue" lights used in the new CSIRO experiments are probably the least representative of solar spectra because they have low intensity in the low as well as the high wavelength region.

Table 9. Summary of environmental chambers whose data were used for aromatics mechanism evaluation.

ID	Brief description and references for additional information
	Chambers at the Statewide Air Pollution Research Center (SAPRC) or the College of Engineering Center for Environmental Research and Technology (CE-CERT) at the University of California at Riverside (UCR)
EC	A 5774-liter evacuable chamber constructed of Teflon-coated aluminum with Quartz end windows. Located at SAPRC. Xenon arc solar simulator light source (see Figure 4 for a representative spectrum). Most experiments at ~50% RH and around 300^{o}K. Experiments were carried out 1975 - 1984. See Carter et al (1995a) for description of chamber and experimental methods and Carter (2000a) for a discussion of the modeling methods used. This chamber is now primarily being used for mechanistic studies.
ITC	One semi-collapsible ~6400-liter reactor constructed of 2 mil FTP Teflon film held in a framework. Blacklight light source (see Figure 4 for spectrum, which was used for all chambers using blacklights). Located at SAPRC. Most experiments at ~50% RH and around 300^{o}K. Experiments were carried out 1982 - 1986. See Carter et al (1995a) for description of chamber and experimental methods and Carter (2000a) for a discussion of the modeling methods used. This chamber is now primarily being used for mechanistic studies.
DTC	Two semi-collapsible ~5000-liter reactors constructed of 2 mil FTP Teflon film held in a framework. Initially located at the outdoor laboratory building at SAPRC, but subsequently relocated to CE-CERT. Two irradiations carried out simultaneously, one in Side "A" and the other in Side "B". Blacklight light source. Most experiments used dry air at around 300^{o}K. Experiments carried out 1993 - 1999. See Carter et al (1995a) for description of chamber and experimental methods and Carter (2000a) for a discussion of the modeling methods used. This chamber no longer exists.
XTC	One semi-collapsible ~5000-liter reactor constructed of 2 mil FTP Teflon film held in a framework. Xenon arc light source (see Figure 4 for a representative spectrum). Located the outdoor laboratory building at SAPRC. Experiments used dry air at around 300^{o}K. Experiments carried out in 1993. See Carter et al (1995a) for description of chamber and experimental methods and Carter (2000a) for a discussion of the modeling methods used. This chamber no longer exists.
CTC (≤82)	Semi-collapsible ~5000-liter reactor constructed of 2 mil FTP Teflon film held in a framework. The same Xenon arc light source was used as the XTC. Located at CE-CERT. Experiments used dry air at around 300^{o}K. Experiments carried out in 1994 - 1995. See Carter et al (1995a) for description of chamber and experimental methods and Carter (2000a) for a discussion of the modeling methods used. This configuration is applicable to runs from 11 through 82.
CTC (≥83)	Two semi-collapsible ~2500-liter reactors constructed of 2 mil FTP Teflon film held in a framework. The same Xenon arc light source was sued. Located at CE-CERT. Experiments used dry air at around 300^{o}K. Experiments carried out in 1995 - 1999. This configuration is applicable to runs 83 and higher. See Carter et al (1995a) for description of chamber and experimental methods and Carter (2000a) for a discussion of the modeling methods used. This chamber no longer exists.
EPA	(Also referred to as the UCR EPA chamber.) Two ~90% collapsible ~100,000-liter reactors constructed of 2 mil FEP Teflon film held on a framework with a moveable top for positive pressure control. Located in a temperature-controlled "clean room" clean room enclosure flushed

Table 9 (continued)

ID	Brief description and references for additional information
	with purified air. Located at CE-CERT. Can use either an argon arc solar simulator light source (see Figure 4 for a representative spectrum) or blacklights. Two irradiations can be carried out simultaneously, one in Side "A" and the other in Side "B". Although the temperature and humidity can be varied, all experiments in this evaluation were carried out with dry air at around 300°K. Experiments were carried out from 2003 through present, with the latest run in this evaluation being carried out in mid-2011. See Carter (2004) and Carter et al (2005) for a description of the chamber and experimental methods and Carter (2004) for a discussion of the modeling methods used. Note that mechanism evaluation experiments in this chamber can be carried out under lower NO_x conditions than the other chambers at UCR or the UNC outdoor chamber. This chamber is still in operation and was employed for most of the new experiments modeled in this study.
	Chamber at the Tennessee Valley Authority (TVA).
TVA	One 28,300-liter reactor constructed of 0.13 mm FEP Teflon film on a rigid frame located inside an enclosure flushed with purified air. Special procedures used to clean between experiments to permit experiments at lower concentrations. The light source consisted of blacklights and sunlamps (see Figure 4 for the spectrum). Experiments carried out at about 15% RH and the temperature varied from ~300-315°K. Experiments carried out in 1993 - 1995. See Simonaitis and Bailey (1995) and Bailey et al (1996) for a description of the chamber and experimental methods and Carter (2004) for a discussion of the modeling methods used. Note that mechanism evaluation experiments in this chamber were carried out under lower NO_x conditions than in the other chambers except for UCR EPA, but the chamber experience high background formaldehyde levels that needed to be taken into account when modeling the experiments (Carter, 2004). This chamber no longer exists.
	Chamber at the Commonwealth Scientific and Industrial Research Organisation in Australia (CSIRO) (Not used for SAPRC-07 mechanism development)
CSI	Single 18,000-liter reactor lined with FEP Teflon film. It is fitted with two UV-A lighting modules, each containing 40 black-light tubes (36W Sylvania Blacklight Blue 350). These lamps emit radiation over the range 350–390 nm, with peak intensity at 366 nm (see Figure 4 for the spectrum). See Hynes et al (2005) and White et al (2010) for a description of the chamber and Azzi et al (2010) for a discussion of the use of data from this chamber for evaluating the SAPRC-07 mechanism. The CSIRO experiments modeled in this work were carried out at around 300 K with a relative humidity of ~3%. The characterization assignments used when modeling the CSIRO experiments for this project were provided by White (2010).

Although use of arc light spectra that better represent sunlight is obviously preferred for mechanism evaluation, it is important to recognize that the spectrum of the light source is taken into account when calculating the photolysis rates. Therefore experiments with light sources with unrepresentative spectra can still be useful for mechanism evaluation as long as the differences in light source spectra are properly taken into account. In fact, the use of experiments with a variety of light sources and spectra provide a more comprehensive evaluation of how well the model can simulate effects of changes in light spectrum that may occur in ambient simulations. The uncertainty arises if the action spectrum of important photolysis reactions are uncertain, as may be the case for photoreactive aromatic products that are not well characterized. The existence of this type of problem would be indicated by the

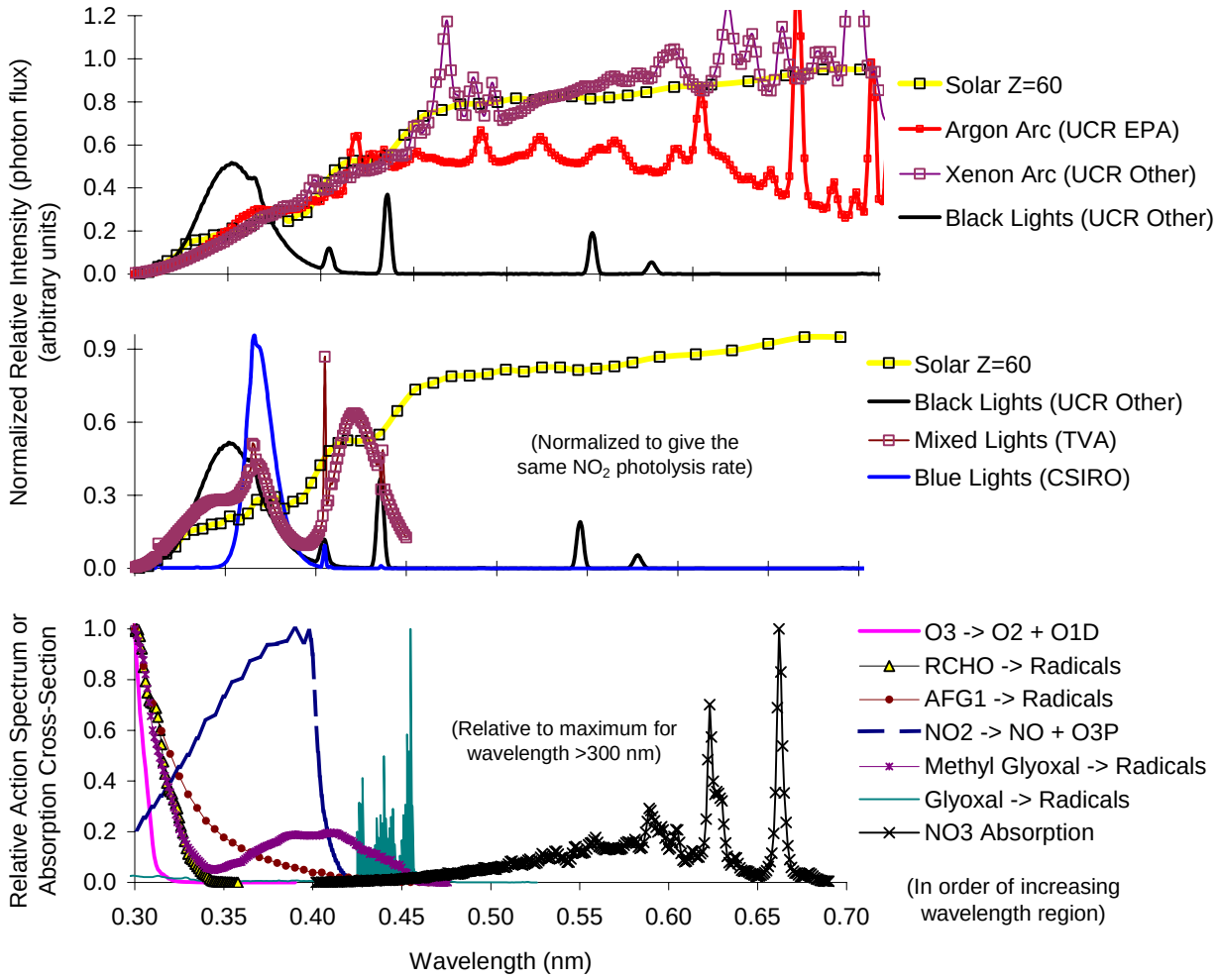

Figure 4. Relative spectral distributions of light sources for the chamber experiments used for mechanism evaluation. Action spectra or absorption cross sections for selected photolysis reactions are also shown.

model performance being different when different light sources are used. Although some compounds only have mechanism evaluation data using blacklights, a few compounds, particularly toluene and m-xylene, have a large number of mechanism evaluation experiments with arc lights as well as blacklights. These data can be used to assess whether there is a significant effect of light source on mechanism evaluation results. This is discussed further in the "Discussion" section of this report.

In addition to the aromatics - NO_x runs listed in Table B-1, the updated mechanism was also evaluated by simulating the results of incremental reactivity experiments where the effects of adding an aromatic compound to a base case reactive organic gas (ROG) surrogate - NO_x experiment. Since no new incremental reactivity experiments with aromatics were conducted since the SAPRC-07 mechanism was developed, these are a subset of the incremental reactivity experiments used in the SAPRC-07 evaluation. These experiments are listed in Table B-2, along with selected conditions and results. See Carter (2010a) for a more complete discussion of these incremental reactivity experiments. The types of incremental reactivity experiments carried out are summarized on Table 10

Modeling Methods

The procedures used when evaluating the mechanism against the chamber data were the same as employed in previous evaluations of the SAPRC-90 (Carter, 1990; Carter and Lurmann, 1991), SAPRC-99 (Carter, 2000a, 2004; Carter and Malkina, 2007), and SAPRC-07 (Carter, 2010a) mechanisms. Briefly, evaluations of mechanisms using chamber data require an appropriate representation of the conditions of the chamber experiments that affect the simulation results. These include initial reactant concentrations, physical conditions such as temperature and dilution, light intensity and spectrum, and the major wall effects such as the chamber radical source, O_3 decays, NO_x offgasing, etc. These considerations are discussed in detail elsewhere (e.g., Carter and Lurmann, 1991, Carter, 2000a and references therein), so are not discussed further here.

The inputs to the chamber simulations concerning initial reactant concentrations, light intensities (as measured by the NO_2 photolysis rate), dilution, temperature, and (if varied) humidity is specified for each experiment depending on the specific procedures or measurements for the experiments. However, other inputs, particularly those concerning chamber wall effects, are assigned for groups of experiments that are judged to have the same chamber effects and thus appropriately use the same characterization parameters. These groupings are done first by chamber and then, depending on the chamber, by groups of runs carried out around the same time that had similar characterization results. For some chambers the characterization results indicate that all the experiments should have the same characterization parameters, but for others the characterization results indicate that some characterization parameters change from time to time and more than one grouping of experiments assigned the same set of parameters is appropriate. This is implemented by assigning each experiment a "characterization set" that is used to obtain input for these variable chamber-dependent parameters. These characterization set assignments are included in the run listing on Table B-1 in Appendix B.

The parameters in the chamber effects model used when modeling the experiments for this mechanism evaluation are given in Table B-4 in Appendix B for each of the chambers and characterization sets used. The table also indicates how these parameters are used in the model and how they were derived. Except for the parameters used to model the chamber-dependent radical source and NO_x offgasing, which tend to vary from reactor to reactor in most UCR chambers, the input data used in modeling the UCR and TVA chamber experiments were the same as used in the SAPRC-07 mechanism evaluation (Carter, 2010a). The chamber effects parameters used when modeling the CSIRO experiments were those developed by the CSIRO group when using these data to evaluate the SAPRC-07 mechanism (White et al, 2010; Azzi et al, 2010), which were provided to us by White (2010).

The most important and variable chamber background effects are the "chamber radical source" first noted by Carter et al (1982) and background NO_x offgasing. The former causes enhanced NO oxidation and O_3 formation in low reactivity experiments, such as CO - NO_x or alkane - NO_x irradiations with no significant radical sources in their gas-phase oxidation mechanisms, while the latter causes O_3 formation in experiments where NO_x has not been added. Both of these effects are attributed to offgasing of HONO, which have been observed experimentally in the SAPHIR outdoor chamber in Jülich, Germany (Brauers et al, 2003, Rohrer et al, 2005) to occur at rates similar to the radial source and NO_x offgasing rates derived for the UCR EPA chamber (Carter et al, 2005). HONO offgasing was also observed in the EUPHORE chamber in Valencia, Spain (Zádor et al., 2006), The magnitudes of the radical source and NO_x offgasing effects are larger in the older chambers (Carter and Lurmann, 1991; Carter et al, 1995a; Carter, 2000a, Carter et al, 2005), but they are still generally comparable to each other, consistent with the assumption that both are due to the same process. This is represented in the chamber model by the parameter RN, which is the rate of HONO offgasing relative to the light intensity as measured by the NO_2 photolysis rate.

Table 10. Types of incremental reactivity experiments used for mechanism evaluation in this work, and codes used to designate these types in the listing of incremental reactivity experiments on Table B-2. See Carter (2010a) for additional discussion.

Designation	Description
Surrogate - NO_x mixtures used as base case in incremental reactivity experiments.	
Surg-8	Standard 8-component "full surrogate" consisting of n-butane, n-octane, ethene, propene, trans-2-butene, toluene, m-xylene and formaldehyde (e.g., Carter et al, 1995b; Carter, 2004)
Surg-7	Standard 8-component "full surrogate", above, but without formaldehyde (e.g. Carter and Malkina, 2005, 2007, Carter et al, 2005)
Surg-3	Standard mini-surrogate consisting of ethene, n-hexane, and m-xylene (e.g., Carter et al, 1993, 1995a).
Surg-NA	Standard 8-componenent "full surrogate" but without aromatics and formaldehyde (unpublished results from this laboratory).
Types of surrogate or incremental reactivity base case experiments	
MIR1	Low ROG/NO_x, MIR-like conditions. NO_x 300-500 ppb (e.g., Carter et al, 1993, 1995b)
MIR2	Low ROG/NO_x, MIR-like conditions, NO_x < 100 ppb (e.g., Carter, 2004; Carter and Malkina, 2005, 2007, Carter et al, 2005)
LN1	Lower NO_x, e.g., MOIR/2. NO_x >100 ppb (e.g., Carter et al, 1993, 1995b)
LN2	Lower NO_x,, e.g. MOIR/2 conditions, NO_x < 50 ppb (e.g., Carter, 2004; Carter and Malkina, 2007, Carter et al, 2005)
vary	Non-standard ROG/NO_x. Conditions varied

Since HONO has not been measured directly in any of the chambers used for mechanism evaluation in this work, the HONO offgasing rate parameter has to be determined by adjusting the parameter so the model calculations can simulate results of the appropriate characterization experiments. The most sensitive experiments are the CO - NO_x and alkane (primarily n-butane) - NO_x experiments used for radical source characterization, and modeling these experiments is the primary method to derive the RN parameters used when modeling the mechanism evaluation runs. The best fit parameters depend to some extent on the chemical mechanism used, particularly the rate constant for the OH + NO_2 reaction, which is the main radical terminating reaction in the characterization experiments. Since this rate constant or other aspects of the mechanism affecting modeling or analysis of the characterization experiments were not changed in the mechanisms developed in this work, the set of RN parameters used in the SAPRC-07 evaluation is also appropriate for this work. These RN parameters are included in the characterization input listing given on Table B-4.

Data Presented and Measures of Model Performance

The performance of the gas-phase mechanism is measured in this work primarily in terms of its ability to simulate maximum O_3 yields, rates of O_3 formation and NO oxidation, and effects of the compounds on OH radical levels. These quantities test different aspects of the mechanism, and are quantified as discussed below.

Maximum Ozone Yields. The maximum O_3 yield in an aromatic - NO_x experiment is the maximum O_3 concentration that would occur if the experiment were run long enough so additional

irradiation time would not yield a significantly higher O_3 concentration in the experiment. In other words, the experiment gives maximum O_3 yield information only if O_3 formation is no longer occurring at a significant rate when the experiment ends. This gives a measure of the maximum O_3 formation potential that is (to a first approximation at least) independent of how rapidly O_3 is formed. If O_3 formation is still occurring at the end of the experiment, then the maximum (i.e., final) O_3 concentration reflects the rate of O_3 formation, not the true maximum O_3 yield that would be observed if the experiment were run sufficiently long. The rate of O_3 formation in the experiment is measured by the rate of change of $\Delta([O_3]\text{-}[NO])$, which is quantified as discussed below.

For the purpose of this mechanism evaluation, the maximum O_3 yield is defined as the maximum O_3 concentration if the maximum occurs some time before the end of the experiment, or the O_3 concentration at the end of the experiment if the O_3 increases by less than 5% in the last 30 minutes of the experiment. If the ozone increases by more than 5% in the last 30 minutes then we conclude that the experiment does not yield information on the maximum O_3 yield, and the data are not used for evaluating this aspect of mechanism performance.

The "model error" for prediction of the maximum O_3 yield is defined as follows, where $[O_3]_{max}^{expt}$ and $[O_3]_{max}^{model}$ are the experimental and calculated maximum O_3 yields, respectively.

$$\text{Maximum } O_3 \text{ Model Error} = ([O_3]_{max}^{model} - [O_3]_{max}^{expt}) \,/\, \text{average}\,([O_3]_{max}^{model}, [O_3]_{max}^{expt}) \qquad \text{(I)}$$

Note that the model error is only defined if the maximum O_3 yield can be derived for *both* the experiment and the model simulation of the experiment, i.e., the O_3 increases by less than 5% in the last 30 minutes of both the experiment and the calculation. Note also that this definition of model error is different than the more commonly used definition where the denominator is the experimentally measured quantity, not the average of the experimental and modeled results. The above definition is preferred here because it gives a symmetrical distribution of model errors in cases of extreme model underprediction or overprediction. This is necessary for averages of model errors for multiple experiments to be meaningful quantities. In particular, by this definition the model errors can range between ±200%, while by the more commonly used definition the model error ranges from -100% to +∞. The two definitions approach the same value when the magnitudes of the model errors are small. In both cases, a negative value means the model is underpredicting the quantity of interest, while a positive value means that the model is overpredicting it.

Ozone Formation and NO Oxidation. The amount of O_3 formed and NO oxidized in the experiments is measured by the quantity $\Delta([O_3]\text{-}[NO])$, which is calculated by

$$\Delta([O_3]\text{-}[NO])_t = ([O_3]_t - [NO]_t) - ([O_3]_0 - [NO]_0) \qquad \text{(II)}$$

where $[O_3]_0$, $[NO]_0$, $[O_3]_t$, and $[NO]_t$ are the initial and time=t concentrations of ozone, and NO, respectively. As discussed previously (e.g., Carter and Atkinson, 1987; Carter, 1990; Carter and Lurmann, 1991), this gives a measure of the ability of the model to simulate the chemical processes that cause ozone formation, and gives a useful measure even where ozone is suppressed by the presence of excess NO. The ability of the mechanism to simulate this quantity in the experiments can be measured by its model error, calculated analogously to Equation (I), above. This definition of model error for $\Delta([O_3]\text{-}[NO])$ is used for the model errors shown on Figure 1 in the Introduction and on Table B-1. However, the primary use of these data is to evaluate the mechanism's ability to simulate the rates of ozone formation and NO oxidation in the aromatics - NO_x experiments, which is defined as discussed below.

For incremental reactivity experiments, the model performance is evaluated by comparing model predictions of the incremental reactivities relative to $\Delta([O3]\text{-}[NO])$, which are defined as follows:

$$\text{IR } \Delta([O_3]\text{-}[NO])_t = \{\Delta([O_3]\text{-}[NO])_t^{Test} - \Delta([O_3]\text{-}[NO])_t^{Base}\} \,/\, \text{amount of test VOC added} \qquad \text{(III)}$$

where t is the time, $\Delta([O_3]\text{-}[NO])_{Base}$ and $\Delta([O_3]\text{-}[NO])_{Test}$ are the Δ([O3]-[NO]) in the base case and the added test VOC experiments, respectively. The IR $\Delta([O_3]\text{-}[NO])$ values are given in molar units (e.g., ppm $\Delta([O_3]\text{-}[NO])$ / ppm VOC added). Model performance in simulating the incremental reactivity experiments is evaluated by comparing plots of experimental and calculated IR $\Delta([O_3]\text{-}[NO])$ values as a function of time. These values are calculated for each hour of the experiments, with the experimental values being derived by linear interpolation if no measurement were made exactly on the hour.

Fits to Rates of NO Oxidation and O_3 Formation. An important measure of model performance is its ability to simulate how rapidly NO is oxidized and O_3 is formed, or the rate of change of $\Delta([O_3]\text{-}[NO])$ when O_3 formation is occurring. This is defined as follows:

$$\Delta([O_3]\text{-}[NO])\ \text{Rate} = \frac{\text{½ Maximum } \Delta([O_3]\text{-}[NO])}{\text{Time to reach ½ maximum } \Delta([O_3]\text{-}[NO]),\ \text{estimated by interpolation}} \qquad \text{(IV)}$$

$$\text{Formation Rate Model Error} = \frac{\Delta([O_3]\text{-}[NO])\ \text{Rate}^{model} - \Delta([O_3]\text{-}[NO])\ \text{Rate}^{expt}}{\text{average } \{\Delta([O_3]\text{-}[NO])\ \text{Rate}^{model}, \Delta([O_3]\text{-}[NO])\ \text{Rate}^{expt}\}}$$

This is determined by summarizing the $\Delta([O_3]\text{-}[NO])$ values at each hour in the experiment or model simulation (with the experimental hourly $\Delta([O_3]\text{-}[NO])$ values being derived by interpolation if necessary, determining the maximum of the hourly values, finding the first hour when the $\Delta([O_3]\text{-}[NO])$ value is greater than half this maximum value, and then deriving an estimated time to achieve this half maximum value by linear interpolation between the time and value at this time and the time and value for the previous hour. Since NO oxidation and O_3 formation is still occurring at the time $\Delta([O_3]\text{-}[NO])$ reaches half its maximum value, this therefore reflects the rate of change of $\Delta([O_3]\text{-}[NO])$ when O_3 formation is occurring.

Another measure of O_3 formation and NO oxidation rates that have been used is the NO to NO_2 crossover time, which measures the NO oxidation rate during the initial stages of experiments where the initial NO is greater than the initial NO_2. However, this is not a very good measure because it is highly dependent on the initial NO_2/NO ratio in the experiments, is affected by interferences on the NO_x analyzers generally employed, and is not defined if the initial NO_2/NO ratio is greater than one. Therefore, we believe that using the measure given by Equation (IV) is a preferable approach.

Integrated Hydroxyl Radical Levels. The ability of the model to simulate the hydroxyl radical (OH) levels in the experiments is also used as a measure of model performance. The quantity used for this purpose is the integrated OH levels, or IntOH. For the aromatic - NO_x experiments, the integrated OH is derived from model calculations using a version of the model where OH radicals are specified as inputs to the calculations, and are adjusted to fit rates of consumption of the aromatic reactant. These are not derived for benzene experiments because the rate of consumption of benzene is too slow to provide a sufficiently precise measure of OH levels, and are not derived for experiments with phenolic compounds because reaction with OH radicals is not their only potentially significant consumption process. For the incremental reactivity experiments the IntOH is derived from the rate of consumption of m-xylene in the base case ROG surrogate mixture, using the rate constant for m-xylene that is given in Table 3. The effect of the test VOC on this quantity is measured by

$$\text{IR IntOH} = \{\text{IntOH}_{Test} - \text{InOH}_{Base}\} / \text{amount of test VOC added} \qquad \text{(V)}$$

where IntOH_{Base} and IntOH_{Test} are the IntOH values derived from the base case and the added test VOC experiments, respectively. They are given in units of ppt-minute per ppm of test VOC added if the test VOC is a compound, or ppt-minute per ppmC of test VOC if it is a complex mixture.

Adjustments to Mechanisms to Fit Data

SAPRC-11 Mechanism. The SAPRC-11 mechanism is the version of the updated aromatic mechanism where no new NO_x-dependence process is assumed in order to improve model performance in the higher NO_x experiments, i.e., where processes "A" and "B" on Figure 2 are assumed to be negligible regardless of the NO_x levels in the experiments. As discussed above in the "Mechanism Description" section and indicated on Table 6, above, the quantum yields for radical production in the photolyses of model species representing the uncharacterized photoreactive aromatic ring-opening products, i.e., the yield ratios for AFG1/(AFG1+AFG2), were adjusted for each compound to optimize fits to chamber data, but no other parameters were adjusted. The metric used in this optimization was the average $\Delta([O_3]-[NO])$ formation rate for all experiments where the initial NO_x was less than 90 ppb. Only the lower NO_x experiments were used for this purpose because the model errors for SAPRC-11 were found to depend on the total NO_x levels for some compounds. Initial NO_x levels of 90 ppb were chosen for the cutoff because this was the highest NO_x level that did not significantly affect the optimization results for benzene and toluene.

For most compounds, the yield ratios for AFG1/(AFG1+AFG2) were adjusted until the magnitude of the average model error for $\Delta([O_3]-[NO])$ formation rate for experiments with NO_x <90 ppb was no greater than about 10%. Somewhat higher magnitudes of model errors were permitted for benzene, phenol, and 2,4-dimethylphenol because the overall scatter of the fits was such that further fine-tuning was not meaningful, and for p-ethyl toluene because the best fit ratio slightly exceeded 100%. The resulting AFG yield ratios (radical forming quantum yields) are summarized on Table 6, above.

SAPRC-11A Mechanism. The SAPRC-11A mechanism is the version of the updated mechanism where an additional NO_x-dependent process, process "A" on Figure 2, is assumed to occur at non-negligible rates for some compounds in order to reduce dependences of model errors on overall NO_x levels. This is not the standard mechanism developed in this project because the rate constants required to fit the data are not consistent with NO_x-dependences of aromatic product yields measured in the laboratory, but assessing its performance is useful for mechanism analysis purposes. For this version of the mechanism the rate constant for the reaction of O_2 with the OH-aromatic adduct is adjusted as well as the AFG1/(AFG1+AFG2) product yield ratio what is adjusted for SAPRC-11.

This separate adjustment was done only for those compounds where the average model error for the $\Delta([O_3]-[NO])$ formation rate for all runs was greater than +20%, which turned out to be the case for benzene, toluene, ethyl benzene, and p-xylene. No separate SAPRC-11A mechanism was developed for the other compounds, where the performance of SAPRC-11 appeared to be satisfactory over the full range of NO_x levels, or where the range of NO_x levels studied was insufficient to unambiguously determine a best fit value for the O_2 + OH-aromatic adduct rate constant.

The adjustment procedure employed was as follows. Starting with the AFG1/(AFG1+AFG2) yield ratio that gave the best fits for SAPRC-11, the rate constant for the OH-aromatic adduct + O_2 reaction was decreased until the average $\Delta([O_3]-[NO])$ formation rate model error for all experiments was within ±10%. If the average model error for the low NO_x experiments differed from the average for all experiments by more than about 10% (absolute), then the adduct + O_2 reaction rate constant was increased or decreased to reduce the difference, and the best fit AFG yield ratios were determined again. The resulting adduct + O_2 rate constants and AFG yield ratios that satisfied these criteria are summarized on Table 8, above.

Results

Table 11 gives a summary of the average performance metrics for the simulations of the aromatic - NO_x experiments with the updated aromatics mechanisms, with results shown for all compounds for SAPRC-11, the standard version of the mechanism, and shown also shown for SAPRC-11A for the four compounds where the additional NO_x dependence incorporated in this version is necessary to fit the data over the full range of NO_x levels. Average model errors are shown graphically, and compared between SAPRC-07 and SAPRC-11 on Figure 5 for all 17 aromatic compounds, and compared between SAPRC-11A and SAPRC-11 on Figure 6 for the four compounds where SAPRC-11A had to be used to fit the data over the full NO_x concentration range. Table 11 gives the average biases and errors for the various metrics, where the biases are the averages of the model errors for the various runs and the errors are the averages of the absolute magnitudes of the model errors. The number of runs used for computing the

Table 11. Average model performance metrics for SAPRC-11 model simulations of the aromatic - NO_x chamber experiments.

Compound	Δ([O_3]-[NO]) formation rate [NO_x]<90 ppb			Δ([O_3]-[NO]) formation rate All Runs			Maximum Ozone Yield			Integrated OH Levels	
	Runs	Bias	Error	Runs	Bias	Error	Runs	Bias	Error	Bias	Error
SAPRC-11 (Standard NO_x Dependence)											
Benzene	4	-3%	5%	14	54%	61%	3	14%	19%		
Toluene	48	3%	17%	76	19%	29%	48	8%	13%	-20%	31%
Ethyl Benzene	5	4%	6%	12	34%	36%	3	14%	15%	-23%	23%
n-Propyl Benzene	3	-4%	4%	4	-6%	7%	1	16%	16%	-17%	17%
Isopropyl Benzene	5	3%	6%	6	3%	6%	1	-1%	5%	-25%	25%
m-Xylene	90	-3%	17%	128	-2%	19%	99	-3%	11%	-38%	38%
o-Xylene	10	1%	10%	27	1%	15%	16	-3%	11%	-32%	34%
p-Xylene	14	4%	13%	29	33%	38%	8	-12%	13%	-12%	40%
m-Ethyl toluene	5	-2%	17%	10	-12%	19%	9	-1%	5%	-40%	40%
o-Ethyl toluene	6	2%	10%	11	-6%	14%	7	-5%	6%	-40%	40%
p-Ethyl toluene	2	-5%	30%	7	-15%	32%	2	-1%	7%	-49%	49%
1,2,3-trimethylbenzene	4	-1%	8%	13	-7%	10%	8	-3%	7%	-38%	38%
1,2,4-trimethylbenzene	11	-4%	10%	27	-2%	28%	10	-6%	8%	-27%	34%
1,3,5-trimethylbenzene	8	2%	5%	25	-13%	15%	21	10%	12%	-29%	29%
Phenol	4	-4%	26%	5	-8%	26%	0	3%	10%		
o-Cresol	4	-4%	14%	7	8%	29%	0	23%	23%		
2,4-Dimethyl phenol	4	5%	23%	4	5%	23%	0	-3%	7%		
SAPRC-11A (Additional NO_x Dependence)											
Benzene	4	-1%	8%	14	-1%	17%	3	-0%	22%	-	-
Toluene	48	2%	17%	76	5%	20%	48	7%	12%	-23%	28%
Ethyl Benzene	5	9%	9%	12	-1%	11%	3	10%	13%	-22%	22%
p-Xylene	14	-1%	14%	29	-3%	17%	8	-15%	15%	-21%	29%

Note: "Bias" is the average of the model errors and "error" is the average of the absolute values of the model errors.

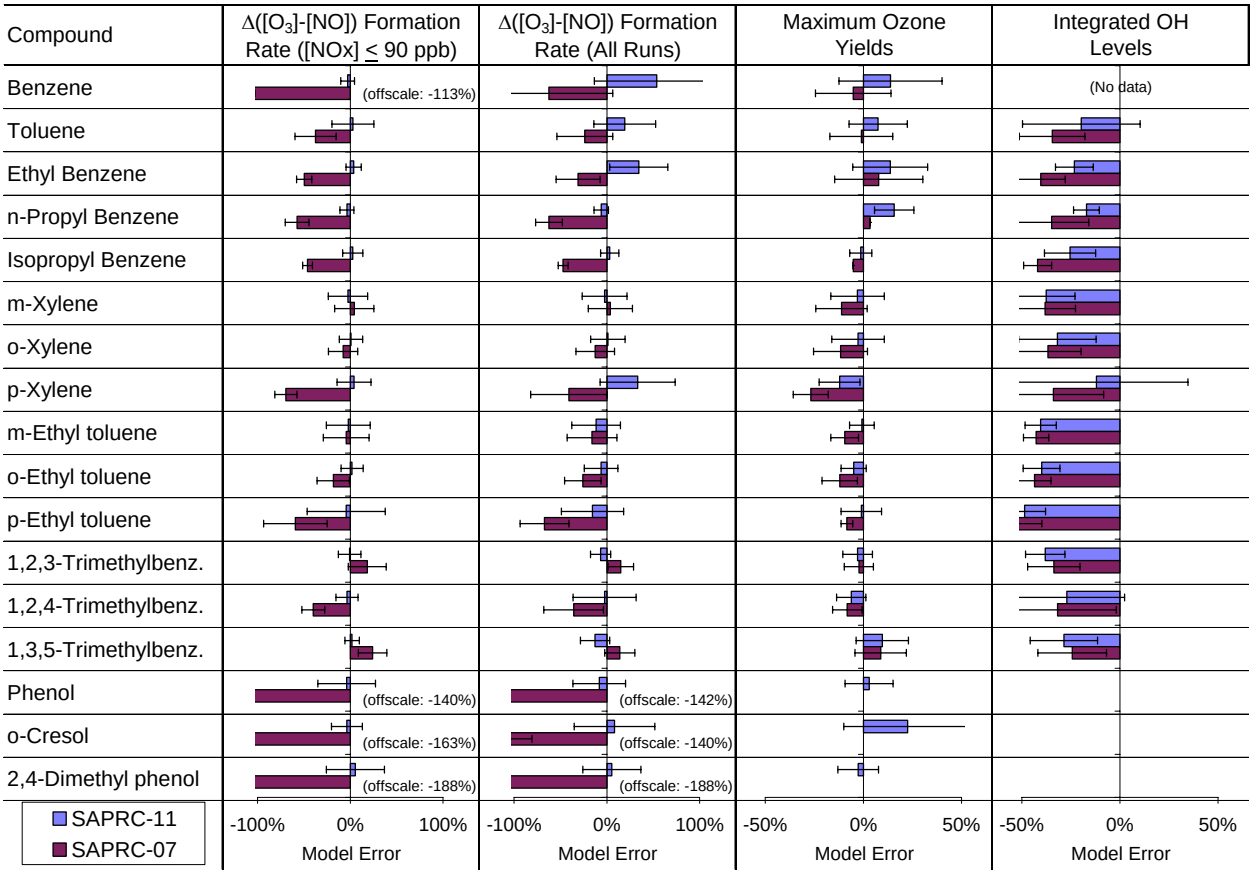

Figure 5. Plots of average model errors for various fit metrics for model simulations of the aromatic - NO_x experiments by SAPRC-11 and SAPRC-07. Standard deviations of the averages are also shown.

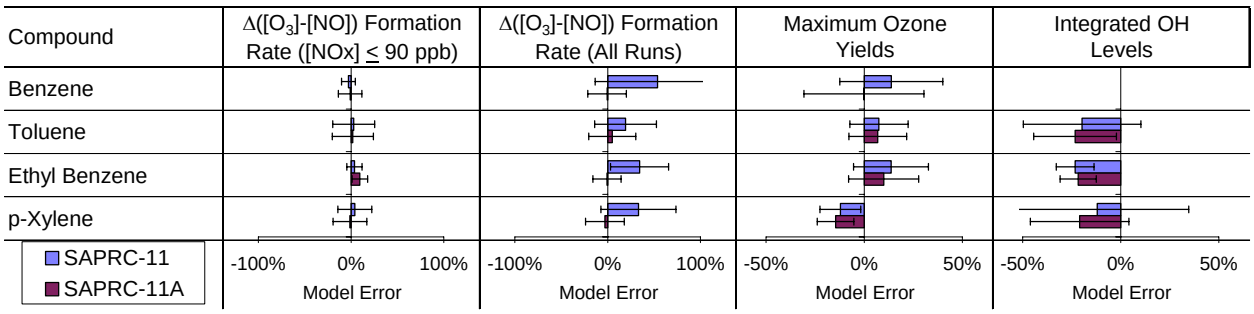

Figure 6. Plots of average model errors for various fit metrics for model simulations of the aromatic - NO_x experiments by SAPRC-11A and SAPRC-11. Standard deviations of the averages are also shown.

averages for the $\Delta([O_3]-[NO])$ formation rate and maximum ozone yield metrics are also shown. In the case of the metrics for the $\Delta([O_3]-[NO])$ formation rate with $NO_x < 90$ ppb this is the number of runs with initial NO_x in this range, while in the case of the maximum O_3 yields this is the number of runs where the increase in O_3 in the last 30 minutes of the run was less than 5% for both the experiment and the model calculation.

Note that the average biases are very low for the SAPRC-11 simulations of the $\Delta([O_3]-[NO])$ formation rates at the lower NO_x levels, and for the SAPRC-11A simulations of $\Delta([O_3]-[NO])$ formation rates for all experiments (see Table 11, Figure 5, and Figure 6) because the parameters for the mechanisms were optimized to minimize these average biases. However, no optimizations were done to improve the simulations of the maximum O_3 yields and the integrated OH radical levels, or to improve results of simulations of incremental reactivity experiments for those compounds that have such data, so these provide more independent tests of the mechanism performance.

Overall, the SAPRC-11 or SAPRC-11A mechanisms give much better fits to the $\Delta([O_3]-[NO])$ formation rates, primarily because they were optimized using this metric, but also because the experiments used to develop SAPRC-07 were much less comprehensive in terms of the range of NO_x conditions that were represented, and there were no experiments with the propyl benzenes or ethyl toluenes, and only one experiment used for cresols. On the other hand, the magnitudes of the average model errors for maximum O_3 yields for benzene and the alkylbenzenes were not significantly better for SAPRC-11 than SAPRC-07. Both mechanisms have a consistent bias towards underpredicting OH levels in aromatic - NO_x experiments, though in most cases this underprediction is slightly less for SAPRC-11 than SAPRC-07.

The results for the individual compounds or groups of compounds are discussed in more detail in the following sections. Figures such as Figure 7 for benzene are given for each compound, showing tables giving various average model performance metrics, plots of model errors for $\Delta([O_3]-[NO])$ formation rates and maximum $\Delta([O_3]-[NO])$ concentrations against both initial NO_x and initial aromatic / NO_x ratios, and plots of initial aromatic vs. initial NO_x levels showing the range of reactant conditions for the experiments are presented. Separate plots are given showing the performance of SAPRC-11A for those compounds for which parameters for this mechanism were derived. In addition, figures showing model performance in simulations of incremental reactivity experiments are shown for those compounds that have such data.

Benzene

Plots and tables of selected model performance results for the individual benzene - NO_x experiments are shown on Figure 7 for the SAPRC-11 mechanism and on Figure 8 for the SAPRC-11A, and plots showing the performance of these mechanisms in simulating selected reactivity results of the incremental reactivity experiments with benzene are shown on Figure 9. Experiments carried out using arc lights are indicted in Figure 7 and Figure 8 in order to provide information on light-source dependences on model performance. Figure 7 also shows that the initial benzene and NO_x concentrations, and also the initial benzene / NO_x ratios in the benzene - NO_x experiments varied by almost two orders of magnitude, indicating that the mechanism was evaluated over a very wide concentration range. No reliable information could be obtained concerning model performance in simulating integrated OH levels in the benzene experiments because benzene reacts too slowly to reliably derive OH levels from its rate of consumption.

Figure 7 shows that the standard SAPRC-11 mechanism gives fair simulations of $\Delta([O_3]-[NO])$ formation rates and O_3 yields at NO_x levels below about 100 ppb, but consistently overpredicts both at

Benzene

Number of Runs	14
Average Model Bias	
Formation Rate (low NOx)	-3%
Formation Rate (all runs)	54%
Maximum Ozone Yield	14%
Average Model Error	
Formation Rate (low NOx)	5%
Formation Rate (all runs)	61%
Maximum Ozone Yield	19%

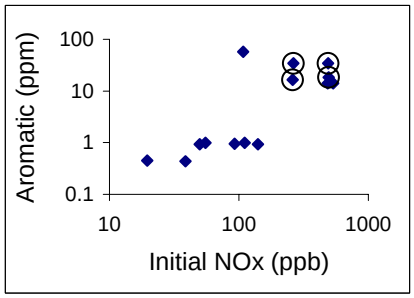

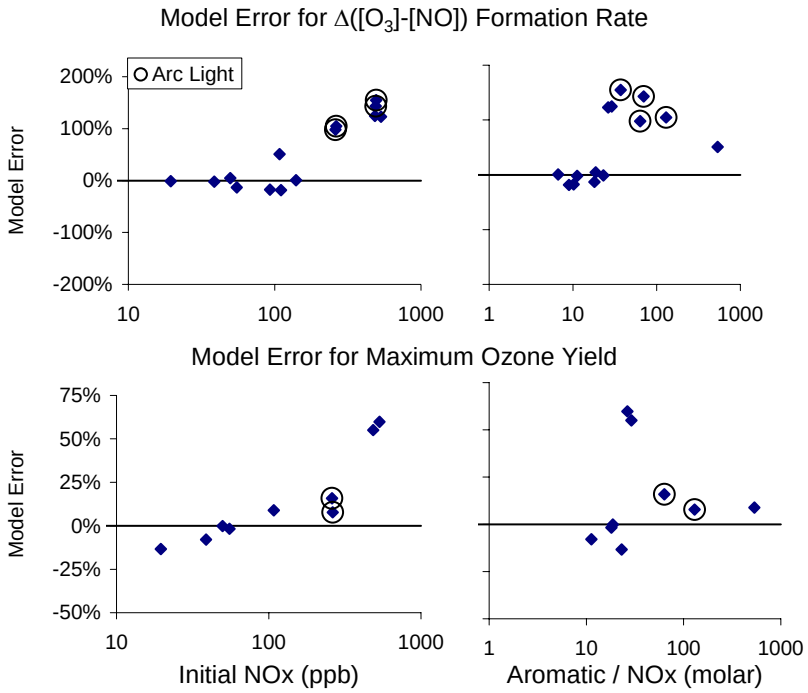

Figure 7. Plots and tables of selected model performance results for the benzene - NO_x experiments using the SAPRC-11 mechanism.

Benzene (Model "A")

Number of Runs	14
Average Model Bias	
Formation Rate (low NOx)	-1%
Formation Rate (all runs)	-1%
Maximum Ozone Yield	0%
Average Model Error	
Formation Rate (low NOx)	8%
Formation Rate (all runs)	17%
Maximum Ozone Yield	22%

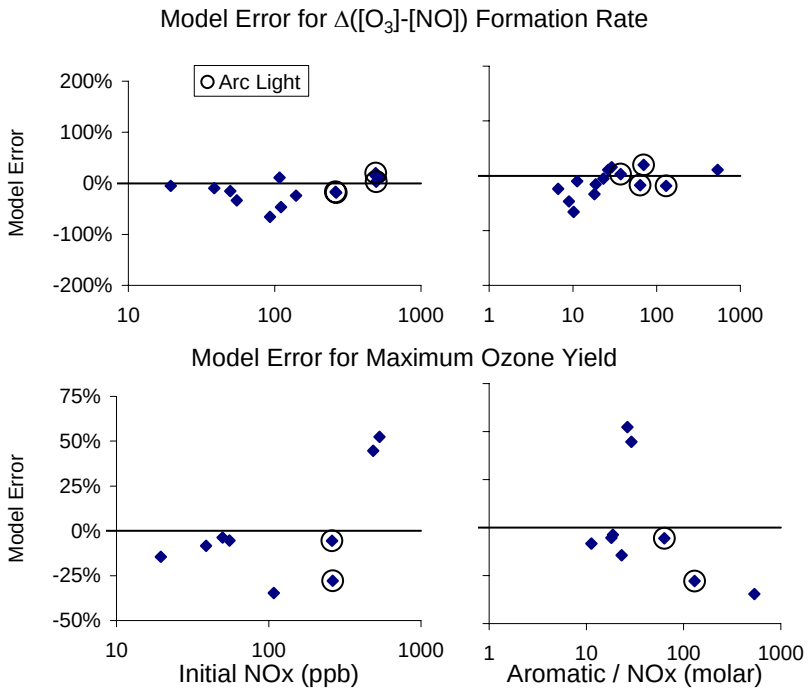

Figure 8. Plots and tables of selected model performance results for the benzene - NO_x experiments using the SAPRC-11A mechanism.

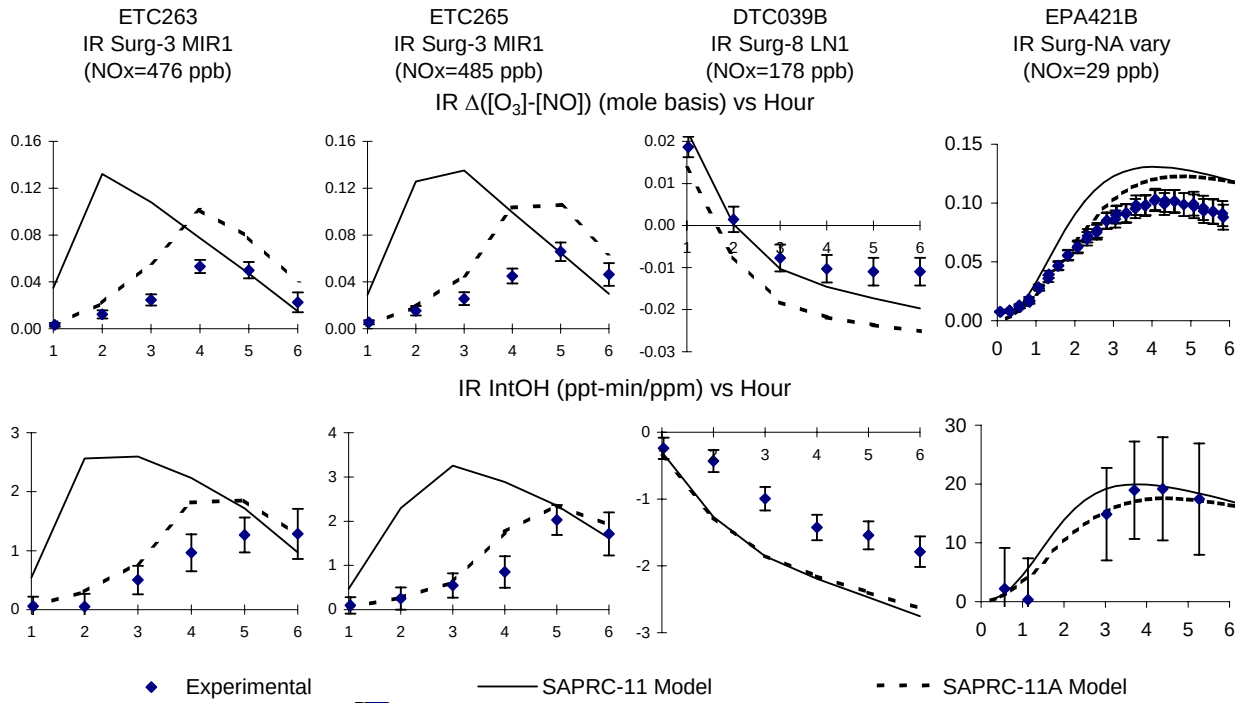

Figure 9. Plots of selected incremental reactivity evaluation results for benzene. Results are shown for both SAPRC-11 (solid lines) and SAPRC-11A (dashed lines).

higher NO_x levels. This large and consistent overprediction bias at higher NO_x is removed if the additional NO_2-dependent process incorporated in SAPRC-11A is included, though there are still some runs that are not particularly well simulated. Figure 6 shows that SAPRC-11A also gives good simulations of the maximum O_3 yields in the benzene experiments, even though the adjustments and optimizations focused only on rates of NO oxidation and O_3 formation.

Figure 9 shows that SAPRC-11 consistently overpredicts the incremental reactivities of benzene with respect to $\Delta([O_3]-[NO])$ formation and Integrated OH levels in the high NO_x, low ROG/NO_x "Surg-3 MIR1" incremental reactivity experiments, but gives better simulations of the reactivity results of the higher ROG/NO_x "Surg-8 LN1" experiment and the non-aromatic surrogate (Surg-NA) experiment carried out at much lower NO_x levels. (See Table 10 for a listing of the designations of the types of incremental reactivity experiments.) The model performance at the higher NO_x experiments is considerably better with the SAPRC-11A mechanism, consistent with the results for the benzene - NO_x experiments discussed above. However, SAPRC-11A still significantly overpredicts the effect of added benzene on the final $\Delta([O_3]-[NO])$ levels in the highest NO_x experiments.

It is not possible to assess the effect of light source on mechanism evaluation results for benzene independently of the effects of NO_x because all the benzene runs with arc lights were carried out with relatively high NO_x levels. However, the light source does not appear to have a significant effect on the evaluation results for the SAPRC-11A mechanism, which appears to simulate the data moderately well at the full range of available NO_x levels.

Toluene

Plots and tables of selected model performance results for the toluene - NO_x experiments are shown on Figure 10 for the SAPRC-11 mechanism and on Figure 11 for the SAPRC-11A, with experiments carried out using arc lights indicated on the plots for the individual runs. Plots showing the performance of these mechanisms in simulating the incremental reactivity experiments are shown on Figure 12. Figure 10 also shows that the initial toluene and NO_x concentrations varied by over two orders of magnitude, and the initial toluene/NO_x ratio varied by almost as much. The average performance of the mechanisms in simulating various measures of model performance, including integrated OH levels, is indicated in Figure 6, above.

Figure 10 shows that, like benzene, SAPRC-11 gives reasonably good simulations of the results of the toluene - NO_x experiments at NO_x levels less than about 100 ppb, but has a consistent bias for overprediction at higher NO_x levels. Figure 11 shows that this consistent bias is removed if the initial NO_x-dependent process incorporated in SAPRC-11A is used, though there is still run-to-run scatter and there is still a consistent dependence of model performance on the initial toluene/NO_x ratio. However, the high NO_x overprediction bias for SAPRC-11 is not as large as is the case for benzene, and the SAPRC-11A parameterization that fits the data for toluene (shown in Table 8, above) indicates that the high NO_x regime (i.e., the NO_2 level above which the rate of the reaction of the OH-aromatic with NO_2 exceeds that for the reaction with O_2) occurs at higher NO_x levels for toluene than was the case for benzene.

As is also the case for benzene, the SAPRC-11 mechanism overpredicts the effects of toluene on $\Delta([O_3]-[NO])$ and integrated OH levels in the high NO_x, low ROG/NO_x "MIR1" experiments but gives reasonably good simulations of the "LN1" experiment at lower NO_x and higher ROG/NO_x levels (Figure 12). The SAPRC-11A mechanism gives the same fits to the LN1 experiment but gives much better fits to the MIR1 experiments, though it tends to overpredict $\Delta([O_3]-[NO])$ reactivities in some of the runs. This is consistent with the results of the simulations of the toluene - NO_x experiments. Figure 6 shows that SAPRC-11 and SAPRC-11A gives similar fits to maximum O_3 yields and integrated OH levels, tending to slightly overpredict maximum O_3 yields and consistently underpredict OH levels in toluene - NO_x experiments.

Figure 13 shows plots of model errors in the simulations of the integrated OH radical levels (IntOH) against initial NO_x and initial aromatic / NO_x ratios. SAPRC-11 tends to underpredict the IntOH model errors except for some of the higher NO_x experiments, and SAPRC-11A underpredicts IntOH over the full range of NO_x levels. Except for SAPRC-11 at higher NO_x levels, there is no apparent dependence of the IntOH model error on initial NO_x and the initial aromatic / NO_x ratios.

The toluene - NO_x experiments provide a better dataset on the effect of light source than is the case for benzene, since arc light experiments were carried out with almost as wide a variety of NO_x levels and toluene / NO_x ratios as was the case for blacklight experiments. No significant effect of light source can be seen in the toluene - NO_x simulations with either SAPRC-11 (Figure 10) or SAPRC-11A (Figure 11).

Ethyl Benzene

Plots and tables of selected model performance results for the ethyl benzene - NO_x experiments are shown on Figure 14 for the SAPRC-11 mechanism and on Figure 15 for the SAPRC-11A, and plots showing the performance of these mechanisms in simulating the incremental reactivity experiments are shown on Figure 16. The average performance of the mechanisms in simulating various measures of model performance, including integrated OH levels, is indicated in Figure 6, above. The number of experiments with ethylbenzene is much more limited than is the case with toluene, and only 3

Toluene

Number of Runs	76
Average Model Bias	
Formation Rate (low NOx)	3%
Formation Rate (all runs)	19%
Maximum Ozone Yield	8%
Average Model Error	
Formation Rate (low NOx)	17%
Formation Rate (all runs)	29%
Maximum Ozone Yield	13%

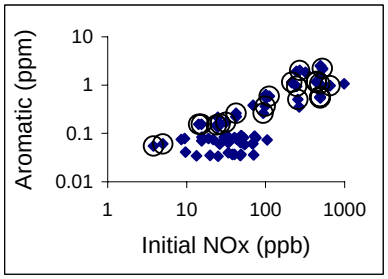

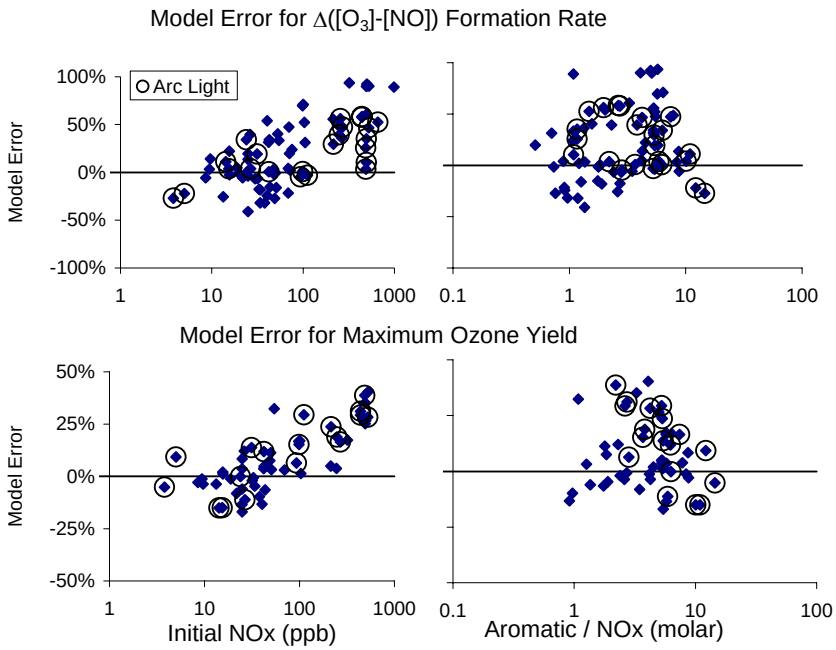

Figure 10. Plots and tables of selected model performance results for the toluene - NO_x experiments using the SAPRC-11 mechanism.

Toluene (Model "A")

Number of Runs	76
Average Model Bias	
Formation Rate (low NOx)	2%
Formation Rate (all runs)	5%
Maximum Ozone Yield	7%
Average Model Error	
Formation Rate (low NOx)	17%
Formation Rate (all runs)	20%
Maximum Ozone Yield	12%

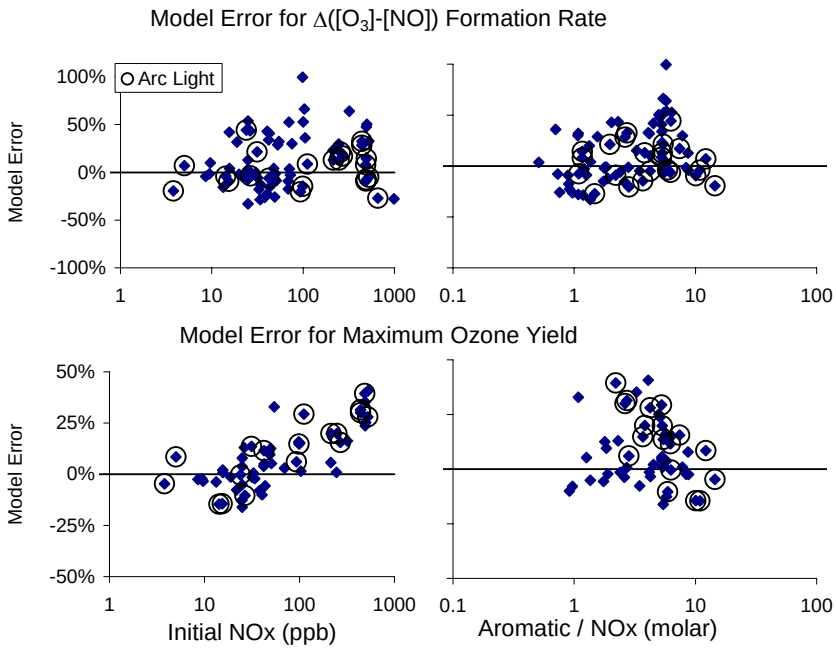

Figure 11. Plots and tables of selected model performance results for the toluene - NO_x experiments using the SAPRC-11A mechanism.

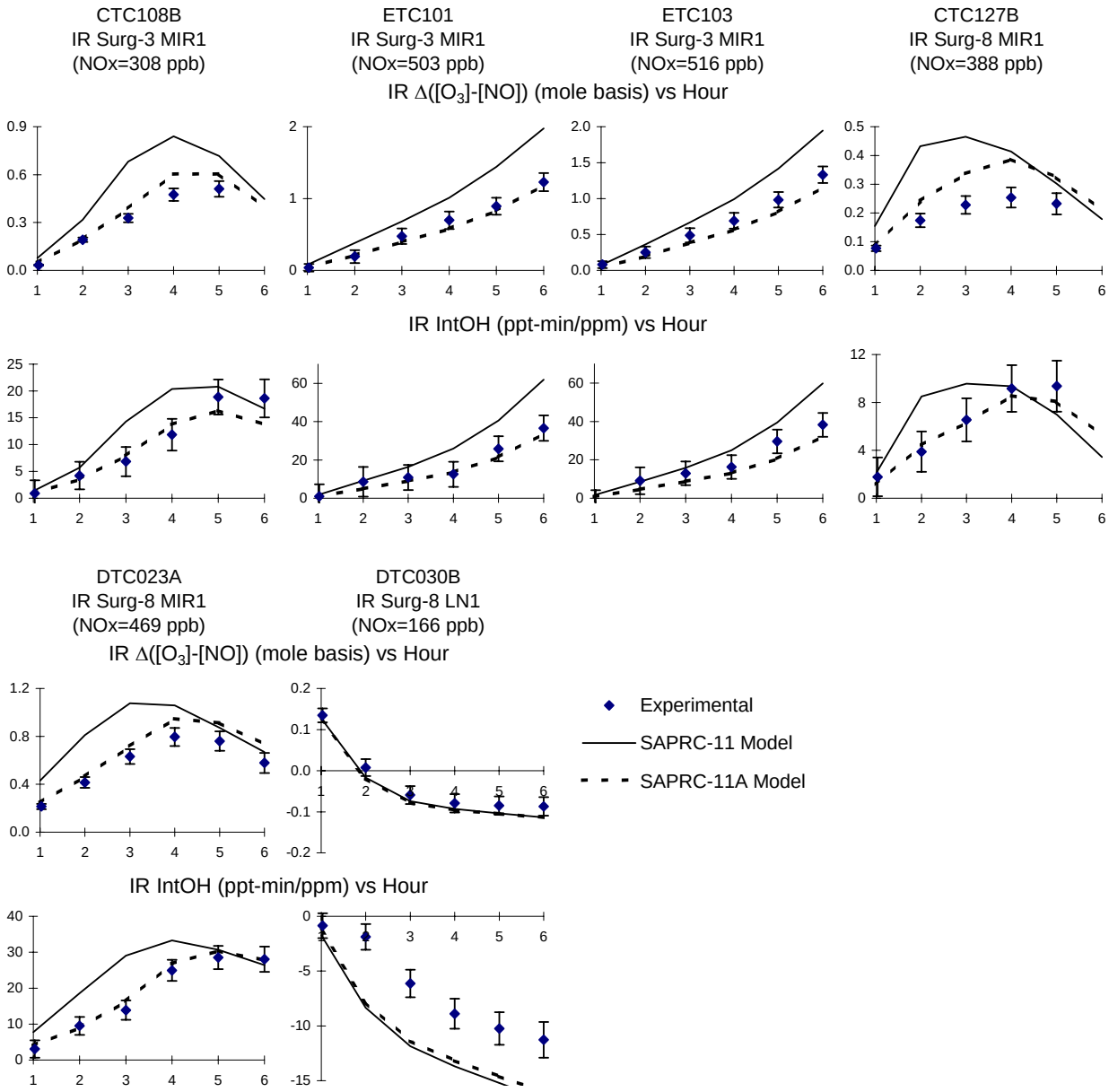

Figure 12. Plots of selected incremental reactivity evaluation results for toluene. Results are shown for both SAPRC-11 (solid lines) and SAPRC-11A (dashed lines).

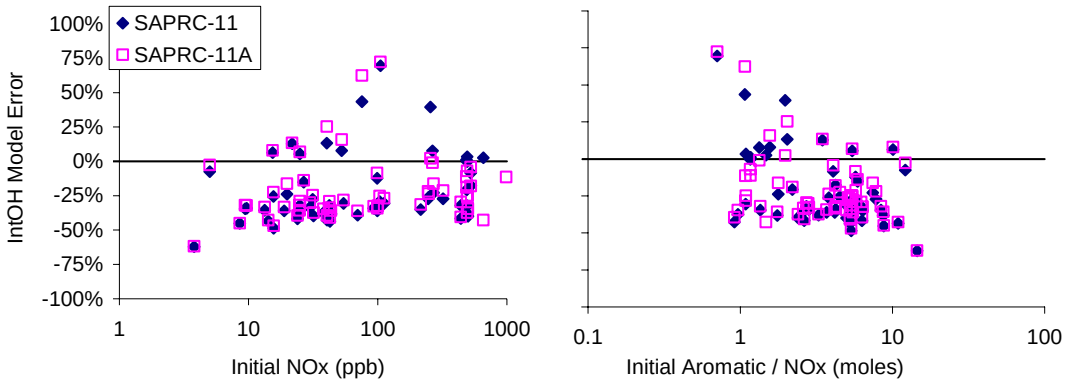

Figure 13. Plots of model errors for simulations of the integrated OH levels in the toluene - NO_x experiments with the SAPRC-11 and SAPRC-11A mechanisms.

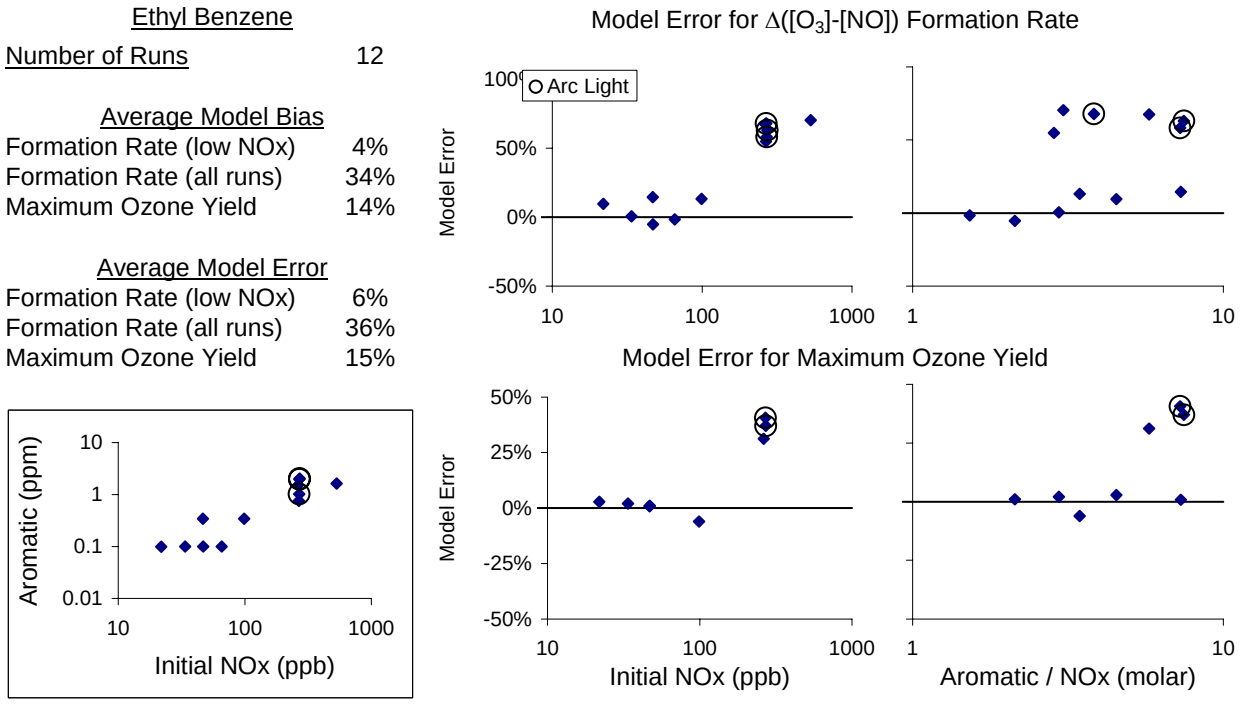

Figure 14. Plots and tables of selected model performance results for the ethylbenzene - NO_x experiments using the SAPRC-11 mechanism.

Ethyl Benzene (Model "A")

Number of Runs	12
Average Model Bias	
Formation Rate (low NOx)	9%
Formation Rate (all runs)	-1%
Maximum Ozone Yield	10%
Average Model Error	
Formation Rate (low NOx)	9%
Formation Rate (all runs)	11%
Maximum Ozone Yield	13%

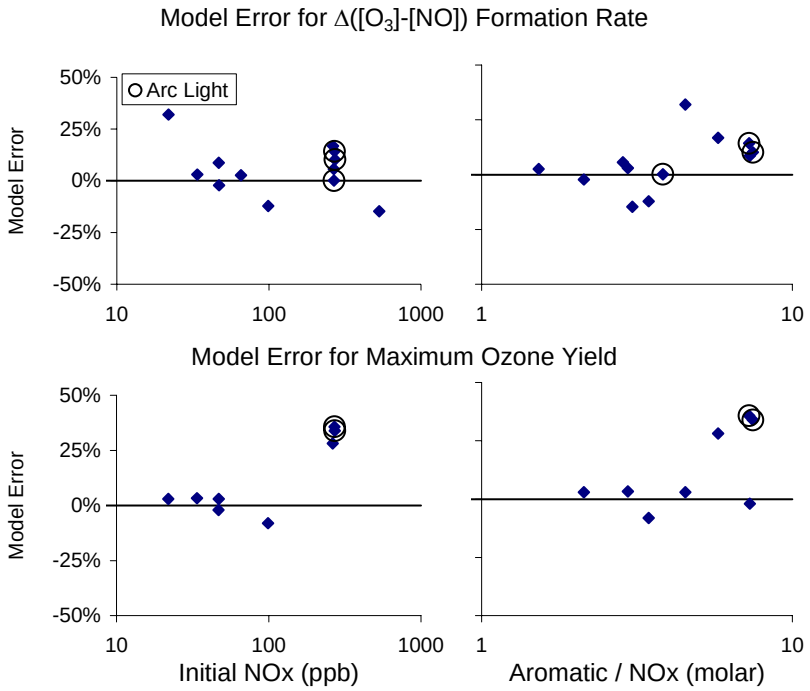

Figure 15. Plots and tables of selected model performance results for the ethylbenzene - NO_x experiments using the SAPRC-11A mechanism.

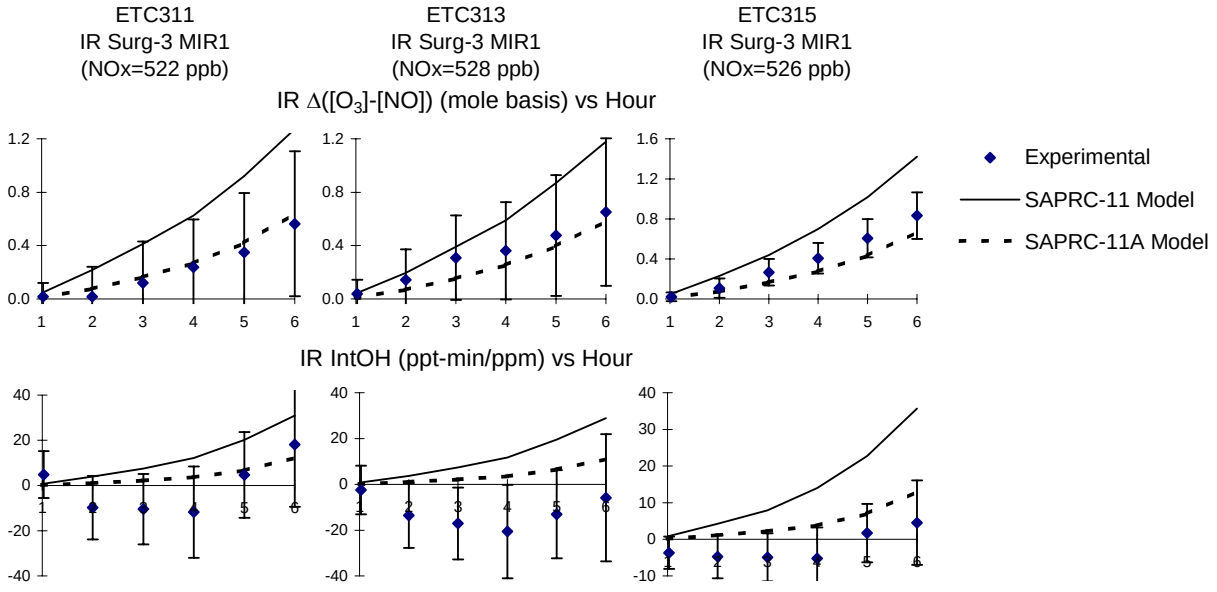

Figure 16. Plots of selected incremental reactivity evaluation results for ethylbenzene. Results are shown for both SAPRC-11 (solid lines) and SAPRC-11A (dashed lines).

experiments were carried out with arc lights, all at high NO_x levels. Nevertheless, the available data cover over an order of magnitude of initial NO_x levels, and almost an order of magnitude of initial ethylbenzene / NO_x ratios.

As was the case with toluene, SAPRC-11 gave reasonably good simulations of the data at NO_x levels of ~100 ppb or less but consistently overpredicted reactivity at high NO_x levels, while SAPRC-11A was reasonably consistent with the data over the full NO_x range. However, the NO_x level corresponding to the high NO_x regime for SAPRC-11A is much lower for ethylbenzene than is the case for toluene, though

it is not as low as fit the data for benzene (see Table 8). There is still a dependence of SAPRC-11A model performance on aromatic / NO_x ratio, as was also the case for toluene, though more experiments may be required to verify that the apparent dependence is outside the scatter of the data. The run-to-run scatter in the simulations of the $\Delta([O_3]-[NO])$ data was less than was the case for toluene, perhaps because of the lower variety of chambers and conditions that were employed.

Figure 16 shows that, as is the case for toluene, SAPRC-11 consistently overpredicts the incremental reactivities of ethyl benzene in the high NO_x, low ROG/NO_x "MIR1" incremental reactivity experiments, and these experiments are simulated much better by SAPRC-11A. In this case, the incremental reactivities in the three ethylbenzene experiments are fit to within the uncertainty of the data. There are no other types of incremental reactivity experiments in the case of ethylbenzene.

Both SAPRC-11 and SAPRC-11A consistently underpredicted integrated OH levels in the ethylbenzene - NO_x experiments, with average underprediction biases of 22±9%. There was no apparent dependence of the underprediction bias on initial NO_x or ethylbenzene / NO_x ratios, so plots of biases for individual experiments are not shown.

Propyl Benzenes

Several propylbenzene - NO_x experiments were carried out as part of our SOA mechanism development project, and these provide the first available mechanism evaluation data for these compounds. Plots and tables of model performance results for the SAPRC-11 mechanism are shown on Figure 17 for n-propyl benzene and on Figure 18 for isopropyl benzene. Both the initial NO_x and the propylbenzene / NO_x ratios were varied for both compounds, though the range of variation was much less than was the case for the compounds discussed previously. The average performance of the mechanisms in simulating various measures of model performance, including integrated OH levels, is indicated in Figure 5, above. There are no incremental reactivity experiments for the propylbenzenes, and propylbenzene mechanisms for SAPRC-11A were not developed because the initial NO_x levels for all these experiments were less than ~130 ppb, so the mechanistic parameter affecting the simulations at higher NO_x levels (the OH-aromatic adduct + O_2 rate constant) could not be determined.

Figure 17 and Figure 18 shows that the SAPRC-11 mechanism simulated the $\Delta([O3]-[NO])$ data from the available propylbenzene - NO_x chamber experiments reasonably well, with no apparent dependence of model errors on initial NO_x and propylbenzene / NO_x ratios. It may be that there would be an overprediction bias at higher NO_x levels that might be corrected by developing a propylbenzene version of SAPRC-11A but this could not be determined, and separate SAPRC-11A mechanisms could not be developed, without experiments at higher NO_x levels.

As with most of the other aromatic compounds studied, the model tended to underpredict the integrated OH levels in the propylbenzene - NO_x experiments, with the average underprediction biases being 16±11% for n-propyl benzene and 26±11% for isopropyl benzene. There was no apparent consistent dependence of IntOH model error on initial reactant concentrations.

n-Propyl Benzene

Number of Runs	4

Average Model Bias

Formation Rate (low NOx)	-4%
Formation Rate (all runs)	-6%
Maximum Ozone Yield	16%

Average Model Error

Formation Rate (low NOx)	4%
Formation Rate (all runs)	7%
Maximum Ozone Yield	16%

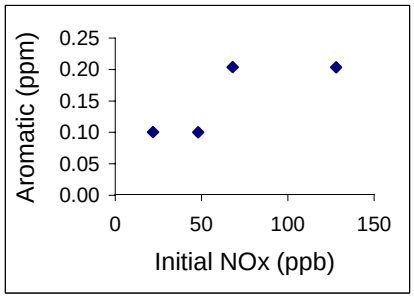

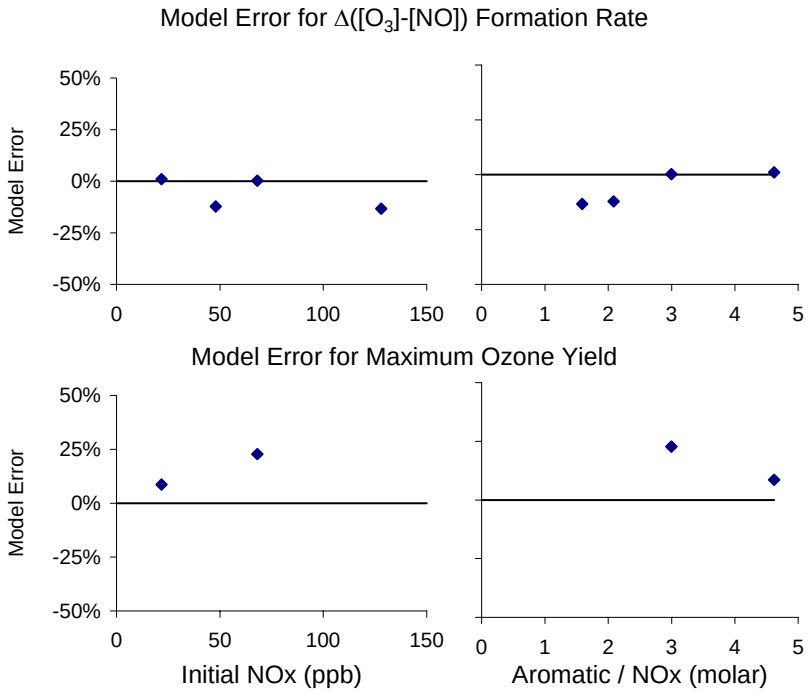

Figure 17. Plots and tables of selected model performance results for the n-propyl benzene - NO_x experiments using the SAPRC-11 mechanism

Isopropyl Benzene

Number of Runs	6

Average Model Bias

Formation Rate (low NOx)	3%
Formation Rate (all runs)	3%
Maximum Ozone Yield	-1%

Average Model Error

Formation Rate (low NOx)	6%
Formation Rate (all runs)	6%
Maximum Ozone Yield	5%

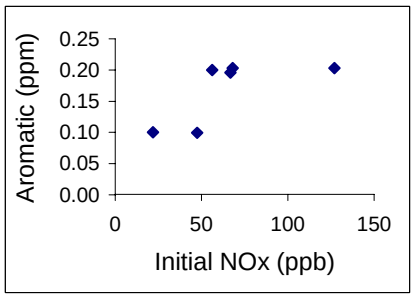

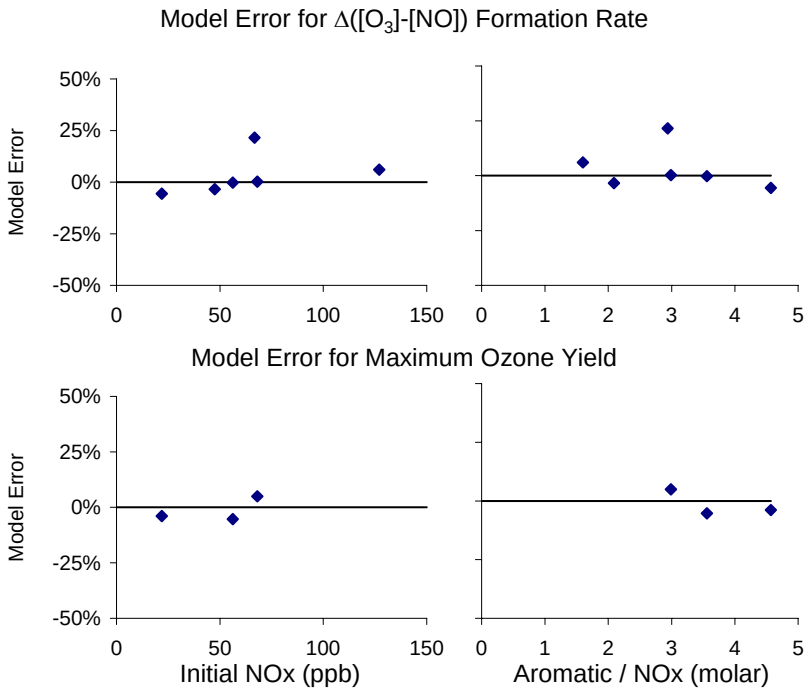

Figure 18. Plots and tables of selected model performance results for the isopropyl benzene - NO_x experiments using the SAPRC-11 mechanism

O- and M-Xylene

The model performance in simulating the experiments with o- and m-xylene were found to be similar, so the results for these two compounds are discussed together. Plots and tables of selected model performance results for the SAPRC-11 mechanism are shown on Figure 19 for m-xylene and on Figure 20 for o-xylene, and plots showing model performance for the incremental reactivity experiments for these compounds are shown on Figure 21 and Figure 22. In addition, Figure 23 shows plots of model errors in simulations of the integrated OH levels against initial NO_x and initial aromatic / NO_x ratios for these two compounds. Figure 19 shows that a very large number of m-xylene - NO_x experiments were carried out, covering about two orders of magnitude in initial NO_x and initial xylene / NO_x concentrations for both blacklight and arc light experiments. Somewhat experiments were carried out with o-xylene, though the range of initial conditions covered was almost as large, though only high NO_x experiments are available with arc lights.

Figure 19 and Figure 20 show similar performance in the SAPRC-11 simulations of the m- and o-xylene - NO_x experiments. It can be seen that there is no apparent dependence of model error on initial NO_x levels for both compounds, which means that there was no need to develop SAPRC-11A mechanisms for these compounds. On the other hand, there is a dependence of model error on aromatic / NO_x ratios for both compounds, as was also seen for toluene with SAPRC-11A (see Figure 11). The model had no significant overall biases in simulations of maximum O_3 yields even though the parameters were optimized to fit NO oxidation and O_3 formation rates. Figure 21 and Figure 22 shows that the SAPRC-11 mechanism also gives reasonably good simulations of Δ([O3]-[NO]) incremental reactivity results.

Figure 5 shows that the SAPRC-11 mechanism tends to underpredict integrated OH radical levels for these xylenes by about the same amount as for most of the other aromatic hydrocarbons. Figure 23 shows that this bias does not have a strong dependence on initial NO_x levels or aromatic / NO_x ratios, though there may be a slight dependence on aromatic / NO_x ratios and the underprediction bias may be slightly less for o-xylene experiments with initial NO_x levels greater than 100 ppb. However, these apparent dependences are not large compared to run-to-run scatter, and may not be significant. Despite the general underprediction bias for integrated OH in the xylene - NO_x experiments, the model gives reasonably good simulations of the effects of adding the xylenes on OH radical levels in the incremental reactivity experiments (Figure 21 and Figure 22).

The m-xylene experiments are also useful for evaluating the effects of the light source on mechanism evaluation results, because both arc light and blacklight experiments covered a wide range of initial reactant levels (see Figure 19). As with toluene (see Figure 10), the results on Figure 19 indicate no significant effect of light source in simulations of the m-xylene - NO_x experiments.

P-Xylene

Somewhat different evaluation results were obtained with p-xylene than the other xylene isomers, so the results with this compound are discussed separately. Plots and tables of selected model performance results in the p-xylene - NO_x experiments are shown on Figure 24 for SAPRC-11 and on Figure 25 for SAPRC-11A, and the performance of these two mechanisms in simulating the results of the single incremental reactivity experiment with p-xylene is shown in Figure 22, above. Figure 26 shows plots of model errors against initial NO_x or initial xylene / NO_x ratios in simulations of the integrated OH levels in the p-xylene - NO_x experiments for the two mechanisms. Figure 24 shows that the p-xylene - NO_x experiments cover a range of initial NO_x levels of almost two orders of magnitude and approximately an order of magnitude range of initial xylene / NO_x ratios. Several arc light experiments

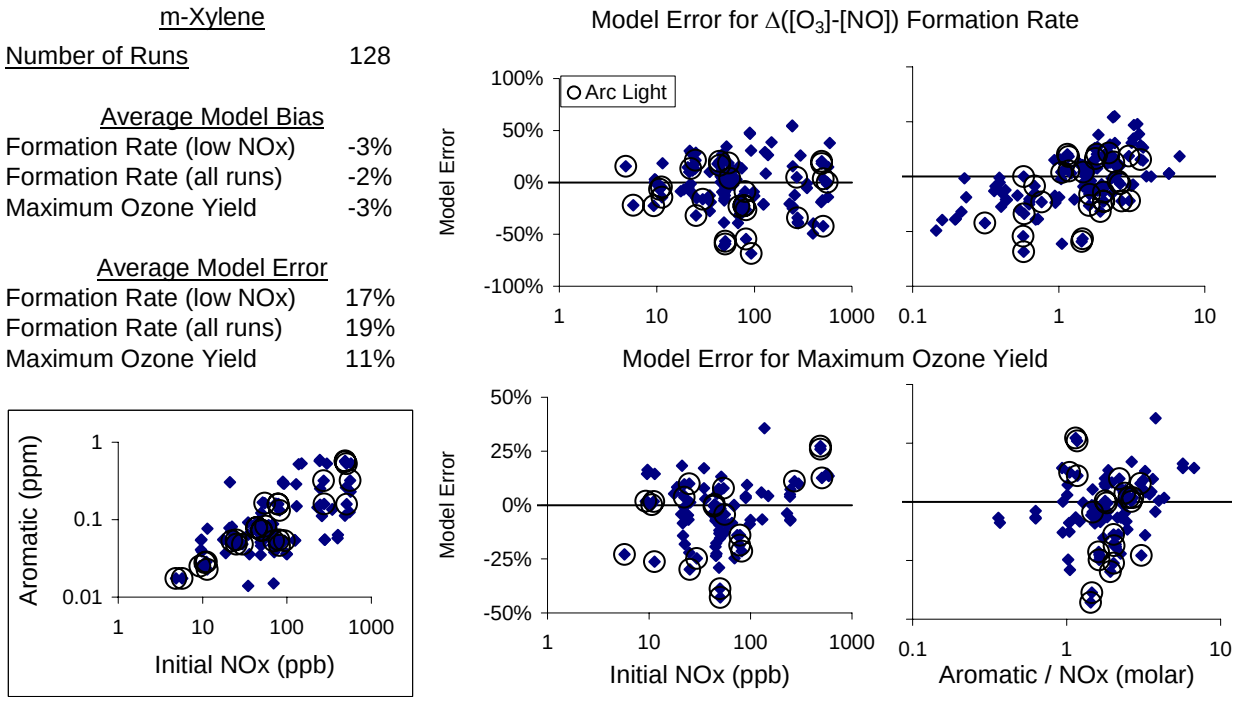

Figure 19. Plots and tables of selected model performance results for the m-xylene - NO_x experiments using the SAPRC-11 mechanism.

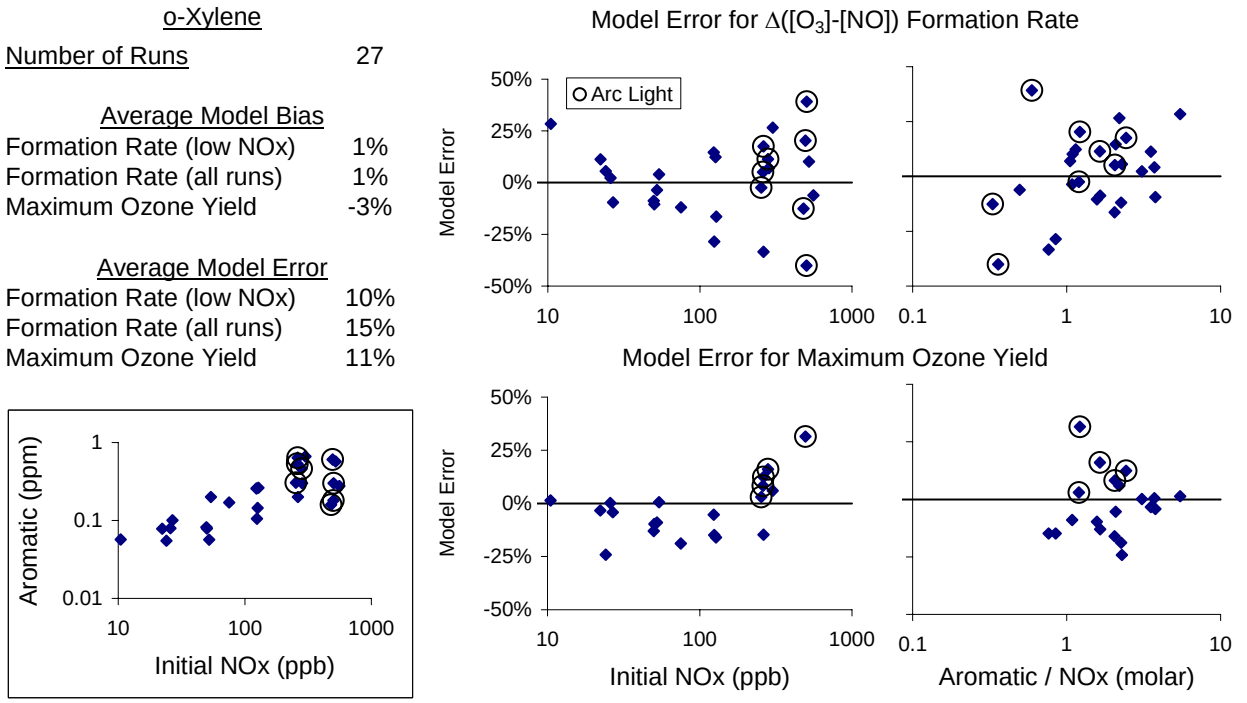

Figure 20. Plots and tables of selected model performance results for the o-xylene - NO_x experiments using the SAPRC-11 mechanism.

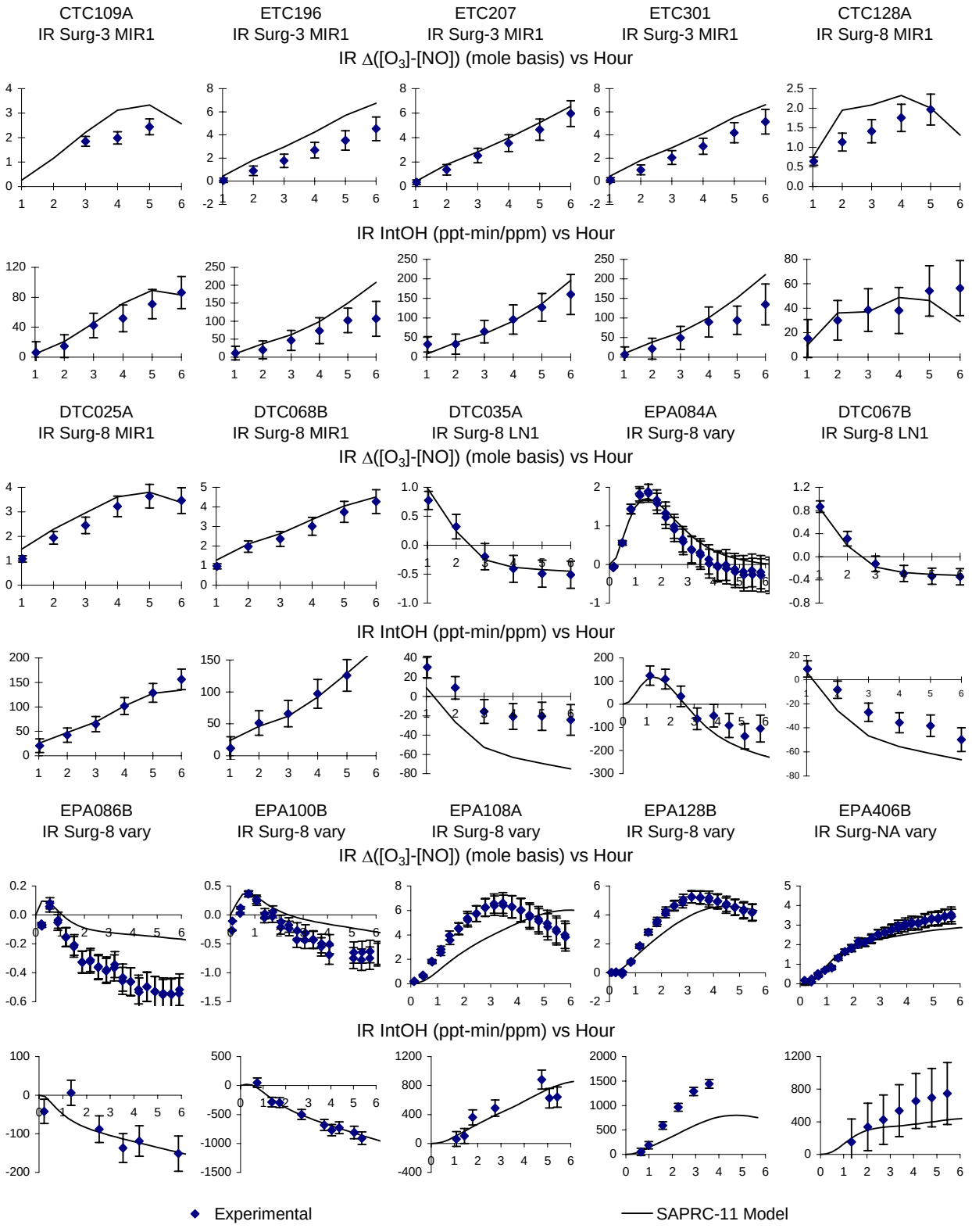

Figure 21. Plots of selected incremental reactivity evaluation results for m-xylene.

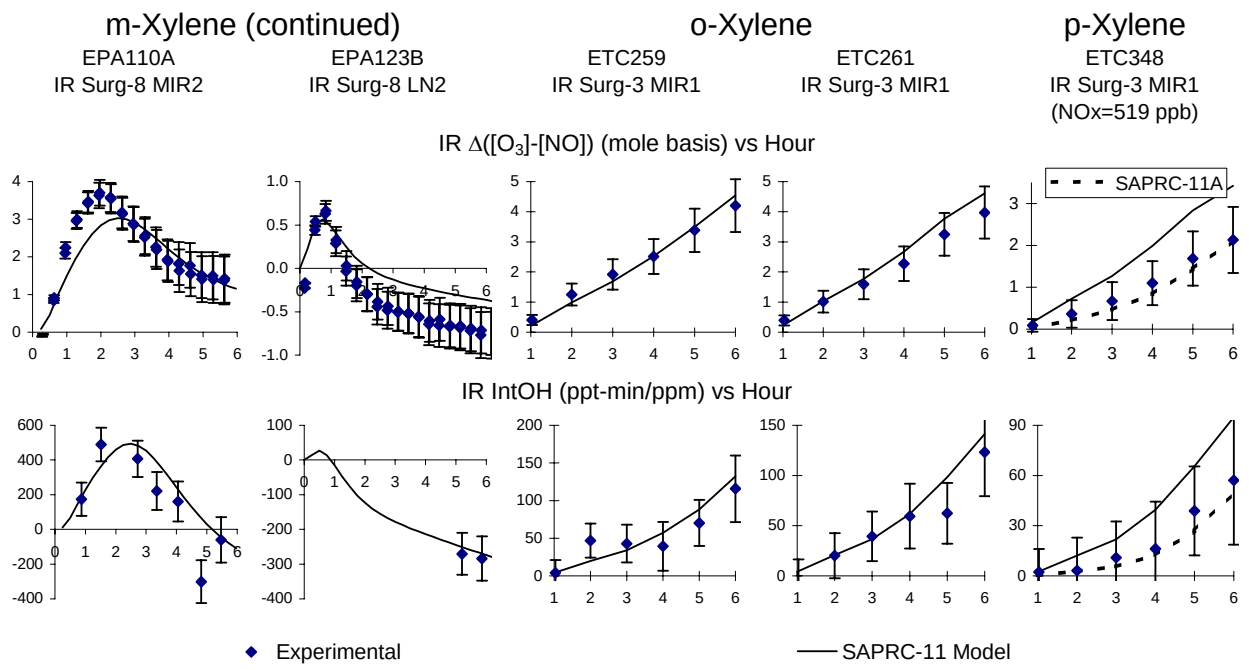

Figure 22. Plots of selected incremental reactivity evaluation results for m-, o- and p-xylenes.

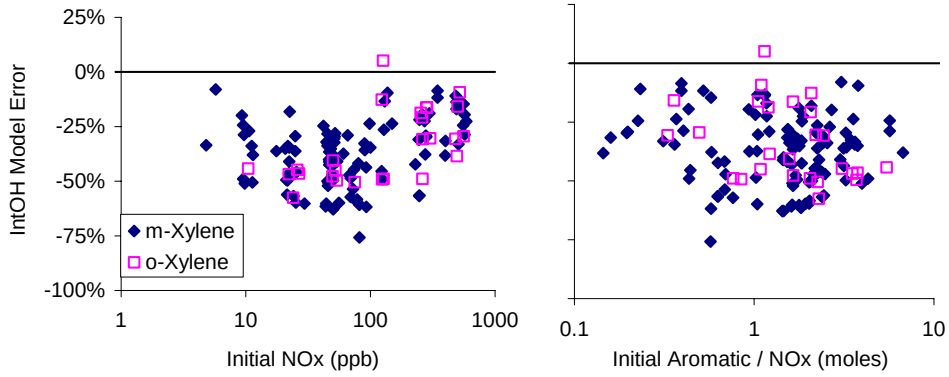

Figure 23. Plots of model errors for simulations of the integrated OH levels in the m- and o-xylene - NO_x experiments with the SAPRC-11 mechanism.

were conducted with this compound, but only for NO_x levels greater than about 250 ppb. On the other hand, only two blacklight experiments were conducted at the higher NO_x levels.

Figure 24 shows that, like benzene, toluene, and ethylbenzene but unlike the other xylene isomers, the SAPRC-11 mechanism consistently underpredicts the $\Delta([O_3]-[NO])$ formation rates at the higher NO_x levels, and Figure 25 shows that this bias can be removed using the SAPRC-11A mechanism with suitable parameters. However, although the additional NO_x-dependence included in SAPRC-11A removes the dependence of the $\Delta([O_3]-[NO])$ formation rate model errors on initial NO_x levels, there is a significant dependence of these model errors for SAPRC-11A on the initial aromatic / NO_x ratios, which

p-Xylene

Number of Runs	29
Average Model Bias	
Formation Rate (low NOx)	4%
Formation Rate (all runs)	33%
Maximum Ozone Yield	-12%
Average Model Error	
Formation Rate (low NOx)	13%
Formation Rate (all runs)	38%
Maximum Ozone Yield	13%

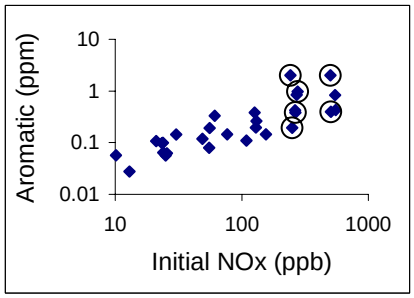

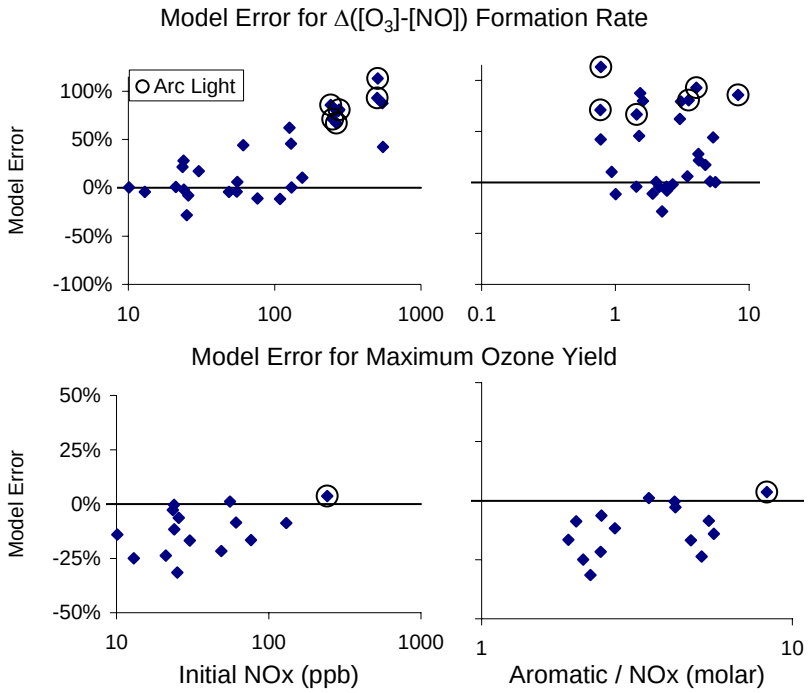

Figure 24. Plots and tables of selected model performance results for the p-xylene - NO_x experiments using the SAPRC-11 mechanism.

p-Xylene (Model "A")

Number of Runs	29
Average Model Bias	
Formation Rate (low NOx)	-1%
Formation Rate (all runs)	-3%
Maximum Ozone Yield	-15%
Average Model Error	
Formation Rate (low NOx)	14%
Formation Rate (all runs)	17%
Maximum Ozone Yield	15%

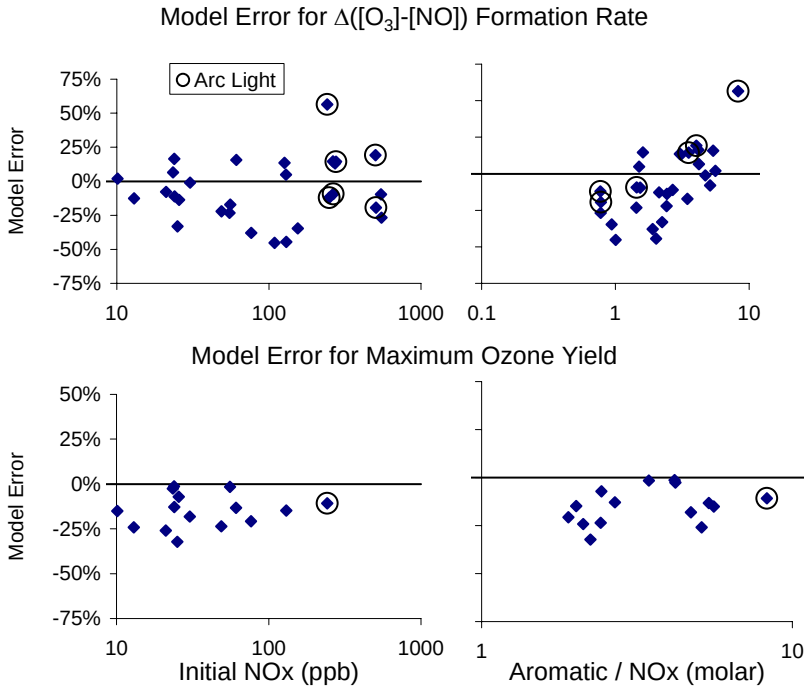

Figure 25. Plots and tables of selected model performance results for the p-xylene - NO_x experiments using the SAPRC-11A mechanism.

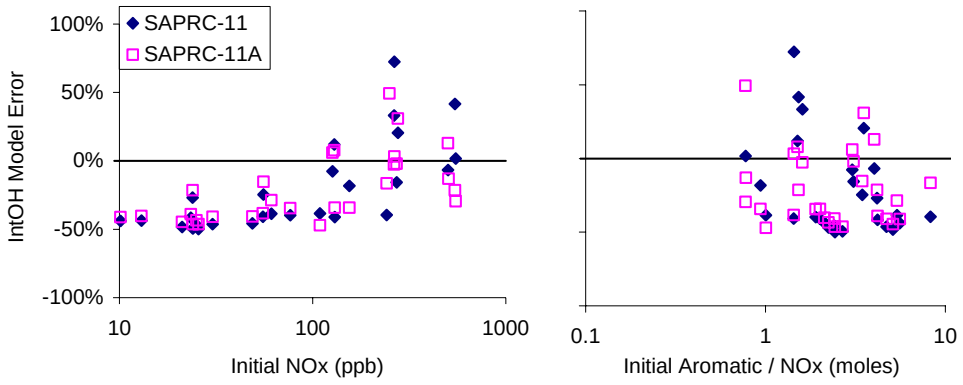

Figure 26. Plots of model errors for simulations of the integrated OH levels in the p-xylene - NO_x experiments with the SAPRC-11 and SAPRC-11A mechanisms.

is not seen for SAPRC-11. The updated mechanisms tend to somewhat underpredict maximum O_3 yields for p-xylene, though this problem is not as great as with SAPRC-07 (see Figure 5).

The single incremental reactivity experiment with p-xylene is shown on the right hand plots on Figure 22. This is a high NO_x, low ROG/NO_x "MIR1" experiment, and, as was the case for benzene (Figure 9), toluene (Figure 12) and ethylbenzene (Figure 16), the SAPRC-11 mechanism overpredicts the $\Delta([O_3]-[NO])$ reactivity in this experiment (right plots on Figure 22). However, this overprediction in the p-xylene reactivity experiment is somewhat less than was the case with the other compounds. As was the case with the other compounds, the SAPRC-11A gave better simulations of the reactivity results with p-xylene, fitting the data to within the experimental uncertainty.p-Xylene tended to have somewhat lower average model errors for underpredicting integrated OH levels in the aromatic - NO_x experiments than was the case for the other aromatics, but also much greater run-to-run variability (see Figure 5 and Figure 6). Figure 26 shows that this is due to the p-xylene experiments at the higher NO_x levels, where SAPRC-11 tends to overpredict OH levels and SAPRC-11A appears to have no net negative bias. When the initial NO_x is less than about 100 ppb the models underpredict OH levels with no apparent dependence on conditions and by about the same amount as observed for the other aromatics.

The possibility that the apparent differences in model performance between the high and low NO_x experiments may be due to a light source effect cannot be totally ruled out, since most of the high NO_x experiments were carried out using arc lights and all of the lower NO_x experiments were carried out using blacklights. However, the evaluation results for the few higher NO_x blacklight experiments were reasonably consistent with the arc light experiments in this concentration range.

Ethyl Toluenes

Several ethyltoluene - NO_x experiments were carried out for each of the three ethyltoluene isomers as part of our SOA mechanism development project, and these provide the first available mechanism evaluation data for these compounds. Plots and tables of model performance results for the SAPRC-11 mechanism are shown on Figure 27, Figure 28, and Figure 29 for o-, m-, and p-ethyltoluene, respectively. Both the initial NO_x and the propylbenzene / NO_x ratios were varied for these compounds, though the range of variation was much less than was the case for some of the compounds discussed previously. The average performance of the mechanisms in simulating various measures of model performance, including integrated OH levels, is indicated in Figure 5, above. There are no incremental reactivity experiments for the ethyltoluenes, and ethyltoluene mechanisms for SAPRC-11A were not

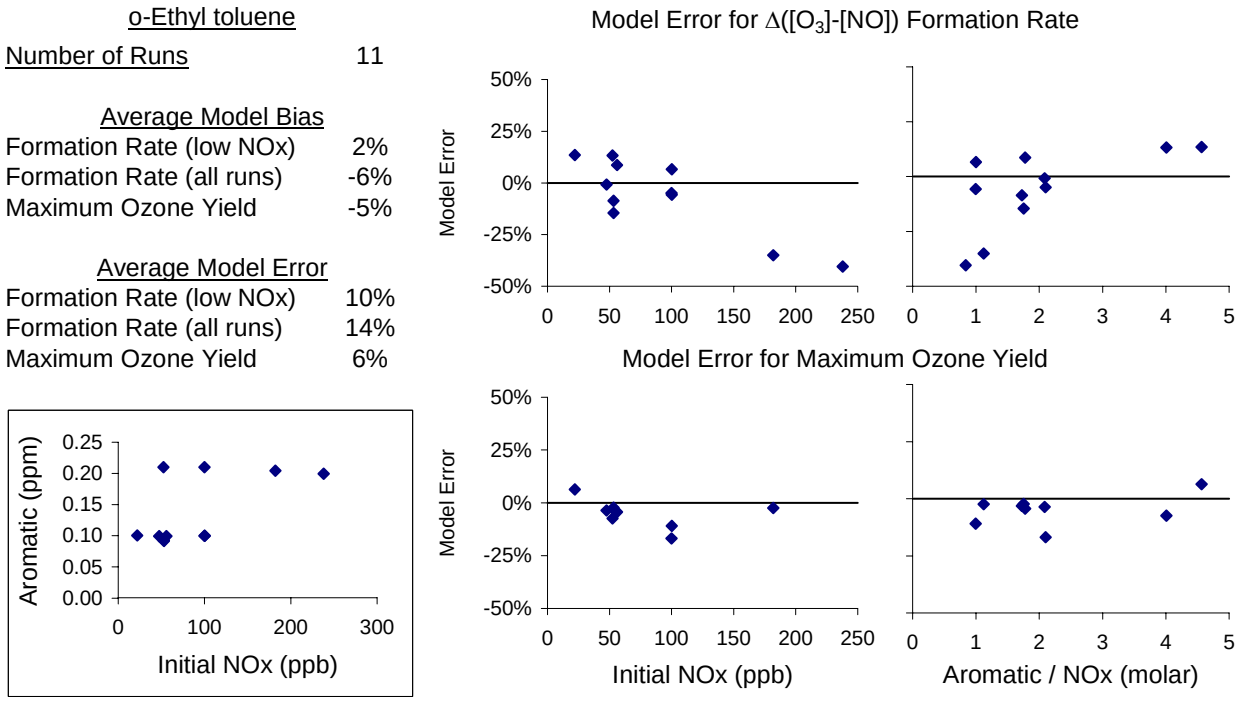

Figure 27. Plots and tables of selected model performance results for the o-ethyl toluene - NO_x experiments using the SAPRC-11 mechanism.

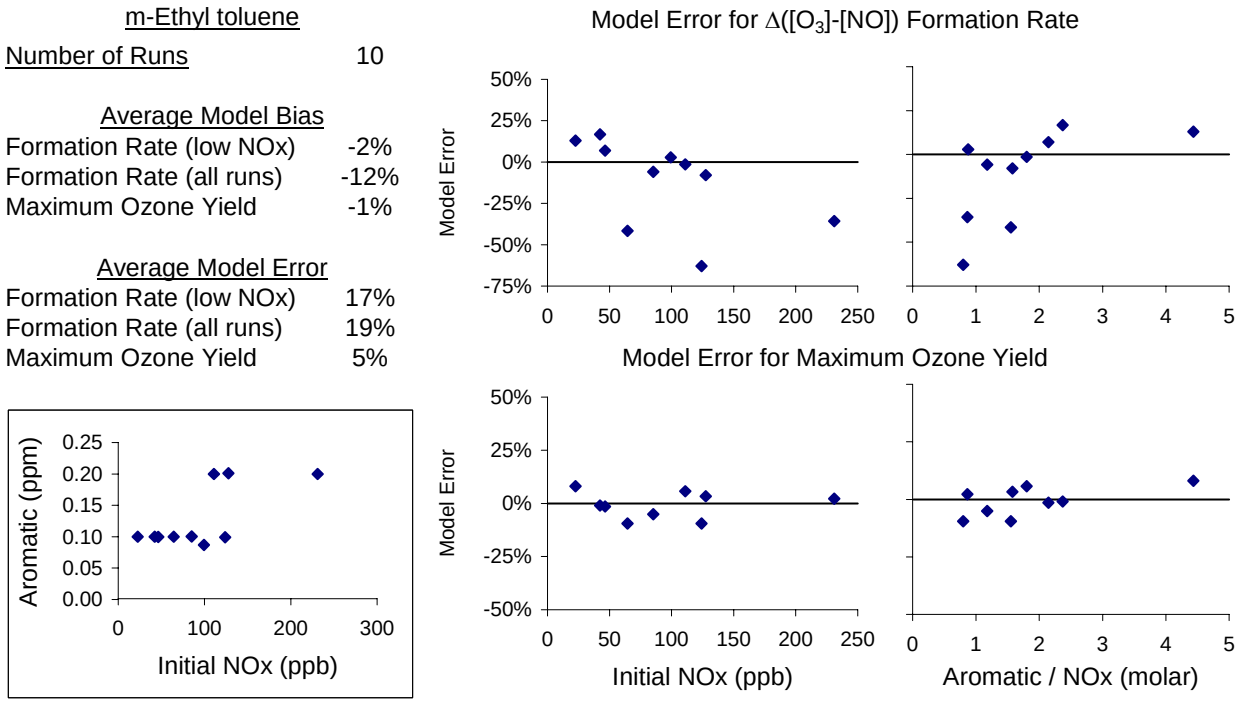

Figure 28. Plots and tables of selected model performance results for the m-ethyl toluene - NO_x experiments using the SAPRC-11 mechanism.

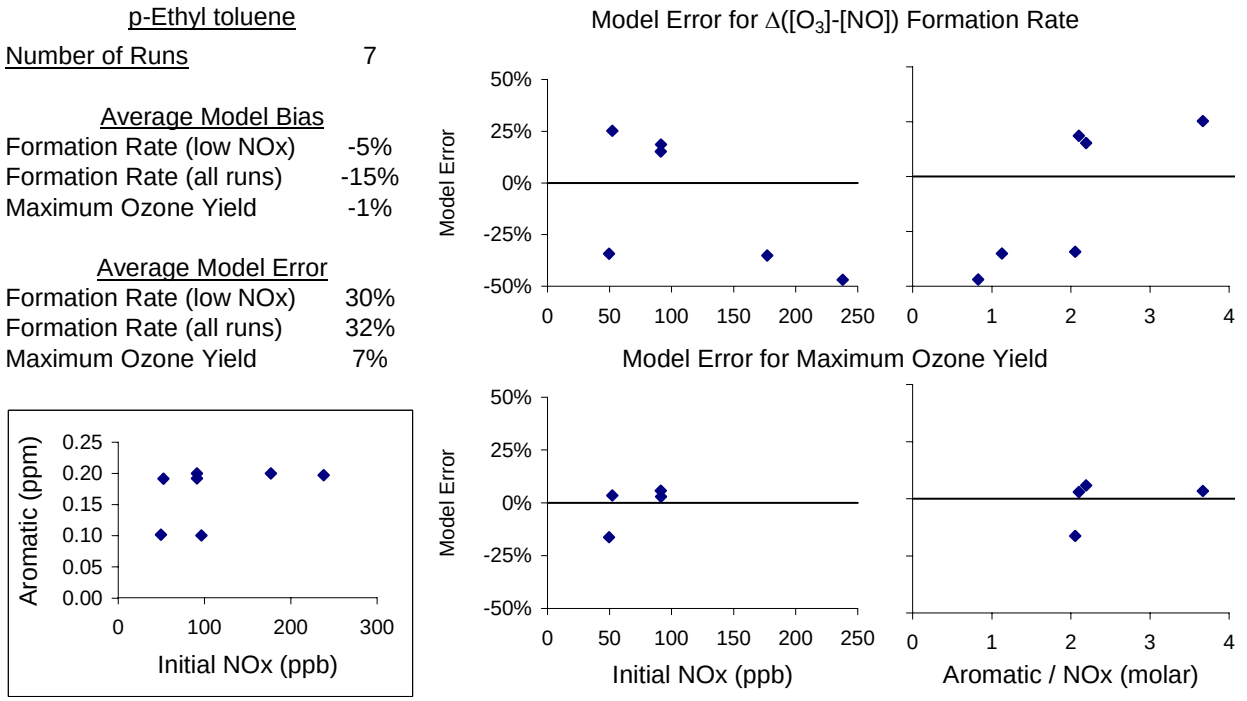

Figure 29. Plots and tables of selected model performance results for the p-ethyl toluene - NO_x experiments using the SAPRC-11 mechanism.

developed because there were no experiments with NO_x levels greater than ~250 ppb, and few with NO_x levels greater than 100 ppb.

Figure 27 through Figure 29 show that the SAPRC-11 mechanism gave moderately good simulations of the $\Delta([O_3]-[NO])$ data, though as with many of the other aromatics there appears to be a tendency for the model error to depend on the initial aromatic / NO_x ratio, with a tendency to underpredict at low ratios. There is no tendency for the model to overpredict reactivity in high NO_x experiments, indicating that use of SAPRC-11A would probably not give better results. (If anything, there might be a slight tendency to underpredict at higher NO_x, but the trend is probably not significant.) Figure 5 shows that the maximum O_3 yields are well simulated for all three compounds, but that the model consistently underpredicts OH levels in the ethyltoluene - NO_x experiments. The OH underprediction is relatively consistent from run to run (as indicated by the relatively small error bars on Figure 5), and is somewhat higher than is the case for the other compounds.

Trimethylbenzenes

Plots and tables of model performance results for the SAPRC-11 mechanism are shown on Figure 30, Figure 31, and Figure 32 for 1,2,3-, 1,2,4-, and 1,3,5-trimethylbenzenes, respectively, and Figure 33 shows model performance for the simulations of the incremental reactivity experiments for these compounds. Plots of model errors for integrated OH levels against initial NO_x and initial trimethylbenzene / NO_x ratios are shown on Figure 34. The average performance of the mechanisms in simulating various measures of model performance, including integrated OH levels, is indicated in Figure 5, above. Experiments with these compounds were carried out with NO_x levels varying by almost two orders of magnitude and with initial trimethylbenzene / NO_x ratios varying by over an order of magnitude.

1,2,3-trimethylbenzene

Number of Runs	13
Average Model Bias	
Formation Rate (low NOx)	-1%
Formation Rate (all runs)	-7%
Maximum Ozone Yield	-3%
Average Model Error	
Formation Rate (low NOx)	8%
Formation Rate (all runs)	10%
Maximum Ozone Yield	7%

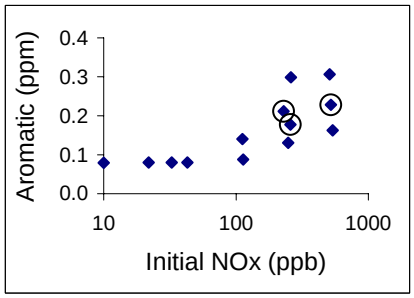

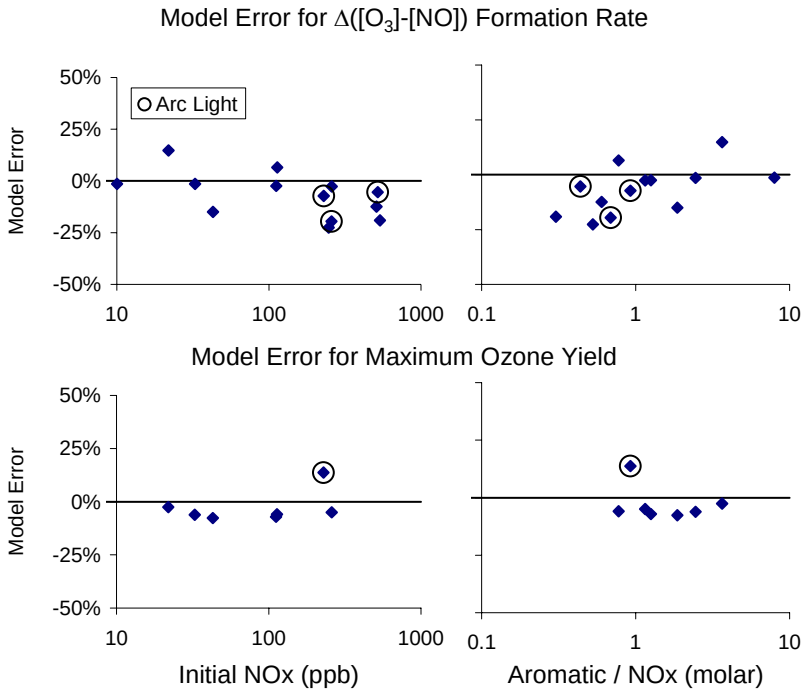

Figure 30. Plots and tables of selected model performance results for the 1,2,3-trimethylbenzene - NO_x experiments using the SAPRC-11 mechanism.

1,2,4-trimethylbenzene

Number of Runs	27
Average Model Bias	
Formation Rate (low NOx)	-4%
Formation Rate (all runs)	-2%
Maximum Ozone Yield	-6%
Average Model Error	
Formation Rate (low NOx)	10%
Formation Rate (all runs)	28%
Maximum Ozone Yield	8%

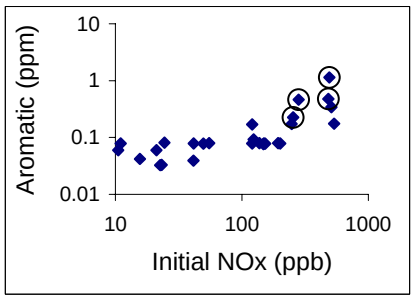

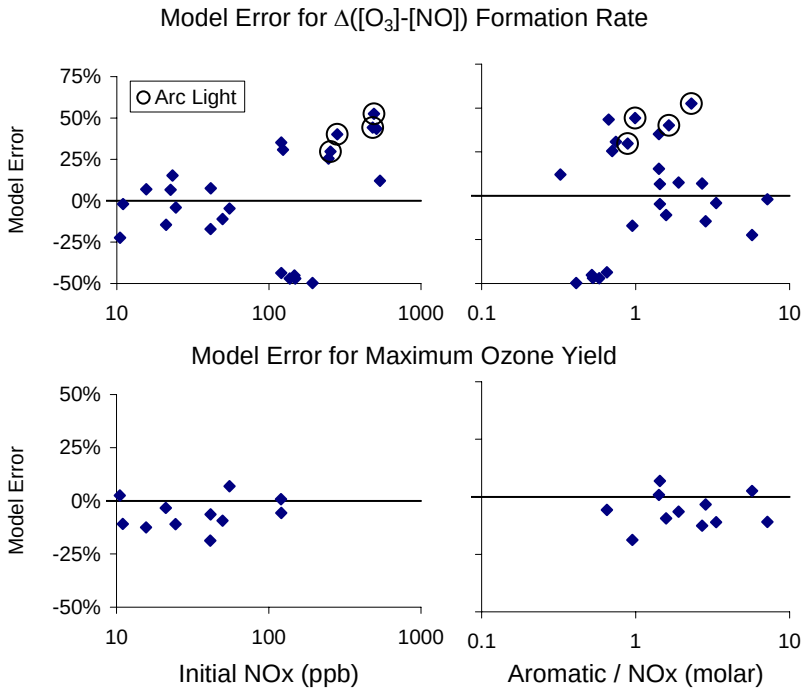

Figure 31. Plots and tables of selected model performance results for the 1,2,4-trimethylbenzene - NO_x experiments using the SAPRC-11 mechanism.

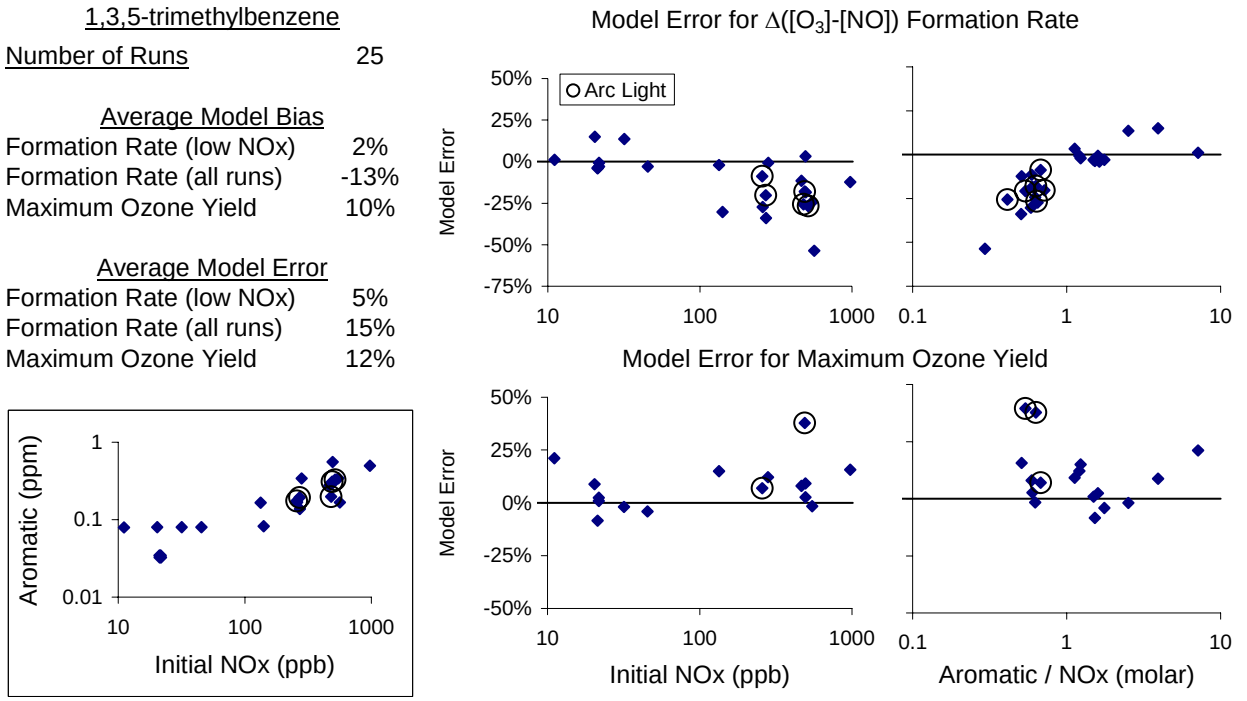

Figure 32. Plots and tables of selected model performance results for the 1,3,5-trimethylbenzene - NO_x experiments using the SAPRC-11 mechanism.

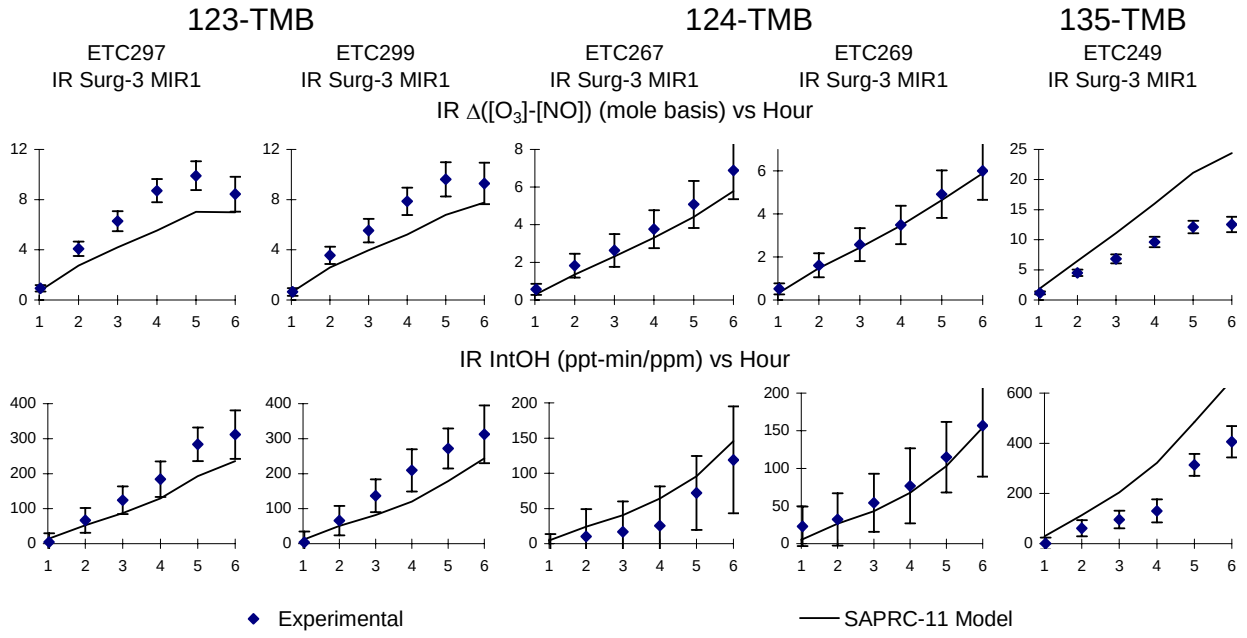

Figure 33. Plots of selected incremental reactivity evaluation results for the trimethylbenzene isomers.

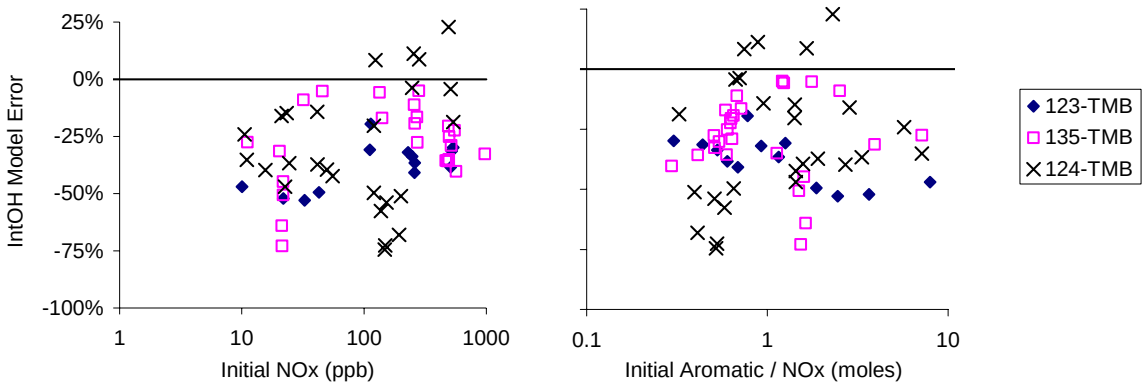

Figure 34. Plots of model errors for simulations of the integrated OH levels in the trimethylbenzene - NO_x experiments with the SAPRC-11 mechanism.

However, arc light experiments are limited to the higher NO_x levels, so comprehensive information on effects of light source is not available.

As with the ethyltoluenes, the SAPRC-11 mechanism gave moderately good simulations of the $\Delta([O_3]-[NO])$ data, though again there appears to be a dependence of $\Delta([O_3]-[NO])$ model error on the initial aromatic / NO_x ratio, with a tendency to underpredict at low ratios. The incremental reactivity results for $\Delta([O_3]-[NO])$ are simulated reasonably well, though the overprediction for the single 1,3,5-trimethylbenzene experiment may be outside the range of experimental uncertainty (see Figure 33). The model gives good simulations of the maximum O_3 yields for the 1,2,3- and 1,3,5- isomers, but tends to underpredict maximum O_3 somewhat for 1,2,4-trimethylbenzene, though probably not outside the run-to-run variability of the data. As with the other aromatics, the model tends to underpredict the integrated OH levels in the experiments, though the run-to-run variability in the model error, as shown on Figure 34, is relatively high, and too great to determine whether there is a dependence of model error on initial reactant concentrations.

Phenolic Compounds

Because of their suspected importance in SOA formation from aromatic compounds, a number of experiments with representative phenolic aromatic oxidation products were carried out as part of our aromatic SOA project. These experiments provide a significant expansion of the mechanism evaluation database for these phenolic compounds, including data with lower NO_x levels than were available previously. The SAPRC-07 uses the model species "CRES" to represent all phenolic compounds, and the mechanism for that model species is based on simulations of only a single o-cresol - NO_x experiment carried out in the SAPRC evacuable chamber (EC281) with about 0.5 ppm NO_x. Data are now available for phenol, o-cresol, and 2,4-dimethylphenol, allowing for separate mechanisms to be developed for these three types of phenolic compounds. Unfortunately all the new experiments with these compounds were carried out using blacklights, with the only experiment with arc lights being the single o-cresol - NO_x run used to develop the CRES model for SAPRC-07.

Plots and tables of model performance results for the SAPRC-11 mechanism are shown on Figure 35, Figure 36, and Figure 37 for phenol, o-cresol, and 2,4-dimethylphenol, respectively, and Figure 38 shows model performance for the simulations of the single incremental reactivity experiment with a phenolic compound, specifically m-cresol. The experiments with phenol and 2,4-dimethylphenol

Phenol

Number of Runs	5

Average Model Bias

Formation Rate (low NOx)	-4%
Formation Rate (all runs)	-8%
Maximum Ozone Yield	3%

Average Model Error

Formation Rate (low NOx)	26%
Formation Rate (all runs)	26%
Maximum Ozone Yield	10%

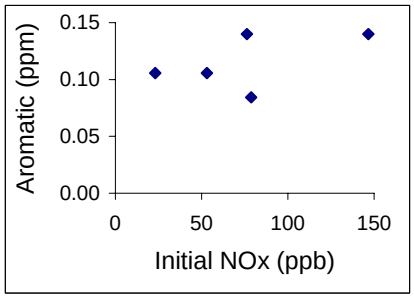

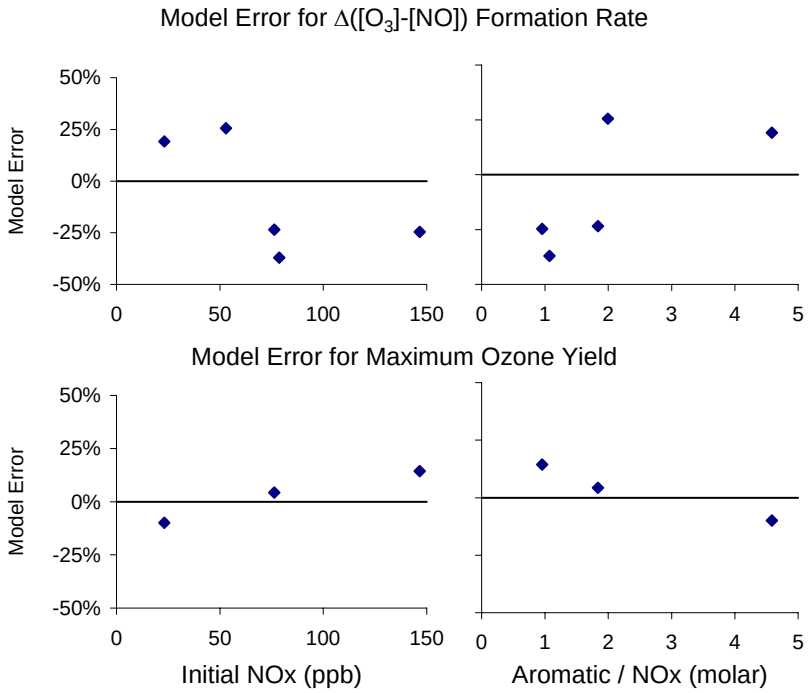

Figure 35. Plots and tables of selected model performance results for the phenol - NO_x experiments using the SAPRC-11 mechanism.

o-Cresol

Number of Runs	7

Average Model Bias

Formation Rate (low NOx)	-4%
Formation Rate (all runs)	8%
Maximum Ozone Yield	23%

Average Model Error

Formation Rate (low NOx)	14%
Formation Rate (all runs)	29%
Maximum Ozone Yield	23%

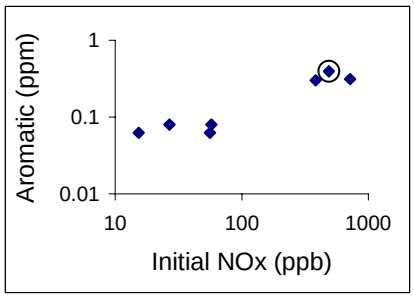

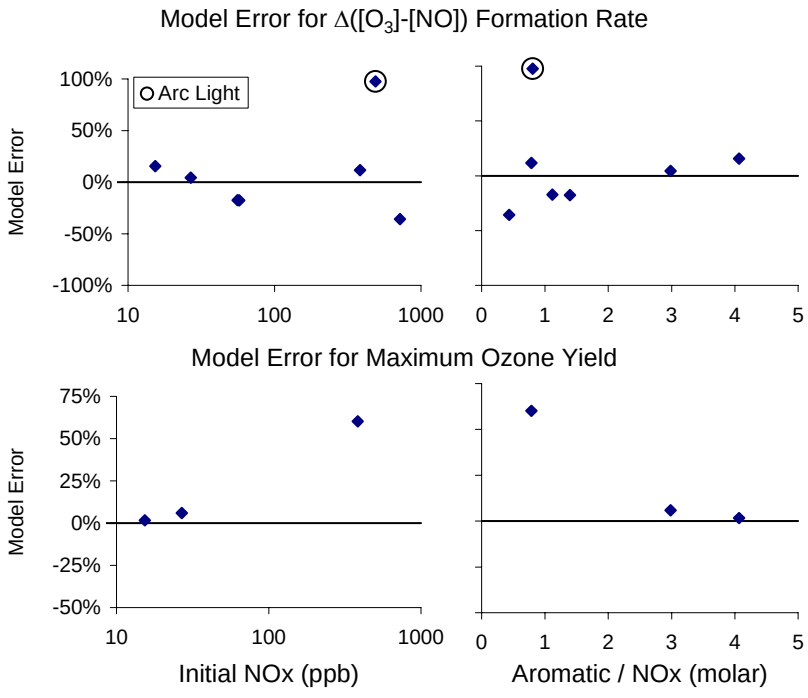

Figure 36. Plots and tables of selected model performance results for the o-cresol - NO_x experiments using the SAPRC-11 mechanism.

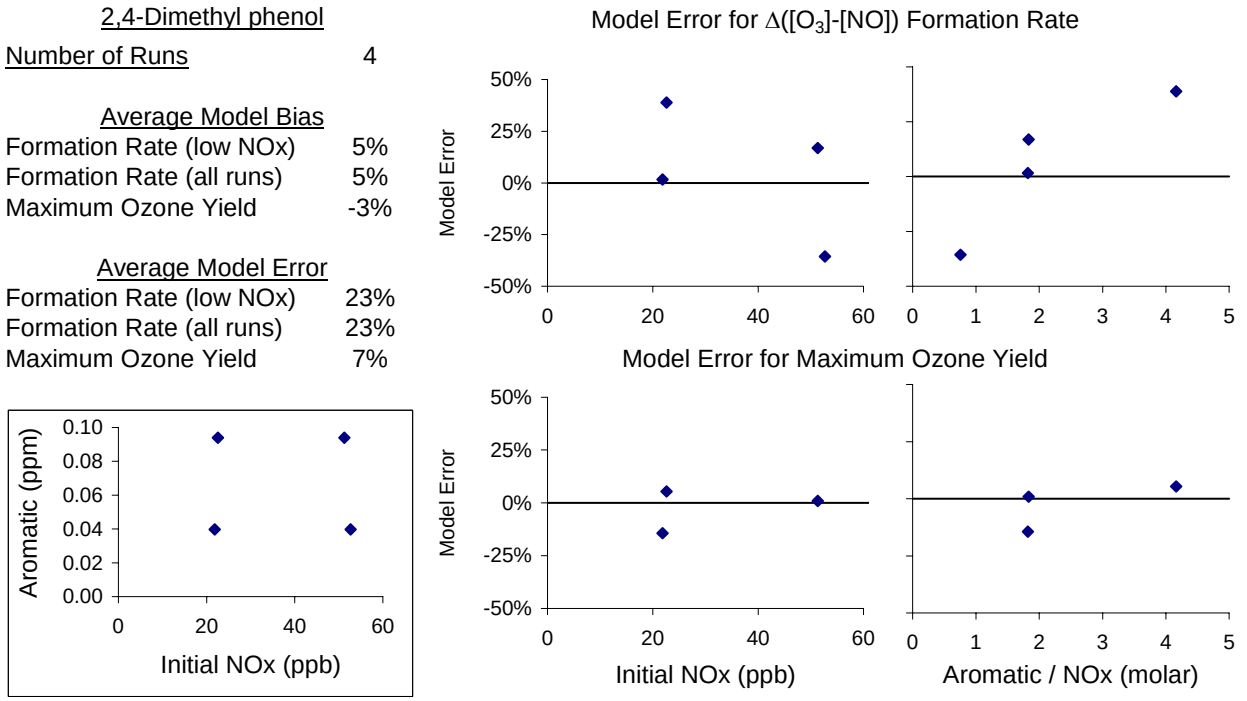

Figure 37. Plots and tables of selected model performance results for the 2,4-dimethyl phenol - NO_x experiments using the SAPRC-11 mechanism.

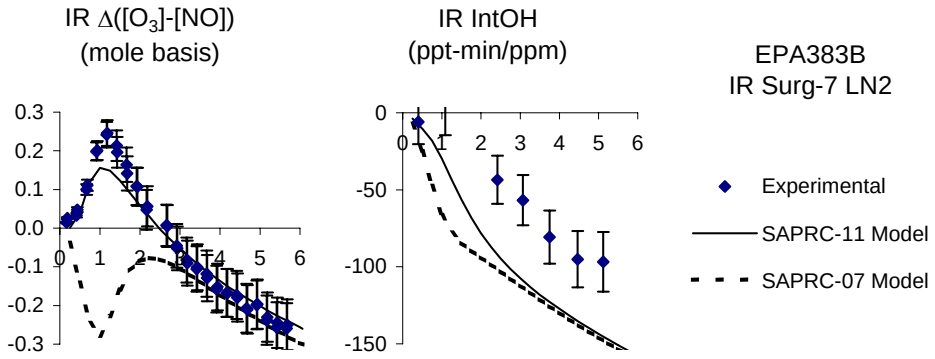

Figure 38. Plots of selected incremental reactivity evaluation results for the m-cresol. Results are shown for both SAPRC-11 (solid lines) and SAPRC-07 (dashed lines).

were carried out over relatively limited concentration ranges, though both initial NO_x and initial compound / NO_x ratios were varied, while the o-cresol experiments were carried out with NO_x levels varying by almost two orders of magnitude and the initial cresol / NO_x ratio varied by approximately a factor of 5. Data could not be obtained on model simulations of OH radical levels because consumption rates of phenolic compounds could not be used to derive OH radical levels due to the fact that they are also consumed by reactions with NO_3 radicals.

Although there is somewhat greater variability than observed with the aromatic hydrocarbons, the model gave fair simulations of the $\Delta([O_3]-[NO])$ data for all three of these compounds, though it should be noted that the parameterized model was formulated and adjusted to simulate these data. The notable outlier is EC281, the single high NO_x, arc light o-cresol experiment used to develop the SAPRC-07 cresol mechanism, which SAPRC-11 significantly overpredicted the rate of NO oxidation and O_3 formation (see the circled point on Figure 36). The SAPRC-07 cresol mechanism was adjusted to fit that single experiment, and consequently it significantly underpredicted the NO oxidation and O_3 formation rates in all the other experiments with the phenolic compounds (see Figure 5). Note that this does not appear to be a concentration effect, since several newer experiments were conducted at a similar concentration range where the performance of SAPRC-11 was comparable to its performance for the lower concentration experiments. Other than the results for EC281 for o-cresol, there does not appear to be any NO_x dependence in the model errors that indicate that use of the additional NO_x dependence in the SAPRC-11A mechanism would give better fits to the data.

The possibility that the differences in results between the o-cresol evacuable chamber experiment EC281 and the more recent UCR EPA chamber experiments is due to a light source effect cannot be ruled out. The evacuable chamber uses an arc light source, while all the newer experiments were carried out using blacklights. Experiments were carried out with other cresol isomers around the time of EC281, and the results are shown on Figure 39, along with the results of a recent blacklight chamber experiments that was carried out using similar initial reactant concentrations. It can be seen that the SAPRC-11 mechanism significantly overpredicted the NO oxidation and O_3 formation rates in these evacuable chamber experiments, with SAPRC-07 performing significantly better for those experiments, while SAPRC-11 performed much better in simulating the recent blacklight experiment with similar initial reactant concentrations. Unfortunately, we were unable to conduct new arc light experiments to test this possibility.

Figure 38 shows that the SAPRC-11 mechanism for cresols gives good simulations of the $\Delta([O_3]-[NO])$ reactivity results in the only incremental reactivity experiment with a phenolic compound. On the other hand, the tendency of the cresol addition to inhibit OH levels is somewhat overpredicted. The performance of the SAPRC-07 cresol mechanism in simulating these data is also shown on Figure 38, where it can be seen that the performance of the updated mechanism is a significant improvement.

Surrogate - NO_x Experiments

It was noted previously (Carter, 2010a,b; Carter et al, 2005) that previous versions of the SAPRC mechanism had a tendency to underpredict $\Delta([O_3]-[NO])$ in ambient surrogate - NO_x experiments carried out in the UCR EPA chamber at lower ROG/NO_x ratios, though it gave generally good simulations at higher ROG/NO_x ratios. Although the reasons for this have not been comprehensively investigated, the bias at low ROG/NO_x was suspected to be due to problems with the aromatics mechanisms. To investigate whether this is also a problem with the updated mechanisms, we simulated the surrogate - NO_x experiments shown in Figure 14 of Carter (2010a) and in Figure 8 of Carter et al (2005) using the SAPRC-11 mechanism, and the results are shown in Figure 40. The results with SAPRC-07 are also shown for comparison. Separate plots are shown for experiments carried out using blacklights and arc lights and also for experiments carried out with aromatics removed from the surrogate ROG mixture.

The results on Figure 40 indicate that the problem with $\Delta([O_3]-[NO])$ underprediction at low ROG/NO_x ratios was improved only slightly when updating SAPRC-07 to SAPRC-11. Although the underprediction bias for SAPRC-11 is not quite as much as that for SAPRC-07 at the lowest ROG/NO_x ratios, it still exists, and there still is a dependence of the bias on this ratio. Note that the results for SAPRC-11 are the same as for SAPRC-07 for the non-aromatic surrogate because the major differences between SAPRC-07 and SAPRC-11 concern the aromatics mechanisms.

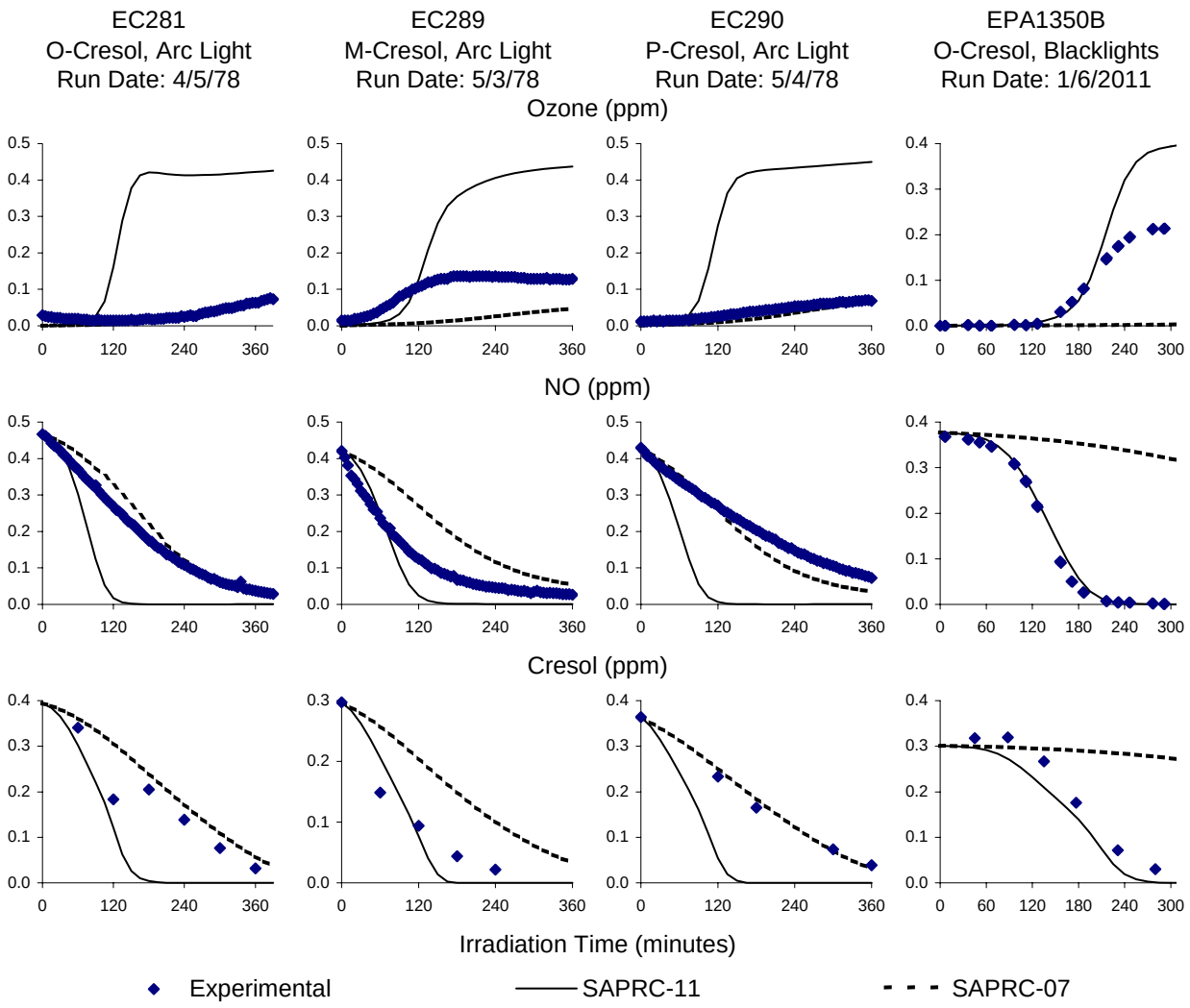

Figure 39. Selected experimental and model calculation results for the cresol - NO_x experiments carried out using different chambers and light sources with similar reactant concentrations.

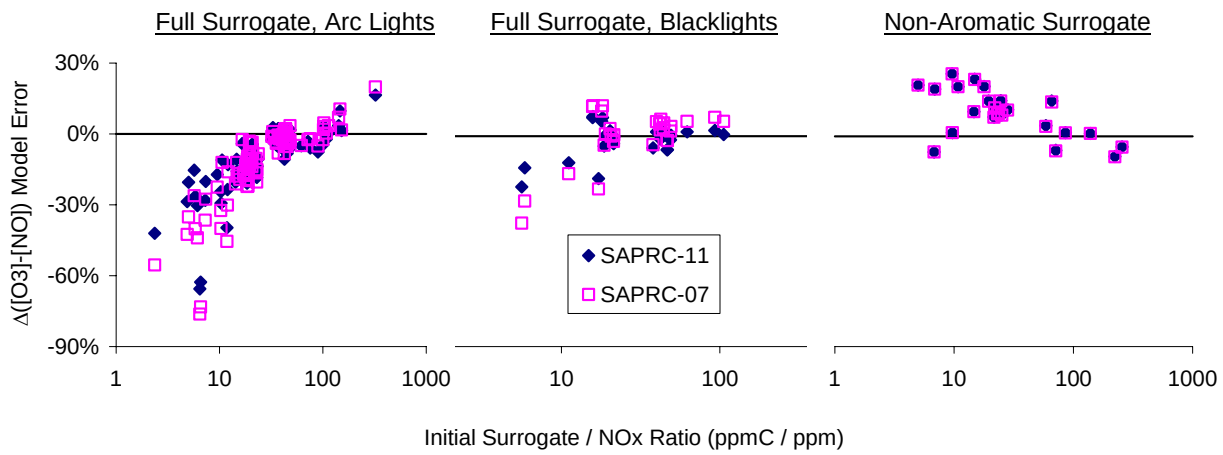

Figure 40. Plots of $\Delta([O_3]-[NO])$ model error against initial ROG/NO_x ratios for the surrogate - NO_x experiments.

ATMOSPHERIC SIMULATIONS

Methods

Atmospheric model simulations were carried out to assess the extent to which the changes in the mechanism from SAPRC-07 to SAPRC-11 affected model predictions of ambient ozone and relative ozone impacts (reactivities) of aromatics and other individual VOCs. The scenarios and methods used were the same as those used when calculating the MIR and other atmospheric ozone reactivity scales, and were described previously (Carter, 1994a,b 2000a, 2010a). The base ROG constituents were represented using the lumping procedures incorporated in the airshed version of the SAPRC-07 mechanism (Carter, 2010a). Note that this differs from the treatment of the base ROG mixture used in the environmental chamber simulations, where each compound was represented explicitly. However, the individual compounds whose reactivities were being assessed were represented explicitly, as was the case for the simulations of the chamber experiments.

As discussed previously (Carter, 1994a, 2010a), the scenarios used in the atmospheric simulations consisted of 1-day box model inputs originally developed by Baugues (1990) to represent ozone episodes in 39 urban areas in the United States, and adapted for reactivity simulations by Carter (1994a,b). The "Base" scenarios utilize the pollutant inputs developed by Baugues (1990) to represent the 39 areas and represent a range of reactive organic gas (ROG) and NO_x inputs and ROG/NO_x ratios. The maximum incremental reactivity (MIR) scenarios have the same inputs as the base scenarios except that the NO_x levels are adjusted for each scenario to yield maximum incremental reactivities of the base ROG inputs, or maximum sensitivity of O_3 to changes in VOC concentrations. These "MIR" scenarios are used as the basis for deriving the MIR scale (Carter, 1994a, 2000a, 2010a) that is used in regulatory and other applications. The NO_x inputs for the MIR scenarios are higher than those for all but one of the base scenarios. Likewise, the NO_x inputs in the maximum ozone incremental reactivity (MOIR) scenarios are adjusted to yield the maximum O_3 concentrations, and those for the equal benefit incremental reactivity (EBIR) scenarios are adjusted such that O_3 is equally sensitive to relative changes in NO_x and ROG inputs. In all cases, the NO_x inputs are MIR > MOIR > EBIR, with MIR and EBIR scenarios representing respectively high and low NO_x conditions where VOC reactivity is relevant for ozone formation. Ozone formation is significantly inhibited by NO_x when NO_x exceeds MIR levels, and is primarily sensitive to NO_x emissions when NO_x is lower than EBIR levels. The MOIR scenarios represent NO_x conditions that are optimum for O_3 formation.

In addition to these various city-specific scenarios, Carter (1994a,b) also developed an "averaged conditions" scenario based on averages of the inputs of the 39 base case scenarios developed by Baugues (1990). These scenarios are used with varying NO_x inputs to assess how mechanism differences vary as a function of NO_x inputs, with all other conditions held constant. In addition, the MIR version of the averaged conditions scenario was used for comparing the effects of the mechanism changes on incremental reactivities of a wide range of individual VOCs. These "averaged conditions MIR" values are generally very close to the standard MIR values calculated by averaging the reactivities in the city-specific MIR scenarios (Carter, 2000a), and provide a useful indication of the effects of mechanism changes on the MIR scale.

The airshed version of the SAPRC-11 mechanism consisted of the base SAPRC-11 mechanism used in the chamber simulations plus the mechanisms for the lumped model species used to represent the emitted VOCs that are not represented explicitly. The mechanisms for the non-aromatic lumped model species, i.e., ALK1 through ALK5, OLE1, OLE2, and TERP are the same as used in SAPRC-07. The mechanisms for the lumped aromatic species ARO1 and ARO2 were derived by averaging the rate

constants and product yield parameters for the aromatic compounds in the ambient mixture used in the reactivity simulations that were used for deriving the ARO_n parameters for SAPRC-07 (see Table 18 in Carter, 2010a). Note that these include other types of aromatic hydrocarbons besides than those that were evaluated using the chamber data as discussed this report. Their mechanisms were derived from those discussed in this report using the same procedures as documented for SAPRC-07 by Carter (2010a). The SAPRC-11 mechanisms for the lumped model species are included with the mechanism listing in Table A-2 in Appendix A.

Results

The maximum O_3 concentrations calculated for the various scenarios using the airshed version of the SAPRC-11 mechanism are shown on Figure 41a as a function of the ROG inputs, and the relative changes in O_3 for SAPRC-11 compared to SAPRC-07 are shown as a function of the ROG/NO_x ratio on Figure 41b. This shows that the mechanism update has an effect on maximum O_3 calculated for these scenarios, with SAPRC-11 generally predicting 1-3% more O_3 in the MOIR and EBIR scenarios, and predicting 3-16% more O_3 in the MIR scenarios. This is consistent with the effect of the ROG/NO_x ratio on the O_3 calculated for the averaged conditions scenarios. The effect of the mechanism change is the greatest, and also the most variable, in the relatively high NO_x MIR scenarios. This is consistent with the generally greater sensitivity of O_3 formation in high NO_x scenarios to mechanism differences.

Table 12 gives the incremental reactivities of the 17 aromatic compounds whose mechanisms were developed for this project, calculated both with the SAPRC-11 and SAPRC-07 mechanisms. Results are shown for both the "averaged conditions" MIR scenario and the standard MIR scale, which are the averages of the reactivities in the city-specific MIR scales. Note that the differences between the "averaged conditions" and the actual MIR values are very small, and that the changes in the averaged conditions MIR values gives a good approximation of the actual MIR values calculated using all the city-

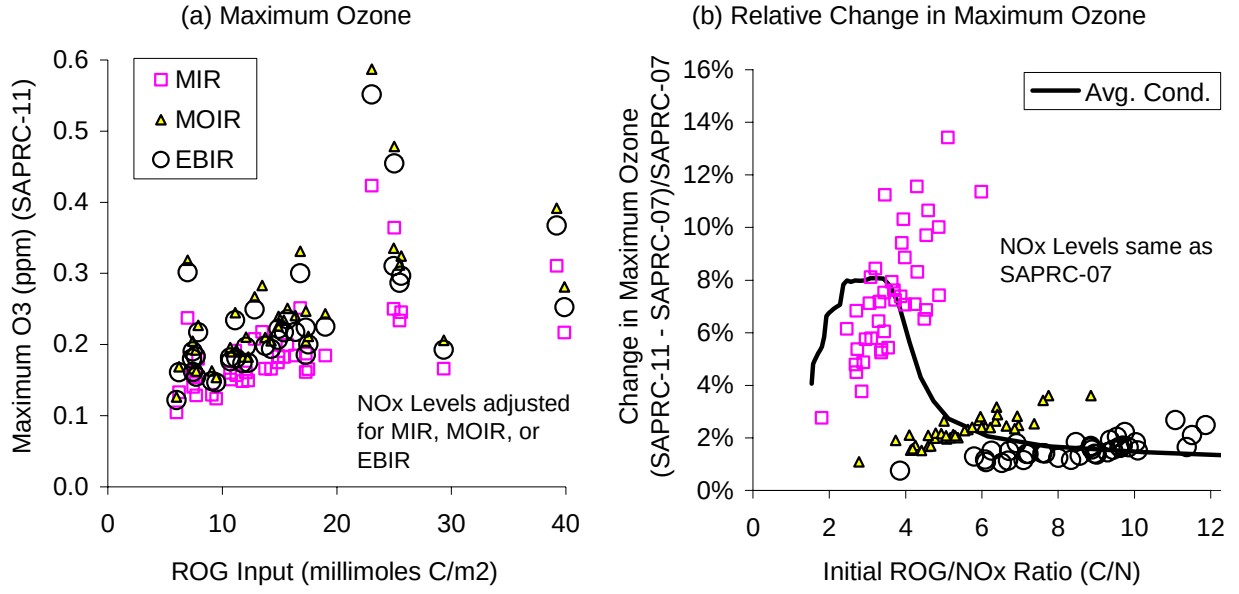

Figure 41. Maximum daily O_3 calculated for the various 1-day scenarios used for reactivity assessments using the SAPRC-11 mechanism, and relative changes in maximum O_3 for SAPRC-11 compared to SAPRC-07.

Table 12. SAPRC-11 and SAPRC-07 MIR values calculated for the aromatic compounds whose mechanisms were developed for this project.

Compound	Averaged Conditions MIR [a,b]			Standard MIR [a,c]		
	SAPRC-11	SAPRC-07	Change	SAPRC-11	SAPRC-07	Change
Benzene	1.46	0.73	99%	1.43	0.72	99%
Toluene	5.42	4.09	33%	5.30	4.00	32%
Ethyl Benzene	4.21	3.10	36%	4.12	3.04	36%
n-Propyl Benzene	2.90	2.06	40%	2.84	2.03	40%
Isopropyl Benzene	3.71	2.56	45%	3.63	2.52	44%
m-Xylene	10.70	10.02	7%	10.37	9.75	6%
o-Xylene	8.97	7.83	15%	8.73	7.64	14%
p-Xylene	7.42	5.99	24%	7.21	5.84	23%
m-Ethyl toluene	8.66	7.59	14%	8.41	7.39	14%
o-Ethyl toluene	6.93	5.72	21%	6.75	5.59	21%
p-Ethyl toluene	5.75	4.55	27%	5.60	4.44	26%
1,2,3-trimethylbenzene	11.78	12.32	-4%	11.41	11.97	-5%
1,2,4-trimethylbenzene	9.65	9.12	6%	9.35	8.87	5%
1,3,5-trimethylbenzene	11.25	12.13	-7%	10.87	11.76	-8%
Phenol	8.54	2.87	198%	8.25	2.76	199%
o-Cresol	9.57	2.50	283%	9.17	2.40	282%
2,4-Dimethyl phenol	9.86	2.21	346%	9.40	2.12	343%

[a] Units are grams O_3 per gram VOC

[b] Incremental reactivities in the single "averaged conditions" MIR scenario.

[c] Averages of incremental reactivities in the 39 city-specific MIR scenarios.

specific MIR scenarios. Figure 42 shows a comparison the averaged conditions MIR values of all individual VOCs represented separately in the mechanisms, other than for those requiring the chlorine or special mechanisms that were not updated for this work.

Although the mechanisms of the non-aromatic compounds (except for acetylene and glyoxal) are unchanged in SAPRC-11 compared to SAPRC-07 their reactivities calculated using SAPRC-11 are about 0.3% greater in magnitude than those calculated using SAPRC-07. This can be attributed to changes in the mechanism for the base case simulation, which includes aromatics (represented by ARO1 and ARO2) in the ambient mixture. The reactivity change for glyoxal, where the mechanism for the OH reaction was modified, is small and in the range observed for the non-aromatic compounds. The reactivity change for acetylene, where only the temperature dependence on the rate constant was also small.

As expected, the changes in averaged conditions MIR values are larger for the aromatic compounds, though the changes are less than 50% except for the phenols and benzene. In the case of the phenols the reactivities are significantly increased based on adjustments to the mechanisms needed to simulate the newer chamber experiments. In the case of benzene, the reactivity increases by a factor of two because of the much higher reactivities seen in the lower concentration experiments. For the aromatics lumped into ARO1 (e.g., toluene and monoalkylbenzenes), the SAPRC-11 reactivities are always higher than those for SAPRC-07, with the average reactivity change being +34±7%. The results

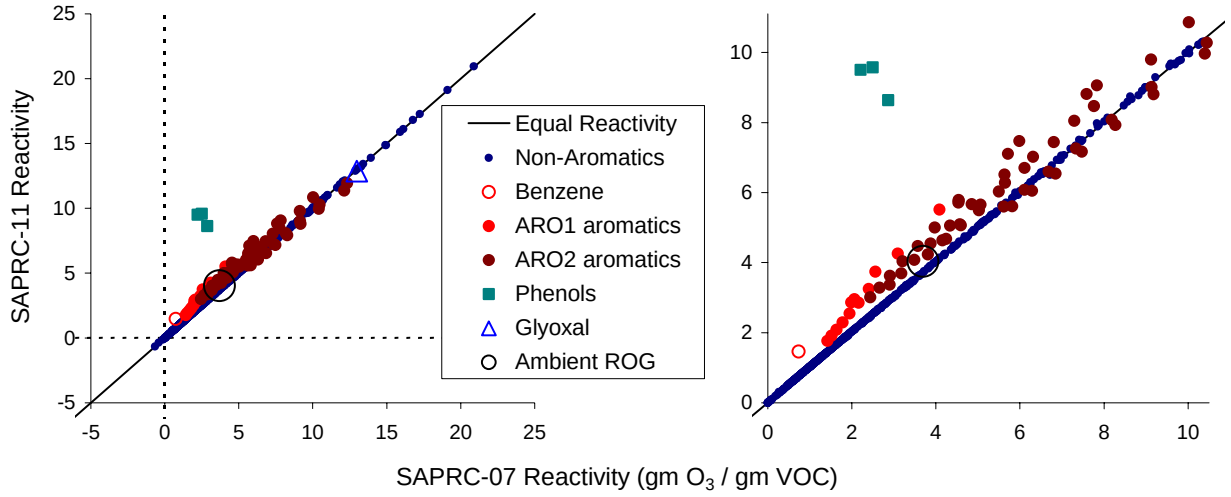

Figure 42. Comparisons of MIR values calculated using the SAPRC-11 and SAPRC-07 mechanisms calculated using the "Averaged Conditions" scenario.

are more variable for the aromatics lumped into ARO2 (xylenes and other di- and polyalkylbenzenes), with the average reactivity change ranging from -3±2% for compounds whose mechanisms are derived from those based on 1,3,5- or 1,2,3-trimethylbenzene, to +25±1% for compounds whose mechanisms are derived based on those for p-xylene or p-ethyl toluene. These are consistent with the changes in standard MIR values for the compounds studied for this project that are shown on Table 12. These changes are due to the effects of the revised mechanisms and reoptimized mechanistic parameters for these compounds.

DISCUSSION AND CONCLUSIONS

Discussion

The recent experiments carried out in our laboratory to investigate SOA formation from aromatics had the additional benefit of significantly enhancing the database of environmental chamber experiments to evaluate gas-phase mechanisms for predicting impacts of aromatics on ozone formation. The new data indicated significant biases in the SAPRC-07 aromatics mechanism towards underpredicting ozone formation at concentration levels representative of ambient conditions in experiments with benzene, toluene and other alkylbenzene, and even greater ozone underprediction bias in experiments with phenolic oxidation products. The new experiments also provided data for evaluating mechanisms for compounds that have not been previously studied. These new data, together with an update of rate constants and product yields to take into account new data in the literature, serve as the basis for the new SAPRC-11 mechanisms developed in this work. The results of the development and evaluation of the new mechanisms, and their implications for the gas-phase mechanisms for the aromatics in general, are discussed below.

Dependence on Mechanism Evaluation Results on Total NO_x Levels

The most significant finding of this mechanism update and evaluation is that it is not possible for the model to simulate the rates of NO oxidation and O_3 formation over the full range of available NO_x conditions for some important aromatic compounds without adding additional NO_x-dependent processes that were not previously considered in aromatics mechanisms used in airshed models. Mechanisms, such as SAPRC-07, that were derived primarily on modeling chamber experiments with NO_x levels greater than about 100 ppb tend to underpredict NO oxidation and O_3 formation rates at lower, more atmospherically relevant, NO_x concentrations, while those, such as the SAPRC-11 aromatics mechanism developed in this work that are adjusted to fit the data at low NO_x conditions, significantly overpredict reactivities in the higher NO_x experiments. This situation is applicable to some but not all aromatic compounds that were studied. The affected compounds are benzene, toluene, ethylbenzene and p-xylene, but not o- or m-xylene, the trimethylbenzenes and (probably) o-cresol. The data are not sufficient to determine whether it is applicable to the propylbenzenes, ethyltoluenes, or other phenolic compounds.

The NO oxidation and O_3 formation rates in the chamber experiments can be simulated over the full range of available NO_x conditions if it is assumed that the OH-aromatic adduct formed from compounds reacts with O_2 sufficiently slowly that reaction of the adduct with NO_2 can become competitive at the NO_x levels in the higher NO_x experiments, and if it is further assumed that the products formed when the adduct reacts with NO_2 are less reactive than those formed when it reacts with O_2. The data can also be simulated if it is assumed that the OH-aromatic-O_2 adduct reacts with NO at a rate competitive with the unimolecular ring opening that is assumed in the current mechanisms, and that the products formed in the NO reaction are less reactive than the products of the unimolecular reactions. Available laboratory data indicate that these additional aromatic adduct + NO_x reactions (OH-aromatic + NO_2 or OH-aromatic-O_2 +NO) indeed occur at sufficiently high NO_x levels, but that for both reactions the NO_x levels required for the reactions to be non-negligible are far higher than occur in any of the chamber experiments used in this study. For example, the published kinetic and mechanistic data indicate that the reactions of the aromatic-OH adduct with NO_2 becomes competitive with the reaction of the adduct with O_2 only with NO_2 concentrations greater than about 1 ppm for benzene (Koch et al, 2007) or ~3 ppm for toluene (Nishino et al, 2010 and references therein), whereas the simulations of the chamber data indicate that these concentrations need to be reduced to 20 ppb for benzene and 200 ppb for toluene (see Table 8, above) in order to simulate reactivities in both the lower and higher NO_x experiments . Therefore, either

there is an inconsistency between the chamber data and the published laboratory results, or there is a different, unknown, process that causes this additional NO_x dependence in the chamber experiments.

Two approaches can be used to address this apparent inconsistency between the laboratory and chamber data and model predictions. One approach, adopted for the standard version of the updated mechanism designated SAPRC-11, is not to use the adduct + NO_x reactions with the rate constants that are inconsistent with the laboratory data and to use only the lower NO_x experiments to derive the parameters for the mechanism. This mechanism may not be inappropriate for atmospheric modeling because the NO_x levels in the atmosphere are generally lower than the ~100 ppb level where SAPRC-11 begins to overpredict reactivities for compounds such as benzene and toluene. Although this limits its range of validity this is not an important limitation when modeling current ambient conditions (at least within most of the United States), and this approach is easier to scientifically justify. The other approach, adopted for the version of the updated mechanism designated SAPRC-11A, is to incorporate this process with the rate constants that give the best simulations of the chamber data for the compounds where this is necessary, despite the apparent inconsistency with the laboratory data. This could be justified by representing this added adduct + NO_x reaction as a surrogate for the actual unknown NO_x-dependent process.

The available data suggest that the need for this additional NO_x-dependent process is the greatest for benzene and the monoalkylbenzenes such as ethylbenzene, and the least for the di-and polysubstituted benzenes such as xylenes and trimethylbenzene. The one exception to this generalization is that this additional process is also necessary to simulate the data for p-xylene, while this is clearly not the case for the other two xylene isomers. p-Xylene differs from the other xylene isomers in being predicted to form unsaturated diketones, but this is also the case for 1,2,4-trimethylbenzene, where this additional process is not needed to fit the data. The NO_x range for the ethyltoluene experiments is insufficient to determine whether p-ethyltoluene is different from the other ethyltoluene isomers in this respect.

Variations of Mechanisms Among Compounds

As with previous versions of the aromatic mechanisms, it is still not possible to derive predictive aromatics mechanisms from first principles of laboratory data alone; is still necessary to optimize uncertain parameters in the mechanisms to satisfactorily simulate the chamber data. For this work, the parameters in the mechanisms were adjusted to optimize simulations of O_3 formation and NO oxidation rates in the chamber experiments, so by design the mechanisms fit these data without overall biases. The mechanistic parameters that were adjusted concerned the effective quantum yields for the photolysis of the photoreactive monounsaturated dicarbonyl products to form radicals, and also, in the case of SAPRC-11A, the rate constant for the reaction of the OH-aromatic adduct with NO_2. The yields of the photoreactive products were determined based on independently measured or estimated yields of their assumed co-products, and the overall photolysis rates were assumed to be rapid, so the only adjustments concerned quantum yields for radical formation. These parameters were adjusted on a compound-by-compound basis, and therefore differed depending on the compound.

The quantum yields for radical formation from the photolysis of the model species that represent the uncharacterized photoreactive products, i.e., the AFG1/(AFG1+AFG2) yield ratios, that best fit the chamber data for the various aromatic hydrocarbons are shown on Figure 43. Also shown are the yields of the model species, AFG1, that photolyzes to form radicals. The results are shown for SAPRC-11A as well as SAPRC-11 for those compounds where chamber data are available for a sufficiently large range of NO_x conditions to permit deriving parameters for SAPRC-11A. Note that for the purpose of this plot the SAPRC-11A mechanism is assumed to be the same as SAPRC-11 for those compounds, such as o- and m-xylene and the trimethylbenzenes, where SAPRC-11 fits the data over the full range of reactant

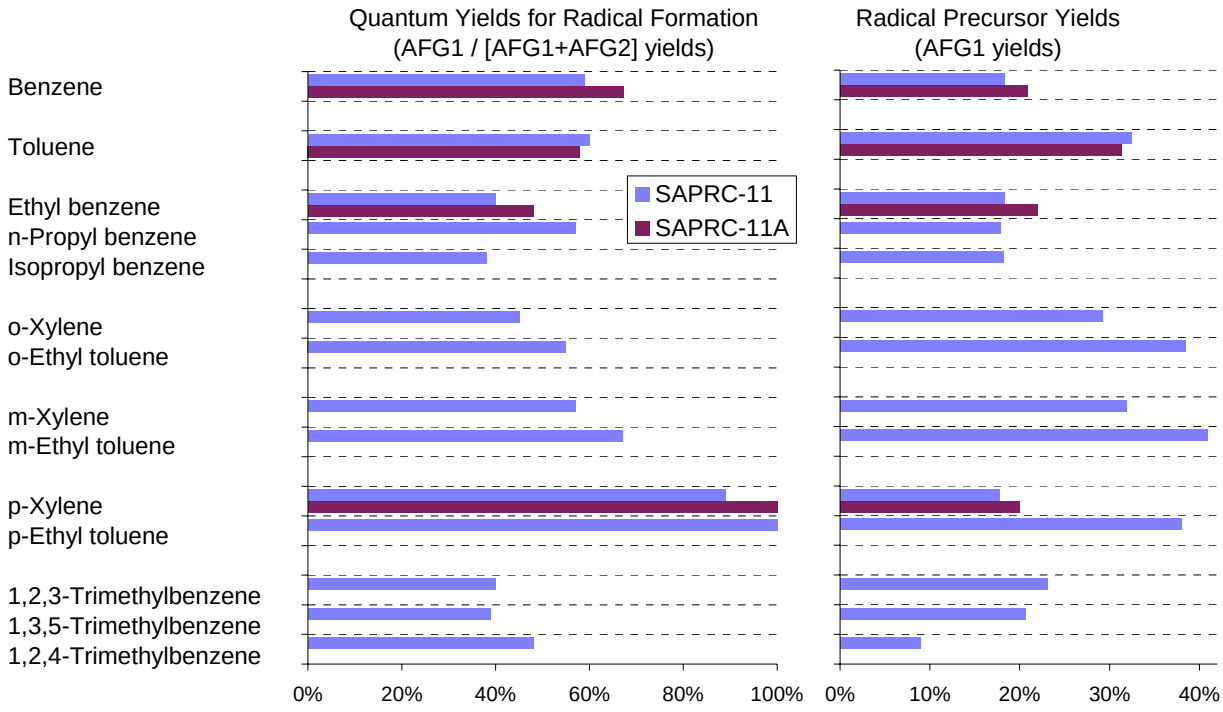

Figure 43. Quantum yields for radical formation and yields of uncharacterized photoreactive products that photolyze to form radicals (AFG1) derived to fit the chamber data for the various aromatic compounds.

concentrations. This is equivalent to assuming that the rate constant for the reaction of the OH-aromatic adduct with NO_2 is small for these compounds.

Figure 43 shows that there is compound-to-compound variability in the radical formation quantum yields that fit the data, though the quantum yields are reasonably consistent for structurally similar compounds. The apparent quantum yields tend to be higher for SAPRC-11A compared to SAPRC-11 (for compounds where SAPRC-11A is necessary to fit all the data) because higher quantum yields are necessary to offset the effects of the reaction of NO_2 with aromatic-OH adducts, which are assumed to form non-photoreactive species. The variability of the quantum yields is somewhat less than the variability in absolute AFG1 yields (particularly for p-xylene and p-ethyl toluene), which is consistent with our assumption that the yields of uncharacterized radical precursor products are linked to predicted yields of monounsaturated dicarbonyl aldehydes. The average apparent quantum yield for all compounds shown on Figure 43 is 57±19%, or 50±10% if the relatively high apparent quantum yields for p-xylene and p-ethyl toluene are excluded from the average.

One possible reason that the apparent quantum yields for p-xylene, p-ethyl toluene, and 1,2,4-trimethylbenzene are higher than those of their isomers is that these compounds are predicted to form monounsaturated 1,4-diketones, which are assumed to be non-photoreactive and therefore are not represented by AFG1+AFG2. If these were assumed to be as photoreactive as the 1,4-dicrbonyl aldehydes and therefore lumped with AFG1+AFG2 then the apparent radical formation quantum yields that fit the data for these compounds would be lower. Although we did not develop versions of SAPRC-11 with this assumption, an approximation to the apparent quantum yields that would result under this assumption can

be obtained from the AFG1 / (AFG1+AFG2+AFG4) ratio, where AFG4 is the model species used to represent the monounsaturated 1,4-diketones. The quantum yields that would result under this assumption are shown on Figure 44, along with the quantum yields derived for SAPRC-11 assuming that the diketones are not photoreactive and the average quantum yields for the other isomers. This figure shows that if the 1,4-diketones were lumped with the other unsaturated 1,4-dicarbonyls then the radical formation quantum yields would be lower for compounds forming these products than those for the other isomers. This is consistent with our assumption that the 1,4-diketones are less photoreactive than the dialdehydes or aldehyde-ketones, but suggests that they may photolyze to form radicals to at least some extent, contrary to what is assumed in the current mechanism.

Of course, it is always possible that the co-products of the measured α-dicarbonyls are compounds other than the monounsaturated 1,4-dicarbonyls that are assumed in the current mechanism. Available product data as discussed by Calvert et al (2002) suggests that this may indeed be the case, but this is uncertain because of difficulties in analyzing and working with these compounds. In this case, AFG1 and AFG2 are surrogates for the unknown photoreactive compounds that are actually formed, and trends in their yields and quantum yields would be difficult to assess without additional information.

Simulations of Benzene Experiments in the Euphore Outdoor Chamber

As an independent evaluation of SAPRC-07 and the mechanisms developed for this project, Goliff (2012) compared the performance of the SAPRC-07, SAPRC-11, and SAPRC-11A in simulating the results of a benzene - NO_x and a benzene - NO_x - HONO experiment carried out in the Euphore outdoor chamber (Bloss et al, 2005a). The initial reactant concentrations are given on Figure 45, along with experimental and calculated concentration-time plots for ozone. Both experiments used natural sunlight irradiation, and measurements were made of several major oxidation products and OH and HO_2 radicals as well as NO_x and ozone. The first experiment falls into the low NO_x category in the mechanism evaluation dataset used in this work, while the second has NO_x levels that are between the low and high NO_x levels in this dataset.

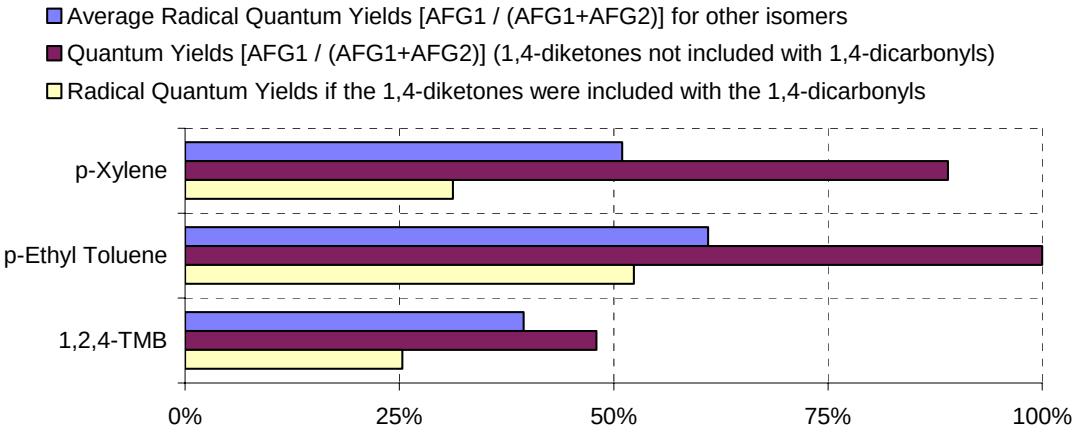

Figure 44. Comparison of radical formation quantum yields for compounds predicted to form unsaturated 1,4-diketones relative to those of isomers that cannot form these products.

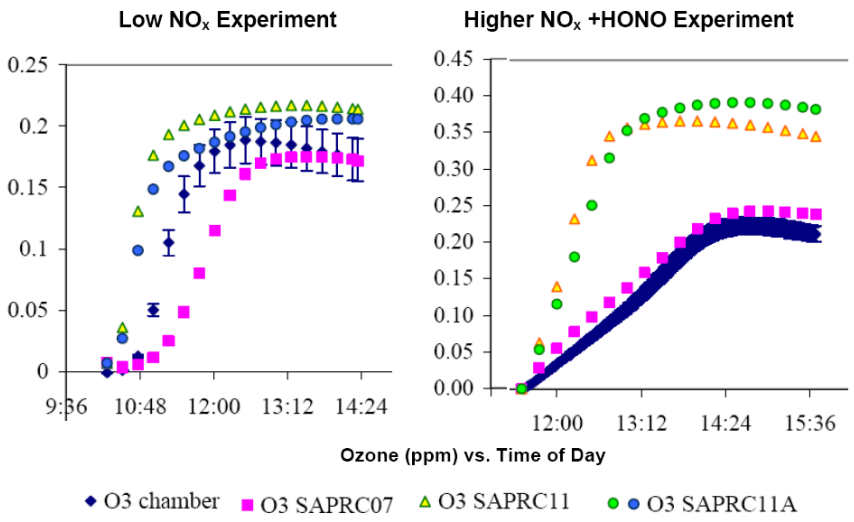

Figure 45. Experimental and calculated concentration-time plots for O_3 in the Euphore benzene - NO_x and benzene - NO_x - HONO experiments. (From Goliff , 2012).

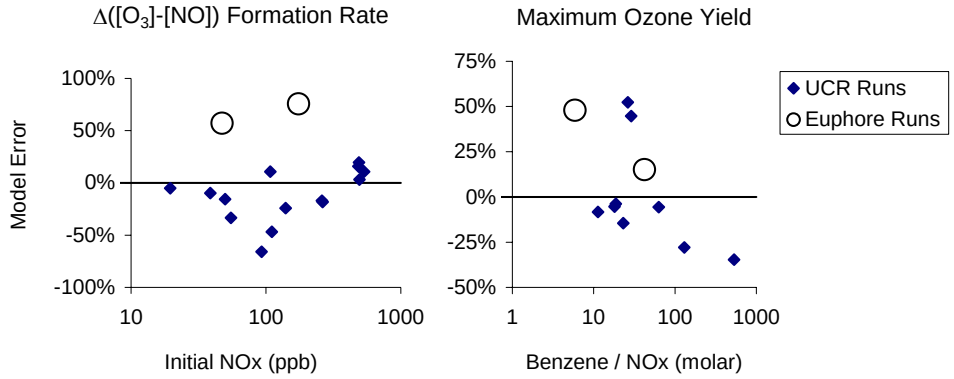

Figure 46. Comparison of model errors for SAPRC-11A simulations of Euphore and UCR benzene experiments.

Figure 45 shows that SAPRC-07 somewhat overpredicted the O_3 formation rate and final O_3 yield in the higher NO_x, added HONO experiment and underpredicted the O_3 formation rate in the lower NO_x experiment, though it gave a good simulation of the final O_3 yield. This is consistent with the fact that SAPRC-07 was adjusted based on fits to higher NO_x experiments and tended to underpredict reactivities in experiments with lower NO_x levels. SAPRC-07 also gave reasonably good simulations of NO, NO_2, phenol and HO_2 in the higher NO_x experiment where it fit the O_3 data, though it tended to somewhat underpredict the OH levels (see Goliff, 2012 for details). The underprediction of OH is consistent with the underprediction of integrated OH in the simulations of most of the alkylbenzene - NO_x experiments with previous versions of the SAPRC mechanisms that were derived to fit the ozone data.

Figure 45 shows that SAPRC-11 and SAPRC-11A tend to overpredict both O_3 formation rates and final O_3 yields in both of these Euphore experiments, with the overprediction being worse in the

higher NO_x experiment. Note that the final O_3 yields in both experiments reflect true O_3 maxima because the experimental NO_2 was completely consumed by the end of both experiments, indicating that additional O_3 would not be formed even if the irradiation were continued for a longer time. The difference between SAPRC-11 and SAPRC-11A is not large for either experiment, perhaps because the NO_x levels are relatively low compared to the high NO_x experiments in the chamber database used to develop SAPRC-11A. For the low NO_x experiment, SAPRC-11 and SAPRC-11A overpredict O_3 formation rates by about the same extent as the underprediction of these rates by SAPRC-07, but the predicted final O_3 yields are similar and only slightly higher than the experimentally measured values. Goliff (2012) showed that the performance of SAPRC-11A in simulating the O_3 formation rate in the higher NO_x experiment can be improved by reducing the rate constant for the reaction of O_2 with OH-aromatic adduct (i.e., increasing the importance of the adduct + NO_2 reaction), but this does not improve the significant overprediction of the final O_3 yields.

Figure 46 shows a comparison of the model errors for the SAPRC-11A mechanism (the version that gives the best fit to the benzene data) for the Euphore and UCR chamber experiments. The model tends to have somewhat more positive biases in simulations of $\Delta([O_3]-[NO])$ formation rates in the Euphore experiments than is the case for the UCR experiments. The biases for the maximum O_3 yields for the Euphore experiments appear to be consistent with the dependence of bias on benzene/NO_x ratio for the UCR experiments, though it should be noted that the presence of HONO in the higher NO_x experiment may tend to make the effective VOC (i.e., reactivity)/NO_x ratio higher. Any differences in biases for the Euphore experiments may be due to greater characterization uncertainties for outdoor chamber experiments, though the differences in light source may also have an effect. The effect of light source on evaluation results is discussed later in this report.

Goliff (2012) also found that while SAPRC-07 and SAPRC-11 gave reasonable simulations of the phenol data (when effects of overprediction of overall reactivity are taken into account, where applicable), SAPRC-11A predicted lower yields of phenol that were not consistent with the measurements. SAPRC-11A predicts lower yields of phenol, α-dicarbonyls, and photoreactive ring fragmentation products under higher NO_x conditions because these are assumed not to be products of the reaction of NO_2 with OH-aromatic adducts that is included in this version of the mechanism. The Euphore data modeled by Goliff (2012) suggest that the phenol yield is not as dependent on NO_x levels in the concentration range of these experiments as predicted by SAPRC-11A. This is consistent with fact that the laboratory data suggest that the NO_x dependence on product yields should not occur until NO_x levels are much higher than those used in the benzene experiments modeled in this work and by Goliff (2012).

Other Model Performance Issues

With suitable adjustments, the SAPRC-11 (or in some cases SAPRC-11A) mechanism can simulate NO oxidation rates and O_3 formation in the chamber experiments reasonably well, suggesting that the mechanisms may be suitable for O_3 simulations in the atmosphere. The lack of overall bias in simulating rates of NO oxidation and O_3 formation is expected because the mechanisms were adjusted so this would be the case, but the mechanisms also give reasonably good simulations of maximum ozone yields in experiments where maximum ozone formation potentials were obtained, and these reflect other aspects of the mechanism besides NO oxidation and O_3 formation rates. However, there are other areas where the mechanism evaluation results are not totally satisfactory and indicate remaining problems with the mechanism or the way the uncertain processes are represented. These were discussed above for the individual compounds, and are summarized below.

The most obvious mechanism performance issue is the consistent underprediction of OH radical levels in almost all of the aromatic - NO_x experiments, including those where good simulations of NO oxidation rates and O_3 formation are obtained. The predicted OH radical levels can be increased by

increasing the yields or rates of photolysis of model species representing the uncharacterized photoreactive products (e.g., AFG1), but this results in overpredictions of NO oxidation and O_3 formation rates. With the mechanism adjusted to fit $\Delta([O_3]-[NO])$ formation rates, the integrated OH levels are underpredicted by ~30% on the average. This is slightly better than the ~36% underprediction bias for SAPRC-07, but this might be because the SAPRC-11 mechanism predicts somewhat greater reactivity for a number of compounds. It is unclear at this point what the source of this discrepancy is and how to modify the mechanism to improve this systematic OH underprediction problem.

Another mechanism performance issue is that the $\Delta([O_3]-[NO])$ formation rate model errors tend to correlate with the initial aromatic / NO_x ratio for many compounds, having a greater tendency to underpredict at low ratios and to overpredict at high ratios. This is the case even after the dependence of model errors on initial NO_x concentrations is removed by using the SAPRC-11A mechanism where necessary. This type of bias is observed for which there were sufficient range of aromatic and NO_x levels to determine this. It is also unclear what the source of this discrepancy is and how to resolve it, and it may be a result of the same problem that is reflected in the problem with simulating integrated OH levels.

Another problem with SAPRC-07 that has not been resolved with this mechanism update is the tendency to underpredict $\Delta([O_3]-[NO])$ at the low ROG / NO_x ratios in the ambient surrogate - NO_x experiments (see Figure 40). This is probably related to the other two problems discussed above.

The model performance in simulating the experiments with benzene was found to be somewhat worse than was the case for the other aromatic hydrocarbons, even after adjusting both the radical input rates from the AFG1 photolysis and the OH-aromatic + NO_2 rate constant to fit the data using SAPRC-11A. Although the UCR experiments with both low and high initial NO_x levels are reasonably well simulated, some experiments with moderate NO_x levels are not well simulated (see Figure 8), and the incremental reactivities in the high NO_x "MIR1" incremental reactivity experiments are significantly overpredicted even with SAPRC-11A (see Figure 9). Also, Goliff (2012) found that the SAPRC-11 mechanisms did not simulate the results of the two Euphore benzene experiments as well as SAPRC-07, with SAPRC-11 overpredicting both O_3 formation rates in both experiments and final O_3 yields in the higher NO_x experiment with added HONO. Note that for benzene experiments with NO_x levels greater than about 100 ppb the SAPRC-11A mechanism predicts most of the reaction is via the OH-aromatic + NO_2 reaction route, and the model species used to represent the lower reactivity products formed in this route (AFG3 + HO_2) may not be appropriate.

The model performance in simulating the experiments with p-xylene was found to be quite different from the simulations of the other di- and tri-alkylbenzene experiments. This is the only di- or trialkylbenzene compound where it was necessary to use the SAPRC-11A mechanism to fit the data over the full range of NO_x conditions, and this is the only compound where the model error for integrated OH levels were not consistently underpredicted at higher NO_x levels. A sufficient number of experiments were conducted with this compound so this is probably not a chamber or light effects issue. p-Xylene differs from the other xylene isomers in that it is predicted to form an unsaturated diketone that is assumed to be less reactive, but this is also the case for p-ethyl toluene and 1,2,4-trimethylbenznee. A similar problem is not seen for those compounds. The range of conditions for p-ethyl toluene may not be sufficient to observe this model performance issue, but the range of conditions for 1,2,4-trimethylbenzene is reasonably comprehensive.

Although the main focus of this mechanism evaluation is simulation of $\Delta([O3]-[NO])$ formation rates, O_3 yields, and integrated OH radical levels, the mechanism can also be evaluated for simulations of measured product yields. However, product yield data are limited for the chamber database used in this evaluation, so the mechanism was not comprehensively evaluated in this regard in this work. With regard to aromatic products, phenol measurements are available for four of the UCR benzene experiments used

in this evaluation, as well as the Euphore benzene experiments discussed above and by Goliff (2012). Figure 47 shows the concentration-time plots for ozone and phenol for these experiments, and indicates that the SAPRC-11 mechanism simulates the phenol data reasonably well but that SAPRC-11A significantly underpredicts phenol yields. This is consistent with the results obtained by Goliff (2012) for the Euphore experiments, and indicates that SAPRC-11A incorrectly predicts the effects of NO_x on phenol yields. There are also data for o-cresol in several of the older UCR chamber toluene - NO_x experiments, and the data are generally consistent with SAPRC-07 and SAPRC-11 model predictions. Although SAPRC-11A predicts lower cresol yields in these experiments, the differences between the mechanisms are less than the scatter and uncertainty of the data in this case.

Finally, although there is no evidence for a light source effect on the mechanism evaluation results for toluene and m-xylene, there may be a light source effect in the evaluation of the mechanism for benzene and the cresols. This is discussed in the next section.

Effect of Light Source on Evaluation Results

One potential area of concern for the current environmental chamber database for mechanism evaluation concerns the large number of experiments employing artificial light sources whose spectra are significantly different from that of sunlight (see Figure 4, above). In principle, differences in light spectra can be taken into account during the mechanism evaluation process by using the measured spectra to calculate photolysis rates when modeling the chamber experiments, and this procedure was employed in this study. Having data from a variety of light sources can be a benefit since it allows for mechanisms to be evaluated under a variety of lighting conditions. However, if data are available from only one type of

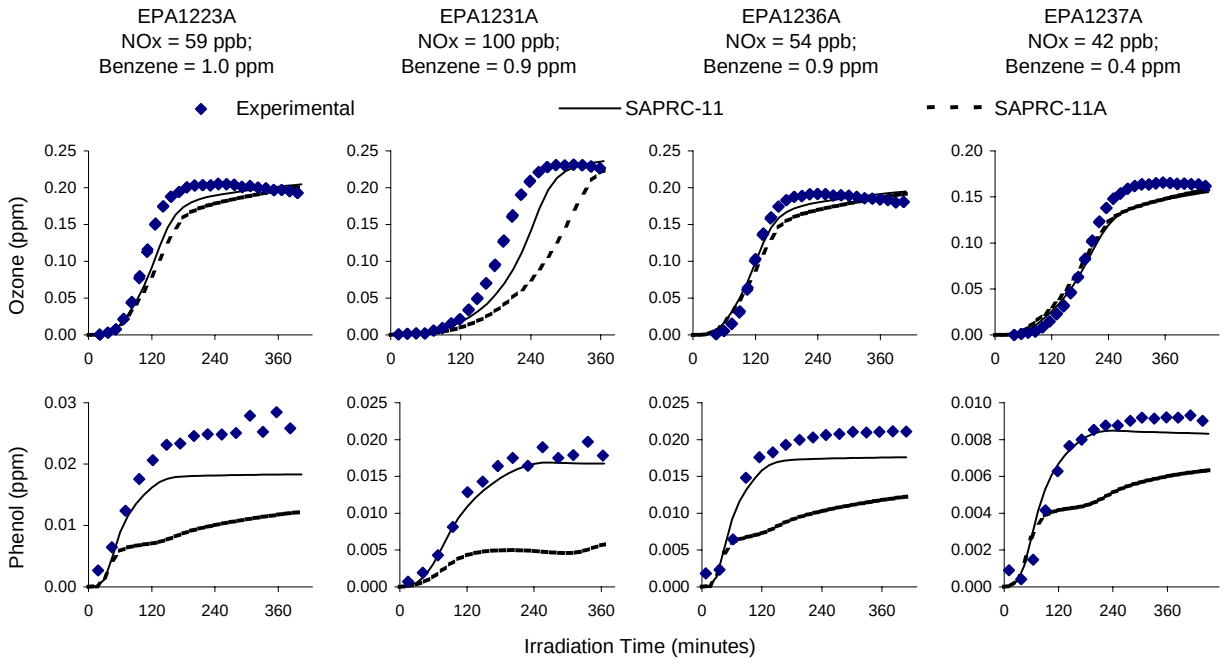

Figure 47. Experimental and calculated concentration-time plots for ozone and phenol for the UCR EPA chamber experiments for which phenol data are available.

light source, and the light source does not represent ambient light conditions, then the mechanism evaluation may be misleading if the model has incorrect action spectra (absorption cross sections and quantum yields) for important photoreactive species.

The light source issues are of particular concern when evaluating mechanisms for aromatics because (1) the identities and therefore the action spectra of the highly photoreactive species whose photolyses are important in affecting aromatic reactivities are uncertain, and (2) the yields and/or quantum yields of these photoreactive species have to be adjusted based on simulations of chamber data. An incorrect action spectrum would result in compensating errors when the yields or quantum yields are adjusted, and if the spectrum used when deriving the adjusted parameters is significantly different than ambient conditions then incorrect simulations of reactivities under ambient conditions may result. This is not as much of an issue for most non-aromatic compounds since the action spectra of the photoreactive products tend to be less uncertain and also less important in affecting model results, and generally either no parameters need to be adjusted or the parameters that have to be adjusted (such as nitrate yields from peroxy radical reactions) do not directly concern photolysis reactions.

Use of arc light sources is less of a concern because their spectra are reasonably representative of sunlight, though there are differences and photolysis rates still need to be calculated for each light source. Blacklights are more of a concern because of the lower relative intensity in the high wavelength region that affects photolyses of α-dicarbonyls and perhaps other aromatic products. Having comprehensive data for both arc and blacklight light sources is a benefit because it provides a means to evaluate the action spectra used for the uncertain photoreactive species, but having data only for blacklights, or having incomplete or limited arc light data can be a concern.

Although there are not comprehensive data for both types of light sources for all the 17 aromatic compounds whose mechanisms were evaluated for this study, the data are reasonably comprehensive for toluene (see Figure 10 and Figure 11) and m-xylene (Figure 19). In both cases, data from both arc light and blacklight irradiated chambers are available over a wide range of NO_x levels and initial aromatic / NO_x ratios, and no significant effect of light source on model performance was observed. Evaluation data for arc light experiments are also available for benzene, ethylbenzene, o- and p-xylenes, and the trimethylbenzenes but only for NO_x levels greater than about 200 ppb. In those cases there are also blacklight chamber data in the high NO_x range and similar evaluation results are obtained. These results tend to indicate that there is no significant light source effect in the mechanism evaluation results at least for the aromatic hydrocarbons, and suggest that if arc light data were available for the other compounds or the lower NO_x ranges then the results should not be significantly different.

The one area of concern is the possibility of significant light source effects in the mechanism evaluation data for the phenolic compounds. There are no arc light chamber data suitable for evaluating mechanisms for phenol or the xylenols and there is only a single arc light experiment for o-cresol, and the mechanism evaluation results for that experiment are significantly different than the results for blacklight experiments with similar reactant concentrations (see Figure 36). Similar results are seen for other cresol experiments carried out around the same time, but not for cresol experiments carried out recently using blacklights (see Figure 39). Unfortunately the arc light in the UCR EPA chamber requires major repairs for which funding has not been available, so new arc light experiments with phenolic compounds could not be carried out.

Discussion of Mechanism Problems and Uncertainties

Despite considerable study in recent years, significant uncertainty in the details of the aromatics photooxidation mechanisms, particularly concerning the aromatic ring opening processes and the identity and reactions of the highly reactive products that are formed. These uncertainties are such that attempts to

develop chemically detailed or explicit mechanisms *a-priori* consist primarily of speculation, and such mechanisms lack predictive capability. For this reason, if the primary objective is to develop predictive mechanisms we still have no choice but to use mechanisms that represent the unknown processes and reactive products using lumped model species whose parameters are adjusted based on simulations of chamber data. Attempts are made to use our knowledge of the possible reactions to guide the representations of these products and processes in the model, and to evaluate the mechanism under as wide a variety of conditions as possible. However, because of the uncertainties and the fact that no single mechanism was found to simulate all the data under all conditions, the possibility that parameterized and adjusted mechanisms may give incorrect predictions when applied beyond the conditions where they were developed cannot be ruled out.

One major finding of this project is that current mechanisms is that they cannot simulate the effects of total NO_x levels on reactivity for benzene and several other compounds without adding an additional reaction of NO_2 with the OH-aromatic adduct that is inconsistent with laboratory data and the dependence of NO_x on aromatic product yields. If the adduct + NO_2 reaction added to the SAPRC-11A mechanism is not the reason for this apparent NO_x dependence, then what is it? The only other mechanistic explanation for this result we could come up with was a reaction between the aromatic-OH-O_2 adduct with NO, but again the rate constant ratios required for the model to simulate the chamber data are inconsistent with laboratory data in the literature. Until the type of process that could account for these results is found, then even explicit mechanisms will not be able to simulate the available data and will not have predictive capability.

Another problem with aromatics mechanisms, which has been realized for some time but not corrected in this work, is that mechanisms adjusted to simulate rates of NO oxidation and O_3 formation tend to systematically underpredict OH radical levels. This may be related to the tendency of the mechanisms to underpredict O_3 formation at low ROG/NO_x ratios, though this may be due to other problems. Radical sources in mechanisms become more important as ROG/NO_x ratios go down. Attempts to revise the representation of uncertain processes to eliminate or reduce this bias has not been successful. Reducing formation of PAN analogues in the aromatics mechanisms may reduce this bias, but this tends to result in increased biases towards overpredictions of final O_3 yields, which are affected by NO_x sink processes such as formation of PAN compounds.

These and other mechanism evaluation problems suggest that the assumptions made in formulating mechanisms concerning the formation, identity, and reactions of reactive products may not be correct. The formation and yields of α-dicarbonyl products are reasonably well characterized, but are the monounsaturated 1,4-dicarbonyls really the only significant co-products formed with them? We assume that they are but the limited and generally highly uncertain product data suggest that this is probably not the case. In addition, the observed yields of phenolic products and α-dicarbonyls do not account for all the reaction pathways, and our assumption that the unknown pathway(s) result in formation of diunsaturated dicarbonyls has not been experimentally verified and may be incorrect. Whatever the unknown products are, at least some of them must be highly reactive and give rise to radicals when they react or the reactivities of aromatics are significantly underpredicted.

Without adequate knowledge of the identity and reaction mechanisms of the highly photoreactive products that must be formed from aromatic compounds, we do not know whether we are appropriately representing them in the parameterized mechanisms. The total amount of radical input from their reactions can be adjusted to simulate reactivities in chamber experiments, but there are different ways to represent this in the model and differing approaches may give different results when using the models to extrapolate from chamber to atmospheric conditions. In the current mechanisms we assume that the photoreactive products photolyze rapidly and we adjust the quantum yields for radical production to fit the data, but the data could also be fit by assuming only radical production occurs and adjusting the total

photolysis rates. The chamber data are not sufficient to determine which approach is best, and different approaches give different predictions of ozone formation in the atmosphere.

Phenolic compounds are important in aromatic mechanisms because of the importance of the NO_x sinks in their reactions in affecting final O_3 yields, and also because of their importance in SOA formation (Carter et al, 2012, and references therein). The new chamber data indicate that SAPRC-07 significantly underpredicts their reactivity with NO_x levels representing ambient conditions, and new mechanisms for these compounds were developed for SAPRC-11. However, even less is known about their reactions than is the case for the parent aromatic hydrocarbons, and the current mechanisms are highly parameterized with many uncertain assumptions. Most of the chamber data are moderately well simulated with the parameterized mechanisms that were developed, but there may be cancellations of errors and not all experiments are well simulated in all respects. Catechols are known to be important products of the reactions of phenolic compounds, and uncertainties in their mechanisms will affect uncertainties in the overall mechanism. However, catechols are not expected to undergo photolysis under atmospheric conditions and mechanisms cannot simulate the chamber data unless significant formation of photoreactive compounds is also assumed. The nature of these compounds, and how best to represent their reactions in the models, is unknown.

Conclusions and Recommendations

The new environmental chamber data that became available after SAPRC-07 was developed indicated that there was a need to update the SAPRC-07 aromatics mechanisms so they could adequately simulate the available data. In this work, the rate constants and yields of known products were updated based on recent literature data, and uncertain parameters that were adjusted to fit chamber data were reoptimized using the new, more comprehensive environmental chamber dataset. Although uncertainties and significant problems still exist as discussed above, the SAPRC-11 mechanism developed in this work performed well in simulating most of the available NO oxidation and O_3 formation data at the lower NO_x levels more representative of ambient conditions. It therefore represents an improvement over SAPRC-07 for use in simulations of ambient ozone or for developing ozone reactivity scales.

One-day box model simulations indicate that the new mechanism gives somewhat higher predictions of ozone in ambient simulations, particularly at low ROG/NO_x ratios, and also generally higher incremental reactivities of aromatic compounds. However, a complete assessment of the effects of these updates on ambient simulations will require implementing the updated mechanism in the 3-D models and using them to simulate various scenarios. This is beyond the scope of this project.

It is important to recognize that this work amounted to only an incremental update of the aromatics mechanism, and not a complete reformulation such as occurred when updating from SAPRC-90 to SAPRC-99 or from SAPRC-99 to SAPRC-07. Other than a complete revision of the parameterized mechanisms for phenolic compounds that was needed to fit the data, the overall approach and assumptions and methods used to represent uncertain processes in the SAPRC-07 mechanism was retained in SAPRC-11. Although alternative approaches for representing uncertain processes, such as the additional NO_x dependence incorporated in SAPRC-11A, were examined in the process of carrying out this aromatic mechanism update process, no alternative approach was found that simulated the available data sufficiently better to justify revising the approach employed, and most resulted in degradations of model performance. The only exception was incorporating the additional NO_x-dependence process into SAPRC-11A, but this mechanism is inconstant with available laboratory and product yield data and is not recommended for use in ambient simulations.

The overall goal in the SAPRC mechanism development effort is to develop mechanisms that have predictive capability when used in atmospheric models and that are also consistent with current

laboratory data and theories of atmospheric chemistry. Ideally the mechanism should be based on an understanding of the individual reactions that occur, with the mechanism used for airshed models being derived directly from explicit mechanisms incorporating all these reactions. Although fully explicit mechanisms such as MCM (Jenkin et al, 1997, 2003; Saunders et al, 2003) could serve this objective, their large size makes them generally impractical for airshed models without at least some condensations. (Even the MCM, whose thousands of species and tens of thousands of reactions make it barely useable for ambient modeling, is useable only because only a subset of emitted compounds are represented, and because only a few of the many possible reaction routes are represented for most represented compounds and reaction products.) In the case of the SAPRC mechanisms for many non-aromatic compounds, traceability to explicit chemistry is achieved by using a computerized mechanism generation system to generate fully explicit mechanisms, and then using various "lumping rules" to derive more condensed mechanisms that are practical to use in airshed models (Carter, 2000, 2010a-c). However, this approach is not yet possible for aromatic compounds.

As discussed above, our knowledge of many aspects of the aromatic reactions mechanisms is insufficient to derive explicit mechanisms that have predictive capability. Although the current version of MCM has a semi-explicit mechanism for aromatics that was developed to be generally consistent with available laboratory data, attempts to make its predictions consistent with environmental chamber data have not been successful (e.g., see Bloss et al, 2005a,b). Unfortunately, the present situation seems to be that mechanism developers have to make a choice between having aromatics mechanisms that appear to be consistent with all the published laboratory results and having mechanisms that can at least approximately simulate ozone formation in environmental chamber experiments. Since it is not yet possible for us to achieve both objectives, the SAPRC mechanism development effort has put the priority on predictive capability because the intention is for the mechanism to be used for predictions. But the validity of the predictions when applied beyond the conditions where the mechanism is evaluated is obviously questionable if the mechanism does not appropriately represent the underlying chemical processes.

This means that the current situation with regard to aromatic mechanisms is still not satisfactory, and efforts to understand more of the details of aromatic photooxidation mechanisms need to continue. We need to know the identities and yields of *all* the products formed in non-negligible yields, and the reaction mechanisms, photolysis rates and quantum yields (if applicable), and secondary products formed for at least the most reactive of these products. Information on compounds that are NO_x sinks and radical sources are particularly important for ozone predictions, but for SOA predictions information is also needed on formation of lower volatility products that may not be important in ozone modeling. This requires improvements to analytical methods so the identities and yields of the unidentified products can be determined. Without such new methods or approaches, it is unlikely that the needed breakthroughs can be obtained. We have probably gone about as far as we can with the current laboratory methods and approaches.

One area of significant recent progress has been expanding the environmental chamber database needed for developing and evaluating aromatics mechanisms. The recent experiments at UCR have been driven by the need for chamber data for developing mechanisms for SOA formation (Carter et al, 2012), but they have also provided a valuable addition to the dataset for ozone modeling. The fact that the recent experiments showed problems when applying SAPRC-07 to lower NO_x conditions illustrates the problems when extrapolating uncertain mechanisms beyond the range of conditions where they were evaluated, and demonstrates the importance of mechanism evaluation data under more varied conditions when our understanding of the underlying chemistry is incomplete. Although the chamber database has been significantly improved since the development of SAPRC-07 there still remain areas where more chamber data are needed.

One major problem with the aromatic chamber database is the limited numbers of well-characterized chamber experiments at more atmospherically relevant concentration levels using light sources that are more representative of sunlight. Indoor chamber experiments are the least uncertain to characterize for mechanism evaluation and provide the only means to systematically study temperature and light intensity effects, but require use of artificial light sources whose spectra are different from that of sunlight. Arc lights provide the best approximation of sunlight but such light sources are expensive and difficult to operate and maintain. Although the UCR EPA chamber has an arc light source as well as blacklights (Carter et al, 2005), the computer controlling its arc light needs to be replaced at an estimated cost of at least $50K. Because of this, most of the database of new chamber experiments, including most at the lower NO_x levels, used the blacklight light source. As discussed above, there does not appear to be light source effect when evaluating ozone predictions for toluene and m-xylene. However, the data are insufficient to determine if there is a light source effect for the other compounds, there are indications that there may be a light source effect when evaluating mechanisms for phenolic compounds, and there are inadequate data for evaluating effects of light source on SOA formation. The arc light is also required to systematically study temperature effects because the intensity of blacklights is affected by temperature. Evaluating temperature effects is particularly important for SOA mechanism evaluation but data are also needed to evaluate predictions of effects of temperature on ozone formation. Temperature effects on aromatic model predictions may be important, for example, for modeling the wintertime ozone formation problem in Wyoming (Carter and Seinfeld, 2012). We are not aware of any other environmental chamber currently being used to generate chamber data for mechanism evaluation that has a functioning arc light source, and the cost of constructing a new one would be far more than the cost of repairing the arc light for the UCR chamber.

The focus of this report has been updating aromatics mechanisms for predicting ozone formation, but there is also a need for developing aromatic mechanisms for predicting SOA (Carter et al, 2012). Improving the gas-phase mechanisms is a necessary precursor to developing and improving SOA mechanisms because the gas-phase processes provide the source of the condensable materials that form the SOA. The uncertainties and performance issues in the gas-phase mechanism discussed above will also cause uncertainties and performance issues in the predictions of SOA. However, SOA formation is much more complex and depends on more environmental factors than ozone formation and therefore the uncertainties and needs for basic mechanistic data for mechanism development and well-characterized environmental chamber data for mechanism evaluation are much greater. Many of the recommendations for data needs for ozone modeling are even more important for development of SOA models. This will be discussed in more detail in our report on developing and evaluating a PM-SAPRC mechanism for aromatic SOA prediction (Carter et al, 2012).

REFERENCES

Anderson, R.S., Czuba, E., Ernst, D., Huang, L., Thompson, A.E., Rudolph, J. (2003): "Method for measuring carbon kinetic isotope effects of gas-phase reactions of light hydrocarbons with the hydroxyl radical," J. Phys. Chem. A 107, 6191-6199.

Anderson, R.S., Iannone, R., Thompson, A.E., Rudolph, J., Huang, L. (2004): "Carbon kinetic isotope effects in the gas-phase reactions ofaromatic hydrocarbons with the OH radical at 296 ± 4 K," Geophysical Research Letters 31, L15108, doi:10.1029/2004GL020089.

Arey, J., Obermeyer, G., Aschmann, S.M., Chattopadhyay, S., Cusick, R.D., Atkinson, R. (2009): "Dicarbonyl products of the OH radical-initiated reaction of a series of aromatic hydrocarbons," Environ. Sci. Technol. 43 (3), 683-689.

Atkinson, R. (1989): "Kinetics and Mechanisms of the Gas-Phase Reactions of the Hydroxyl Radical with Organic Compounds," J. Phys. Chem. Ref. Data, Monograph no 1.

Atkinson, R. and S. M. Aschmann (1994): "Products of the gas-phase reactions of aromatic hydrocarbons: effect of NO_2 concentration," Int. J. Chem. Kinet., 26, 929-944.

Atkinson, R. and J. Arey (2003): "Atmospheric Degradation of Volatile Organic Compounds," Chem. Rev. 103, 4605-4638

Atkinson, R., Aschmann, S.M., Arey, J. (1991): "Formation of ring-retaining products from the OH radical-initiated reactions of o-, m-, and p-xylene," International Journal of Chemical Kinetics 23, 77-97.

Azzi M., S. J. White, D. E. Angove, I. M. Jamie, A, Kaduewela (2010): "Evaluation of the SAPRC-07 mechanism against CSIRO smog chamber data," Atmos. Environ. 44, 1707-1713.

Bailey, E. M., C. H. Copeland and R. Simonaitis (1996): "Smog Chamber Studies at Low VOC and NO_x Concentrations," Report on Interagency Agreement DW64936024 to EPA/NREL, Research Triangle Park, NC.

Bandow, H. N. and N. Washida (1985a): "Ring-cleavage reactions of aromatic hydrocarbons studied by FT-IR spectroscopy. II. Photooxidation of o-, m- and p-xylenes in the NOx -air system," Bull. Chem. Soc. Jpn., 58, 2541-2548.

Bandow, H. N. and N. Washida (1985b): "Ring-cleavage reactions of aromatic hydrocarbons studied by FT-IR spectroscopy. III. Photooxidation of 1,2,3-, 1,2,4-, and 1,3,5-trimethylbenzenes in the NOx -air system," Bull. Chem. Soc. Jpn., 58, 2549-2555.

Bandow, H., N. Washida, and H. Akimoto (1985): "Ring-cleavage reactions of aromatic hydrocarbons studied by FT-IR spectroscopy. I. Photooxidation of toluene and benzene in the NOx -air system," Bull. Chem. Soc. Jpn., 58, 2531-2540.

Baugues, K. (1990): "Preliminary Planning Information for Updating the Ozone Regulatory Impact Analysis Version of EKMA," Draft Document, Source Receptor Analysis Branch, Technical Support Division, U. S. Environmental Protection Agency, Research Triangle Park, NC, January.

Berndt, T. and O. Böge (2003): "Gas-phase reaction of OH radicals with phenol," Phys. Chem. Chem. Phys. 5, 342-350.

Berndt, T. and O. Böge (2006): "Formation of phenol and carbonyls from the atmospheric reaction of OH radicals with benzene," Phys. Chem. Chem. Phys 8, 1205-1214.

Bethel, H.L., Atkinson, R., Arey, J. (2000): "Products of the gas-phase reactions of OH radicals with p-xylene and 1,2,3- and 1,2,4-trimethylbenzene: effect of NO2 concentration," J. Phys. Chem. A 104, 8922-8929.

Bierbach, A., Barnes, I., Becker, K.H., Wiesen, E. (1994): "Atmospheric chemistry of unsaturated carbonyls: Butendial, 4-oxo-2-pentenal, 3-hexene-2,5-dione, maleic anhydride, 3H-furan-2-one, and 5-methyl-3H-furan-2-one," Environmental Science & Technology 28, 715-729.

Bloss, C., V. Wagner, A. Bonzanini, M. E. Jenkin, K.Wirtz, M. Martin-Reviejo, and M. J. Pilling (2005a): "Evaluation of detailed aromatic mechanisms (MCMv3 and MCMv3.1) against environmental chamber data", Atmos. Chem. Phys., 5, 623–639.

Bloss, C., Wagner, V., Jenkin, M. E., Volkamer, R., Bloss, W. J., Lee, J. D., Heard, D. E., Wirtz, K., Martin-Reviejo, M., Rea, G., Wenger, J. C., and Pilling, M. J. (2005b): "Development of a detailed chemical mechanism (MCMv3.1) for the atmospheric oxidation of aromatic hydrocarbons," Atmos. Chem. Phys., 5, 641-664.

Bohn, B. and C. Zetzsch, (1999): "Gas-phase Reaction of the OH-Benzene Adduct with O_2: Reversibility and Secondary Formation of HO_2," Phys. Chem. Chem. Phys. 1, 5097-5107.

Brauers, T., B. Bohn, F.-J. Johnen, F. Rohrer, S. Rodriguez Bares, R. Tillmann, and A. Wahner (2003): "The Atmosphere Simulation Chamber SAPHIR: a Tool for the Investigation of Photochemistry," Presented at the EGS - AGU - EUG Joint Assembly, Nice, France, April 11, 2003. See also http://www.fz-juelich.de/icg/icg-ii/saphir/home.

Calvert, J. G., R. Atkinson, J. A. Kerr, S. Madronich, G. K. Moortgat, T. J. Wallington and G. Yarwood (2000): "The Mechanisms of Atmospheric Oxidation of Alkenes," Oxford University Press, New York.

Calvert, J. G., R. Atkinson, K. H. Becker, R. M. Kamens, J. H. Seinfeld, T. J. Wallington and G. Yarwood (2002): "The Mechanisms of Atmospheric Oxidation of Aromatic Hydrocarbons," Oxford University Press, New York, 566p.

Carter, W. P. L. (1994a): "Development of Ozone Reactivity Scales for Volatile Organic Compounds," J. Air & Waste Manage. Assoc., 44, 881-899.

Carter, W. P. L. (1994b): "Calculation of Reactivity Scales Using an Updated Carbon Bond IV Mechanism," Report Prepared for Systems Applications International Under Funding from the Auto/Oil Air Quality Improvement Research Program, April 12.

Carter, W. P. L. (1990): "A Detailed Mechanism for the Gas-Phase Atmospheric Reactions of Organic Compounds," Atmos. Environ. 24A, 481-518.

Carter, W. P. L. (2000a): "Documentation of the SAPRC-99 Chemical Mechanism for VOC Reactivity Assessment," Report to the California Air Resources Board, Contracts 92-329 and 95-308, May 8. Available at http://cert.ucr.edu/~carter/absts.htm#saprc99 and http://www.cert.ucr.edu/~carter/reactdat.htm.

Carter, W. P. L. (2000b): "Implementation of the SAPRC-99 Chemical Mechanism into the Models-3 Framework," Report to the United States Environmental Protection Agency, January 29. Available at http://www.cert.ucr.edu/~carter/absts.htm#s99mod3.

Carter, W. P. L. (2004): Evaluation of a Gas-Phase Atmospheric Reaction Mechanism for Low NO_x Conditions," Final Report to California Air Resources Board Contract No. 01-305, May 5. Available at http://www.cert.ucr.edu/~carter/absts.htm#lnoxrpt.

Carter, W. P. L. (2010a): "Development of the SAPRC-07 Chemical Mechanism and Updated Ozone Reactivity Scales," Final report to the California Air Resources Board Contract No. 03-318, 06-408, and 07-730. January 27. Available at www.cert.ucr.edu/~carter/SAPRC.

Carter, W. P. L. (2010b): "Development of the SAPRC-07 chemical mechanism," Atmospheric Environment 44, 5324-5335.

Carter, W. P. L. (2010c): "Development of a Condensed SAPRC-07 Chemical Mechanism," Final Report to the California Air Resources Board, January 28. Available at http://www.cert.ucr.edu/~carter/absts.htm#csaprc07.

Carter, W. P. L., R. Atkinson, A. M. Winer, and J. N. Pitts, Jr. (1982): "Experimental Investigation of Chamber-Dependent Radical Sources," Int. J. Chem. Kinet., 14, 1071.

Carter, W. P. L. and F. W. Lurmann (1991): "Evaluation of a Detailed Gas-Phase Atmospheric Reaction Mechanism using Environmental Chamber Data," Atm. Environ. 25A, 2771-2806.

Carter, W. P. L., J. A. Pierce, I. L. Malkina, D. Luo and W. D. Long (1993): "Environmental Chamber Studies of Maximum Incremental Reactivities of Volatile Organic Compounds," Report to Coordinating Research Council, Project No. ME-9, California Air Resources Board Contract No. A032-0692; South Coast Air Quality Management District Contract No. C91323, United States Environmental Protection Agency Cooperative Agreement No. CR-814396-01-0, University Corporation for Atmospheric Research Contract No. 59166, and Dow Corning Corporation. April 1. Available at http://www.cert.ucr.edu/~carter/absts.htm#rct1rept

Carter, W. P. L., D. Luo, I. L. Malkina, and D. Fitz (1995a): "The University of California, Riverside Environmental Chamber Data Base for Evaluating Oxidant Mechanism. Indoor Chamber Experiments through 1993," Report submitted to the U. S. Environmental Protection Agency, EPA/AREAL, Research Triangle Park, NC, March 20.

Carter, W. P. L., D. Luo, I. L. Malkina, and J. A. Pierce (1995b): "Environmental Chamber Studies of Atmospheric Reactivities of Volatile Organic Compounds. Effects of Varying ROG Surrogate and NO_x," Final report to Coordinating Research Council, Inc., Project ME-9, California Air Resources Board, Contract A032-0692, and South Coast Air Quality Management District, Contract C91323. March 24.

Carter, W. P. L., D. R. Cocker III, D. R. Fitz, I. L. Malkina, K. Bumiller, C. G. Sauer, J. T. Pisano, C. Bufalino, and C. Song (2005): "A New Environmental Chamber for Evaluation of Gas-Phase Chemical Mechanisms and Secondary Aerosol Formation", Atmos. Environ. 39 7768-7788.

Carter, W. P. L. and I. L. Malkina (2005): "Evaluation of Atmospheric Impacts of Selected Coatings VOC Emissions," Final report to the California Air Resources Board Contract No. 00-333, March 21. Available at http://www.cert.ucr.edu/~carter/absts.htm#coatrpt.

Carter, W. P. L. and I. L. Malkina (2007): "Investigation of the Atmospheric Impacts of Selected Pesticides," Final Report to the California Air Resources Board Contract 04-334, January 10. Available at http://www.cert.ucr.edu/~carter/absts.htm#pestrep.

Carter, W. P. L. and J. H. Seinfeld (2012): "Winter ozone formation and VOC incremental reactivities in the Upper Green River Basin of Wyoming," Atmospheric Environment, in press. doi:10.1016/j.atmosenv.2011.12.025

Carter, W. P. L., Gookyoung Heo, David R. Cocker III, and Shunsuke Nakao (2012): "SOA Formation: Chamber Study and Model Development," Final report to CARB contract 08-326, May 21. Available at http://www.cert.ucr.edu/~carter/absts.htm #pmchrpt

Dodge, M. C. (2000): "Chemical Oxidant Mechanisms for Air Quality Modeling, Critical Review Paper for 1998 Ozone Assessment," Atmos. Environ, 34, 2103-2130.

Goliff, W. (2012), "An Analysis of the Benzene Scheme for Three Versions of the SAPRC Mechanism," Draft report to CARB contract 07-730, December 20.

Gómez Alvarez, E., Viidanoja, J., Muñoz, A., Wirtz, K., Hjorth, J. (2007): "Experimental confirmation of the dicarbonyl route in the photo-oxidation of toluene and benzene," Environmental Science & Technology 41, 8362-8369.

Hoshino, M., Akimoto, H., Okuda, M. (1978): "Photochemical oxidation of benzene, toluene, and ethylbenzene initiated by OH radicals in the gas phase," Bulletin of the Chemical Society of Japan 51, 718-724.

Hynes, R. G., D. E. Angove, S, M. Saunders, V. Haverd, and M. Azzi (2005): "Evaluation of two MCM v3.1 alkene mechanisms using indoor environmental chamber data," Atmos. Environ., 39, 7251-7262.

IUPAC (2006): "Evaluated Kinetic and Photochemical Data". IUPAC Subcommittee on Gas Kinetic Data Evaluation for Atmospheric Chemistry. Web Version. Available at http://www.iupac-kinetic.ch.cam.ac.uk. Latest data sheets dated June, 2006.

IUPAC (2008a): http://www.iupac-kinetic.ch.cam.ac.uk/datasheets/pdf/HOx_VOC16_HO_(CHO)2.pdf

IUPAC (2008b): http://www.iupac-kinetic.ch.cam.ac.uk/datasheets/pdf/HOx_AROM4_HO_o-cresol.pdf

IUPAC (2008c): http://www.iupac-kinetic.ch.cam.ac.uk/datasheets/pdf/NO3_AROM4_NO3_o-cresol.pdf

IUPAC (2008d): http://www.iupac-kinetic.ch.cam.ac.uk/datasheets/pdf/HOx_AROM6_HO_phenol.pdf

IUPAC (2008e): http://www.iupac-kinetic.ch.cam.ac.uk/datasheets/pdf/HOx_AROM8_HO_1,2-hydroxy-3-methylbenzene.pdf

IUPAC (2008f): http://www.iupac-kinetic.ch.cam.ac.uk/datasheets/pdf/NO3_AROM8_NO3_1,2-dihydroxy-3-methylbenzene.pdf

IUPAC (2008g): http://www.iupac-kinetic.ch.cam.ac.uk/datasheets/pdf/NO3_AROM6_NO3_phenol.pdf

IUPAC (2009): http://www.iupac-kinetic.ch.cam.ac.uk/datasheets/pdf/HOx_VOC54_HO2_CH3CO3.pdf

Jenkin, M. E., S. M. Saunders, and M. J. Pilling (1997): "The tropospheric degradation of volatile organic compounds: A protocol for mechanism development," Atmos Environ, 31(1), 81-104.

Jenkin, M. E., S. M. Saunders, V. Wagner, and M. J. Pilling (2003): "Protocol for the development of the Master Chemical Mechanism, MCM v3 (Part B): tropospheric degradation of aromatic volatile organic compounds," Atmos Chem Phys, 3, 181-193.

Klotz, B., R. Volkamer, M. D. Hurley, M. P. S. Andersen, M. P. S.; O. J. Nielsen, I. Barnes, T. Imamura, K. Wirtz, K.-H. Becker, U. Platt, T. J. Wallington, and N. Washida (2002): "OH-Initiated Oxidation of Benzene: Part II. Influence of Elevanted NO_x Concentrations," Phys. Chem. Chem. Phys. 4, 4399-4411.

Koch, R., R. Knispel, M. Elend, M. Siese, and C. Zetzsch (2007): "Consecutive reactions of aromatic-OH adducts with NO, NO_2 and O_2: benzene, naphthalene, toluene, m- and p-xylene, hexamethylbenzene, phenol, m-cresol and aniline," Atmos. Chem. Phys. 7, 2057-2071.

Lloyd, A.C., K.R. Darnall, A.M. Winer, and J.N. Pitts, Jr. (1976): "Relative rate constants for reaction of the hydroxyl radical with a series of alkanes, alkenes, and aromatic hydrocarbons," J. Phys. Chem. 80(8), 789-794.

NASA (2006): "Chemical Kinetics and Photochemical Data for Use in Stratospheric Modeling, Evaluation Number 15," JPL Publication 06-2, Jet Propulsion Laboratory, Pasadena, California, July.

NASA (2011): "Chemical Kinetics and Photochemical Data for Use in Stratospheric Modeling, Evaluation Number 17," JPL Publication 10-6, Jet Propulsion Laboratory, Pasadena, California, July. From http://jpldataeval.jpl.nasa.gov.

Nishino, N., Arey, J., Atkinson, R. (2010): " Formation yields of glyoxal and methylglyoxal from the gas-phase OH radical-initiated reactions of toluene, xylenes, and trimethylbenzenes as a function of NO2 concentration," J. Phys. Chem. A 114, 10140-10147.

Noda, J., Volkamer, R., Molina, M.J. (2009): "Dealkylation of alkylbenzenes: a significant pathway in the toluene, o-, m-, and p-xylene þ OH reaction," Journal of Physical Chemistry A 113, 9658-9666.

Ohta, T., Ohyama, T. (1985): "A set of rate constants for the reactions of OH radicals with aromatic hydrocarbons," Bull. Chem. Soc. Jpn. 58, 3029-3020.

Olariu, R. I., B. Klotz, I. Barnes, K.H. Becker, and R. Mocanu (2002): "FT-IR study of the ring-retaining products from the reaction of OH radicals with phenol, o-, m-, and p-cresol," Atmos. Environ. 36, 3685-3697.

Ravishankara, A.R., Wagner, S., Fischer, S., Smith, G., Schiff, R., Watson, R.T., Tesi, G., Davis, D.D. (1978): "A kinetic study of the reactions of OH with several aromatic and olefinic compounds," International Journal of Chemical Kinetics 10, 783-804.

Rohrer, F., Bohn, B., Brauers, T., Brüning, D., Johnen, F. -J., Wahner, A. and Kleffmann, J. (2005): "Characterisation of the photolytic HONO-source in the atmosphere simulation chamber SAPHIR," Atmos. Chem. Phys. 5, 2189-2201. Available at http://www.atmos-chem-phys.org/5/2189/2005/acp-5-2189-2005.pdf

Saunders, S. M., M. E. Jenkin, R. G. Derwent, and M. J. Pilling (2003): "Protocol for the development of the Master Chemical Mechanism, MCM v3 (Part A): tropospheric degradation of non-aromatic volatile organic compounds," Atmos Chem Phys, 3, 161-180.

Smith, D.F., McIver, C.D., Kleindienst, T.E. (1998): "Primary product distribution from the reaction of hydroxyl radicals with toluene at ppb NOx mixing ratios," Journal of Atmospheric Chemistry 30, 209-228.

Smith, D.F., Kleindienst, T.E., McIver, C.D. (1999): "Primary product distributions from the reaction of OH with m-, p-xylene, 1,2,4- and 1`,3,5-trimethylbenzene," Journal of Atmospheric Chemistry 34, 339-364.

Simonaitis, R. and E. M. Bailey (1995): "Smog Chamber Studies at Low VOC and NO_x Concentrations: Phase I," Report on Interagency Agreement DW64936024 to EPA/NREL, Research Triangle Park, NC.

Simonaitis, R., J. Meagher, and E. M. Bailey (1997): "Evaluation of the condensed Carbon Bond Mechanism against smog chamber data at low VOC and NOx Concentrations," Atmos. Environ. 31, 27-43

Thüner, L. P., B. P. Bardini, G. J. Rea, and J.C. Wenger (2004): "Kinetics of the Gas-Phase Reactions of OH and NO3 Radicals with Dimethylphenols," J. Phys. Chem. A 108, 11019-11025

Tuazon E.C., R. Atkinson R. and W. P. L. Carter W.P.L. (1985): "Atmospheric Chemistry of cis- and trans-3-Hexene-2,5-dione,". Environ. Sci. Technol., 19, 265-269.

Tuazon, E. C., H. MacLeod, R. Atkinson, and W. P. L. Carter (1986): "α-Dicarbonyl yields from the NOx -air photooxidations of a series of aromatic hydrocarbons in air," Environ. Sci. Technol. 20, 33-387.

Volkamer, R., Platt, U., Wirtz, K. (2001): "Primary and secondary glyoxal formation from aromatics: experimental evidence for the bicycloalkyl-radical pathway from benzene, toluene, and p-xylene," J. Phys. Chem. A 105, 7865-7874.

Volkamer, R., B. Klotz, I. Barnes, T. Imamura, K. Wirtz, N. Washida, K. H. Becker, and U. Platt (2002): "OH-initiated oxidation of benzene. Part I. Phenol formation under atmospheric conditions," Phys. Chem. Chem. Phys. 4, 1598-1610.

Volkamer, R., P. Spietz, J. Burrows, and U. Platt (2005): "High-resolution absorption cross sections of glyoxal in the UV-vis and IR spectral ranges," J. Photochem. Photobiol. A: Chemistry 172, 35-46.

White, S.J., M. Azzi, D. E. Angove, and I. M. Jamie (2010): "Modelling the photooxidation of ULP, E5 and E1 in the CSIRO smog chamber," Atmos. Environ. 44(14), 1707-1713

White, S. J. (2010): Stephen. J. White, Commonwealth Scientific and Industrial Research Organisation, personal communication.

Zádor, J., Turányi, T., Wirtz, K., Pilling, M.J. (2006): "Measurement and investigation of chamber radical sources in the European Photoreactor (EUPHORE)," Journal of Atmospheric Chemistry 55, 147-166.

APPENDIX A. MECHANISM LISTING TABLES

This appendix contains the tables giving a complete listing of the SAPRC-11 mechanism developed in this work. Note that the SAPRC-11 mechanism is the same as SAPRC-07 except as indicated on Table 1 and Table 2, so these tables, and the SAPRC-07 mechanism documentation (Carter, 2010a,b) should be consulted for details.

Table A-1. List of model species used in the SAPRC-11 mechanism.

Type and Name	Description
Constant Species.	
O2	Oxygen
M	Air
H2O	Water
H2	Hydrogen Molecules
HV	Light
Active Inorganic Species.	
O3	Ozone
NO	Nitric Oxide
NO2	Nitrogen Dioxide
NO3	Nitrate Radical
N2O5	Nitrogen Pentoxide
HONO	Nitrous Acid
HNO3	Nitric Acid
HNO4	Peroxynitric Acid
HO2H	Hydrogen Peroxide
CO	Carbon Monoxide
SO2	Sulfur Dioxide
Active Radical Species and Operators.	
OH	Hydroxyl Radicals
HO2	Hydroperoxide Radicals
MEO2	Methyl Peroxy Radicals
RO2C	Peroxy Radical Operator representing NO to NO2 and NO3 to NO2 conversions, and the effects of peroxy radical reactions on acyl peroxy and other peroxy radicals.
RO2XC	Peroxy Radical Operator representing NO consumption (used in conjunction with organic nitrate formation), and the effects of peroxy radical reactions on NO3, acyl peroxy radicals, and other peroxy radicals.
MECO3	Acetyl Peroxy Radicals
RCO3	Peroxy Propionyl and higher peroxy acyl Radicals
BZCO3	Peroxyacyl radical formed from Aromatic Aldehydes
MACO3	Peroxyacyl radicals formed from methacrolein and other acroleins.

Table A-1 (continued)

Type and Name	Description
Steady State Radical Species	
O3P	Ground State Oxygen Atoms
O1D	Excited Oxygen Atoms
TBUO	t-Butoxy Radicals
BZO	Phenoxy Radicals
HCOCO3	HC(O)C(O)OO Radicals
PAN and PAN Analogues	
PAN	Peroxy Acetyl Nitrate
PAN2	PPN and other higher alkyl PAN analogues
PBZN	PAN analogues formed from Aromatic Aldehydes
MAPAN	PAN analogue formed from Methacrolein
Explicit and Lumped Molecule Reactive Organic Product Species	
HCHO	Formaldehyde
CCHO	Acetaldehyde
RCHO	Lumped C3+ Aldehydes (mechanism based on propionaldehyde)
ACET	Acetone
MEK	Ketones and other non-aldehyde oxygenated products which react with OH radicals faster than 5 x 10-13 but slower than 5 x 10-12 cm3 molec-2 sec-1. (Based on mechanism for methyl ethyl ketone).
MEOH	Methanol
HCOOH	Formic Acid
CCOOH	Acetic Acid. Also used for peroxyacetic acid.
RCOOH	Higher organic acids and peroxy acids (mechanism based on propionic acid).
COOH	Methyl Hydroperoxide
ROOH	Lumped organic hydroperoxides with 2-4 carbons. Mechanism based on that estimated for n-propyl hydroperoxide.
R6OOH	Lumped organic hydroperoxides with 5 or more carbons, and organic hydroperoxides formed from aromatics that do not participate in SOA formation. Mechanism based on that estimated for 3-hexyl hydroperoxide.
RAOOH	Organic hydroperoxides formed from aromatic hydrocarbons that condense to form SOA (see Carter et al, 2012 for a complete listing of the mechanism and model species used for modeling aromatic SOA formation.)
GLY	Glyoxal
MGLY	Methyl Glyoxal
BACL	Biacetyl
PHEN	Phenol
CRES	Cresols
XYNL	Xylenols and higher alkylphenols
CATL	Catechols
NPHE	Nitrophenols
BALD	Aromatic aldehydes (e.g., benzaldehyde)
MACR	Methacrolein
MVK	Methyl Vinyl Ketone

Table A-1 (continued)

Type and Name	Description
IPRD	Lumped isoprene product species
Aromatic unsaturated ring fragmentation products	
AFG1	Monounsaturated dialdehydes or aldehyde-ketones formed from aromatics. - Most photoreactive
AFG2	Monounsaturated dialdehydes or aldehyde-ketones formed from aromatics. - Least photoreactive
AFG3	Diunsaturatred dicarbonyl aromatic fragmentation products that are assumed not to photolyze rapidly
AFG4	3-hexene-2,5-dione and other monounsaturated diketone aromatic products.
Lumped Parameter Products	
PROD2	Ketones and other non-aldehyde oxygenated products which react with OH radicals faster than 5 x 10-12 cm3 molec-2 sec-1.
RNO3	Lumped Organic Nitrates
Steady state operators used to represent radical or product formation in peroxy radical reactions.	
xHO2	Formation of HO2 from alkoxy radicals formed in peroxy radical reactions with NO and NO3 (100% yields) and RO2 (50% yields)
xOH	As above, but for OH
xNO2	As above, but for NO2
xMEO2	As above, but for MEO2
xMECO3	As above, but for MECO3
xRCO3	As above, but for RCO3
xMACO3	As above, but for MACO3
xTBUO	As above, but for TBUO
xCO	As above, but for CO
xHCHO	As above, but for HCHO
xCCHO	As above, but for CCHO
xRCHO	As above, but for RCHO
xACET	As above, but for ACET
xMEK	As above, but for MEK
xPROD2	As above, but for PROD2
xBALD	As above, but for BALD
xGLY	As above, but for GLY
xMGLY	As above, but for MGLY
xBACL	As above, but for BACL
xAFG1	As above, but for AFG1
xAFG2	As above, but for AFG2
xAFG4	As above, but for AFG4
xMACR	As above, but for MACR
xMVK	As above, but for MVK
xIPRD	As above, but for IPRD
xRNO3	As above, but for RNO3
zRNO3	Formation of RNO3 in the RO2 + NO, reaction, or formation of corresponding non-nitrate products (represented by PROD2) formed from alkoxy radicals formed in RO2 + NO3 and (in 50% yields) RO2 + RO2 reactions.

Table A-1 (continued)

Type and Name	Description
yROOH	Formation of ROOH following RO2 + HO2 reactions, or formation of H-shift disproportionation products (represented by MEK) in the RO2 + RCO3 and (in 50% yields) RO2 + RO2 reactions.
yR6OOH	As above, but the RO2 + HO2 product is represented by R6OOH and the H-shift products are represented by PROD2.
yRAOOH	Like yROOH or yR6OOH but for RAOOH
Non-Reacting Species	
CO2	Carbon Dioxide
SULF	Sulfates (SO3 or H2SO4)
XC	Lost Carbon or carbon in unreactive products
XN	Lost Nitrogen or nitrogen in unreactive products
Primary Organics Represented explicitly	
CH4	Methane
ETHENE	Ethene
ISOPRENE	Isoprene
ACETYLEN	Acetylene
BENZENE	Benzene
Species used in Lumped Mechanisms for Base Case and Ambient Simulations	
ALK1	Alkanes and other non-aromatic compounds that react only with OH, and have kOH between 2 and 5 x 102 ppm-1 min-1. (Primarily ethane)
ALK2	Alkanes and other non-aromatic compounds that react only with OH, and have kOH between 5 x 102 and 2.5 x 103 ppm-1 min-1. (Primarily propane)
ALK3	Alkanes and other non-aromatic compounds that react only with OH, and have kOH between 2.5 x 103 and 5 x 103 ppm-1 min-1.
ALK4	Alkanes and other non-aromatic compounds that react only with OH, and have kOH between 5 x 103 and 1 x 104 ppm-1 min-1.
ALK5	Alkanes and other non-aromatic compounds that react only with OH, and have kOH greater than 1 x 104 ppm-1 min-1.
ARO1	Aromatics with kOH < $2x10^4$ ppm^{-1} min^{-1}.
ARO2	Aromatics with kOH > $2x10^4$ ppm^{-1} min^{-1}.
OLE1	Alkenes (other than ethene) with kOH < 7x104 ppm-1 min-1.
OLE2	Alkenes with kOH > $7x10^4$ ppm^{-1} min^{-1}.
TERP	Terpenes
Non-aromatic compounds represented explicitly in chamber simulations. (Not in base mechanism)	
ETHANE	Ethane
PROPANE	Propane
N-C4	n-Butane
N-C6	n-Hexane
N-C8	n-Octane
PROPENE	Propene
T-2-BUTE	trans-2-Butene
N-C6F14	Perfluorohexane

Table A-1 (continued)

Type and Name	Description
Aromatic compounds represented explicitly in chamber simulations (not in base mechanism)	
TOLUENE	Toluene
C2-BENZ	Ethyl Benzene
N-C3-BEN	n-Propyl Benzene
I-C3-BEN	Isopropyl Benzene
M-XYLENE	m-Xylene
O-XYLENE	o-Xylene
P-XYLENE	p-Xylene
M-ET-TOL	m-Ethyl toluene
O-ET-TOL	o-Ethyl toluene
P-ET-TOL	p-Ethyl toluene
123-TMB	1,2,3-trimethylbenzene
124-TMB	1,2,4-trimethylbenzene
135-TMB	1,3,5-trimethylbenzene
Steady-State species used in the SAPRC-11A version only.	
BENZOH TOLOH ETBOH PXYOH	Used to represent OH-aromatic adducts in the benzene, toluene, ethyl benzene and p-xylene mechanisms to represent the competition between the adduct + NO_2 and adduct + O_2 reactions.

Table A-2. Listing of reactions and rate parameters in the base SAPRC-07 mechanism.

Label	Reaction and Products [a]	Rate Parameters [b]			
		k(300)	A	Ea	B
Inorganic Reactions					
1	NO2 + HV = NO + O3P	Phot Set= NO2-06			
2	O3P + O2 + M = O3 + M	5.68e-34	5.68e-34	0.00	-2.60
3	O3P + O3 = #2 O2	8.34e-15	8.00e-12	4.09	
4	O3P + NO = NO2	1.64e-12	Falloff, F=0.60, N=1.00		
			0: 9.00e-32	0.00	-1.50
			inf: 3.00e-11	0.00	0.00
5	O3P + NO2 = NO + O2	1.03e-11	5.50e-12	-0.37	
6	O3P + NO2 = NO3	3.24e-12	Falloff, F=0.60, N=1.00		
			0: 2.50e-31	0.00	-1.80
			inf: 2.20e-11	0.00	-0.70
7	O3 + NO = NO2 + O2	2.02e-14	3.00e-12	2.98	
8	O3 + NO2 = O2 + NO3	3.72e-17	1.40e-13	4.91	
9	NO + NO3 = #2 NO2	2.60e-11	1.80e-11	-0.22	
10	NO + NO + O2 = #2 NO2	1.93e-38	3.30e-39	-1.05	
11	NO2 + NO3 = N2O5	1.24e-12	Falloff, F=0.35, N=1.33		
			0: 3.60e-30	0.00	-4.10
			inf: 1.90e-12	0.00	0.20
12	N2O5 = NO2 + NO3	5.69e-2	Falloff, F=0.35, N=1.33		
			0: 1.30e-3	21.86	-3.50
			inf: 9.70e+14	22.02	0.10
13	N2O5 + H2O = #2 HNO3	2.50e-22			
14	N2O5 + H2O + H2O = #2 HNO3 + H2O	1.80e-39			
15	NO2 + NO3 = NO + NO2 + O2	6.75e-16	4.50e-14	2.50	
16	NO3 + HV = NO + O2	Phot Set= NO3NO-06			
17	NO3 + HV = NO2 + O3P	Phot Set= NO3NO2-6			
18	O3 + HV = O1D + O2	Phot Set= O3O1D-06			
19	O3 + HV = O3P + O2	Phot Set= O3O3P-06			
20	O1D + H2O = #2 OH	1.99e-10	1.63e-10	-0.12	
21	O1D + M = O3P + M	3.28e-11	2.38e-11	-0.19	
22	OH + NO = HONO	7.31e-12	Falloff, F=0.60, N=1.00		
			0: 7.00e-31	0.00	-2.60
			inf: 3.60e-11	0.00	-0.10
23	HONO + HV = OH + NO	Phot Set= HONO-06			
24	OH + HONO = H2O + NO2	5.95e-12	2.50e-12	-0.52	
25	OH + NO2 = HNO3	1.05e-11	Falloff, F=0.60, N=1.00		
			0: 1.80e-30	0.00	-3.00
			inf: 2.80e-11	0.00	0.00
26	OH + NO3 = HO2 + NO2	2.00e-11			
27	OH + HNO3 = H2O + NO3	1.51e-13	k = k0+k3M/(1+k3M/k2)		

Table A-2 (continued)

Label	Reaction and Products [a]	Rate Parameters [b]			
		k(300)	A	Ea	B
		k0:	2.40e-14	-0.91	0.00
		k2:	2.70e-17	-4.37	0.00
		k3:	6.50e-34	-2.65	0.00
28	HNO3 + HV = OH + NO2	Phot Set= HNO3			
29	OH + CO = HO2 + CO2	2.28e-13	k = k1 + k2 [M]		
		k1:	1.44e-13	0.00	0.00
		k2:	3.43e-33	0.00	0.00
30	OH + O3 = HO2 + O2	7.41e-14	1.70e-12	1.87	
31	HO2 + NO = OH + NO2	8.85e-12	3.60e-12	-0.54	
32	HO2 + NO2 = HNO4	1.12e-12	Falloff, F=0.60, N=1.00		
		0:	2.00e-31	0.00	-3.40
		inf:	2.90e-12	0.00	-1.10
33	HNO4 = HO2 + NO2	1.07e-1	Falloff, F=0.60, N=1.00		
		0:	3.72e-5	21.16	-2.40
		inf:	5.42e+15	22.20	-2.30
34	HNO4 + HV = #.61 {HO2 + NO2} + #.39 {OH + NO3}	Phot Set= HNO4-06			
35	HNO4 + OH = H2O + NO2 + O2	4.61e-12	1.30e-12	-0.76	
36	HO2 + O3 = OH + #2 O2	2.05e-15	2.03e-16	-1.38	4.57
37	HO2 + HO2 = HO2H + O2	2.84e-12	k = k1 + k2 [M]		
		k1:	2.20e-13	-1.19	0.00
		k2:	1.90e-33	-1.95	0.00
38	HO2 + HO2 + H2O = HO2H + O2 + H2O	6.09e-30	k = k1 + k2 [M]		
		k1:	3.08e-34	-5.56	0.00
		k2:	2.66e-54	-6.32	0.00
39	NO3 + HO2 = #.8 {OH + NO2 + O2} + #.2 {HNO3 + O2}	4.00e-12			
40	NO3 + NO3 = #2 NO2 + O2	2.41e-16	8.50e-13	4.87	
41	HO2H + HV = #2 OH	Phot Set= H2O2			
42	HO2H + OH = HO2 + H2O	1.80e-12	1.80e-12	0.00	
43	OH + HO2 = H2O + O2	1.10e-10	4.80e-11	-0.50	
44	OH + SO2 = HO2 + SULF	9.49e-13	Falloff, F=0.60, N=1.00		
		0:	3.30e-31	0.00	-4.30
		inf:	1.60e-12	0.00	0.00
45	OH + H2 = HO2 + H2O	7.02e-15	7.70e-12	4.17	
Methyl peroxy and methoxy reactions					
BR01	MEO2 + NO = NO2 + HCHO + HO2	7.64e-12	2.30e-12	-0.72	
BR02	MEO2 + HO2 = COOH + O2	4.65e-12	3.46e-13	-1.55	0.36
BR03	MEO2 + HO2 = HCHO + O2 + H2O	4.50e-13	3.34e-14	-1.55	-3.53
BR04	MEO2 + NO3 = HCHO + HO2 + NO2	1.30e-12			
BR05	MEO2 + MEO2 = MEOH + HCHO + O2	2.16e-13	6.39e-14	-0.73	-1.80
BR06	MEO2 + MEO2 = #2 {HCHO + HO2}	1.31e-13	7.40e-13	1.03	

Table A-2 (continued)

Label	Reaction and Products [a]	Rate Parameters [b] k(300)	A	Ea	B
Active Peroxy Racical Operators					
BR07	RO2C + NO = NO2	9.23e-12	2.60e-12	-0.76	
BR08	RO2C + HO2 =	7.63e-12	3.80e-13	-1.79	
BR09	RO2C + NO3 = NO2	2.30e-12			
BR10	RO2C + MEO2 = #.5 HO2 + #.75 HCHO + #.25 MEOH	2.00e-13			
BR11	RO2C + RO2C =	3.50e-14			
BR12	RO2XC + NO = XN	Same k as rxn BR07			
BR13	RO2XC + HO2 =	Same k as rxn BR08			
BR14	RO2XC + NO3 = NO2	Same k as rxn BR09			
BR15	RO2XC + MEO2 = #.5 HO2 + #.75 HCHO + #.25 MEOH	Same k as rxn BR10			
BR16	RO2XC + RO2C =	Same k as rxn BR11			
BR17	RO2XC + RO2XC =	Same k as rxn BR11			
Reactions of Acyl Peroxy Radicals, PAN, and PAN analogues					
BR18	MECO3 + NO2 = PAN	9.37e-12	Falloff, F=0.30, N=1.41		
		0:	2.70e-28	0.00	-7.10
		inf:	1.21e-11	0.00	-0.90
BR19	PAN = MECO3 + NO2	6.27e-4	Falloff, F=0.30, N=1.41		
		0:	4.90e-3	24.05	0.00
		inf:	4.00e+16	27.03	0.00
BR20	PAN + HV = #.6 {MECO3 + NO2} + #.4 {MEO2 + CO2 + NO3}	Phot Set= PAN			
BR21	MECO3 + NO = MEO2 + CO2 + NO2	1.97e-11	7.50e-12	-0.58	
BR22	MECO3 + HO2 = #.44 {OH + MEO2 + CO2} + #.41 CCOOH + #.15 {O3 + CCOOH}	1.36e-11	5.20e-13	-1.95	
BR23	MECO3 + NO3 = MEO2 + CO2 + NO2 + O2	Same k as rxn BR09			
BR24	MECO3 + MEO2 = #.1 {CCOOH + HCHO + O2} + #.9 {HCHO + HO2 + MEO2 + CO2}	1.06e-11	2.00e-12	-0.99	
BR25	MECO3 + RO2C = MEO2 + CO2	1.56e-11	4.40e-13	-2.13	
BR26	MECO3 + RO2XC = MEO2 + CO2	Same k as rxn BR25			
BR27	MECO3 + MECO3 = #2 {MEO2 + CO2} + O2	1.54e-11	2.90e-12	-0.99	
BR28	RCO3 + NO2 = PAN2	1.21e-11	1.21e-11	0.00	-1.07
BR29	PAN2 = RCO3 + NO2	5.48e-4	8.30e+16	27.70	
BR30	PAN2 + HV = #.6 {RCO3 + NO2} + #.4 {RO2C + xHO2 + yROOH + xCCHO + CO2 + NO3}	Phot Set= PAN			
BR31	RCO3 + NO = NO2 + RO2C + xHO2 + yROOH + xCCHO + CO2	2.08e-11	6.70e-12	-0.68	
BR32	RCO3 + HO2 = #.44 {OH + RO2C + xHO2 + xCCHO + yROOH + CO2} + #.41 RCOOH + #.15 {O3 + RCOOH}	Same k as rxn BR22			
BR33	RCO3 + NO3 = NO2 + RO2C + xHO2 + yROOH + xCCHO + CO2 + O2	Same k as rxn BR09			

Table A-2 (continued)

Label	Reaction and Products [a]	Rate Parameters [b]			
		k(300)	A	Ea	B
BR34	RCO3 + MEO2 = HCHO + HO2 + RO2C + xHO2 + xCCHO + yROOH + CO2	Same k as rxn BR24			
BR35	RCO3 + RO2C = RO2C + xHO2 + xCCHO + yROOH + CO2	Same k as rxn BR25			
BR36	RCO3 + RO2XC = RO2C + xHO2 + xCCHO + yROOH + CO2	Same k as rxn BR25			
BR37	RCO3 + MECO3 = #2 CO2 + MEO2 + RO2C + xHO2 + yROOH + xCCHO + O2	Same k as rxn BR27			
BR38	RCO3 + RCO3 = #2 {RO2C + xHO2 + xCCHO + yROOH + CO2}	Same k as rxn BR27			
BR39	BZCO3 + NO2 = PBZN	1.37e-11			
BR40	PBZN = BZCO3 + NO2	4.27e-4	7.90e+16	27.82	
BR41	PBZN + HV = #.6 {BZCO3 + NO2} + #.4 {CO2 + BZO + RO2C + NO3}	Phot Set= PAN			
BR42	BZCO3 + NO = NO2 + CO2 + BZO + RO2C	Same k as rxn BR31			
BR43	BZCO3 + HO2 = #.44 {OH + BZO + RO2C + CO2} + #.41 RCOOH + #.15 {O3 + RCOOH} + #2.24 XC	Same k as rxn BR22			
BR44	BZCO3 + NO3 = NO2 + CO2 + BZO + RO2C + O2	Same k as rxn BR09			
BR45	BZCO3 + MEO2 = HCHO + HO2 + RO2C + BZO + CO2	Same k as rxn BR24			
BR46	BZCO3 + RO2C = RO2C + BZO + CO2	Same k as rxn BR25			
BR47	BZCO3 + RO2XC = RO2C + BZO + CO2	Same k as rxn BR25			
BR48	BZCO3 + MECO3 = #2 CO2 + MEO2 + BZO + RO2C	Same k as rxn BR27			
BR49	BZCO3 + RCO3 = #2 CO2 + RO2C + xHO2 + yROOH + xCCHO + BZO + RO2C	Same k as rxn BR27			
BR50	BZCO3 + BZCO3 = #2 {BZO + RO2C + CO2}	Same k as rxn BR27			
BR51	MACO3 + NO2 = MAPAN	Same k as rxn BR28			
BR52	MAPAN = MACO3 + NO2	4.79e-4	1.60e+16	26.80	
BR53	MAPAN + HV = #.6 {MACO3 + NO2} + #.4 {CO2 + HCHO + MECO3 + NO3}	Phot Set= PAN			
BR54	MACO3 + NO = NO2 + CO2 + HCHO + MECO3	Same k as rxn BR31			
BR55	MACO3 + HO2 = #.44 {OH + HCHO + MECO3 + CO2} + #.41 RCOOH + #.15 {O3 + RCOOH} + #.56 XC	Same k as rxn BR22			
BR56	MACO3 + NO3 = NO2 + CO2 + HCHO + MECO3 + O2	Same k as rxn BR09			
BR57	MACO3 + MEO2 = #2 HCHO + HO2 + CO2 + MECO3	Same k as rxn BR24			
BR58	MACO3 + RO2C = CO2 + HCHO + MECO3	Same k as rxn BR25			
BR59	MACO3 + RO2XC = CO2 + HCHO + MECO3	Same k as rxn BR25			
BR60	MACO3 + MECO3 = #2 CO2 + MEO2 + HCHO + MECO3 + O2	Same k as rxn BR27			
BR61	MACO3 + RCO3 = HCHO + MECO3 + RO2C + xHO2 + yROOH + xCCHO + #2 CO2	Same k as rxn BR27			
BR62	MACO3 + BZCO3 = HCHO + MECO3 + BZO + RO2C + #2 CO2	Same k as rxn BR27			
BR63	MACO3 + MACO3 = #2 {HCHO + MECO3 + CO2}	Same k as rxn BR27			

Table A-2 (continued)

Label	Reaction and Products [a]	Rate Parameters [b] k(300)	A	Ea	B
Other Organic Radical Species					
BR64	TBUO + NO2 = RNO3 + #-2 XC	2.40e-11			
BR65	TBUO = ACET + MEO2	1.18e+3	7.50e+14	16.20	
BR66	BZO + NO2 = NPHE	3.79e-11	2.30e-11	-0.30	
BR67	BZO + HO2 = CRES + #-1 XC	Same k as rxn BR08			
BR68	BZO = CRES + RO2C + xHO2 + #-1 XC	1.00e-3			
Steady-State Peroxy Radical operators (for formation of inorganic and radical products)					
RO01	xHO2 = HO2	k is variable parameter: RO2RO			
RO02	xHO2 =	k is variable parameter: RO2XRO			
RO03	xOH = OH	k is variable parameter: RO2RO			
RO04	xOH =	k is variable parameter: RO2XRO			
RO05	xNO2 = NO2	k is variable parameter: RO2RO			
RO06	xNO2 = XN	k is variable parameter: RO2XRO			
RO07	xMEO2 = MEO2	k is variable parameter: RO2RO			
RO08	xMEO2 = XC	k is variable parameter: RO2XRO			
RO09	xMECO3 = MECO3	k is variable parameter: RO2RO			
RO10	xMECO3 = #2 XC	k is variable parameter: RO2XRO			
RO11	xRCO3 = RCO3	k is variable parameter: RO2RO			
RO12	xRCO3 = #3 XC	k is variable parameter: RO2XRO			
RO13	xMACO3 = MACO3	k is variable parameter: RO2RO			
RO14	xMACO3 = #4 XC	k is variable parameter: RO2XRO			
RO15	xTBUO = TBUO	k is variable parameter: RO2RO			
RO16	xTBUO = #4 XC	k is variable parameter: RO2XRO			
RO17	xCO = CO	k is variable parameter: RO2RO			
RO18	xCO = XC	k is variable parameter: RO2XRO			
Explicit and Lumped Molecule Organic Products					
BP01	HCHO + HV = #2 HO2 + CO	Phot Set= HCHOR-06			
BP02	HCHO + HV = H2 + CO	Phot Set= HCHOM-06			
BP03	HCHO + OH = HO2 + CO + H2O	8.47e-12	5.40e-12	-0.27	
BP04	HCHO + HO2 = HOCOO	Assumed to be negligible			
BP07	HCHO + NO3 = HNO3 + HO2 + CO	6.06e-16	2.00e-12	4.83	
BP08	CCHO + OH = MECO3 + H2O	1.49e-11	4.40e-12	-0.73	
BP09	CCHO + HV = CO + HO2 + MEO2	Phot Set= CCHO_R			
BP10	CCHO + NO3 = HNO3 + MECO3	2.84e-15	1.40e-12	3.70	
BP11	RCHO + OH = #.965 RCO3 + #.035 {RO2C + xHO2 + xCO + xCCHO + yROOH}	1.97e-11	5.10e-12	-0.80	
BP12	RCHO + HV = RO2C + xHO2 + yROOH + xCCHO + CO + HO2	Phot Set= C2CHO			
BP13	RCHO + NO3 = HNO3 + RCO3	6.74e-15	1.40e-12	3.18	
BP14	ACET + OH = RO2C + xMECO3 + xHCHO + yROOH	1.91e-13	4.56e-14	-0.85	3.65
BP15	ACET + HV = #.62 MECO3 + #1.38 MEO2 + #.38 CO	Phot Set= ACET-06, qy= 0.5			

Table A-2 (continued)

Label	Reaction and Products [a]	Rate Parameters [b]			
		k(300)	A	Ea	B
BP16	MEK + OH = #.967 RO2C + #.039 {RO2XC + zRNO3} + #.376 xHO2 + #.51 xMECO3 + #.074 xRCO3 + #.088 xHCHO + #.504 xCCHO + #.376 xRCHO + yROOH + #.3 XC	1.20e-12	1.30e-12	0.05	2.00
BP17	MEK + HV = MECO3 + RO2C + xHO2 + xCCHO + yROOH	Phot Set= MEK-06, qy= 0.175			
BP18	MEOH + OH = HCHO + HO2	9.02e-13	2.85e-12	0.69	
BP19	HCOOH + OH = HO2 + CO2	4.50e-13			
BP20	CCOOH + OH = #.509 MEO2 + #.491 RO2C + #.509 CO2 + #.491 xHO2 + #.491 xMGLY + #.491 yROOH + #-0.491 XC	7.26e-13	4.20e-14	-1.70	
BP21	RCOOH + OH = RO2C + xHO2 + #.143 CO2 + #.142 xCCHO + #.4 xRCHO + #.457 xBACL + yROOH + #-0.455 XC	1.20e-12			
BP22	COOH + OH = H2O + #.3 {HCHO + OH} + #.7 MEO2	7.40e-12	3.80e-12	-0.40	
BP23	COOH + HV = HCHO + HO2 + OH	Phot Set= COOH			
BP24	ROOH + OH = #.744 OH + #.251 RO2C + #.004 RO2XC + #.004 zRNO3 + #.744 RCHO + #.239 xHO2 + #.012 xOH + #.012 xHCHO + #.012 xCCHO + #.205 xRCHO + #.034 xPROD2 + #.256 yROOH + #-0.111 XC	2.50e-11			
BP25	ROOH + HV = RCHO + HO2 + OH	Phot Set= COOH			
BP26	R6OOH + OH = #.84 OH + #.222 RO2C + #.029 RO2XC + #.029 zRNO3 + #.84 PROD2 + #.09 xHO2 + #.041 xOH + #.02 xCCHO + #.075 xRCHO + #.084 xPROD2 + #.16 yROOH + #.017 XC	5.60e-11			
BP27	R6OOH + HV = OH + #.142 HO2 + #.782 RO2C + #.077 RO2XC + #.077 zRNO3 + #.085 RCHO + #.142 PROD2 + #.782 xHO2 + #.026 xCCHO + #.058 xRCHO + #.698 xPROD2 + #.858 yR6OOH + #.017 XC	Phot Set= COOH			
Isoprene Products					
BP54	MACR + OH = #.5 MACO3 + #.5 {RO2C + xHO2} + #.416 xCO + #.084 xHCHO + #.416 xMEK + #.084 xMGLY + #.5 yROOH + #-0.416 XC	2.84e-11	8.00e-12	-0.76	
BP55	MACR + O3 = #.208 OH + #.108 HO2 + #.1 RO2C + #.45 CO + #.117 CO2 + #.1 HCHO + #.9 MGLY + #.333 HCOOH + #.1 xRCO3 + #.1 xHCHO + #.1 yROOH + #-0.1 XC	1.28e-18	1.40e-15	4.17	
BP56	MACR + NO3 = #.5 {MACO3 + RO2C + HNO3 + xHO2 + xCO} + #.5 yROOH + #1.5 XC + #.5 XN	3.54e-15	1.50e-12	3.61	
BP57	MACR + O3P = RCHO + XC	6.34e-12			
BP58	MACR + HV = #.33 OH + #.67 HO2 + #.34 MECO3 + #.33 MACO3 + #.33 RO2C + #.67 CO + #.34 HCHO + #.33 xMECO3 + #.33 xHCHO + #.33 yROOH	Phot Set= MACR-06			

Table A-2 (continued)

Label	Reaction and Products [a]	Rate Parameters [b]			
		k(300)	A	Ea	B
BP59	MVK + OH = #.975 RO2C + #.025 {RO2XC + zRNO3} + #.3 xHO2 + #.675 xMECO3 + #.3 xHCHO + #.675 xRCHO + #.3 xMGLY + yROOH + #-0.725 XC	1.99e-11	2.60e-12	-1.21	
BP60	MVK + O3 = #.164 OH + #.064 HO2 + #.05 {RO2C + xHO2} + #.475 CO + #.124 CO2 + #.05 HCHO + #.95 MGLY + #.351 HCOOH + #.05 xRCO3 + #.05 xHCHO + #.05 yROOH + #-0.05 XC	5.36e-18	8.50e-16	3.02	
BP61	MVK + NO3 = #4 XC + XN		(Slow)		
BP62	MVK + O3P = #.45 RCHO + #.55 MEK + #.45 XC	4.32e-12			
BP63	MVK + HV = #.4 MEO2 + #.6 CO + #.6 PROD2 + #.4 MACO3 + #-2.2 XC		Phot Set= MVK-06		
BP64	IPRD + OH = #.289 MACO3 + #.67 {RO2C + xHO2} + #.041 {RO2XC + zRNO3} + #.336 xCO + #.055 xHCHO + #.129 xCCHO + #.013 xRCHO + #.15 xMEK + #.332 xPROD2 + #.15 xGLY + #.174 xMGLY + #-0.504 XC + #.711 yR6OOH	6.19e-11			
BP65	IPRD + O3 = #.285 OH + #.4 HO2 + #.048 {RO2C + xRCO3} + #.498 CO + #.14 CO2 + #.124 HCHO + #.21 MEK + #.023 GLY + #.742 MGLY + #.1 HCOOH + #.372 RCOOH + #.047 xCCHO + #.001 xHCHO + #.048 yR6OOH + #-.329 XC	4.18e-18			
BP66	IPRD + NO3 = #.15 {MACO3 + HNO3} + #.799 {RO2C + xHO2} + #.051 {RO2XC + zRNO3} + #.572 xCO + #.227 xHCHO + #.218 xRCHO + #.008 xMGLY + #.572 xRNO3 + #.85 yR6OOH + #.278 XN + #-.815 XC	1.00e-13			
BP67	IPRD + HV = #1.233 HO2 + #.467 MECO3 + #.3 RCO3 + #1.233 CO + #.3 HCHO + #.467 CCHO + #.233 MEK + #-.233 XC		Phot Set= MACR-06		
Lumped Parameter Organic Products					
BP68	PROD2 + OH = #.472 HO2 + #.379 xHO2 + #.029 xMECO3 + #.049 xRCO3 + #.473 RO2C + #.071 RO2XC + #.071 zRNO3 + #.002 HCHO + #.211 xHCHO + #.001 CCHO + #.083 xCCHO + #.143 RCHO + #.402 xRCHO + #.115 xMEK + #.329 PROD2 + #.007 xPROD2 + #.528 yR6OOH + #.877 XC	1.55e-11			
BP69	PROD2 + HV = #.913 xHO2 + #.4 MECO3 + #.6 RCO3 + #1.59 RO2C + #.087 RO2XC + #.087 zRNO3 + #.303 xHCHO + #.163 xCCHO + #.78 xRCHO + yR6OOH + #-.091 XC		Phot Set= MEK-06, qy= 4.86e-3		
BP70	RNO3 + OH = #.189 HO2 + #.305 xHO2 + #.019 NO2 + #.313 xNO2 + #.976 RO2C + #.175 RO2XC + #.175 zRNO3 + #.011 xHCHO + #.429 xCCHO + #.001 RCHO + #.036 xRCHO + #.004 xACET + #.01 MEK + #.17 xMEK + #.008 PROD2 + #.031 xPROD2 + #.189 RNO3 + #.305 xRNO3 + #.157 yROOH + #.636 yR6OOH + #.174 XN + #.04 XC	7.20e-12			

Table A-2 (continued)

Label	Reaction and Products [a]	Rate Parameters [b] k(300)	A	Ea	B
BP71	RNO3 + HV = #.344 HO2 + #.554 xHO2 + NO2 + #.721 RO2C + #.102 RO2XC + #.102 zRNO3 + #.074 HCHO + #.061 xHCHO + #.214 CCHO + #.23 xCCHO + #.074 RCHO + #.063 xRCHO + #.008 xACET + #.124 MEK + #.083 xMEK + #.19 PROD2 + #.261 xPROD2 + #.066 yROOH + #.591 yR6OOH + #.396 XC	Phot Set= IC3ONO2			
Aromatic Products					
BP30	GLY + HV = #2 {CO + HO2}	Phot Set= GLY-07R			
BP31	GLY + HV = HCHO + CO	Phot Set= GLY-07M			
BP32	GLY + OH = #.7 HO2 + #1.4 CO + #.3 HCOCO3	9.63e-12	3.10e-12	-0.68	
BP33	GLY + NO3 = HNO3 + #.7 HO2 + #1.4 CO + #.3 HCOCO3	1.02e-15	2.80e-12	4.72	
BP80	HCOCO3 + NO = HO2 + CO + CO2 + NO2	Same k as rxn BR31			
BP81	HCOCO3 + NO2 = HO2 + CO + CO2 + NO3	Same k as rxn BR28			
BP82	HCOCO3 + HO2 = #.44 {OH + HO2 + CO + CO2} + #.56 GLY + #.15 O3	Same k as rxn BR22			
BP34	MGLY + HV = HO2 + CO + MECO3	Phot Set= MGLY-06			
BP35	MGLY + OH = CO + MECO3	1.50e-11			
BP36	MGLY + NO3 = HNO3 + CO + MECO3	2.53e-15	1.40e-12	3.77	
BP37	BACL + HV = #2 MECO3	Phot Set= BACL-07			
BP40	NPHE + OH = BZO + XN	3.50e-12			
BP41	NPHE + HV = HONO + #6 XC	Phot Set= NO2-06, qy= 1.5e-3			
BP42	NPHE + HV = #6 XC + XN	Phot Set= NO2-06, qy= 1.5e-2			
BP43	BALD + OH = BZCO3	1.20e-11			
BP44	BALD + HV = #7 XC	Phot Set= BALD-06, qy= 0.06			
BP45	BALD + NO3 = HNO3 + BZCO3	2.73e-15	1.34e-12	3.70	
BP83	PHEN + OH = #.7 HO2 + #.1 BZO + #.095 xHO2 + #.105 OH + #.095 RO2C + #.7 CATL + #.105 AFG3 + #.048 xAFG1 + #.048 xAFG2 + #.095 xGLY + #.095 yRAOOH	2.74e-11	4.70e-13	-2.42	
BP84	PHEN + NO3 = #.1 HNO3 + #.9 XN + #.7 HO2 + #.1 BZO + #.095 xHO2 + #.105 OH + #.095 RO2C + #.7 CATL + #.105 AFG3 + #.048 xAFG1 + #.048 xAFG2 + #.095 xGLY + #.095 yRAOOH	3.80e-12			
BP38	CRES + OH = #.7 HO2 + #.1 BZO + #.17 xHO2 + #.03 OH + #.17 RO2C + #.7 CATL + #.03 AFG3 + #.085 xAFG1 + #.085 xAFG2 + #.085 xGLY + #.085 xMGLY + #.17 yRAOOH	4.06e-11	1.60e-12	-1.93	
BP39	CRES + NO3 = #.1 HNO3 + #.9 XN + #.7 HO2 + #.1 BZO + #.17 xHO2 + #.03 OH + #.17 RO2C + #.7 CATL + #.03 AFG3 + #.085 xAFG1 + #.085 xAFG2 + #.085 xGLY + #.085 xMGLY + #.170 yRAOOH	1.40e-11			
BP85	XYNL + OH = #.7 HO2 + #.07 BZO + #.23 xHO2 + #.23 RO2C + #.7 CATL + #.115 xAFG1 + #.115 xAFG2 + #.115 xGLY + #.115 xMGLY + #.23 yRAOOH	7.38e-11			

Table A-2 (continued)

Label	Reaction and Products [a]	Rate Parameters [b]			
		k(300)	A	Ea	B
BP86	XYNL + NO3 = #.07 HNO3 + #.93 XN + #.7 HO2 + #.07 BZO + #.23 xHO2 + #.23 RO2C + #.7 CATL + #.115 xAFG1 + #.115 xAFG2 + #.115 xGLY + #.115 xMGLY + #.23 yRAOOH	3.06e-11			
BP87	CATL + OH = #.4 HO2 + #.2 BZO + #.2 xHO2 + #.2 OH + #.2 RO2C + #.2 AFG3 + #.1 xAFG1 + #.1 xAFG2 + #.1 xGLY + #.1 xMGLY + #.33 CNDPP + #.2 yRAOOH	2.00e-10			
BP88	CATL + NO3 = #.2 HNO3 + #.8 XN + #.4 HO2 + #.2 BZO + #.2 xHO2 + #.2 OH + #.2 RO2C + #.2 AFG3 + #.1 xAFG1 + #.1 xAFG2 + #.1 xGLY + #.1 xMGLY + #.2 yRAOOH	1.70e-10			
BP46	AFG1 + OH = #.217 MACO3 + #.723 RO2C + #.060 {RO2XC + zRNO3} + #.521 xHO2 + #.201 xMECO3 + #.334 xCO + #.407 xRCHO + #.129 xMEK + #.107 xGLY + #.267 xMGLY + #.783 yR6OOH + #.284 XC	7.40e-11			
BP48	AFG1 + HV = #1.023 HO2 + #.173 MEO2 + #.305 MECO3 + #.500 MACO3 + #.695 CO + #.195 GLY + #.305 MGLY + #.217 XC		Phot Set= AFG1		
BP49	AFG2 + OH = #.217 MACO3 + #.723 RO2C + #.060 {RO2XC + zRNO3} + #.521 xHO2 + #.201 xMECO3 + #.334 xCO + #.407 xRCHO + #.129 xMEK + #.107 xGLY + #.267 xMGLY + #.783 yR6OOH + #.284 XC	7.40e-11			
BP51	AFG2 + HV = PROD2 + #-1 XC		Phot Set= AFG1		
BP52	AFG3 + OH = #.206 MACO3 + #.733 RO2C + #.117 {RO2XC + zRNO3} + #.561 xHO2 + #.117 xMECO3 + #.114 xCO + #.274 xGLY + #.153 xMGLY + #.019 xBACL + #.195 xAFG1 + #.195 xAFG2 + #.231 xIPRD + #.794 yR6OOH + #.938 XC	9.35e-11			
BP53	AFG3 + O3 = #.471 OH + #.554 HO2 + #.013 MECO3 + #.258 RO2C + #.007 {RO2XC + zRNO3} + #.580 CO + #.190 CO2 + #.366 GLY + #.184 MGLY + #.350 AFG1 + #.350 AFG2 + #.139 AFG3 + #.003 MACR + #.004 MVK + #.003 IPRD + #.095 xHO2 + #.163 xRCO3 + #.163 xHCHO + #.095 xMGLY + #.264 yR6OOH + #-.575 XC	1.43e-17			
BP89	AFG4 + OH = #.902 RO2C + #.098 RO2XC + #.098 zRNO3 + #.902 xMECO3 + #.902 xRCHO + yROOH + #.902 XC	6.30e-11			
BP28	RAOOH + OH = #.139 OH + #.148 HO2 + #.589 RO2C + #.124 RO2XC + #.124 zRNO3 + #.074 PROD2 + #.147 MGLY + #.139 IPRD + #.565 xHO2 + #.024 xOH + #.448 xRCHO + #.026 xGLY + #.030 xMEK + #.252 xMGLY + #.073 xAFG1 + #.073 xAFG2 + #.713 yR6OOH + #1.674 XC	1.41e-10			
BP29	RAOOH + HV = OH + HO2 + #.5 {GLY + MGLY + AFG1 + AFG2} + #-.5 XC		Phot Set= COOH		

Steady-State Peroxy Radical operators (for formation of organic product species)

PO01	xHCHO = HCHO	k is variable parameter: RO2RO
PO02	xHCHO = XC	k is variable parameter: RO2XRO
PO03	xCCHO = CCHO	k is variable parameter: RO2RO

Table A-2 (continued)

Label	Reaction and Products [a]	Rate Parameters [b]			
		k(300)	A	Ea	B
PO04	xCCHO = #2 XC	k is variable parameter: RO2XRO			
PO05	xRCHO = RCHO	k is variable parameter: RO2RO			
PO06	xRCHO = #3 XC	k is variable parameter: RO2XRO			
PO07	xACET = ACET	k is variable parameter: RO2RO			
PO08	xACET = #3 XC	k is variable parameter: RO2XRO			
PO09	xMEK = MEK	k is variable parameter: RO2RO			
PO10	xMEK = #4 XC	k is variable parameter: RO2XRO			
PO11	xPROD2 = PROD2	k is variable parameter: RO2RO			
PO12	xPROD2 = #6 XC	k is variable parameter: RO2XRO			
PO27	xMACR = MACR	k is variable parameter: RO2RO			
PO28	xMACR = #4 XC	k is variable parameter: RO2XRO			
PO29	xMVK = MVK	k is variable parameter: RO2RO			
PO30	xMVK = #4 XC	k is variable parameter: RO2XRO			
PO31	xIPRD = IPRD	k is variable parameter: RO2RO			
PO32	xIPRD = #5 XC	k is variable parameter: RO2XRO			
PO33	xRNO3 = RNO3	k is variable parameter: RO2RO			
PO34	xRNO3 = #6 XC + XN	k is variable parameter: RO2XRO			
PO13	xGLY = GLY	k is variable parameter: RO2RO			
PO14	xGLY = #2 XC	k is variable parameter: RO2XRO			
PO15	xMGLY = MGLY	k is variable parameter: RO2RO			
PO16	xMGLY = #3 XC	k is variable parameter: RO2XRO			
PO17	xBACL = BACL	k is variable parameter: RO2RO			
PO18	xBACL = #4 XC	k is variable parameter: RO2XRO			
PO19	xBALD = BALD	k is variable parameter: RO2RO			
PO20	xBALD = #7 XC	k is variable parameter: RO2XRO			
PO21	xAFG1 = AFG1	k is variable parameter: RO2RO			
PO22	xAFG1 = #5 XC	k is variable parameter: RO2XRO			
PO23	xAFG2 = AFG2	k is variable parameter: RO2RO			
PO24	xAFG2 = #5 XC	k is variable parameter: RO2XRO			
PO50	xAFG4 = #6 XC	k is variable parameter: RO2XRO			
PO51	xAFG4 = AFG4	k is variable parameter: RO2RO			
PO35	zRNO3 = RNO3 + #-1 XN	k is variable parameter: RO2NO			
PO36	zRNO3 = PROD2 + HO2	k is variable parameter: RO22NN			
PO37	zRNO3 = #6 XC	k is variable parameter: RO2XRO			
PO38	yROOH = ROOH + #-3 XC	k is variable parameter: RO2HO2			
PO39	yROOH = MEK + #-4 XC	k is variable parameter: RO2RO2M			
PO40	yROOH =	k is variable parameter: RO2RO			
PO41	yR6OOH = R6OOH + #-6 XC	k is variable parameter: RO2HO2			
PO42	yR6OOH = PROD2 + #-6 XC	k is variable parameter: RO2RO2M			
PO43	yR6OOH =	k is variable parameter: RO2RO			
PO44	yRAOOH = RAOOH + #-7 XC	k is variable parameter: RO2HO2			

Table A-2 (continued)

Label	Reaction and Products [a]	Rate Parameters [b]			
		k(300)	A	Ea	B
PO45	yRAOOH = PROD2 + #-6 XC	k is variable parameter: RO2RO2M			
PO46	yRAOOH =	k is variable parameter: RO2RO			
Explicitly Represented Primary Organics					
BE01	CH4 + OH = H2O + MEO2	6.62e-15	1.85e-12	3.36	
BE02	ETHENE + OH = RO2C + xHO2 + #1.61 xHCHO + #.195 xCCHO + yROOH	8.15e-12	Falloff, F=0.60, N=1.00		
		0:	1.00e-28	0.00	-4.50
		inf:	8.80e-12	0.00	-0.85
BE03	ETHENE + O3 = #.16 OH + #.16 HO2 + #.51 CO + #.12 CO2 + HCHO + #.37 HCOOH	1.68e-18	9.14e-15	5.13	
BE04	ETHENE + NO3 = RO2C + xHO2 + xRCHO + yROOH + #-1 XC + XN	2.24e-16	3.30e-12	5.72	2.00
BE05	ETHENE + O3P = #.8 HO2 + #.51 MEO2 + #.29 RO2C + #.51 CO + #.1 CCHO + #.29 xHO2 + #.278 xCO + #.278 xHCHO + #.012 xGLY + #.29 yROOH + #.2 XC	7.43e-13	1.07e-11	1.59	
BE06	ISOPRENE + OH = #.986 RO2C + #.093 {RO2XC + zRNO3} + #.907 xHO2 + #.624 xHCHO + #.23 xMACR + #.32 xMVK + #.357 xIPRD + yR6OOH + #-0.167 XC	9.96e-11	2.54e-11	-0.81	
BE07	ISOPRENE + O3 = #.266 OH + #.066 HO2 + #.192 RO2C + #.008 {RO2XC + zRNO3} + #.275 CO + #.122 CO2 + #.4 HCHO + #.1 PROD2 + #.39 MACR + #.16 MVK + #.15 IPRD + #.204 HCOOH + #.192 {xMACO3 + xHCHO} + #.2 yR6OOH + #-0.559 XC	1.34e-17	7.86e-15	3.80	
BE08	ISOPRENE + NO3 = #.936 RO2C + #.064 {RO2XC + zRNO3} + #.749 xHO2 + #.187 xNO2 + #.936 xIPRD + yR6OOH + #-0.064 XC + #.813 XN	6.81e-13	3.03e-12	0.89	
BE09	ISOPRENE + O3P = #.25 MEO2 + #.24 RO2C + #.01 {RO2XC + zRNO3} + #.75 PROD2 + #.24 xMACO3 + #.24 xHCHO + #.25 yR6OOH + #-1.01 XC	3.50e-11			
BE10	ACETYLEN + OH = #.7 OH + #.3 HO2 + #.3 CO + #.7 GLY + #.3 HCOOH	7.56e-13	Falloff, F=0.60, N=1.00		
		0:	5.50e-30	0.00	0.00
		inf:	8.30e-13	0.00	-2.00
BE11	ACETYLEN + O3 = #.5 OH + #1.5 HO2 + #1.5 CO + #.5 CO2	1.16e-20	1.00e-14	8.15	
BE12 [c]	BENZENE + OH = #.027 RO2XC + #.31 RO2C + #.57 HO2 + #.31 xHO2 + #.027 zRNO3 + #.57 PHEN + #.31 xGLY + #.183 xAFG1 + #.127 xAFG2 + #.337 yRAOOH + #.093 OH + #.093 AFG3 + #-0.403 XC	1.22e-12	2.33e-12	0.38	
Lumped Species used in Atmospheric Reactivity Simulations					
BL01	ALK1 + OH = xHO2 + RO2C + xCCHO + yROOH	2.54e-13	1.34e-12	0.99	2.00
BL02	ALK2 + OH = #.965 xHO2 + #.965 RO2C + #.035 RO2XC + #.035 zRNO3 + #.261 xRCHO + #.704 xACET + yROOH + #-.105 XC	1.11e-12	1.49e-12	0.17	2.00

Table A-2 (continued)

Label	Reaction and Products [a]	Rate Parameters [b]			
		k(300)	A	Ea	B
BL03	ALK3 + OH = #.695 xHO2 + #.236 xTBUO + #1.253 RO2C + #.07 RO2XC + #.07 zRNO3 + #.026 xHCHO + #.445 xCCHO + #.122 xRCHO + #.024 xACET + #.332 xMEK + #.983 yROOH + #.017 yR6OOH + #-.046 XC	2.31e-12	1.51e-12	-0.25	
BL04	ALK4 + OH = #.83 xHO2 + #.01 xMEO2 + #.011 xMECO3 + #1.763 RO2C + #.149 RO2XC + #.149 zRNO3 + #.002 xCO + #.029 xHCHO + #.438 xCCHO + #.236 xRCHO + #.426 xACET + #.106 xMEK + #.146 xPROD2 + yR6OOH + #-.119 XC	4.34e-12	3.75e-12	-0.09	
BL05	ALK5 + OH = #.647 xHO2 + #1.605 RO2C + #.353 RO2XC + #.353 zRNO3 + #.04 xHCHO + #.106 xCCHO + #.209 xRCHO + #.071 xACET + #.086 xMEK + #.407 xPROD2 + yR6OOH + #2.004 XC	9.40e-12	2.70e-12	-0.74	
BL06	OLE1 + OH = #.904 xHO2 + #.001 xMEO2 + #1.138 RO2C + #.095 RO2XC + #.095 zRNO3 + #.7 xHCHO + #.301 xCCHO + #.47 xRCHO + #.005 xACET + #.026 xMACR + #.008 xMVK + #.006 xIPRD + #.119 xPROD2 + #.413 yROOH + #.587 yR6OOH + #.822 XC	3.29e-11	6.18e-12	-1.00	
BL07	OLE1 + O3 = #.116 HO2 + #.04 xHO2 + #.193 OH + #.104 MEO2 + #.063 RO2C + #.004 RO2XC + #.004 zRNO3 + #.368 CO + #.125 CO2 + #.5 HCHO + #.147 CCHO + #.007 xCCHO + #.353 RCHO + #.031 xRCHO + #.002 xACET + #.006 MEK + #.185 HCOOH + #.022 CCOOH + #.112 RCOOH + #.189 PROD2 + #.007 yROOH + #.037 yR6OOH + #.69 XC	1.09e-17	3.15e-15	3.38	
BL08	OLE1 + NO3 = #.824 xHO2 + #1.312 RO2C + #.176 RO2XC + #.176 zRNO3 + #.009 xCCHO + #.002 xRCHO + #.024 xACET + #.546 xRNO3 + #.413 yROOH + #.587 yR6OOH + #.454 XN + #.572 XC	1.44e-14	4.73e-13	2.08	
BL09	OLE1 + O3P = #.45 RCHO + #.437 MEK + #.113 PROD2 + #1.224 XC	5.02e-12	1.49e-11	0.65	
BL10	OLE2 + OH = #.914 xHO2 + #.966 RO2C + #.086 RO2XC + #.086 zRNO3 + #.209 xHCHO + #.788 xCCHO + #.481 xRCHO + #.136 xACET + #.076 xMEK + #.027 xMACR + #.002 xMVK + #.037 xIPRD + #.022 xPROD2 + #.357 yROOH + #.643 yR6OOH + #.111 XC	6.42e-11	1.26e-11	-0.97	
BL11	OLE2 + O3 = #.093 HO2 + #.039 xHO2 + #.423 OH + #.29 MEO2 + #.147 xMECO3 + #.008 xRCO3 + #.2 RO2C + #.003 RO2XC + #.003 zRNO3 + #.297 CO + #.162 CO2 + #.152 HCHO + #.108 xHCHO + #.428 CCHO + #.067 xCCHO + #.315 RCHO + #.018 xRCHO + #.048 ACET + #.031 MEK + #.001 xMEK + #.033 HCOOH + #.061 CCOOH + #.222 RCOOH + #.028 MACR + #.021 MVK + #.042 PROD2 + #.069 yROOH + #.128 yR6OOH + #.125 XC	1.24e-16	8.14e-15	2.49	

Table A-2 (continued)

Label	Reaction and Products [a]	Rate Parameters [b]			
		k(300)	A	Ea	B
BL12	OLE2 + NO3 = #.423 xHO2 + #.409 xNO2 + #.033 xMEO2 + #1.185 RO2C + #.136 RO2XC + #.136 zRNO3 + #.074 xHCHO + #.546 xCCHO + #.154 xRCHO + #.11 xACET + #.002 xMEK + #.026 xMVK + #.007 xIPRD + #.322 xRNO3 + #.357 yROOH + #.643 yR6OOH + #.269 XN + #.114 XC	7.85e-13	2.20e-13	-0.76	
BL13	OLE2 + O3P = #.014 HO2 + #.007 xHO2 + #.007 xMACO3 + #.013 RO2C + #.001 RO2XC + #.001 zRNO3 + #.006 xCO + #.074 RCHO + #.709 MEK + #.006 xMACR + #.202 PROD2 + #.014 yROOH + #.666 XC	2.07e-11	1.43e-11	-0.22	
BL14	ARO1 + OH = #.089 RO2XC + #.622 RO2C + #.167 HO2 + #.612 xHO2 + #.089 zRNO3 + #.14 yR6OOH + #.007 xMEO2 + #.049 xBALD + #.064 xPROD2 + #.003 xCCHO + #.006 xRCHO + #.135 CRES + #.032 XYNL + #.268 xGLY + #.231 xMGLY + #.283 xAFG1 + #.216 xAFG2 + #.567 yRAOOH + #.126 OH + #.126 AFG3 + #-0.099 XC	6.07e-12	1.97e-12	-0.67	
BL15	ARO2 + OH = #.126 RO2XC + #.651 RO2C + #.083 HO2 + #.649 xHO2 + #.126 zRNO3 + #.079 yR6OOH + #.002 xMEO2 + #.038 xBALD + #.025 xPROD2 + #.004 xRCHO + #.083 XYNL + #.14 xGLY + #.336 xMGLY + #.109 xBACL + #.093 xAFG4 + #.252 xAFG1 + #.24 xAFG2 + #.698 yRAOOH + #.14 OH + #.14 AFG3 + #1.428 XC	2.60e-11			
BL16	TERP + OH = #.759 xHO2 + #.042 xRCO3 + #1.147 RO2C + #.2 RO2XC + #.2 zRNO3 + #.001 xCO + #.264 xHCHO + #.533 xRCHO + #.036 xACET + #.005 xMEK + #.009 xMGLY + #.014 xBACL + #.002 xMVK + #.001 xIPRD + #.255 xPROD2 + yR6OOH + #5.056 XC	7.98e-11	1.87e-11	-0.86	
BL17	TERP + O3 = #.052 HO2 + #.067 xHO2 + #.585 OH + #.126 xMECO3 + #.149 xRCO3 + #.875 RO2C + #.203 RO2XC + #.203 zRNO3 + #.166 CO + #.019 xCO + #.045 CO2 + #.079 HCHO + #.15 xHCHO + #.22 xRCHO + #.165 xACET + #.004 MEK + #.107 HCOOH + #.043 RCOOH + #.001 xGLY + #.002 xMGLY + #.055 xBACL + #.001 xMACR + #.001 xIPRD + #.409 PROD2 + #.545 yR6OOH + #3.526 XC	6.99e-17	9.57e-16	1.56	
BL18	TERP + NO3 = #.162 xHO2 + #.421 xNO2 + #.019 xRCO3 + #1.509 RO2C + #.397 RO2XC + #.397 zRNO3 + #.01 xCO + #.017 xHCHO + #.001 xCCHO + #.509 xRCHO + #.175 xACET + #.001 xMGLY + #.003 xMACR + #.001 xMVK + #.002 xIPRD + #.163 xRNO3 + yR6OOH + #.416 XN + #4.473 XC	6.53e-12	1.28e-12	-0.97	
BL19	TERP + O3P = #.147 RCHO + #.853 PROD2 + #4.441 XC	3.71e-11			
Non-aromatic VOCs represented in chamber simulations					
CH01	ETHANE + OH = RO2C + xHO2 + xCCHO + yROOH	2.54e-13	1.34e-12	0.99	2.00
CH03	PROPANE + OH = #.965 RO2C + #.035 RO2XC + #.035 zRNO3 + #.965 xHO2 + #.261 xRCHO + #.704 xACET + yROOH + #-.105 XC	1.11e-12	1.49e-12	0.17	2.00

Table A-2 (continued)

Label	Reaction and Products [a]	Rate Parameters [b]			
		k(300)	A	Ea	B
CH05	N-C4 + OH = #1.334 RO2C + #.079 RO2XC + #.079 zRNO3 + #.921 xHO2 + #.632 xCCHO + #.120 xRCHO + #.485 xMEK + yROOH + #-.038 XC	2.38e-12	1.63e-12	-0.23	2.00
CH07	N-C6 + OH = #1.562 RO2C + #.225 RO2XC + #.225 zRNO3 + #.775 xHO2 + #.011 xCCHO + #.113 xRCHO + #.688 xPROD2 + yR6OOH + #.161 XC	5.25e-12	7.62e-12	0.22	1.00
CH09	N-C8 + OH = #1.432 RO2C + #.354 RO2XC + #.354 zRNO3 + #.646 xHO2 + #.024 xRCHO + #.622 xPROD2 + yR6OOH + #2.072 XC	8.16e-12	2.45e-12	-0.72	2.00
CH11	PROPENE + OH = #.984 RO2C + #.016 RO2XC + #.016 zRNO3 + #.984 xHO2 + #.984 xHCHO + #.984 xCCHO + yROOH + #-.048 XC	2.60e-11	4.85e-12	-1.00	
CH12	PROPENE + O3 = #.350 OH + #.165 HO2 + #.355 MEO2 + #.525 CO + #.215 CO2 + #.500 HCHO + #.500 CCHO + #.185 HCOOH + #.075 CCOOH + #.070 XC	1.05e-17	5.51e-15	3.73	
CH13	PROPENE + NO3 = #.949 RO2C + #.051 RO2XC + #.051 zRNO3 + #.949 xHO2 + yROOH + #2.694 XC + XN	9.73e-15	4.59e-13	2.30	
CH14	PROPENE + O3P = #.450 RCHO + #.550 MEK + #-.550 XC	4.01e-12	1.02e-11	0.56	
CH16	T-2-BUTE + OH = #.965 RO2C + #.035 RO2XC + #.035 zRNO3 + #.965 xHO2 + #1.930 xCCHO + yROOH + #-.070 XC	6.32e-11	1.01e-11	-1.09	
CH17	T-2-BUTE + O3 = #.540 OH + #.170 HO2 + #.710 MEO2 + #.540 CO + #.310 CO2 + CCHO + #.150 CCOOH + #.140 XC	1.95e-16	6.64e-15	2.10	
CH18	T-2-BUTE + NO3 = #.920 RO2C + #.080 RO2XC + #.080 zRNO3 + #.705 xNO2 + #.215 xHO2 + #1.410 xCCHO + #.215 xRNO3 + yROOH + #-.590 XC + #.080 XN	3.93e-13	1.10e-13	-0.76	2.00
CH19	T-2-BUTE + O3P = MEK	1.99e-11	1.09e-11	-0.36	
CH29	N-C6F14 + OH = #6 XC	0.00e+0			
<u>Aromatic VOCs represented in chamber simulations (SAPRC-11)</u>					
AR01 [c]	TOLUENE + OH = #.074 RO2XC + #.605 RO2C + #.18 HO2 + #.605 xHO2 + #.074 zRNO3 + #.073 yR6OOH + #.065 xBALD + #.18 CRES + #.29 xGLY + #.25 xMGLY + #.324 xAFG1 + #.216 xAFG2 + #.606 yRAOOH + #.141 OH + #.141 AFG3 + #-0.176 XC	5.58e-12	1.81e-12	-0.67	
AR02 [c]	C2-BENZ + OH = #.105 RO2XC + #.642 RO2C + #.153 HO2 + #.642 xHO2 + #.105 zRNO3 + #.213 yR6OOH + #.161 xPROD2 + #.023 xRCHO + #.153 XYNL + #.246 xGLY + #.212 xMGLY + #.183 xAFG1 + #.275 xAFG2 + #.533 yRAOOH + #.101 OH + #.101 AFG3 + #.986 XC	6.50e-12			
AR03	N-C3-BEN + OH = #.14 RO2XC + #.698 RO2C + #.105 HO2 + #.698 xHO2 + #.14 zRNO3 + #.46 yR6OOH + #.36 xPROD2 + #.023 xRCHO + #.105 XYNL + #.169 xGLY + #.146 xMGLY + #.179 xAFG1 + #.135 xAFG2 + #.377 yRAOOH + #.057 OH + #.057 AFG3 + #2.346 XC	6.13e-12			

Table A-2 (continued)

Label	Reaction and Products [a]	Rate Parameters [b]			
		k(300)	A	Ea	B
AR04	I-C3-BEN + OH = #.126 RO2XC + #.627 RO2C + #.16 HO2 + #.526 xHO2 + #.126 zRNO3 + #.176 yR6OOH + #.1 xMEO2 + #.1 xPROD2 + #.046 xRCHO + #.16 XYNL + #.258 xGLY + #.222 xMGLY + #.182 xAFG1 + #.298 xAFG2 + #.577 yRAOOH + #.088 OH + #.088 AFG3 + #1.928 XC	6.20e-12			
AR05	M-XYLENE + OH = #.098 RO2XC + #.6 RO2C + #.11 HO2 + #.6 xHO2 + #.098 zRNO3 + #.046 yR6OOH + #.04 xBALD + #.11 XYNL + #.11 xGLY + #.45 xMGLY + #.319 xAFG1 + #.241 xAFG2 + #.651 yRAOOH + #.192 OH + #.192 AFG3 + #.538 XC	2.31e-11			
AR06	O-XYLENE + OH = #.114 RO2XC + #.695 RO2C + #.11 HO2 + #.695 xHO2 + #.114 zRNO3 + #.053 yR6OOH + #.045 xBALD + #.11 XYNL + #.13 xGLY + #.33 xMGLY + #.19 xBACL + #.293 xAFG1 + #.358 xAFG2 + #.756 yRAOOH + #.081 OH + #.081 AFG3 + #.289 XC	1.36e-11			
AR07 [c]	P-XYLENE + OH = #.107 RO2XC + #.655 RO2C + #.13 HO2 + #.655 xHO2 + #.107 zRNO3 + #.099 yR6OOH + #.085 xBALD + #.13 XYNL + #.37 xGLY + #.2 xMGLY + #.37 xAFG4 + #.178 xAFG1 + #.022 xAFG2 + #.663 yRAOOH + #.108 OH + #.108 AFG3 + #.407 XC	1.43e-11			
AR08	M-ET-TOL + OH = #.123 RO2XC + #.612 RO2C + #.104 HO2 + #.612 xHO2 + #.123 zRNO3 + #.1 yR6OOH + #.021 xBALD + #.054 xPROD2 + #.008 xRCHO + #.104 XYNL + #.104 xGLY + #.425 xMGLY + #.354 xAFG1 + #.174 xAFG2 + #.634 yRAOOH + #.162 OH + #.162 AFG3 + #1.678 XC	1.86e-11			
AR09	O-ET-TOL + OH = #.142 RO2XC + #.709 RO2C + #.098 HO2 + #.709 xHO2 + #.142 zRNO3 + #.156 yR6OOH + #.033 xBALD + #.085 xPROD2 + #.012 xRCHO + #.098 XYNL + #.116 xGLY + #.294 xMGLY + #.169 xBACL + #.318 xAFG1 + #.261 xAFG2 + #.695 yRAOOH + #.05 OH + #.05 AFG3 + #1.552 XC	1.19e-11			
AR10	P-ET-TOL + OH = #.133 RO2XC + #.664 RO2C + #.122 HO2 + #.664 xHO2 + #.133 zRNO3 + #.158 yR6OOH + #.033 xBALD + #.086 xPROD2 + #.012 xRCHO + #.122 XYNL + #.346 xGLY + #.187 xMGLY + #.346 xAFG4 + #.187 xAFG1 + #.64 yRAOOH + #.081 OH + #.081 AFG3 + #1.612 XC	1.18e-11			
AR11	123-TMB + OH = #.148 RO2XC + #.736 RO2C + #.031 HO2 + #.736 xHO2 + #.148 zRNO3 + #.044 yR6OOH + #.036 xBALD + #.031 XYNL + #.06 xGLY + #.17 xMGLY + #.47 xBACL + #.28 xAFG1 + #.42 xAFG2 + #.841 yRAOOH + #.085 OH + #.085 AFG3 + #1.007 XC	3.27e-11			
AR12	124-TMB + OH = #.117 RO2XC + #.581 RO2C + #.022 HO2 + #.581 xHO2 + #.117 zRNO3 + #.04 yR6OOH + #.034 xBALD + #.022 XYNL + #.077 xGLY + #.36 xMGLY + #.11 xBACL + #.167 xAFG4 + #.182 xAFG1 + #.198 xAFG2 + #.657 yRAOOH + #.281 OH + #.281 AFG3 + #1.341 XC	3.25e-11			

Table A-2 (continued)

Label	Reaction and Products [a]	Rate Parameters [b]			
		k(300)	A	Ea	B
AR13	135-TMB + OH = #.128 RO2XC + #.638 RO2C + #.04 HO2 + #.638 xHO2 + #.128 zRNO3 + #.034 yR6OOH + #.028 xBALD + #.04 XYNL + #.61 xMGLY + #.238 xAFG1 + #.372 xAFG2 + #.732 yRAOOH + #.194 OH + #.194 AFG3 + #1.478 XC	5.67e-11			
Aromatic VOCs represented in chamber simulations (SAPRC-11A) [d]					
BZOH	BENZENE + OH = BENZOH [e]	1.22e-12	2.33e-12	0.38	
BZN2	BENZOH + NO2 = NO + HO2 + AFG3	3.60e-11			
BZO2	BENZOH + O2 + #BZNF = #.027 RO2XC + #.31 RO2C +#.57 HO2 +#.31 xHO2 + #.027 zRNO3 + #.189 yR6OOH + #.57 PHEN + #.31 xGLY + #.208 xAFG1 + #B.102 xAFG2 +#.148 yRAOOH + #.093 OH +#.093 AFG3	3.44e-18			
TLOH	TOLUENE + OH = #.065 {RO2C + xHO2 + xBALD} + #.008 {RO2XC + zRNO3} + #0.073 yR6OOH + #.927 TOLOH	5.58e-12	1.81e-12	-0.67	
TLN2	TOLOH + NO2 = NO + HO2 + AFG3	3.60e-11			
TLO2	TOLOH + O2 + #TLNF = #.072 RO2XC + #.583 RO2C + #.194 HO2 + #.583 xHO2 + #.072 zRNO3 + #.458 yR6OOH + #.194 CRES + #.313 xGLY + #.27 xMGLY + #.338 xAFG1 + #.245 xAFG2 + #.196 yRAOOH + #.152 OH + #.152 AFG3	3.44e-17			
EBOH	C2-BENZ + OH = #.183 {RO2C + xHO2} + #.030 {RO2XC + zRNO3} + #.161 xPROD2 + #.023 xRCHO + #.213 yR6OOH + #.787 ETBOH	6.50e-12			
EBN2	ETBOH + NO2 = NO + HO2 + AFG3	3.60e-11			
EBO2	ETBOH + O2 + #EBNF = #.095 RO2XC + #.583 RO2C + #.194 HO2 + #.583 xHO2 + #.095 zRNO3 + #.034 yR6OOH + #.194 XYNL + #.313 xGLY + #.27 xMGLY + #.280 xAFG1 + #.303 xAFG2 + #.644 yRAOOH + #.128 OH + #.128 AFG3	8.60e-18			
PXOH	P-XYLENE + OH = #.085 {RO2C + xHO2 + xBALD} + #.014 {RO2XC + zRNO3} + #0.099 yR6OOH + #.901 PXYOH	1.43e-11			
PXN2	PXYOH + NO2 = NO + HO2 + AFG3	3.60e-11			
PXO2	PXYOH + O2 + #PXNF = #.103 RO2XC + #.633 RO2C + #.144 HO2 + #.633 xHO2 + #.103 zRNO3 + #.515 yR6OOH + #.144 XYNL + #.411 xGLY + #.222 xMGLY + #.411 xAFG4 + #.222 xAFG1 + #.221 yRAOOH + #.12 OH + #.12 AFG3	5.16e-18			

[a] Format of reaction listing: "=" separates reactants from products; "*#number*" indicates stoichiometric coefficient, "*#coefficient* {*product list*}" means that the stoichiometric coefficient is applied to all the products listed.

[b] Except as indicated, the rate constants are given by $k(T) = A \cdot (T/300)^B \cdot e^{-Ea/RT}$, where the units of k and A are $cm^3\ molec^{-1}\ s^{-1}$, Ea are kcal mol^{-1}, T is ^oK, and R=0.0019872 kcal $mol^{-1}\ deg^{-1}$. The following special rate constant expressions are used:

Table A-2 (continued)

Phot Set = *name*: The absorption cross sections and (if applicable) quantum yields for the photolysis reaction are given by Carter (2010a), where "*name*" indicates the photolysis set used. If a "qy=*number*" notation is given, the number given is the overall quantum yield, which is assumed to be wavelength independent.

Falloff: The rate constant as a function of temperature and pressure is calculated using $k(T,M) = \{k0(T)\cdot[M]/[1 + k0(T)\cdot[M]/kinf(T)]\}\cdot F^{Z}$, where $Z = \{1 + [\log10\{k0(T)\cdot[M])/kinf(T)\}/N]^2\}^{-1}$, [M] is the total pressure in molecules cm^{-3}, F and N are as indicated on the table, and the temperature dependences of k and kinf are as indicated on the table.

k = k0+k3M(1+k3M/k2): The rate constant as a function of temperature and pressure is calculated using $k(T,M) = k0(T) + k3(T)\cdot[M] \cdot(1 + k3(T)\cdot[M]/k2(T))$, where [M] is the total bath gas (air) concentration in molecules cm-3, and the temperature dependences for k0, k2 and k3 are as indicated on the table.

k = k1 + k2 [M]: The rate constant as a function of temperature and pressure is calculated using $k(T,M) = k1(T) + k2(T)\cdot[M]$, where [M] is the total bath gas (air) concentration in molecules cm-3, and the temperature dependences for k1, and k2 are as indicated on the table.

Same K as Rxn xx: Uses the same rate constant as the reaction in the base mechanism with the same label.

[c] Not used in SAPRC-11A.

[d] The species BENZOH, TOLOH, ETBOH, and PXYOH represent the OH-aromatic adduct are only used for SAPRC-11A and are not included in the species list in Table A-1.

[e] This reaction is used in place of reaction BL12 for SAPRC-11A.

APPENDIX B. LIST OF ENVIRONMENTAL CHAMBER EXPERIMENTS

Table B-1. List of environmental chamber experiments used to develop and evaluate the aromatics mechanisms developed for this project.

Run	New [a]	Char [b]	Experimental Conditions					Results [d]		Model Results [d,e]		
			NO_x (ppb)	Arom. (ppm)	CO (ppm)	Light [c] Type	k1	Hours	O_3 (ppb)	O_3 (ppb)	Model Error Rate	Model Error O_3^{max}
						Benzene						
ITC560		3	108	57.5		Black	0.36	6	321	338	51%	9%
ITC698		6	485	14.05		Black	0.35	10	370	562	125%	55%
ITC710		6	534	14.08		Black	0.35	12	363	563	123%	60%
CTC159A		6	263	34.3		Arc	0.18	10	386	349	105%	8%
CTC159B		6	260	16.49		Arc	0.18	10	338	358	98%	16%
CTC160A		2	494	18.39		Arc	0.18	10	(31)	453	155%	
CTC160B		2	490	34.3		Arc	0.18	10	(292)	439	143%	
EPA1223A	yes	9	55	0.99		Black	0.40	12	205	201	-13%	-2%
EPA1223B	yes	9	111	0.99		Black	0.40	10	(244)	(221)	-18%	
EPA1231A	yes	9	93	0.95		Black	0.40	10	230	(223)	-17%	
EPA1236A	yes	9	50	0.93		Black	0.40	12	192	191	4%	0%
EPA1236B	yes	9	140	0.93		Black	0.40	12	(178)	(172)	1%	
EPA1237A	yes	9	39	0.44		Black	0.40	14	165	153	-2%	-8%
EPA1237B	yes	9	20	0.45		Black	0.40	12	132	116	-1%	-13%
						Toluene						
CSI321	yes	1	69	0.062		Blue	0.80	12	(282)	(232)	-22%	
CSI339	yes	1	50	0.089		Blue	0.80	12	277	310	-1%	11%
CSI340	yes	1	51	0.064		Blue	0.80	12	278	287	-16%	3%
CSI341	yes	1	49	0.037		Blue	0.80	12	(163)	(108)	-27%	
CSI412	yes	1	33	0.089		Blue	0.43	12	186	184	-18%	-1%
CSI413	yes	1	34	0.064		Blue	0.43	12	179	171	-18%	-5%
CSI414	yes	1	34	0.040		Blue	0.43	12	(155)	(96)	-32%	
CSI429	yes	1	73	0.088		Blue	0.41	12	(150)	(140)	2%	
CSI430	yes	1	69	0.061		Blue	0.41	12	(71)	(59)	4%	
CSI431	yes	1	49	0.090		Blue	0.41	12	181	195	0%	8%
CSI432	yes	1	48	0.065		Blue	0.41	12	(138)	(134)	3%	
CSI434	yes	1	48	0.035		Blue	0.40	12	(39)	(31)	-2%	
CSI436	yes	1	71	0.036		Blue	0.40	12	(16)	(14)	20%	
TVA047		1	105	0.074		Mix	0.39	16	(94)	152	31%	
TVA071		1	266	0.35		Mix	0.39	8	(270)	(408)	36%	
TVA080		1	54	0.059		Mix	0.39	12	107	148	33%	32%
EC264		1	440	1.16		Arc	0.34	8	417	530	58%	29%
EC266		1	440	1.20		Arc	0.34	12	401	479	58%	31%
EC269		1	485	0.57		Arc	0.34	12	(297)	519	26%	
EC271		1	215	1.15		Arc	0.35	12	294	342	30%	24%
EC273		1	112	0.59		Arc	0.40	12	214	288	-3%	29%
EC293		1	487	1.07		Arc	0.40	12	411	543	3%	39%
EC327		1	492	0.57		Arc	0.41	12	(375)	560	35%	
EC340		1	493	0.54		Arc	0.36	10	(317)	(533)	10%	
ITC534		3	526	2.15		Black	0.36	10	483	702	90%	40%
ITC699		6	493	1.62		Black	0.35	8	476	667	61%	35%
DTC042A		1	986	1.07		Black	0.39	12	(29)	(294)	89%	
DTC042B		1	99	0.56		Black	0.39	12	255	302	70%	17%

Table B-1 (continued)

Run	New [a]	Char [b]	Experimental Conditions					Results [d]		Model Results [d,e]		
			NO_x (ppb)	Arom. (ppm)	CO (ppm)	Light [c] Type	k1	Hours	O_3 (ppb)	O_3 (ppb)	Model Error Rate	Model Error O_3^{max}
DTC151A		3	321	1.84		Black	0.25	12	392	423	94%	17%
DTC155A		3	100	0.64		Black	0.25	12	202	240	71%	17%
DTC158A		3	499	2.49		Black	0.25	12	473	541	93%	27%
DTC170A		3	493	2.52		Black	0.24	12	473	537	90%	25%
CTC026		1	270	2.01		Arc	0.20	10	347	407	47%	16%
CTC034		1	524	2.21		Arc	0.20	10	466	616	47%	28%
CTC048		2	248	0.95		Arc	0.20	12	313	378	39%	19%
CTC065		2	657	0.97		Arc	0.19	10	(18)	(83)	52%	
CTC079		3	256	0.50		Arc	0.19	10	(62)	(247)	56%	
XTC106		1	245	1.92		Mix	0.25	10	394	400	49%	4%
EPA066A		2	4	0.055	24	Arc	0.26	22	97	92	-27%	-5%
EPA066B		2	5	0.061		Arc	0.26	22	57	62	-22%	9%
EPA072A		2	14	0.155	25	Arc	0.26	10	146	126	11%	-15%
EPA072B		2	15	0.155	27	Arc	0.26	10	156	134	4%	-15%
EPA074A		2	24	0.151		Arc	0.26	12	123	123	34%	0%
EPA074B		2	27	0.157	45	Arc	0.26	12	258	231	4%	-11%
EPA088A		3A	25	0.143	93	Black	0.26	24	298	260	1%	-13%
EPA088B		3B	25	0.135	93	Black	0.26	24	304	257	-4%	-17%
EPA091A		3A	25	0.144		Black	0.17	24	113	117	20%	4%
EPA094B		3B	26	0.060		Black	0.17	24	94	106	39%	12%
EPA099A		3A	42	0.22		Black	0.17	24	144	150	31%	4%
EPA099B		3B	42	0.22		Black	0.17	24	143	150	34%	5%
EPA102A		3A	103	0.56		Black	0.17	22	229	232	52%	1%
EPA102B		3A	70	0.38		Black	0.17	22	185	191	47%	3%
EPA106A		3A	214	1.13		Black	0.17	20	317	333	56%	5%
EPA106B		3A	16	0.070		Black	0.17	20	83	85	22%	2%
EPA210A		3A	42	0.26		Arc	0.26	12	158	178	1%	12%
EPA210B		3B	93	0.26		Arc	0.26	12	231	246	-5%	6%
EPA289B		3B	25	0.22		Black	0.17	16	99	108	13%	8%
EPA443A		4	31	0.170		Arc	0.26	12	127	146	19%	14%
EPA443B		4	99	0.36		Arc	0.26	12	223	260	1%	15%
EPA1095B	yes	8B	75	0.081		Black	0.12	6	(3)	(1)	24%	
EPA1096A	yes	8A	53	0.082		Black	0.12	18	(47)	(72)	40%	
EPA1096B	yes	8B	40	0.082		Black	0.12	12	(26)	(48)	54%	
EPA1098A	yes	8A	16	0.084		Black	0.12	18	66	67	-3%	1%
EPA1098B	yes	8B	30	0.084		Black	0.12	12	75	(72)	-7%	
EPA1099A	yes	8A	20	0.035		Black	0.12	16	(55)	(48)	-1%	
EPA1099B	yes	8B	10	0.041		Black	0.12	14	46	44	14%	-4%
EPA1100A	yes	8A	22	0.075	101	Black	0.12	16	147	136	-6%	-8%
EPA1100B	yes	8B	9	0.075	101	Black	0.12	16	86	83	-6%	-3%
EPA1101A	yes	8A	19	0.079		Black	0.40	16	133	132	5%	-1%
EPA1101B	yes	8B	9	0.079		Black	0.40	12	84	83	3%	-1%
EPA1102A	yes	8A	43	0.076		Black	0.40	14	182	171	-15%	-7%
EPA1102B	yes	8B	32	0.076		Black	0.40	14	156	153	-6%	-2%
EPA1106A	yes	8A	25	0.034		Black	0.40	20	136	128	-41%	-6%
EPA1106B	yes	8B	13	0.035		Black	0.40	20	103	100	-26%	-4%
EPA1107A	yes	8A	40	0.037		Black	0.40	19	153	134	-24%	-13%
EPA1107B	yes	8B	38	0.037		Black	0.40	18	145	132	-32%	-10%

Table B-1 (continued)

Run	New [a]	Char [b]	Experimental Conditions					Results [d]		Model Results [d,e]		
			NO_x (ppb)	Arom. (ppm)	CO (ppm)	Light [c] Type	k1	Hours	O_3 (ppb)	O_3 (ppb)	Model Error Rate	O_3^{max}
						Ethyl Benzene						
DTC223A		3	264	1.52		Black	0.22	10	332	446	67%	31%
DTC223B		3	267	0.76		Black	0.22	12	(206)	398	55%	
DTC224A		3	531	1.62		Black	0.22	10	(100)	(654)	70%	
CTC057		2	272	2.03		Arc	0.20	12	306	436	63%	37%
CTC092A		4	268	1.03		Arc	0.19	10	(85)	(414)	68%	
CTC092B		4	270	1.96		Arc	0.19	12	296	428	58%	41%
EPA1142A	yes	8A	47	0.100		Black	0.40	12	169	171	-5%	1%
EPA1142B	yes	8B	66	0.100		Black	0.40	10	(110)	(108)	-2%	
EPA1146A	yes	8A	22	0.099		Black	0.40	14	130	134	10%	3%
EPA1146B	yes	8B	34	0.100		Black	0.40	12	147	150	1%	2%
EPA1147A	yes	8A	99	0.34		Black	0.40	10	278	262	13%	-6%
EPA1147B	yes	8B	47	0.34		Black	0.40	10	191	192	15%	1%
						n-Propyl Benzene						
EPA1245A	yes	9	22	0.101		Black	0.40	13	111	121	1%	9%
EPA1245B	yes	9	48	0.100		Black	0.40	11	(103)	(93)	-12%	
EPA1246A	yes	9	68	0.20		Black	0.40	13	176	221	0%	23%
EPA1246B	yes	9	128	0.20		Black	0.40	12	(99)	(85)	-13%	
						Isopropyl Benzene						
EPA1247A	yes	9	22	0.100		Black	0.40	15	133	127	-6%	-4%
EPA1247B	yes	9	48	0.099		Black	0.40	12	162	(158)	-3%	
EPA1250A	yes	9	68	0.20		Black	0.40	12	208	218	0%	5%
EPA1250B	yes	9	127	0.20		Black	0.40	11	(139)	(163)	6%	
EPA1253A	yes	9	56	0.20		Black	0.40	11	208	197	0%	-5%
EPA1253B	yes	9	67	0.20		Black	0.40	11	(159)	(225)	22%	
						m-Xylene						
CSI416	yes	1	69	0.088		Blue	0.43	12	312	311	-21%	0%
CSI418	yes	1	69	0.065		Blue	0.43	12	295	295	-24%	0%
CSI419	yes	1	71	0.038		Blue	0.43	12	218	(174)	-30%	
CSI420	yes	1	70	0.015		Blue	0.43	12	(49)	(27)	-32%	
CSI421	yes	1	47	0.069		Blue	0.42	12	247	260	-9%	5%
CSI423	yes	1	49	0.086		Blue	0.42	12	242	261	-11%	8%
CSI424	yes	1	49	0.035		Blue	0.42	12	222	(197)	-39%	
CSI425	yes	1	35	0.064		Blue	0.42	12	200	216	-13%	8%
CSI426	yes	1	36	0.036		Blue	0.42	12	194	200	-19%	3%
CSI427	yes	1	35	0.014		Blue	0.41	12	(85)	(63)	-28%	
CSI428	yes	1	35	0.092		Blue	0.41	12	177	210	10%	17%
CSI433	yes	1	19	0.037		Blue	0.40	12	136	148	-7%	8%
TVA048		1	100	0.036		Mix	0.39	14	154	143	-13%	-7%
TVA049		1	98	0.036		Mix	0.39	14	165	148	-9%	-9%
DTC073A		1	485	0.113		Black	0.39	12	71	(51)	-19%	
DTC188A		3	553	0.125		Black	0.23	12	(17)	(17)	-2%	
DTC188B		3	569	0.23		Black	0.23	12	(236)	(148)	-14%	
DTC189A		3	247	0.25		Black	0.23	12	388	418	16%	7%
DTC189B		3	259	0.112		Black	0.23	12	(192)	(141)	-12%	
DTC191A		3	570	0.53		Black	0.23	12	586	672	15%	14%
DTC191B		3	591	1.10		Black	0.23	12	612	572	38%	13%
DTC192A		3	297	0.53		Black	0.23	10	419	449	26%	10%
DTC192B		3	150	0.53		Black	0.23	12	265	256	39%	4%
DTC193A		3	128	0.29		Black	0.23	12	263	279	29%	6%
DTC193B		3	130	0.150		Black	0.23	12	280	262	8%	-7%

Table B-1 (continued)

Run	New [a]	Char [b]	Experimental Conditions					Results [d]		Model Results [d,e]		
			NO_x (ppb)	Arom. (ppm)	CO (ppm)	Light [c] Type	k1	Hours	O_3 (ppb)	O_3 (ppb)	Model Error Rate	O_3^{max}
CTC029		1	271	0.32		Arc	0.20	12	416	465	5%	11%
CTC035		1	276	0.160		Arc	0.20	12	(357)	(275)	-34%	
CTC036		1	509	0.159		Arc	0.20	12	(92)	(34)	-42%	
CTC066		2	558	0.32		Arc	0.19	12	(325)	(355)	0%	
CTC080		3	507	0.53		Arc	0.19	12	543	614	4%	13%
CTC094A		4	489	0.56		Arc	0.19	10	455	599	20%	27%
CTC094B		4	490	0.57		Arc	0.19	10	456	591	18%	26%
EPA067A		2	5	0.018		Arc	0.26	12	(58)	49	16%	
EPA067B		2	6	0.018	47	Arc	0.26	12	119	94	-22%	-23%
EPA104A	yes	3A	66	0.080		Black	0.19	18	225	207	3%	-8%
EPA104B	yes	3B	22	0.081		Black	0.19	18	103	114	29%	10%
EPA107A	yes	3A	92	0.29		Black	0.19	24	229	251	31%	9%
EPA107B	yes	3A	52	0.167		Black	0.19	22	163	186	35%	13%
EPA129A		3A	48	0.086		Black	0.19	20	165	176	25%	7%
EPA129B		3A	47	0.086		Black	0.19	20	174	173	27%	-1%
EPA149A		3A	56	0.082		Arc	0.26	16	242	232	4%	-4%
EPA149B		3A	54	0.164		Arc	0.26	14	199	215	19%	8%
EPA154A		3A	400	0.064		Black	0.18	14	(8)	(3)	-40%	
EPA154B	yes	3A	61	0.063		Black	0.18	14	188	172	-2%	-9%
EPA155A		3A	398	0.058		Black	0.19	12	(4)	(2)	-49%	
EPA155B		3A	56	0.058	98	Black	0.19	12	338	298	4%	-13%
EPA157A	yes	3A	345	0.136		Black	0.18	8	(19)	(13)	-5%	
EPA157B	yes	3A	346	0.136		Black	0.18	8	(18)	(13)	-1%	
EPA164A		3A	47	0.068		Black	0.18	16	165	162	10%	-1%
EPA164B		3A	47	0.068		Black	0.18	14	164	155	10%	-6%
EPA178A		3A	11	0.028		Arc	0.26	12	86	86	-7%	0%
EPA178B		3B	11	0.028		Arc	0.26	12	85	87	-4%	2%
EPA186A		3A	9	0.025		Arc	0.26	10	72	73	-22%	2%
EPA186B		3B	93	0.054		Arc	0.26	10	(243)	(145)	-69%	
EPA200B	yes	3B	82	0.047	86	Arc	0.26	10	(471)	(324)	-55%	
EPA217A		3A	10	0.041		Black	0.18	20	71	72	0%	2%
EPA217B		3B	10	0.039		Black	0.18	20	71	72	0%	0%
EPA219A		3A	10	0.054		Black	0.18	12	53	61	3%	14%
EPA219B		3B	10	0.055		Black	0.18	12	51	60	2%	16%
EPA222A		3A	123	0.054		Black	0.18	20	(191)	(126)	-21%	
EPA222B		3B	125	0.054		Black	0.18	22	199	(136)	-21%	
EPA223A	yes	3A	282	0.055		Black	0.18	20	(23)	(9)	-39%	
EPA223B	yes	3B	279	0.055		Black	0.18	20	(22)	(9)	-39%	
EPA249A	yes	2	246	0.155		Black	0.17	24	409	381	-23%	-7%
EPA249B	yes	3A	247	0.155		Black	0.17	24	408	381	-25%	-7%
EPA288A		3A	18	0.055		Black	0.17	16	85	89	-9%	5%
EPA290A		3A	26	0.059		Black	0.17	20	118	119	-15%	1%
EPA293A		3A	22	0.051		Black	0.17	14	100	99	-1%	-1%
EPA302A	yes	3A	21	0.30		Black	0.17	14	96	115	-5%	18%
EPA302B	yes	3B	22	0.070		Black	0.17	14	133	115	-7%	-14%
EPA365A		4	22	0.053		Arc	0.26	10	117	121	13%	4%
EPA365B		4	70	0.053		Arc	0.26	10	213	(188)	-23%	
EPA368A		4	23	0.047		Black	0.17	12	105	88	-9%	-18%
EPA368B		4	68	0.047		Black	0.17	10	(149)	(76)	-39%	
EPA385A		4	23	0.050	32	Black	0.16	14	170	159	12%	-7%
EPA385B		4	72	0.050	32	Black	0.16	14	282	(234)	-15%	
EPA396A		4	22	0.053		Black	0.16	12	82	86	31%	5%

Table B-1 (continued)

Run	New [a]	Char [b]	Experimental Conditions					Results [d]		Model Results [d,e]		
			NO_x (ppb)	Arom. (ppm)	CO (ppm)	Light [c] Type	k1	Hours	O_3 (ppb)	O_3 (ppb)	Model Error Rate	O_3^{max}
EPA396B		4	22	0.053	50	Black	0.16	12	165	152	10%	-8%
EPA410A		4	137	0.52		Black	0.15	12	177	253	26%	36%
EPA419A	yes	4	499	0.26		Black	0.15	18	(474)	(330)	-17%	
EPA424A		4	229	0.144	25	Black	0.15	22	480	462	-20%	-4%
EPA441A		4	25	0.055		Arc	0.26	10	106	117	21%	10%
EPA441B		4	80	0.055		Arc	0.26	12	201	(195)	-9%	
EPA485A	yes	5	45	0.095		Black	0.14	16	151	125	21%	-19%
EPA485B	yes	5	46	0.094		Black	0.14	16	150	126	19%	-18%
EPA488A	yes	5	50	0.087		Black	0.14	14	150	129	8%	-15%
EPA492A	yes	5	46	0.075		Black	0.14	18	164	129	11%	-24%
EPA492B	yes	5	46	0.075		Black	0.14	18	163	130	11%	-23%
EPA497A	yes	5	49	0.051		Black	0.14	16	167	125	-61%	-29%
EPA498B	yes	5	25	0.056		Black	0.14	18	118	95	29%	-22%
EPA501B	yes	5	49	0.122		Black	0.14	20	161	143	2%	-12%
EPA516B	yes	5	74	0.161	26	Black	0.14	20	283	246	14%	-14%
EPA527A	yes	5	49	0.046		Black	0.14	20	162	142	-17%	-13%
EPA541A	yes	5	50	0.072		Arc	0.16	20	213	138	-59%	-43%
EPA541B	yes	5	50	0.073		Arc	0.16	18	199	135	-57%	-39%
EPA556A		5	78	0.160		Arc	0.26	22	276	229	-22%	-19%
EPA556B		5	79	0.159		Arc	0.26	22	264	229	-22%	-14%
EPA557A	yes	5	25	0.048		Arc	0.26	16	152	112	-32%	-30%
EPA557B	yes	5	11	0.023		Arc	0.26	16	93	71	-14%	-26%
EPA558A	yes	5	82	0.132		Arc	0.26	16	265	214	-26%	-21%
EPA558B	yes	5	30	0.048		Arc	0.26	16	154	120	-16%	-25%
EPA566A	yes	5	50	0.084		Black	0.14	22	160	153	-13%	-4%
EPA566B	yes	5	49	0.080		Black	0.14	22	156	152	-15%	-2%
EPA618A	yes	5	44	0.080		Arc	0.26	22	190	189	20%	-1%
EPA618B	yes	5	44	0.079		Arc	0.26	22	189	190	16%	0%
EPA749A	yes	5	50	0.076		Black	0.13	24	157	143	-9%	-9%
EPA749B	yes	6	51	0.076		Black	0.13	22	144	141	-5%	-2%
EPA758A	yes	5	11	0.077		Black	0.12	20	53	61	18%	14%
EPA764A	yes	5	69	0.071		Black	0.12	24	213	167	15%	-25%
EPA820A	yes	5	21	0.078		Black	0.13	24	91	88	15%	-4%
EPA1091A	yes	8A	24	0.055		Black	0.12	12	84	78	13%	-7%
EPA1091B	yes	8B	24	0.058		Black	0.12	12	81	78	17%	-5%
EPA1092A	yes	8A	90	0.29		Black	0.12	18	175	182	47%	4%
EPA1092B	yes	8B	90	0.31		Black	0.12	12	169	175	48%	3%
EPA1097A	yes	8A	245	0.57		Black	0.12	16	281	283	54%	4%
EPA1097B	yes	8B	245	0.59		Black	0.12	12	278	285	55%	5%
EPA1105A	yes	8A	61	0.084	8	Black	0.40	16	(159)	203	11%	
EPA1105B	yes	8B	61	0.084	8	Black	0.40	16	(153)	202	12%	
EPA1175A	yes	9	51	0.085		Black	0.13	15	138	127	-4%	-9%
EPA1175B	yes	9	51	0.084		Black	0.13	15	136	127	-7%	-7%
EPA1190A	yes	9	46	0.070		Black	0.40	16	218	210	0%	-3%
EPA1190B	yes	9	47	0.077		Black	0.40	15	215	204	4%	-5%
EPA1191A	yes	9	52	0.080		Black	0.13	17	137	131	7%	-5%
EPA1191B	yes	9	46	0.084		Black	0.13	17	130	122	8%	-7%
EPA1192A	yes	9	42	0.077		Black	0.12	18	123	118	18%	-4%
EPA1192B	yes	9	44	0.077		Black	0.12	18	125	122	9%	-3%
EPA1193A	yes	9	45	0.071		Black	0.13	14	125	116	6%	-7%
EPA1193B	yes	9	45	0.070		Black	0.13	15	122	118	0%	-3%

Table B-1 (continued)

Run	New [a]	Char [b]	Experimental Conditions					Results [d]		Model Results [d,e]		
			NO_x (ppb)	Arom. (ppm)	CO (ppm)	Light [c] Type	k1	Hours	O_3 (ppb)	O_3 (ppb)	Model Error Rate	O_3^{max}
						o-Xylene						
EC288		1	502	0.180		Arc	0.38	12	(253)	(268)	-40%	
EC291		1	495	0.60		Arc	0.39	12	457	607	20%	31%
DTC207A		3	284	0.30		Black	0.23	12	(384)	(408)	7%	
DTC207B		3	302	0.66		Black	0.23	10	414	421	27%	6%
DTC208A		3	521	0.57		Black	0.23	10	(493)	(530)	10%	
DTC208B		3	559	0.28		Black	0.23	12	(104)	(79)	-6%	
DTC209A		3	123	0.26		Black	0.23	10	281	266	15%	-5%
DTC209B		3	127	0.145		Black	0.23	10	(240)	(225)	12%	
CTC038		1	253	0.30		Arc	0.20	12	382	394	-2%	3%
CTC039		1	481	0.159		Arc	0.20	10	(2)	(5)	-13%	
CTC046		2	503	0.30		Arc	0.20	10	(10)	(70)	39%	
CTC068		2	262	0.64		Arc	0.19	12	379	429	18%	12%
CTC081		3	260	0.54		Arc	0.19	10	358	389	5%	8%
CTC091A		4	281	0.46		Arc	0.19	10	347	408	11%	16%
EPA503A	yes	5	75	0.170		Black	0.14	22	222	184	-12%	-19%
EPA504A	yes	5	128	0.26		Black	0.14	22	289	246	-16%	-16%
EPA508A	yes	5	24	0.055		Black	0.14	18	120	94	6%	-24%
EPA517A	yes	5	124	0.105		Black	0.14	20	227	195	-29%	-15%
EPA517B	yes	5	27	0.101		Black	0.14	20	97	93	-10%	-4%
EPA518A	yes	5	262	0.20		Black	0.14	22	347	299	-33%	-15%
EPA518B	yes	5	54	0.20		Black	0.14	22	140	141	4%	1%
EPA522A	yes	5	52	0.057		Black	0.14	22	151	138	-4%	-9%
EPA522B	yes	5	10	0.057		Black	0.14	20	62	63	28%	1%
EPA1315A	yes	9	50	0.082		Black	0.40	11	208	183	-9%	-13%
EPA1315B	yes	9	22	0.078		Black	0.40	11	125	121	11%	-3%
EPA1437A	yes	9	26	0.080		Black	0.40	16	145	145	2%	0%
EPA1437B	yes	9	50	0.079		Black	0.40	9	183	166	-10%	-10%
						p-Xylene						
DTC198A		3	264	0.42		Black	0.23	10	(113)	(387)	80%	
DTC198B		3	272	0.84		Black	0.23	10	(350)	420	80%	
DTC199A		3	546	0.83		Black	0.23	10	(69)	(554)	87%	
DTC199B		3	550	0.43		Black	0.23	12	(22)	(133)	42%	
DTC200A		3	126	0.38		Black	0.23	10	(262)	286	62%	
DTC200B		3	129	0.20		Black	0.23	12	(187)	250	46%	
CTC041		1	265	0.38		Arc	0.20	12	(109)	(355)	67%	
CTC043		2	250	0.193		Arc	0.20	12	(7)	(90)	71%	
CTC044		2	506	0.39		Arc	0.20	12	(5)	(84)	113%	
CTC047		2	276	0.97		Arc	0.20	10	(284)	456	81%	
CTC069		2	242	2.00		Arc	0.19	12	389	401	86%	4%
CTC070		2	502	2.02		Arc	0.19	12	(537)	634	93%	
EPA422A		4	23	0.099	46	Black	0.15	12	151	147	22%	-3%
EPA422B		4	24	0.100		Black	0.15	12	102	101	28%	0%
EPA498A	yes	5	25	0.056		Black	0.14	18	120	87	-28%	-32%
EPA501A	yes	5	49	0.118		Black	0.14	20	172	139	-4%	-22%
EPA502A	yes	5	21	0.108		Black	0.14	22	118	93	1%	-24%
EPA502B	yes	5	109	0.110		Black	0.14	22	(180)	(128)	-12%	
EPA503B	yes	5	76	0.146		Black	0.14	22	216	183	-11%	-17%
EPA504B	yes	5	130	0.26		Black	0.14	22	277	254	0%	-9%
EPA508B	yes	5	13	0.028		Black	0.14	18	78	61	-4%	-25%
EPA509A	yes	5	30	0.143		Black	0.14	24	144	122	17%	-17%

Table B-1 (continued)

Run	New [a]	Char [b]	Experimental Conditions					Results [d]		Model Results [d,e]		
			NO_x (ppb)	Arom. (ppm)	CO (ppm)	Light [c] Type	k1	Hours	O_3 (ppb)	O_3 (ppb)	Model Error Rate	O_3^{max}
EPA509B	yes	5	155	0.145		Black	0.14	24	(178)	(174)	10%	
EPA519B	yes	5	56	0.192		Black	0.14	22	159	161	6%	1%
EPA525A	yes	5	10	0.057		Black	0.14	20	70	61	0%	-14%
EPA525B	yes	5	61	0.33		Black	0.14	20	183	168	44%	-9%
EPA1308A	yes	9	55	0.079		Black	0.40	9	172	(169)	-4%	
EPA1432A	yes	9	26	0.062		Black	0.40	15	149	140	-8%	-6%
EPA1432B	yes	9	24	0.064		Black	0.40	12	143	127	-2%	-12%
m-Ethyl toluene												
EPA1151A	yes	8A	99	0.087		Black	0.40	8	(234)	(237)	3%	
EPA1199A	yes	9	42	0.100		Black	0.40	14	195	194	17%	-1%
EPA1199B	yes	9	85	0.100		Black	0.40	12	286	272	-6%	-5%
EPA1222A	yes	9	124	0.099		Black	0.40	14	357	325	-63%	-9%
EPA1222B	yes	9	64	0.100		Black	0.40	10	245	223	-42%	-10%
EPA1226A	yes	9	231	0.20		Black	0.40	14	486	497	-36%	2%
EPA1226B	yes	9	128	0.20		Black	0.40	10	327	338	-8%	3%
EPA1232A	yes	9	111	0.20		Black	0.40	12	311	329	-1%	6%
EPA1421A	yes	9	23	0.100		Black	0.40	17	128	138	13%	8%
EPA1421B	yes	9	46	0.099		Black	0.40	10	179	176	7%	-1%
o-Ethyl toluene												
EPA1168B	yes	8B	100	0.100		Black	0.40	12	279	250	-6%	-11%
EPA1179A	yes	9	53	0.092		Black	0.40	16	216	210	-9%	-3%
EPA1202A	yes	9	56	0.099		Black	0.40	14	229	219	9%	-4%
EPA1202B	yes	9	100	0.100		Black	0.40	10	(232)	(214)	7%	
EPA1215A	yes	9	100	0.21		Black	0.40	10	338	286	-5%	-17%
EPA1215B	yes	9	52	0.21		Black	0.40	8	207	192	13%	-7%
EPA1233A	yes	9	182	0.20		Black	0.40	12	405	396	-35%	-2%
EPA1233B	yes	9	238	0.20		Black	0.40	12	449	(325)	-40%	
EPA1179B	yes	9	53	0.093		Black	0.40	17	222	217	-15%	-2%
EPA1413A	yes	9	22	0.100		Black	0.40	17	131	140	13%	6%
EPA1413B	yes	9	48	0.099		Black	0.40	13	198	191	-1%	-4%
p-Ethyl toluene												
EPA1194A	yes	9	91	0.20		Black	0.40	18	284	301	15%	6%
EPA1197A	yes	9	52	0.192		Black	0.40	14	215	223	25%	3%
EPA1197B	yes	9	91	0.192		Black	0.40	12	275	283	19%	3%
EPA1214A	yes	9	96	0.101		Black	0.40	12	290	(163)	-51%	
EPA1214B	yes	9	50	0.102		Black	0.40	10	213	181	-34%	-16%
EPA1229A	yes	9	177	0.20		Black	0.40	16	403	(388)	-35%	
EPA1229B	yes	9	238	0.20		Black	0.40	12	(372)	(142)	-47%	
1,2,3-trimethylbenzene												
DTC211A		3	247	0.131		Black	0.23	10	(315)	(225)	-23%	
DTC211B		3	259	0.30		Black	0.23	10	415	393	-3%	-5%
DTC212A		3	510	0.31		Black	0.23	10	477	(382)	-12%	
DTC212B		3	537	0.163		Black	0.23	12	(156)	(117)	-19%	
DTC213A		3	112	0.140		Black	0.23	10	275	256	-2%	-7%
DTC213B		3	113	0.088		Black	0.23	12	246	232	6%	-6%
CTC054		2	229	0.21		Arc	0.20	12	345	396	-7%	14%
CTC075		3	520	0.23		Arc	0.19	12	(277)	(265)	-5%	
CTC076		3	258	0.177		Arc	0.19	12	344	(350)	-20%	
EPA1158A	yes	8A	10	0.080		Black	0.40	12	(74)	84	-1%	
EPA1158B	yes	8B	22	0.080		Black	0.40	10	123	120	15%	-3%
EPA1162A	yes	8A	33	0.080		Black	0.40	12	177	167	-1%	-6%

Table B-1 (continued)

Run	New [a]	Char [b]	Experimental Conditions					Results [d]		Model Results [d,e]		
			NO_x (ppb)	Arom. (ppm)	CO (ppm)	Light [c] Type	k1	Hours	O_3 (ppb)	O_3 (ppb)	Model Error Rate	O_3^{max}
EPA1162B	yes	8B	43	0.080		Black	0.40	10	194	180	-15%	-8%
1,2,4-trimethylbenzene												
DTC201A		3	247	0.173		Black	0.23	10	(182)	(217)	25%	
DTC203A		3	511	0.34		Black	0.23	10	(135)	(258)	43%	
DTC203B		3	537	0.175		Black	0.23	12	(38)	(55)	12%	
DTC204A		3	120	0.170		Black	0.23	12	286	288	35%	1%
DTC204B		3	124	0.092		Black	0.23	10	(138)	(160)	31%	
CTC056		2	254	0.23		Arc	0.20	12	(300)	(373)	30%	
CTC091B		4	281	0.46		Arc	0.19	10	(340)	442	40%	
CTC093A		4	482	0.48		Arc	0.19	10	(181)	(416)	44%	
CTC093B		4	491	1.13		Arc	0.19	10	(499)	609	52%	
EPA416A		4	23	0.033	48	Black	0.15	12	(148)	(134)	7%	
EPA416B		4	23	0.033		Black	0.15	12	93	(95)	15%	
EPA1117A	yes	8A	11	0.060		Black	0.40	16	101	104	-22%	3%
EPA1117B	yes	8B	21	0.060		Black	0.40	16	158	152	-15%	-3%
EPA1119A	yes	8A	50	0.078		Black	0.40	14	260	236	-11%	-9%
EPA1119B	yes	8B	41	0.079		Black	0.40	14	227	213	8%	-6%
EPA1126A	yes	8A	11	0.079		Black	0.40	12	101	91	-2%	-11%
EPA1126B	yes	8B	24	0.081		Black	0.40	12	161	145	-4%	-11%
EPA1129A	yes	8A	41	0.039		Black	0.40	12	222	184	-17%	-19%
EPA1129B	yes	8B	16	0.042		Black	0.40	12	126	112	7%	-13%
EPA1352A	yes	9	193	0.079		Black	0.40	15	396	(199)	-50%	
EPA1352B	yes	9	137	0.079		Black	0.40	14	338	(247)	-47%	
EPA1354A	yes	9	200	0.079		Black	0.40	17	417	(230)	-51%	
EPA1354B	yes	9	153	0.078		Black	0.40	17	388	(289)	-55%	
EPA1356A	yes	9	121	0.079		Black	0.40	15	305	288	-44%	-6%
EPA1356B	yes	9	149	0.079		Black	0.40	16	349	(283)	-47%	
EPA1374B	yes	9	148	0.077		Black	0.40	16	303	(263)	-45%	
EPA1380B	yes	9	55	0.079		Black	0.40	11	177	190	-5%	7%
1,3,5-trimethylbenzene												
EC901		1	490	0.31		Arc	0.27	12	382	560	-18%	38%
EC903		1	1011	0.55		Arc	0.27	12	500	737	-21%	39%
ITC703		6	495	0.56		Black	0.35	8	702	769	3%	9%
ITC706		6	466	0.28		Black	0.35	12	635	687	-12%	8%
ITC709		6	973	0.50		Black	0.35	12	773	905	-12%	16%
DTC194A		3	259	0.169		Black	0.23	12	428	(397)	-27%	
DTC194B		3	281	0.34		Black	0.23	10	410	453	-1%	12%
DTC195A		3	548	0.34		Black	0.23	12	632	(622)	-24%	-2%
DTC195B		3	565	0.167		Black	0.23	12	(316)	(143)	-54%	
DTC196A		3	134	0.165		Black	0.23	12	281	326	-2%	15%
DTC196B		3	141	0.082		Black	0.23	10	268	(200)	-30%	
DTC206A		3	272	0.138		Black	0.23	12	411	(290)	-34%	
CTC050		2	271	0.194		Arc	0.20	10	347	(424)	-20%	
CTC071		2	517	0.329		Arc	0.19	10	582	(563)	-27%	
CTC073		3	257	0.175		Arc	0.19	12	359	385	-9%	7%
CTC098A		4	480	0.198		Arc	0.19	10	(278)	(197)	-26%	
XTC103		1	496	0.297		Mix	0.25	12	671	689	-18%	3%
EPA402A		4	22	0.033		Black	0.16	12	89	90	-3%	1%
EPA402B		4	21	0.033	50	Black	0.16	12	160	147	-4%	-8%
EPA403A		4	21	0.035	49	Black	0.16	10	148	(135)	-4%	
EPA403B		4	22	0.035		Black	0.16	10	81	83	-1%	2%

Table B-1 (continued)

Run	New [a]	Char [b]	Experimental Conditions					Results [d]		Model Results [d,e]		
			NO_x (ppb)	Arom. (ppm)	CO (ppm)	Light [c] Type	k1	Hours	O_3 (ppb)	O_3 (ppb)	Model Error Rate	Model Error O_3^{max}
EPA1153A	yes	8A	11	0.079		Black	0.40	12	73	90	1%	21%
EPA1153B	yes	8B	20	0.080		Black	0.40	10	109	119	15%	9%
EPA1156A	yes	8A	32	0.080		Black	0.40	14	180	177	14%	-2%
EPA1156B	yes	8B	45	0.080		Black	0.40	10	202	194	-3%	-4%
						Phenol						
EPA1219A	yes	9	147	0.140		Black	0.40	17	194	224	-25%	14%
EPA1219B	yes	9	76	0.140		Black	0.40	17	170	177	-24%	4%
EPA1273A	yes	9	23	0.106		Black	0.40	9	99	90	19%	-10%
EPA1273B	yes	9	53	0.106		Black	0.40	9	(93)	(124)	26%	
EPA1289B	yes	9	79	0.084		Black	0.40	7	(10)	(7)	-37%	
						o-Cresol						
EC281		1	488	0.394		Arc	0.37	13	(73)	426	98%	
EPA1260A	yes	9	15	0.062		Black	0.40	7	70	71	16%	2%
EPA1279A	yes	9	27	0.080		Black	0.40	7	96	102	4%	6%
EPA1260B	yes	9	56	0.062		Black	0.40	6	(106)	(83)	-17%	
EPA1279B	yes	9	57	0.080		Black	0.40	7	143	(139)	-18%	
EPA1350A	yes	9	718	0.312		Black	0.40	10	(55)	(29)	-36%	
EPA1350B	yes	9	384	0.301		Black	0.40	10	212	394	12%	60%
						1,4-Dimethyl phenol						
EPA1275A	yes	9	22	0.040		Black	0.40	8	111	96	2%	-14%
EPA1275B	yes	9	53	0.040		Black	0.40	8	(165)	(107)	-36%	
EPA1277A	yes	9	23	0.094		Black	0.40	7	100	106	39%	5%
EPA1277B	yes	9	51	0.094		Black	0.40	7	166	168	17%	1%

[a] "new" = experiment not used for SAPRC-07 mechanism evaluation (Carter, 2010a,b)

[b] Characterization set used to assign chamber effects parameters. Chamber effect parameters used for each chamber and characterization set are given in Table B-4.

[c] "k1" is the NO_2 photolysis rate in min^{-1}. Light source types used are as follows: "black" = blacklights; "mix" = mix of fluorescent lights; "blue" = fluorescent blue lights (low in UV); "arc" = xenon or argon arc lights.

[d] The maximum O_3 concentration is shown if the maximum O_3 value in the experiment or model simulation is greater than the final O_3 value, or if the O_3 increased by less than 5% in the last half hour of the experiment (i.e., the experiment or model gives a measure of the maximum O_3 yield). Otherwise, the final O_3 concentration is shown in parentheses.

[e] Model calculations shown are for the SAPRC-11 mechanism. Model error in simulations of the formation rate of $\Delta([O_3]-[NO])$ and maximum O_3 yields are given by (experimental - model) / average (experimental, model). "Rate" is the model error for the $\Delta([O_3]-[NO])$ formation rate, and "O_3^{max}" is model error the maximum O_3 concentration, which is not calculated if the O_3 increases by less than 5% in the last half hour of the experiment or the model calculation. These are derived as discussed in the model evaluation methods section.

Table B-2. Summary of incremental reactivity experiments with aromatic compounds that were used for aromatics mechanism evaluation.

Run ID	Test VOC and Run Type [a]	Initial Reactants			Char Set [b]	Light [c]	Hrs.	Max Δ([O_3]-[NO]) (ppb)			
		Test (ppm)	NOx (ppb)	ROG (ppmC)				Experimental		Model [d]	
								Test	Base	Test	Base
	Benzene										
ETC263	IR Surg-3 MIR1	6.77	476	4.40	2	Bl	6	958	806	1128	763
ETC265	IR Surg-3 MIR1	5.78	485	4.51	2	Bl	6	959	700	1182	718
DTC039B	IR Surg-8 LN1	7.39	178	4.05	1	Bl	6	527	612	525	698
EPA421B	IR Surg-NA vary	0.45	29	0.55	4B	Bl	6	132	92	133	80
	Toluene										
CTC108B	IR Surg-3 MIR1	0.48	308	4.99	5	A	5	646	402	780	609
ETC101	IR Surg-3 MIR1	0.17	503	3.52	2	Bl	6	645	435	733	517
ETC103	IR Surg-3 MIR1	0.18	516	3.55	2	Bl	6	678	444	725	509
CTC127B	IR Surg-8 MIR1	0.77	388	4.62	5	A	5	708	539	868	728
DTC023A	IR Surg-8 MIR1	0.57	469	3.49	1	Bl	6	1081	800	1194	859
DTC030B	IR Surg-8 LN1	1.13	166	3.41	1	Bl	6	502	598	551	668
	ethyl benzene										
ETC311	IR Surg-3 MIR1	0.11	522	4.44	2	Bl	6	608	548	665	579
ETC313	IR Surg-3 MIR1	0.10	528	4.21	2	Bl	6	643	576	598	523
ETC315	IR Surg-3 MIR1	0.25	526	4.16	2	Bl	6	781	575	724	543
	m-xylene										
CTC109A	IR Surg-3 MIR1	0.21	307	3.85	5	A	5	630	433	741	610
ETC196	IR Surg-3 MIR1	0.16	477	3.96	2	Bl	6	922	659	1106	716
ETC207	IR Surg-3 MIR1	0.15	508	3.61	2	Bl	6	978	645	1043	676
ETC301	IR Surg-3 MIR1	0.15	462	3.64	2	Bl	6	969	687	1058	695
CTC128A	IR Surg-8 MIR1	0.22	407	4.88	5	A	5	748	599	879	804
DTC025A	IR Surg-8 MIR1	0.16	467	3.56	1	Bl	6	1141	848	1218	932
DTC068B	IR Surg-8 MIR1	0.14	484	3.15	1	Bl	6	997	722	1094	803
DTC035A	IR Surg-8 LN1	0.18	166	3.38	1	Bl	6	557	611	630	677
DTC067B	IR Surg-8 LN1	0.25	171	3.11	1	Bl	6	537	597	627	683
EPA110A	IR Surg-8 MIR2	0.03	31	0.49	3A	A	5	185	168	169	150
EPA123B	IR Surg-8 LN2	0.05	22	0.81	3B	A	6	155	174	155	164
EPA084A	IR Surg-8 vary	0.05	50	0.97	3A	A	6	287	294	262	262
EPA086B	IR Surg-8 vary	0.06	10	0.91	3B	A	6	84	103	95	101
EPA100B	IR Surg-8 vary	0.02	5	0.29	3B	A	6	62	72	64	68
EPA108A	IR Surg-8 vary	0.03	76	0.78	3A	A	6	328	257	272	203
EPA128B	IR Surg-8 vary	0.03	48	0.47	3B	A	5	233	165	201	130
EPA406B	IR Surg-NA vary	0.01	26	0.60	4B	Bl	5	111	73	112	90
	o-xylene										
ETC259	IR Surg-3 MIR1	0.06	490	4.50	2	Bl	6	948	681	1004	716
ETC261	IR Surg-3 MIR1	0.06	476	4.49	2	Bl	6	1000	743	1063	765
	p-xylene										
ETC348	IR Surg-3 MIR1	0.08	519	5.13	2	Bl	6	1070	909	1144	886
	1,2,3-trimethyl benzene										
ETC297	IR Surg-3 MIR1	0.04	462	4.44	2	Bl	6	1217	854	1159	858
ETC299	IR Surg-3 MIR1	0.04	481	4.39	2	Bl	6	1166	834	1067	789
	1,2,4-trimethyl benzene										
ETC267	IR Surg-3 MIR1	0.04	486	4.59	2	Bl	6	932	678	910	697
ETC269	IR Surg-3 MIR1	0.04	484	4.47	2	Bl	6	1023	775	977	734

Table B-2 (continued)

Run ID	Test VOC and Run Type [a]	Initial Reactants Test (ppm)	NOx (ppb)	ROG (ppmC)	Char Set [b]	Light [c]	Hrs.	Max Δ([O3]-[NO]) (ppb) Experimental Test	Experimental Base	Model [d] Test	Model [d] Base
	1,3,5-trimethyl benzene										
ETC249	IR Surg-3 MIR1	0.05	494	5.02	2	Bl	6	1264	697	1293	192
	m-cresol										
EPA383B	IR Surg-7 LN2	0.08	26	1.05	4B	Bl	5	112	128	115	137

[a] See Table 10 for a description of the designations or codes used.

[b] See Table B-4 for the characterization model input used for the characterization sets indicated.

[c] A = arc light (Xenon or Argon); Bl = blacklights.

[d] The SAPRC-11A model is used for benzene, toluene, and ethylbenzene because the standard SAPRC-11 model consistently overpredicts reactivity of experiments with NO_x levels greater than ~100 ppb. See plots of incremental reactivity results in the "Mechanism Evaluation Results" section for the performance of the standard SAPRC-11 mechanism in fitting these data

Table B-3. Summary of surrogate - NO_x experiments that were used for the data shown on Figure 40.

Run ID	Surrogate Type	Light	Char Set	Hours	Initial Reactants NOx (ppb)	Initial Reactants ROG (ppmC)	Final Δ([O3]-[NO]) Expt (ppb)	Final Δ([O3]-[NO]) Model (ppb)	Model Error
					Full Surrogate, Arc Lights				
EPA211B	Surg-8	A	3B	5	181	0.43	43	28	-42%
EPA207B	Surg-8	A	3B	6	192	0.94	178	133	-29%
EPA211A	Surg-8	A	3A	5	85	0.43	75	61	-20%
EPA206B	Surg-8	A	3B	5	315	1.80	284	243	-15%
EPA190B	Surg-8	A	3B	6	97	0.57	131	100	-26%
EPA193B	Surg-8	A	3B	5	48	0.29	65	48	-30%
EPA096B	Surg-8	A	3B	5	111	0.72	213	108	-66%
EPA096A	Surg-8	A	3A	6	109	0.72	252	132	-63%
EPA201B	Surg-8	A	3B	5	69	0.50	124	94	-28%
EPA212B	Surg-8	A	3B	5	136	1.00	214	175	-20%
EPA182A	Surg-8	A	3A	6	111	1.06	292	246	-17%
EPA190A	Surg-8	A	3A	6	54	0.56	201	157	-24%
EPA193A	Surg-8	A	3A	5	28	0.29	99	74	-29%
EPA197A	Surg-8	A	3A	5	193	2.05	459	411	-11%
EPA108B	Surg-8	A	3B	5	76	0.90	257	172	-40%
EPA128A	Surg-8	A	3A	5	48	0.57	165	130	-24%
EPA212A	Surg-8	A	3A	6	81	0.98	310	273	-13%
EPA198B	Surg-8	A	3B	6	72	1.03	325	265	-20%
EPA207A	Surg-8	A	3A	6	62	0.91	293	263	-11%
EPA113A	Surg-8	A	3A	6	69	1.03	299	255	-16%
EPA201A	Surg-8	A	3A	5	31	0.49	165	140	-17%
EPA206A	Surg-8	A	3A	5	107	1.79	412	395	-4%
EPA238B	Surg-7	A	3B	6	33	0.56	190	165	-14%
EPA235A	Surg-7	A	2	6	32	0.55	199	173	-14%
EPA235B	Surg-7	A	2	6	32	0.56	202	175	-14%
EPA319B	Surg-7	A	3B	5	31	0.56	175	147	-18%
EPA230A	Surg-7	A	3A	5	33	0.60	176	156	-12%

Table B-3 (continued)

Run ID	Surrogate Type	Light	Char Set	Hours	Initial Reactants		Final Δ([O_3]-[NO])		
					NOx (ppb)	ROG (ppmC)	Expt (ppb)	Model (ppb)	Model Error
EPA226A	Surg-7	A	2	6	31	0.56	192	173	-11%
EPA277B	Surg-7	A	3B	6	32	0.59	208	168	-21%
EPA349A	Surg-7	A	4A	5	33	0.60	178	159	-11%
EPA143A	Surg-8	A	3A	6	29	0.53	181	154	-17%
EPA226B	Surg-7	A	2	6	31	0.58	191	174	-9%
EPA187A	Surg-8	A	3A	6	56	1.04	286	257	-11%
EPA151B	Surg-8	A	3B	6	30	0.56	197	164	-18%
EPA352A	Surg-7	A	4A	6	31	0.58	188	168	-11%
EPA143B	Surg-8	A	3B	6	29	0.55	188	155	-20%
EPA167A	Surg-8	A	3A	6	29	0.56	189	168	-12%
EPA278A	Surg-7	A	3A	5	32	0.62	184	160	-14%
EPA127B	Surg-8	A	3B	5	29	0.56	168	145	-15%
EPA110B	Surg-8	A	3B	5	31	0.60	168	150	-11%
EPA257A	Surg-7	A	3A	6	33	0.63	188	166	-12%
EPA168B	Surg-8	A	3B	6	29	0.55	192	165	-15%
EPA244A	Surg-7	A	3A	6	32	0.63	197	181	-8%
EPA181A	Surg-8	A	3A	5	108	2.12	445	421	-6%
EPA323A	Surg-7	A	3A	5	27	0.53	157	143	-10%
EPA197B	Surg-8	A	3B	6	104	2.05	457	432	-6%
EPA188A	Surg-8	A	3A	5	27	0.54	165	150	-9%
EPA137A	Surg-8	A	3A	5	29	0.59	177	155	-13%
EPA229B	Surg-7	A	3B	5	32	0.66	178	165	-8%
EPA182B	Surg-8	A	3B	6	53	1.09	278	266	-4%
EPA083A	Surg-8	A	3A	6	48	1.01	269	247	-9%
EPA191A	Surg-8	A	3A	6	13	0.29	108	95	-14%
EPA191B	Surg-8	A	3B	5	13	0.29	103	86	-18%
EPA084B	Surg-8	A	3B	6	51	1.16	294	262	-12%
EPA163B	Surg-8	A	3B	6	24	0.53	177	151	-16%
EPA198A	Surg-8	A	3A	6	43	1.02	252	227	-10%
EPA095B	Surg-8	A	3B	5	25	0.80	167	162	-3%
EPA203A	Surg-8	A	3A	6	6	0.20	67	69	3%
EPA258A	Surg-8	A	3A	6	32	1.09	209	201	-4%
EPA192A	Surg-8	A	3A	5	14	0.50	117	112	-5%
EPA098A	Surg-8	A	3A	5	5	0.18	53	50	-5%
EPA098B	Surg-8	A	3B	6	5	0.18	53	54	2%
EPA188B	Surg-8	A	3B	5	14	0.54	115	112	-3%
EPA233B	Surg-7	A	2	6	27	1.10	193	190	-2%
EPA232B	Surg-7	A	3B	6	27	1.12	190	182	-4%
EPA233A	Surg-7	A	2	6	27	1.11	193	190	-1%
EPA231A	Surg-7	A	3A	5	27	1.10	176	170	-4%
EPA187B	Surg-8	A	3B	6	25	1.05	189	170	-11%
EPA180A	Surg-8	A	3A	5	52	2.21	281	279	-1%
EPA180B	Surg-8	A	3B	5	52	2.21	284	277	-2%
EPA253B	Surg-7	A	3B	5	27	1.16	177	171	-3%
EPA240B	Surg-7	A	3B	6	27	1.16	188	178	-6%
EPA237A	Surg-7	A	3A	6	26	1.13	192	179	-7%
EPA227A	Surg-7	A	2	6	25	1.10	181	182	1%
EPA245A	Surg-7	A	3A	6	27	1.17	185	185	0%
EPA239B	Surg-7	A	3B	6	27	1.20	190	183	-4%
EPA243A	Surg-7	A	3A	6	27	1.17	190	180	-5%
EPA242A	Surg-7	A	3A	6	26	1.16	190	181	-5%
EPA250A	Surg-7	A	3A	6	27	1.21	196	184	-6%

Table B-3 (continued)

Run ID	Surrogate Type	Light	Char Set	Hours	Initial Reactants		Final Δ([O_3]-[NO])		
					NOx (ppb)	ROG (ppmC)	Expt (ppb)	Model (ppb)	Model Error
EPA123A	Surg-8	A	3A	6	22	0.99	174	164	-6%
EPA227B	Surg-7	A	2	6	25	1.14	182	181	0%
EPA126A	Surg-8	A	3A	5	23	1.03	169	156	-8%
EPA252B	Surg-7	A	3B	6	27	1.23	193	185	-4%
EPA139A	Surg-8	A	3A	6	20	0.90	163	155	-5%
EPA334A	Surg-7	A	3A	6	28	2.86	203	210	3%
EPA334B	Surg-7	A	3B	5	28	2.86	195	197	1%
EPA353A	Surg-7	A	4A	6	26	1.18	189	182	-4%
EPA081B	Surg-8	A	2	6	50	2.30	297	279	-6%
EPA080A	Surg-8	A	3A	6	92	4.25	437	411	-6%
EPA080B	Surg-8	A	3B	6	92	4.25	440	411	-7%
EPA081A	Surg-8	A	2	6	50	2.31	299	280	-7%
EPA124B	Surg-8	A	3B	6	23	1.07	173	164	-6%
EPA138A	Surg-8	A	3A	6	22	1.05	161	164	2%
EPA189A	Surg-8	A	3A	6	21	0.99	163	155	-5%
EPA100A	Surg-8	A	3A	6	5	0.33	72	68	-5%
EPA192B	Surg-8	A	3B	6	7	0.50	83	80	-3%
EPA189B	Surg-8	A	3B	5	13	1.01	116	110	-6%
EPA181B	Surg-8	A	3B	5	24	2.15	181	168	-8%
EPA097A	Surg-8	A	3A	5	5	0.53	68	65	-5%
EPA097B	Surg-8	A	3B	6	5	0.53	67	67	1%
EPA086A	Surg-8	A	3A	6	10	1.08	103	101	-2%
EPA085A	Surg-8	A	3A	6	10	1.11	96	96	0%
EPA209B	Surg-8	A	3B	5	13	1.91	111	115	4%
EPA152A	Surg-8	A	3A	6	24	0.93	178	172	-3%
EPA101B	Surg-8	A	3B	5	2	0.31	32	35	10%
EPA101A	Surg-8	A	3A	6	2	0.32	40	41	1%
EPA209A	Surg-8	A	3A	6	6	1.90	60	70	16%
			Full Surrogate, Blacklights						
EPA292B	Surg-8	Bl	3B	6	48	0.27	34	28	-22%
EPA387A	Surg-8	Bl	4A	6	100	0.58	62	54	-13%
EPA387B	Surg-8	Bl	4B	5	53	0.59	88	78	-11%
EPA393A	Surg-8	Bl	4A	6	159	2.50	358	387	8%
EPA393B	Surg-8	Bl	4B	6	159	2.51	357	388	8%
EPA394A	Surg-8	Bl	4A	6	18	0.30	78	65	-18%
EPA392B	Surg-8	Bl	4B	6	271	4.87	588	627	6%
EPA392A	Surg-8	Bl	4A	5	270	4.91	563	610	8%
EPA273B	Surg-7	Bl	3B	5	32	0.60	114	109	-4%
EPA354A	Surg-7	Bl	4A	6	31	0.59	120	120	0%
EPA318A	Surg-7	Bl	3A	6	29	0.60	121	124	2%
EPA318B	Surg-7	Bl	3B	6	30	0.62	127	126	-1%
EPA294B	Surg-7	Bl	3B	6	28	0.59	129	125	-3%
EPA294A	Surg-7	Bl	3A	6	27	0.58	125	124	0%
EPA394B	Surg-8	Bl	4B	5	8	0.30	55	53	-5%
EPA383A	Surg-7	Bl	4A	5	26	1.05	128	131	2%
EPA379B	Surg-7	Bl	4B	6	28	1.15	142	144	1%
EPA380A	Surg-7	Bl	4A	6	26	1.11	140	139	-1%
EPA379A	Surg-7	Bl	4A	5	27	1.15	132	136	3%
EPA162B	Surg-8	Bl	3A	6	23	1.00	138	139	0%
EPA162A	Surg-8	Bl	3A	6	23	1.01	135	139	2%
EPA161A	Surg-8	Bl	3A	5	20	0.95	131	124	-6%

Table B-3 (continued)

Run ID	Surrogate Type	Light	Char Set	Hours	Initial Reactants NOx (ppb)	Initial Reactants ROG (ppmC)	Final Δ([O_3]-[NO]) Expt (ppb)	Final Δ([O_3]-[NO]) Model (ppb)	Final Δ([O_3]-[NO]) Model Error
EPA161B	Surg-8	Bl	3A	5	20	0.96	132	124	-6%
EPA291B	Surg-7	Bl	3B	6	26	1.28	148	146	-2%
EPA291A	Surg-7	Bl	3A	6	26	1.28	145	146	0%
EPA388A	Surg-8	Bl	4A	6	18	1.10	104	106	2%
EPA388B	Surg-8	Bl	4B	6	12	1.10	78	80	2%
EPA282B	Surg-8	Bl	3B	6	26	2.74	135	136	1%
				Non-aromatic surrogate					
EPA427A	Surg-NA	A	4A	6	47	1.12	198	219	10%
EPA427B	Surg-NA	A	4B	6	17	1.12	139	162	15%
EPA305B	Surg-NA	Bl	3B	5	222	1.11	46	58	22%
EPA389A	Surg-NA	Bl	4A	6	87	0.59	49	46	-7%
EPA395B	Surg-NA	Bl	4B	6	90	0.62	42	52	20%
EPA397B	Surg-NA	Bl	4B	6	128	1.24	100	131	27%
EPA389B	Surg-NA	Bl	4B	6	61	0.59	59	60	2%
EPA395A	Surg-NA	Bl	4A	6	57	0.61	57	70	21%
EPA400B	Surg-NA	Bl	4B	5	42	0.62	64	72	11%
EPA398B	Surg-NA	Bl	4B	6	164	2.44	239	306	24%
EPA305A	Surg-NA	Bl	3A	6	60	1.08	123	153	21%
EPA299B	Surg-NA	Bl	3B	5	60	1.17	136	159	15%
EPA404A	Surg-NA	Bl	4A	6	27	0.59	81	88	8%
EPA408A	Surg-NA	Bl	4A	6	27	0.59	80	91	12%
EPA406A	Surg-NA	Bl	4A	5	26	0.60	73	80	10%
EPA398A	Surg-NA	Bl	4A	6	99	2.44	279	325	15%
EPA400A	Surg-NA	Bl	4A	6	25	0.62	88	96	9%
EPA397A	Surg-NA	Bl	4A	6	43	1.20	155	174	11%
EPA300A	Surg-NA	Bl	3A	6	19	1.14	129	135	5%
EPA304B	Surg-NA	Bl	3B	5	16	1.14	120	113	-6%
EPA390A	Surg-NA	Bl	4A	5	29	2.53	164	167	2%
EPA390B	Surg-NA	Bl	4B	5	18	2.53	115	117	1%
EPA304A	Surg-NA	Bl	3A	5	5	1.14	57	52	-9%
EPA300B	Surg-NA	Bl	3B	6	4	1.14	52	50	-5%

[a] See Table 10. for a description of the designations or codes used.

[b] See Table B-4 for the characterization input used for the characterization sets indicated.

Table B-4. Chamber wall effect and background characterization parameters used in the environmental chamber model simulations for aromatics mechanism evaluation.

Cham.	Set(s)	Value	Discussion
RN-I (ppb)			Ratio of the rate of wall + hν -> HONO to the NO_2 photolysis rate.
EPA	2	0.0075	Average of values that gave best fits to n-butane - NO_x and CO - NO_x, radical source characterization and CO - air NO_x offgasing characterization experiments carried out in this chamber. Note that for Set 3 the best fit RN-I values depended on the reactor.
	3A	0.0165	
	3B	0.0115	
	4	0.0055	
	5	0.0110	
	6	0.0150	
	7	0.0100	
	8A	0.0173	
	8B	0.0118	
	9	0.0062	
ITC	All	0.0475	Average of value of RS-I that gave best fits to n-butane - NO_x radical source characterization chamber experiments carried out in this chamber.
DTC	1	0.058	Same procedure as above
	3	0.210	
	4	0.300	
	10	0.055	
	11	0.092	
	12	0.310	
	13	0.170	
	14	0.095	
	15	0.063	
	16	0.240	
	17	0.083	
	18	0.074	
XTC	All	0.085	Same procedure as above
CTC	1	0.06	Same procedure as above
	2,3	0.10	
	4-8	0.095	
	9	0.115	
	10	0.08	
EC	1	0.235	Based on the NO_2 dependence radical source derived by Carter et al (1982), adjusted to reduce biases in simulations of n-butane - NO_x experiments carried out in this chamber using this mechanism. The NO_2-dependent radical source term, RS-S, was reduced by an equal factor.
TVA	All	0.008	Estimated value. Could not be determined by modeling radical source characterization because of the large formaldehyde offgasing. See Carter (2004).
CSI	All	0.004	From characterization input file provided by White (2010). This and the other characterization inputs on this table were used by Azzi et al (2010) when evaluating the SAPRC-07 mechanism using CSIRO chamber data.

Table B-4. (continued)

Cham.	Set(s)	Value	Discussion
RS-S (unitless)			Ratio of the rate of NO_2 + hv -> 0.5 HONO + 0.5 wall NO_x to the NO_2 photolysis rate.
EC	1	0.0017	Based on the NO_2 dependence radical source derived by Carter et al (1982), adjusted downward by 20% to reduce biases in simulations of n-butane - NO_x experiments carried out in this chamber. The NO2-independent radical source term, RN-I, was reduced by an equal factor.
All others		0	Any dependence of apparent radical source on initial NOx levels in Teflon bag chambers was found to be much less than the run-to-run variability.
HONO-I (ppb)			Initial HONO in experiment, assumed to be independent of other reactants unless indicated.
EPA	All	0.05	Value that usually gives best fits to model simulations of results of n-butane - NO_x and CO - NO_x experiments in this chamber.
ITC	All	1.7	Average of initial HONO value that gave best fits to n-butane - NO_x chamber experiments carried out in this chamber. The RN-I parameter was optimized at the same time. The best fit initial HONO values appear to be approximately independent of the initial NO_2.
ITC	All	1.7	Similar procedure as above.
TVA	All	0.5	Similar procedure as above.
DTC	1	0.001 x [NO_2]init	Similar procedure as above, except for this chamber the best fit initial HONO appeared to be correlated with the initial NO_2 concentrations.
	3,4	0.004 x [NO_2]init	
	10,18	0.008 x [NO_2]init	
	11,14	0.006 x [NO_2]init	
	12,16	0.005 x [NO_2]init	
	13	0.009 x [NO_2]init	
	15	0.007 x [NO_2]init	
	17	0.003 x [NO_2]init	
XTC	All	0.012 x [NO_2]init	Similar procedure as above
CTC	All	0.008 x [NO_2]init	Similar procedure as above
EC	All	0.07 x [NO_2]init	Similar procedure as above
CSI	All	0	From CSIRO characterization input file provided by White (2010).
E-NO2/K1 (ppb)			Ratio of rate of NO_2 offgasing from the walls to the NO_2 photolysis rate.
EC	1	0.10	Adjusted to fit O_3 formation in acetaldehyde/air run EC-253.
All others		0	The NO_x offgasing caused by representing the radical source by HONO offgasing appears to be sufficient for accounting for NO_x offgasing effects in most cases. RN-I parameters adjusted to fit experiments sensitive to the radical source are consistent with NOx offgasing rates adjusted to fit pure air or aldehyde - air runs, to within the uncertainty and variability.
K(NO2W) (min^{-1})			Rate of unimolecular loss (or hydrolysis) of NO_2 to the walls.
EC	1	2.8e-4	Based on dark NO_2 decay and HONO formation measured in the EC by Pitts et al. (1984).
CSI	All	7.2e-5	From CSIRO characterization input file provided by White (2010).
All Others		1.6e-4	Based on dark NO_2 decay and HONO formation measured in a Teflon film chamber by Pitts et al. (1984). Assumed to be the same in all Teflon bag chambers, regardless of volume.
YHONO			Yield of HONO in the unimolecular reaction (hydrolysis) of NO_2 on the walls.
EC	1	0.5	Based on dark NO2 decay and HONO formation measured in the EC by Pitts et al. (1984).

Table B-4. (continued)

Cham.	Set(s)	Value	Discussion
CSI	All	0.42	From CSIRO characterization input file provided by White (2010).
All Others		0.2	Based on dark NO2 decay and HONO formation measured in a Teflon film chamber by Pitts et al. (1984). Assumed to be the same in all Teflon bag chambers, regardless of volume.
E-ALD/K1 (ppb)			Ratio of rate of formaldehyde offgasing from the walls to the NO_2 photolysis rate.
EPA	All	0.01	Gives best fits to formaldehyde data in most pure air irradiations and other experiments where formaldehyde should not otherwise be present.
TVA	All	0.045 + other sources (see discussion)	This chamber had significant wall offgasing of formaldehyde and assuming a constant offgasing rate did not give best fits to the data. The additional process required to fit the data, derived by Simonaitis et al (1997) and used by Carter (2004), are as follows: Walls + hν → WALLVOC; rate = NO_2 photolysis rate x 0.135 ppb WALLVOC + OH → HO2 + 0.2 HCHO; k = 2 x 10^4 ppm^{-1} min^{-1}
All other chambers		0	Simulations of characterization experiments do not require assuming formaldehyde offgasing. Formaldehyde measurements not sufficiently sensitive to determine formaldehyde offgasing.
K(O3W) (min^{-1})			Unimolecular loss rate of O_3 to the walls.
EPA	All	1.08e-4	Based on results of O_3 decays carried out in this chamber
ITC, DTC, XTC		1.5e-4	Based on results of O_3 decay in Teflon bag chambers experiments as discussed by Carter et al (1995a).
CTC	All	8.5e-5	Based on results of O_3 decay experiments in this chamber
OTC	All	1.67e-4	Similar procedure as above
EC	All	1.1e-3	Similar procedure as above
TVA	All	7.0e-4	Similar procedure as above
CSI	All	1.2e-5	From CSIRO characterization input file provided by White (2010).
k(N25I) (min^{-1})			Rate constant for N2O5 -> 2 Wall-NO_x. This represents the humidity-independent portion of the wall loss of N_2O_5, or the intercept of plots of rates of N_2O_5 loss against humidity.
EC	1	4.7e-3	Based on N_2O_5 decay rate measurements made by Tuazon et al (1983) for the EC. See also Carter et al (1995a).
CSI	All	6.0e-4	From CSIRO characterization input file provided by White (2010).
All other chambers		2.8e-3	Based on N_2O_5 decay rate measurements made by Tuazon et al (1983) for a Teflon film chamber. Assumed to be independent of chamber size (Carter et al, 1995a).
k(N25S) (ppm^{-1} min^{-1})			Rate constant for N2O5 + H2O -> 2 Wall-NOx**.** This represents the humidity dependent portion of the wall loss of N_2O_5, or the slope of plots of rates of N_2O_5 loss against humidity. Note that this is in addition to the N_2O_5 hydrolysis reaction in the gas-phase mechanism.
EC	1	1.8e-6	Based on N_2O_5 decay rate measurements made by Tuazon et al (1983) for the EC. See also Carter et al (1995a).
EPA	All	0	Assumed to be negligible compared to the homogeneous process already in the base mechanism
CSI	All	1.5e-5	From CSIRO characterization input file provided by White (2010).

Table B-4. (continued)

Cham.	Set(s)	Value	Discussion
All other chambers		1.1e-6	Based on N_2O_5 decay rate measurements made by Tuazon et al (1983) for a Teflon film chamber. Assumed to be independent of chamber size (Carter et al, 1995a).
k(XSHC) (min^{-1})			Rate constant for OH -> HO2. This represents the effects of reaction of OH with reactive VOCs in the background air or offgassed from the chamber walls. This parameter does not significantly affect model simulations of experiments other than pure air runs.
EC	1	0	Assumed to be negligible because the EC is generally evacuated overnight between experiments (Carter et al, 1995a).
EPA, TVA		0	Assumed to be negligible because steps are taken to reduce background effects for low concentration experiments.
CSI	All	250	From CSIRO characterization input file provided by White (2010).
All Teflon Bag Chambers		250	Estimated from modeling several pure air in the ITC (Carter et al, 1996d), and also consistent with simulations of pure air runs in a Teflon film chamber (Carter et al, 1997a).
H2O (ppm)			Default water vapor concentration for runs where no humidity data are available.
EPA	All	3.4e+2	The EPA chamber experiments used for mechanism evaluation to date were not humidified. This is the expected upper limit water concentration.
ITC	All	2.0e+4	This corresponds to ~50% RH at 303K, which is the condition for most experiments in this chamber.
EC	1	2.0e+4	This corresponds to ~50% RH at 303K, which is the condition for most experiments in this chamber. Humidity data are available for most EC runs, so the default is usually not used.
TVA		(no default)	The water concentration is specified in the input files for all experiments.
All other experiments in this evaluation		1.0e+3	Experiments in these chambers used in this evaluation were carried out using dried purified air. The limited humidity data for such runs indicate that the humidity was less than 5%, probably no more than ~2.5%, and possibly much less than that. The default value corresponds to ~2.5 - 3% RH for the conditions of most experiments.
Dilution rate (min^{-1})			Default rate of dilution in the experiment (used for most experiments if no dilution specified for the experiment)
EPA	All	0	Dilution expected to be small because of the design of the chamber
ITC	All	0	Dilution not well characterized but assumed to be small.
DTC	1	5.3e-5	Similar procedure as above
	3,4	1.8e-4	
	10-18	5.3e-5	
XTC	All	2.7e-5	Similar procedure as above
CTC	All	6.7e-5	Similar procedure as above
OTC	All	6.7e-5	Similar procedure as above
EC	All	2.0e-4	Similar procedure as above
TVA		(no default)	Dilution specified in input files for each experiment
CSI	All	0	From CSIRO characterization input file provided by White (2010).